https://ntrs.nasa.gov/search.jsp?R=19790019307 2020-03-21T22:40:26+00:00Z

NASA CR-134781
Creare TN-289

(NASA-CR-134781) DESIGN, DEVELOPMENT, AND TEST OF A LASER VELOCIMETER FOR A SMALL 8:1 PRESSURE RATIO CENTRIFUGAL COMPRESSOR, Final Report (Creare, Inc.), 206 p HC A10/MF A01 CSCL 14B G3/35

N79-27478

Unclas
21510

DESIGN, DEVELOPMENT, AND TEST OF A LASER VELOCIMETER FOR A SMALL 8:1 PRESSURE RATIO CENTRIFUGAL COMPRESSOR

by Francis X. Dolan, and Peter W. Runstadler, Jr.

CREARE INCORPORATED

prepared for

NATIONAL AERONAUTICS AND SPACE ADMINISTRATION

NASA Lewis Research Center
Contract NAS 3-17860

JUL 1979
RECEIVED
NASA STI FACILITY
ACCESS DEPT.

1 Report No	2 Government Accession No	3. Recipient's Catalog No
NASA CR-134781		

4. Title and Subtitle	5 Report Date
DESIGN, DEVELOPMENT, AND TEST OF A LASER VELOCIMETER FOR A SMALL 8:1 PRESSURE RATIO CENTRIFUGAL COMPRESSOR	March 1979
	6 Performing Organization Code

7 Author(s)	8 Performing Organization Report No
Francis X. Dolan Peter W. Runstadler, Jr.	TN-289
	10 Work Unit No

9 Performing Organization Name and Address	11. Contract or Grant No
Creare Incorporated P.O. Box 71 Hanover, N. H. 03755	NAS3-17860
	13 Type of Report and Period Covered
	Contractor Report

12 Sponsoring Agency Name and Address	14 Sponsoring Agency Code
U. S. Army Research and Technology Laboratory (AVRADCOM) Moffett Field, California National Aeronautics and Space Administration Washington, D. C.	

15 Supplementary Notes
FINAL REPORT
Project Manager, Jerry R. Wood, Lewis Research Center and U. S. Army Research and Technology Laboratories (Propulsion Lab), Cleveland, Ohio

16 Abstract

This report describes the design, development, and test of a laser velocimeter (LV) instrument to map the velocity fields in a small, high speed, 8:1 pressure ratio, 0.91 kg/s centrifugal compressor. The instrument was designed as a diagnostic tool for the study of the basic fluid dynamics of the inducer, impeller, and diffuser regions of this type compressor.

The LV instrumentation has been optimized to measure instantaneous velocities up to approximately 500 m/s, measured in absolute coordinates, within the rotating compressor impeller and in the two-dimensional radial plane of the diffuser. Some measurements have been made within the diffuser and the impeller inlet flows; however, attempts to make detailed measurements of the velocity field have not been successful. Difficulties in maintaining high seed particle rates within the probe volume and the improper operation of the blade gating optics may explain the lack of success. Recommendations are made to further pursue these problems.

At 100% speed the stage attained a total-static pressure ratio of 7.5:1 at 75% total-static efficiency. Flow range from choke-to-surge was 6.8% of choking mass flow rate. Performance was lower than the design intent of 8:1 pressure ratio at 77% efficiency and 12% flow range.

Detailed measurements of the stage components are presented which show the reasons for the stage performance deficiencies. Recommendations are made for further studies to understand these deficiencies and as a means to improve basic centrifugal compressor designs and performance.

17 Key Words (Suggested by Author(s))	18 Distribution Statement
Laser Velocimeter Centrifugal Compressor High Pressure Ratio Compressor Aerodynamic Measurements	Unclassified – Unlimited

19 Security Classif. (of this report)	20 Security Classif (of this page)	21 No of Pages	22 Price*
Unclassified	Unclassified	195	$3.00

* For sale by the National Technical Information Service, Springfield Virginia 22161

NASA-C-168 (Rev 10-75)

TABLE OF CONTENTS

PRECEDING PAGE BLANK NOT FILMED

TABLE OF CONTENTS (CONTINUED)

LIST OF TABLES

LIST OF FIGURES

LIST OF FIGURES (CONTINUED)

LIST OF FIGURES (CONTINUED)

LIST OF FIGURES (CONTINUED)

LIST OF FIGURES (CONTINUED)

LIST OF FIGURES (CONTINUED)

SUMMARY

The design, development, and test of a laser velocimeter (LV) instrument and the aerodynamic measurements made in a workhorse high pressure ratio centrifugal compressor are presented in this report.

While some examples of the successful measurement of flow velocity vectors within the diffuser and impeller inlet of the workhorse centrifugal compressor are displayed, repeated attempts to measure the details of the velocity fields in the impeller inducer and diffuser were unsuccessful. Two major problems appear to be the cause for this lack of success:

1) continually decreasing concentration of proper size seed particles within the LV probe volume with time, and

2) unstable operation of the acoustic optic (A/O) modulating system between continual and gated data acquisition modes.

Of these two problems, the first, while making measurements lengthy and tedious, is not insurmountable. The second problem apparently has been a continual one in attempts to make successful measurements within the impeller and diffuser during gated operation; gated operation is essential in order to obtain the velocity information required. This difficulty with the A/O modulating system was recognized as a problem only toward the conclusion of the contract experimental work. The recommendation is made to pursue and understand this problem with the A/O modulator before abandoning the LV system as a viable research tool.

Under the continuous mode of operation, the LV system has made successful measurements. The instrument has been optimized to make instantaneous velocity measurements up to order of 500 m/s within an extremely small probe volume with minor dimension (width) of approximately 0.06 mm and a major dimension (length) of approximately 0.6 mm. Electronic strobing and timing equipment has been designed to accurately synchronize and time the acquisition of data relative to a small, high speed, rotating impeller system. This system permits the timing of the data acquisition electronics to acquire velocity data for less than 0.5% of blade pitch rotation using the 19-bladed workhorse impeller, rotating at 53,500 RPM. The time required to measure the velocity of a single particle is approximately 0.1 μs at 200 m/s and 0.08 μs at 500 m/s.

The aerodynamic measurements were made on the workhorse compressor using time-average pressure and temperature techniques and time-dependent, high response pressure transducers. This compressor was designed and mechanically checked out on a separate companion program. The stage has a backswept centrifugal impeller and a vane-island diffuser designed for air operation at 75,000 RPM and 0.907 kg/s mass flow rate with a stage pressure ratio of 8:1. Equivalent design speed with the low speed of sound test gas used in this program is 52,600 RPM. The measurements were made using two diffuser designs (Builds I and II) and two identically designed impellers (S/N 001 and S/N 002 impellers--S/N 001 having been damaged midway through the test program).

The aerodynamic performance did not meet design specifications. The following performance was obtained with the Build II diffuser design:

	Measured	Design Intent
pr_{TS}	7.5:1	8:1
η_{TS}	75%	77%
$\frac{m_{choke} - m_{surge}}{m_{choke}}$	0.068	0.12

At design speed the vaned diffuser chokes at a flow rate 1% less than design flow rate. The inducer, when tested with the vaneless diffuser, choked at design flow rate. The diffuser is responsible for stage choke at all speeds tested.

The detailed static pressure measurements along the impeller shroud and throughout the diffuser appear to demonstrate that the impeller performs about as designed but that the design point incidence and performance occur at a flow rate slightly lower than design intent of 0.907 kg/s.

The diffuser, however, falls short in pressure recovery C_{pD} by about 8 points ($C_{pD} = 0.61$ as measured compared to the design value of 0.686). Based upon the measured diffuser channel throat static and total pressures, the channel pressure recovery meets the design intent and agrees with laboratory channel diffuser recovery data. The decrement in overall diffuser pressure recovery, and hence in stage pressure ratio and efficiency, appears to be caused by a large loss in stagnation pressure between the calculated value at impeller exit and the measured value at the diffuser throat.

Unsteady pressure transducer measurements and detailed diffuser vane suction surface pressure measurements reveal interesting and important unsteady flow and high Mach number shock structure phenomena that are believed important to the surge characteristics of this and other high pressure ratio, vaned diffuser stages. It is recommended that these phenomena be further explored and understood.

A discussion and analysis of the diffuser, impeller, and stage performance and measurements is presented. Recommendations are made to follow this program with further testing of this stage using the vaneless diffuser configuration and with redesigned diffuser geometry to understand the large stagnation pressure loss and to provide improved design information for increasing diffuser recovery and flow range from choke to surge.

INTRODUCTION

This report describes the development and test of a laser velocimeter to map the velocity fields in a small, high speed, centrifugal compressor. This compressor was designed for 8:1 pressure ratio and 0.907 kg/s (2 lb_m/s) flow rate (Reference 14). Also displayed are the results of aerodynamic tests made on the centrifugal compressor at several rotational speeds.

This instrument was to be used as a diagnostic tool for the study of the basic fluid dynamics of the inducer, impeller and the diffuser region of high pressure ratio, centrifugal compressors. It was foreseen that studies using this LV equipment would assist the analysis and improve understanding of the fluid dynamics of centrifugal stages. Such understanding is believed to be essential to the development of improved design tools to enable high pressure ratio centrifugals to achieve the ultimate performance for which they are believed capable (see Figure 1).

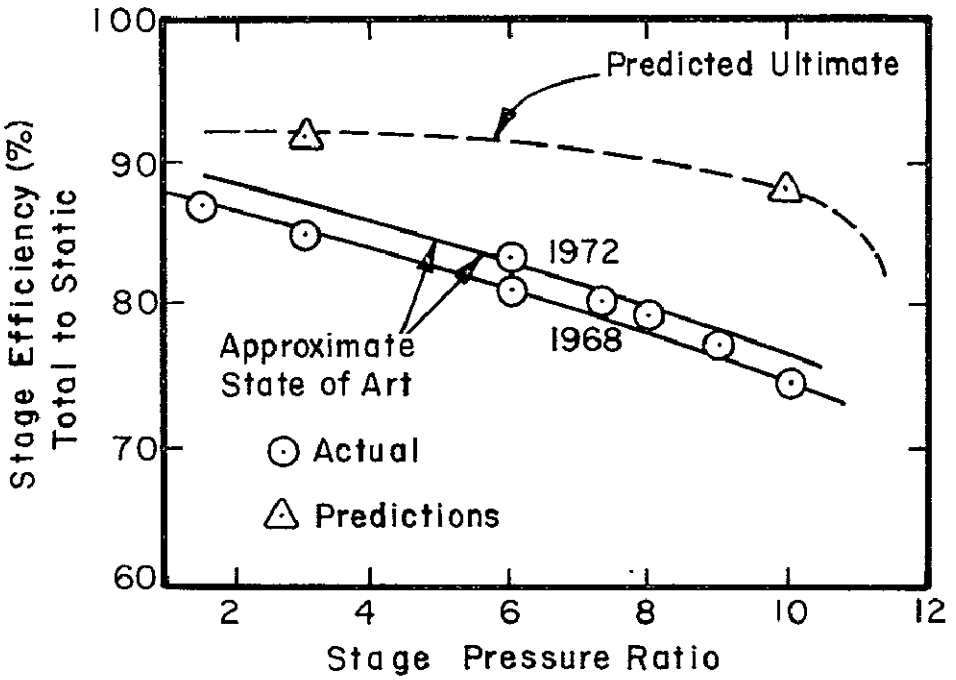

Figure 1. Performance of Small Centrifugal Compressor

Centrifugal compressor performance has continually advanced over the past forty years since centrifugals became important to supercharging high performance aircraft engines. The development of the jet engine near the end of World War II provided some impetus for improved centrifugal compressor technology. However, because of the superiority of the axial compressor for the high thrust jet engine, continued development of centrifugal compressors waned until the late 1960's, when the U. S. Army Research and Technology Laboratory (USARTL) (formerly U. S. Army AVLABS) produced a surge of centrifugal compressor development for helicopter engines. Centrifugal compressor development, sparked by these AVLABS' programs, continues to this day. Higher efficiency and greater stability to accommodate inlet distortion and engine transients without surging are being sought for the low mass flow rate, 0.9 to 2.25 kg/s (2 to 5 lb_m/s), high pressure ratio (8-12) centrifugal compressor.

Many of the gains made in centrifugal compressor performance have been brought about by a classical, "cut and try", development. The fluid dynamics of the centrifugal compressor, which involves transonic flow, compressible three-dimensional boundary layers, secondary flow and separation, centrifugal and Coriolis force fields, shock waves and important regions of unsteady flow, are, in spite of performance advances made, not well understood. Our lack of knowledge about centrifugal compressor fluid dynamics is, in part, due to the complexity of the flow, but also is due to the difficulty of making the required fluid dynamic measurements needed to correlate theory and experiment.

Most data obtained from high pressure ratio centrifugals consist of impeller and diffuser cover static pressure, mass flow rate and overall temperature and pressure rise measurements across the stage. Sometimes time-averaged total temperature and total pressure data may also be obtained at the impeller exit and in the diffuser. While useful in helping to diagnose and improve stage performance, these measurements leave much of the fluid dynamics of the centrifugal unknown.

Research has provided some additional types of information. Hot wire anemometer velocity measurements have been made, but to our knowledge only within lower speed, centrifugal stages (e.g., Reference 1). Schlieren studies of the vaned diffuser flow (e.g., Reference 2) have helped resolve what we know today about high Mach number, vaned, centrifugal diffusers. The complicated jet/wake mixing process at the impeller exit/diffuser entry region has recently been studied (References 3, 4, and 5) for the radial, vaneless diffuser only.

The laser velocimeter (LV) is a novel instrumentation technique developed over the past decade that makes possible velocity measurements within high speed turbomachinery. The field of laser anemometry has grown significantly since the first published report (Reference 6). Applications of this velocity measurement technique range from boundary layer studies in simple pipe flows to the investigation of tip vortex generation of aircraft, and many other situations where the remote sensing and non-contacting characteristics of laser anemometry make it the only practical candidate method.

Measurements of the interblade velocity fields in axial compressors for both subsonic and transonic stages have been reported (References 7, 8, and 9). LV systems have been designed for application in large axial turbines (Reference 10). Laser velocimeter methods, using the dual focus technique, have also been successfully applied to a high pressure ratio centrifugal stage by DFVLR in Germany. References 11 and 12 describe the velocimeter system and measurements made within and at the exit of a radial bladed centrifugal compressor operating with a vaneless diffuser configuration. That test compressor was approximately eight times larger than the compressor selected for test under this program.

The LV instrumentation developed on this program employs the technique commonly known as the "fringe" method. In the fringe method, two beams of coherent radiation, each having the same wave length are obtained from a single laser using a beam splitter. Where the two beams intersect, a "measuring volume" is formed. In this volume, interference fringes are created by the crossing of the two coherent beams of light. As a particle, carried by the flow, passes through these fringes, light is scattered from it only when it is in a "bright" portion of the interference pattern. The frequency at which the light is scattered from this particle is proportional to the velocity component perpendicular to the orientation of the fringes.

The optics and mechanical equipment are designed to allow the incident and reflected laser beams to pass through a window in the turbomachinery passage. The incident beams cross at a point in the flow where the fluid velocity is to be measured. The scattered light is collected by a photomultiplier tube which provides the electrical output signal whose frequency is proportional to the flow velocity.

The LV equipment was designed specifically for use in the low speed modeling (LSM) compressor test facility at Creare Incorporated. The low speed modeling compressor test facility utilizes the technology of low-speed-of-sound modeling developed under a former U. S. USARTL contract (see Reference 13). In this facility, similarity of geometry, Mach number, Reynolds

number and ratio of specific heats are retained by utilizing a gas with a lower speed of sound than air. High speed compressors can be tested at rotational speeds approximately 0.65 to 0.70 of the values that must be used in air. The basic advantage of the LSM facility for LV work is that lower absolute fluid velocities in LSM testing reduce the design contraints placed upon the LV instrumentation.

The details of the LV design were tightly constrained to optimize the system performance in this specific compressor and test facility. Some of the important variables considered in specifying the LV system were the size of the sampling volume relative to the compressor scale, available signal processing methods, data sampling in a flow field with spatial and temporal fluctuations and positioning of the probe volume within the compressor hardware. Thus the design and development program had to consider the following technical areas:

1) the LV optics design to match the compressor hardware and test facilities,

2) the LV mechanical sub-systems design to permit proper positioning of the probe measuring volume and remote operation of the equipment during compressor test,

3) the electronic equipment design to provide for data sampling, validation, and storage, and

4) the design of equipment adequate to meet specifications for the aerodynamic research needs.

In the following sections of this report dealing with the LV system design, each of these areas will be developed in greater detail and trade-offs among various of them made during the design stage will be displayed.

The remaining sections of the report describe the specifications and design parameters of the LV system, the LV system hardware development, assembly, checkout and testing and data reduction procedures. A discussion is presented of the problems encountered in applying the LV technique to this compressor facility. The limited results and conclusions from this LV work, and the aerodynamic measurements made on the 8:1 pr compressor are displayed. Recommendations for the future application of this LV equipment are displayed.

HARDWARE DEVELOPMENT

CENTRIFUGAL COMPRESSOR DESIGN

Under a companion contract (NASA USARTL Contract, NAS3-17848), a low mass flow (0.91 kg/s), high pressure ratio (8:1), centrifugal compressor was designed as a test vehicle for demonstrating the LV concept in small, high speed turbomachinery. The details of the design methods used for this centrifugal compressor configuration have been summarized in detail in Reference 14.

After tests of the compressor stage at speeds up to 100% N_D (design speed), alterations were made to the primary diffuser design (presented in Reference 14) in order to better match the diffuser throat choking conditions to the impeller choked flow. The modifications were also made in an attempt to increase the range to surge at 100% N_D. The diffuser geometry was designated Build II. The modifications that were made are summarized as follows:

1) The diffuser vanes were cut back from the lead edge by 8.66 mm.
2) The pressure surface was surface ground to uniformly remove 0.43 mm of material.
3) A technician then hand-honed the lead edge shape to an approximately semi-circular configuration with the final lead edge vane thickness being on the order of 0.30 to 0.36 mm with an included wedge angle of approximately 5°.
4) Each vane was rotated toward tangential 2 degrees about the center of the first clamping bolt (the clamping bolt circle was located at a radius of 101.6 mm).

These alterations provided the following:

1) an 8% increase in diffuser throat area,
2) an increase in vane lead edge radius from $r_3 = 85.85$ mm ($R_3 = 1.076$) to $r_3 = 90.09$ mm ($R_3 = 1.129$),
3) a reduction in estimated Mach number at the vane lead edge from $M_3 = 1.02$ to $M_3 = 0.964$, and
4) an increase in vane suction surface angle (measured to radial) from approximately $\beta_3 = 70.4°$ to $\beta_3 = 72.3°$.

A tabulation of the final diffuser vane geometric parameters is given in Table I.

The compressor hardware was designed to fit within the LSM compressor test facility. Figure 2 shows a schematic meridional

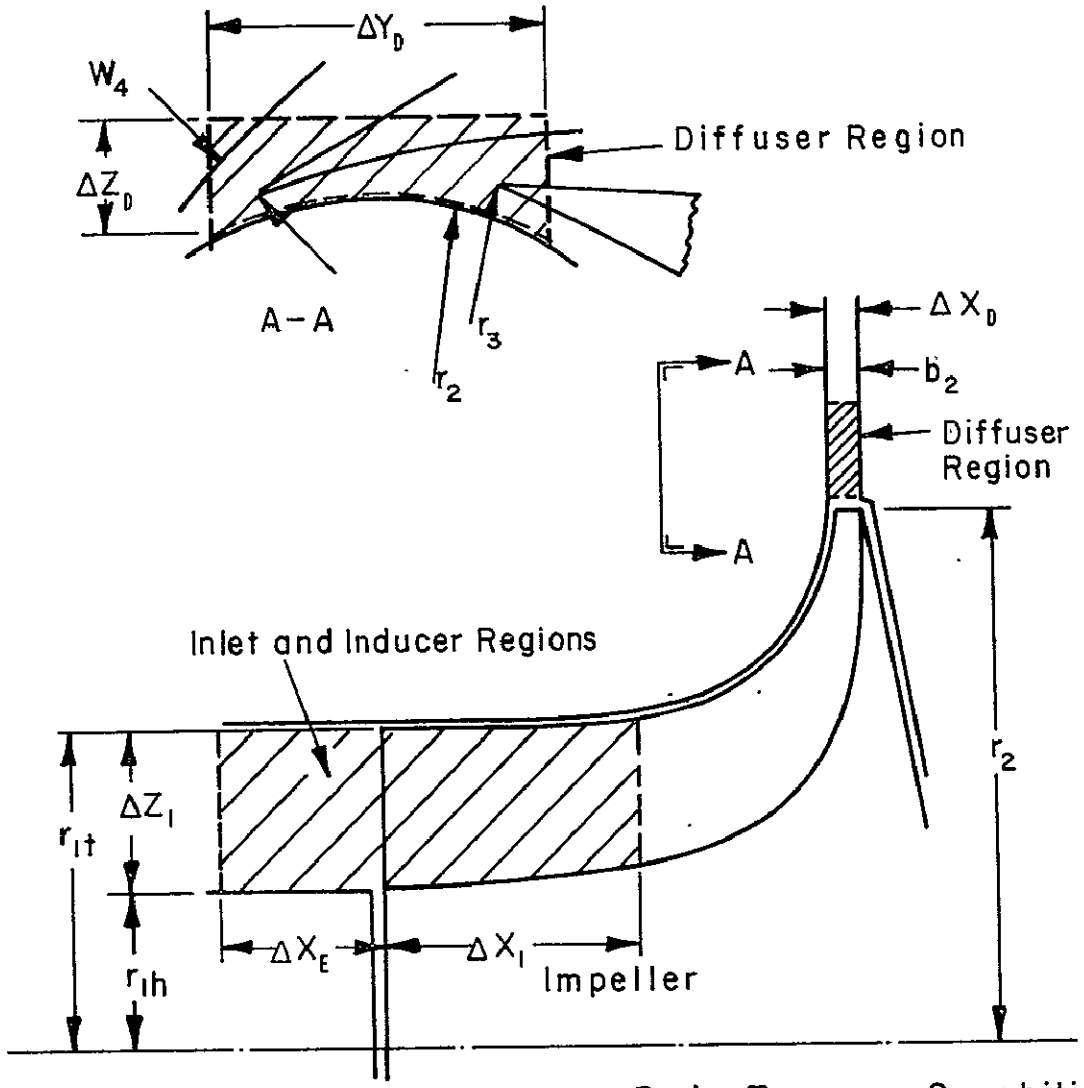

Compressor Geometry

r_{1h} = 21.8 mm
r_{1t} = 43.7 mm
r_2 = 79.8 mm
r_3 = 85.85 mm
b_2 = 3.22 mm
W_4 = 10.5 mm

Probe Traverse Capability

ΔX_E = 6.35 mm
ΔX_I = 15.3 mm
ΔZ_I = 21.9 mm
ΔX_D = 3.22 mm
ΔY_D = 50 mm
ΔZ_D = 20 mm

Figure 2. Compressor Regions of Interest in LDV Measurements. (Dimensions are for Build I Diffuser Geometry)

view of the impeller and diffuser regions of interest in the LV design. Table II displays the principal design and operating characteristics for the compressor in air and LSM gas.

The LV measures fluid velocity in a fixed reference frame and thus measures those absolute velocities designated in Table II as C_{x1}, C_{2J}, C_{2W}, C_{2*} and C_4. Figures 3a, 3b, and 3c show typical absolute velocity vectors in the centrifugal compressor which are of interest in the present program.

TABLE I. - PRINCIPAL DIFFUSER VANE CHANNEL GEOMETRIC PARAMETERS — BUILD II DIFFUSER GEOMETRY

β_p = 66.46°	2θ = 10°
β_s = 72.26°	L = 185.7 mm
r_2 = 79.76 mm	t = 0.356 mm
r_3 = 90.09 mm	L/W_4 = 14.9
W_4 = 12.45 mm	

As will be discussed in the next section, the compressor hardware constraints permit only that measurement of the flow velocity vector in a plane normal to the LV optical axis. The optical axis is oriented in a radial direction in the inducer and in the axial direction in the impeller exit/diffuser entry region. Therefore the velocity vector is only measured tangent to circumferential planes in the impeller inlet region and only in radial planes in the impeller exit/diffuser entry region; however, because the actual mean flow velocity vectors are expected to lie primarily in these planes, this is not considered a major problem in understanding the flow fields in these two regions. In addition, flow velocities normal to these planes could be deduced by steamtube mass balances and, in the inducer region, may actually be measured by orienting the optical axis at slightly off the radial direction.

The remainder of this section describes the laser velocimeter design required to meet the system specifications and constraints imposed by this compressor test vehicle and the low speed modeling facility in which it is used.

BASIC LV SYSTEM CONSTRAINTS

The principal objective of the LV system is to make mean velocity measurements in the centrifugal compressor in the regions of interest shown in Figure 2. This objective requires that:

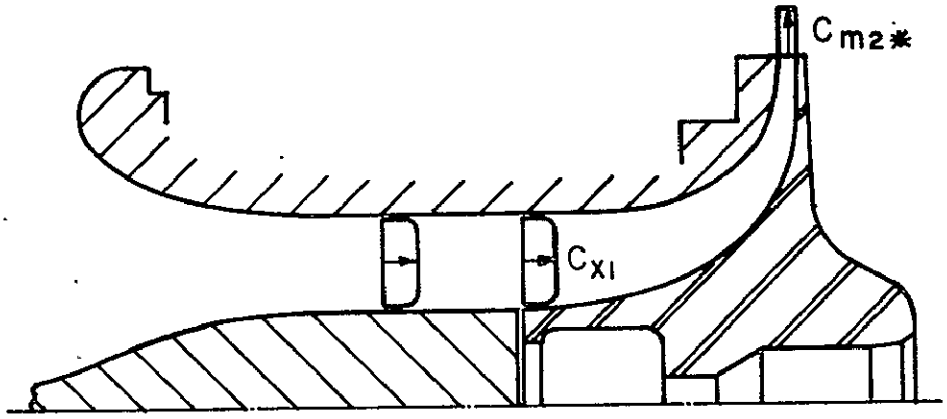

(a.) Impeller Inlet and Discharge (Meridional View)

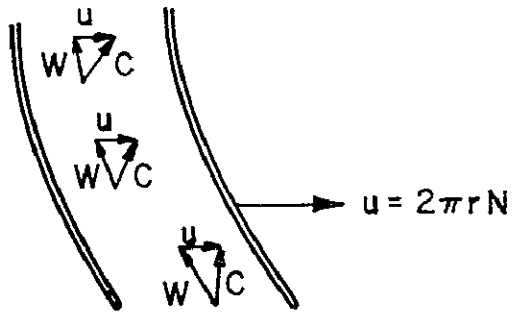

(b.) Impeller Inlet (Circumferential View)

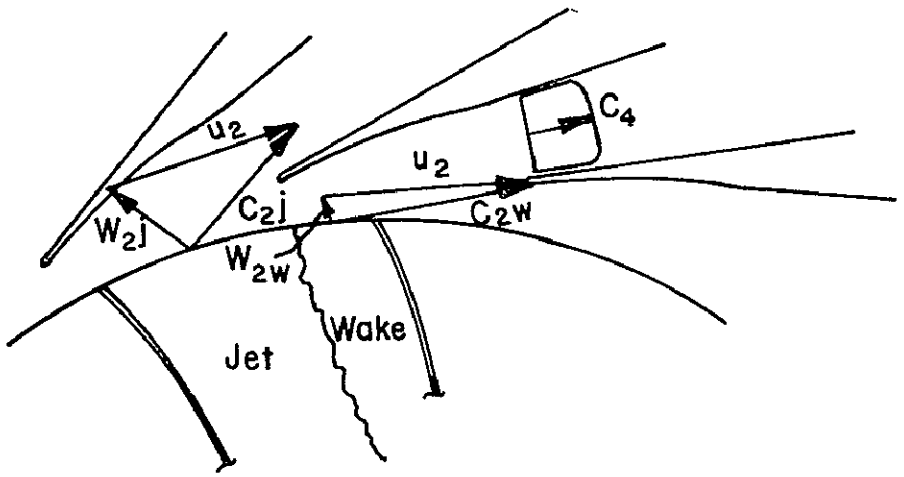

(c.) Impeller Exit / Diffuser Entry (Axial View).

Figure 3. Velocity Vectors of Interest in LV Measurements.

TABLE II. - AIR AND LSM OPERATING CONDITIONS FOR CENTRIFUGAL COMPRESSOR AT DESIGN POINT

Parameter	Air Design Value	LSM Actual Value	Ratio LSM/ Air
Design Speed, N_D, (RPM)	75,000	52,600	0.70
Flow Rate, $\dot{m}$, (kg/s)	0.91	1.17	-
Stage Pressure Ratio, pr	8.0	8.0	1.0
Stage Efficiency, η_{T-S} (%)	77	77	1.0
Actual Power, W_{xT}, (kW)	276	174	0.63
Plenum Pressure, p_{oo}, (kN/m^2)	101.13	78.5	-
Collector Pressure, p_{col}, (kN/m^2)	810	627	-
Plenum Temperature, T_{oo}, (°K)	288	286	-
Collector Temperature, T_{coll}, (°K)	585	558	-
Inlet Speed of Sound, a_o, (m/s)	341	239	0.70
Inlet Specific Heat Ratio, k_o	1.4	1.4	1.0
Discharge Specific Heat Ratio, k_{coll}	1.37	1.33	-
Inlet Relative Mach Number at Tip	1.2	1.2	1.0
Inlet Reynolds Number	-	-	1.0
Stage Geometry	-	-	1.0
Inlet Axial Velocity, C_{x1}, (m/s)	193	135	0.70
Impeller Exit Velocity (mixed), C_{2*}, (m/s)	485	340	0.70
Impeller Exit Jet Velocity, C_{2J} (m/s)	498	348	0.70
Impeller Exit Wake Velocity, C_{2w}, (m/s)	585	409	0.70
Diffuser Throat Velocity, C_4, (m/s)	423	296	0.70

1) the laser probe volume be moved to any position within the measurement space and done so remotely while the compressor is under test on the test stand,

2) the probe volume dimensions be small (compared to the compressor dimensions and expected velocity gradients) to obtain good spatial resolution,

3) the highest anticipated velocities occurring within the compressor can be measured, and

4) the velocity data can be obtained when the impeller is at a known rotational position.

These fundamental specifications will be explored in this section and used to define the preliminary LV design. The details of the LV design and system trade-offs are then presented in the following section.

The first step will be to show how these specifications define the basic system for the centrifugal compressor application.

The laser velocimeter measures the frequency of radiation scattered from a particle passing through a beam of incident light. If the particle is moving with the fluid, the frequency measured is directly proportional to the fluid velocity. One embodiment of this concept involves heterodyning (mixing) of the shifted frequency from two beams incident at different angles to the moving particle and is commonly called the dual-beam differential method. For the present study, we are concerned only with this dual-beam method.

If the two beams of light are incident on the particle simultaneously, the resultant shift is seen as the difference in frequencies of scattered radiation from the two beams. A generalized dual-beam arrangement is shown in Figure 4a. It is assumed that the velocity vector v_o and the detector lie in the plane containing the two beams. v_o is at an angle α to the bisector of the crossing beams 1a and 1b and the detector is placed at an arbitrary angle ψ to the bisector. ϕ is the included angle between the two incident beams. The projections of v_o are drawn, as shown, onto the directions 1a, 1b, and D2. At the detector, the resultant shift is:

$$\Delta f_D = |f_b - f_a| \qquad (1)$$

where f_a and f_b are the frequencies of the scattered light from each beam resulting from the passage of a particle through the intersection region with a velocity v_o. If f_L is the frequency of the incident laser beam,

$$f_a = f_L\left(1 - \frac{v_{o2}}{c} - \frac{v_{o1a}}{c}\right) \qquad (2)$$

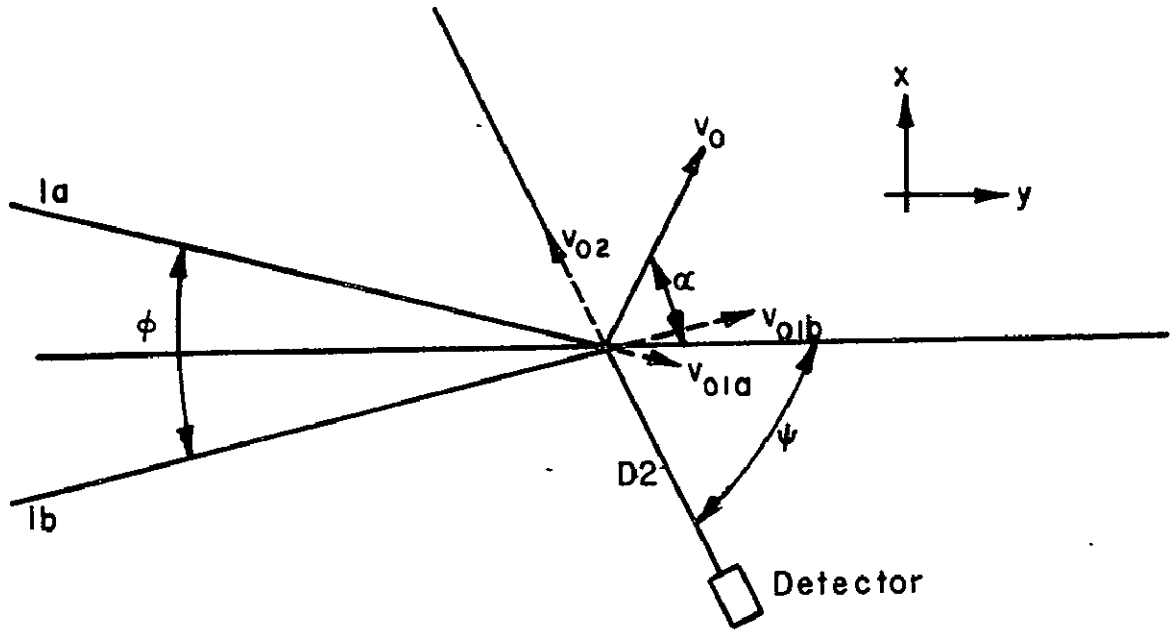

Figure 4a. Generalized Two-Beam Model.

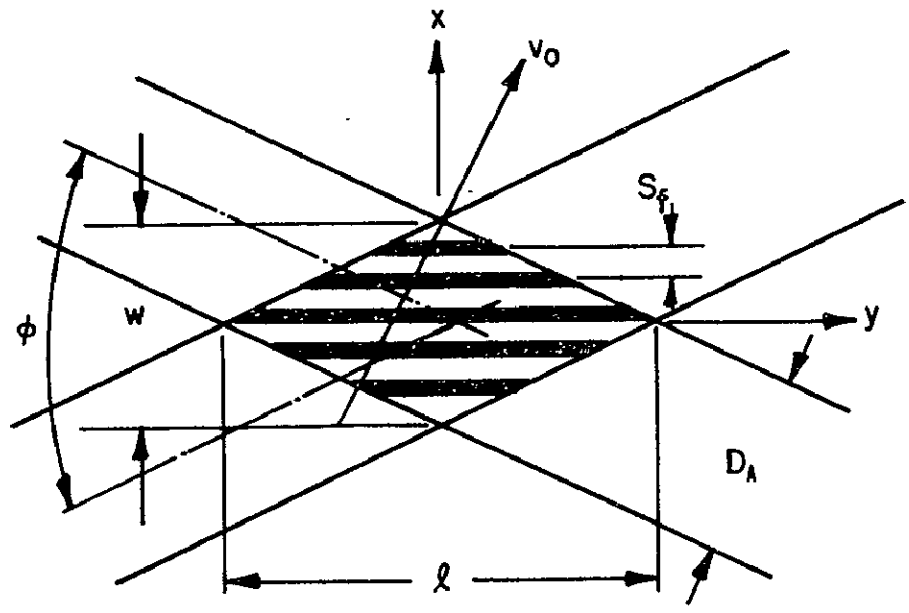

Figure 4b. Fringe Model Geometry.

$$f_b = f_L\left(1 - \frac{v_{o2}}{c} - \frac{v_{o2b}}{c}\right) \tag{3}$$

where c is the velocity of light. From simple trigonometric considerations,

$$v_{ola} = v_o \cos\left(\alpha+\frac{\phi}{2}\right) \tag{4}$$

$$v_{olb} = v_o \cos\left(\alpha-\frac{\phi}{2}\right) \tag{5}$$

$$v_{o2} = v_o \cos(\pi-\alpha-\psi) = -v_o \cos(\alpha+\psi) \tag{6}$$

Then,

$$f_a = f_L\left[1 + \frac{v_o}{c}\cos(\alpha+\psi) - \frac{v_o}{c}\cos\left(\alpha+\frac{\phi}{2}\right)\right] \tag{7}$$

$$f_b = f_L\left[1 + \frac{v_o}{c}\cos(\alpha+\psi) - \frac{v_o}{c}\cos\left(\alpha-\frac{\phi}{2}\right)\right] \tag{8}$$

$$\Delta f_D = \left| f_L \frac{v_o}{c}\left[\cos\left(\alpha+\frac{\phi}{2}\right) - \cos\left(\alpha-\frac{\phi}{2}\right)\right]\right| \tag{9a}$$

$$= 2f_L \frac{v_o}{c}\sin\alpha \sin\frac{\phi}{2} \tag{9b}$$

The component of velocity perpendicular to the bisector is:

$$v_x = v_o \cos\left(\frac{\pi}{2}-\alpha\right) = v_o \sin\alpha \tag{10}$$

Since $c = f_L\lambda$, where λ is the wave length of the scattered radiation, the detected frequency becomes:

$$\Delta f_D = 2\frac{v_x}{\lambda}\sin\frac{\phi}{2} \tag{11}$$

Another way to view the two beam laser velocimeter concept is to consider the fringe pattern established within the crossing region of the two beams as shown in Figure 4b. These fringes are formed as alternating bands of light and dark by the interference of plane wave fronts in the volume formed by the crossing beams. The spacing between fringes is:

$$S_f = \frac{\lambda}{2\sin\frac{\phi}{2}} \tag{12}$$

Then the frequency of light scattered from the particle as it traverses the fringe pattern is:

$$f_{sc} = \frac{v_x}{S_f} = 2\frac{v_x}{\lambda}\sin\frac{\phi}{2} \tag{13}$$

It is seen that the scattering frequency (Equation 13) is identical to the differential Doppler frequency (Equation 11).

A typical dual-beam LV optical system is shown below.

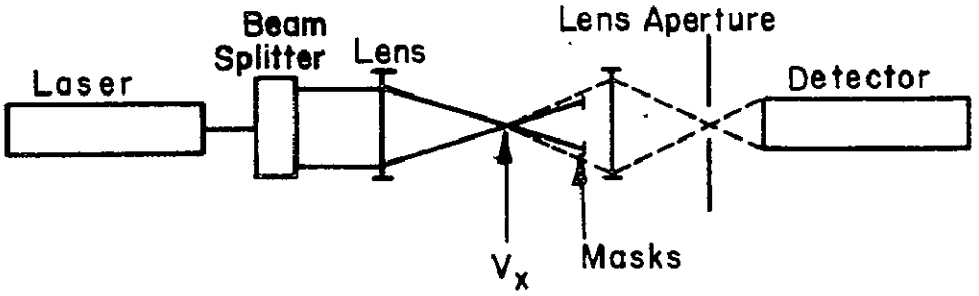

The output from a laser is split into two parallel, equal intensity beams. These beams cross at the focal point of the input lens and there form the probe volume. Light scattered from particles passing through this volume is collected by the second lens, using a mask to eliminate the incident beams if necessary, focused through an aperture to eliminate stray light, and is converted to an electrical signal by the photodetector.

This optical arrangement thus provides a method of measuring a single component of the total velocity vector. The component measured is that perpendicular to the beam bisector and lying in the plane of the beams. A second component may be obtained by rotating the plane of the beams around the axis described by the bisector of the two beams, thereby describing the total velocity in a plane normal to the axis.

For a laser beam with a Gaussian energy distribution passing through a lens, the diffraction limit (diameter of the beams at the lens focal point) to the first order is given by Reference 15:

$$D_A = \frac{4}{\pi} \lambda \frac{f}{D_L} \tag{14}$$

where D_L is the distance of the laser beams at the $\frac{1}{e^2}$ intensity point. If we assume that the probe volume is formed by the intersection of two cylinders of diameter D_A, at an angle ϕ, the size of the volume may be estimated.

$$w = \frac{D_A}{\cos\phi/2} = \frac{4}{\pi} \lambda \frac{f}{D_L} \frac{1}{\cos\phi/2} \tag{15}$$

$$\ell = \frac{D_A}{\sin\phi/2} = \frac{4}{\pi} \lambda \frac{f}{D_L} \frac{1}{\sin\phi/2} \tag{16}$$

where ℓ and w are the major and minor dimensions, respectively, of the probe volume. The number of fringes N_f across the width (minor diameter) of the probe volume is simply,

$$N_f = \frac{w}{S_f} = \frac{8}{\pi} \frac{f}{D_L} \tan \frac{\phi}{2} \qquad (17)$$

Figures 5a, 5b, and 5c display these basic relationships for a wide range of optical parameters. λ is the wave length of the argon ion laser, 514.5 nm.

Two additional important contraints which have not yet been discussed are:

1) optimum particle size, and

2) frequency measurement techniques.

Particle size selection is a somewhat complicated process. Large particles scatter more radiation than do smaller ones, but they may not faithfully reproduce the velocity field of interest. References 16 and 17 review particle fluid dynamics with particular reference to LV measurements. Reference 17 also reviews Mie scattering from aerosols and discusses experience with several types of "seed" materials. In this design, the choice is clearly one of sizing the particles so that they will follow expected velocity fluctuations to a reasonable accuracy and to design the optical system to accept radiation scattered from these particles and produce a good signal to noise ratio at the photodetector. Particles in the 0.5 to 1.0 μm diameter range should give good replication of the velocity fields through most of the regions of interest in the compressor.

The selection of the most desirable particle size range "set the stage" for trade-off studies in selecting appropriate data acquisition and processing equipment and in designing the optics package to achieve desired probe volume dimensions.

At the outset of this work the predominant frequency measurement systems developed and used by others consisted of automatic frequency trackers or automatic frequency counters. For a number of reasons, particularly signal dropout in highly fluctuating flow fields*, the frequency tracking method was eliminated as a possible signal processor.

*For these compressor studies, the wake and jet absolute velocities at the impeller exit, C_{2W} and C_{2J} show a difference of about 20% in velocity with fluctuations occurring at a frequency of around 20 kHz.

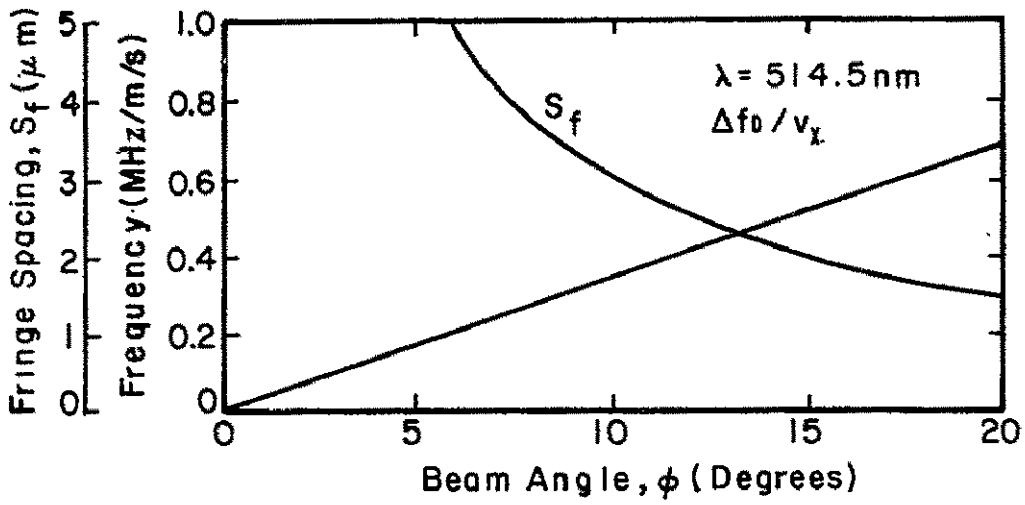

Figure 5 a. Fringe Spacing and Normalized Frequency as Function of Beam Crossing Angle.

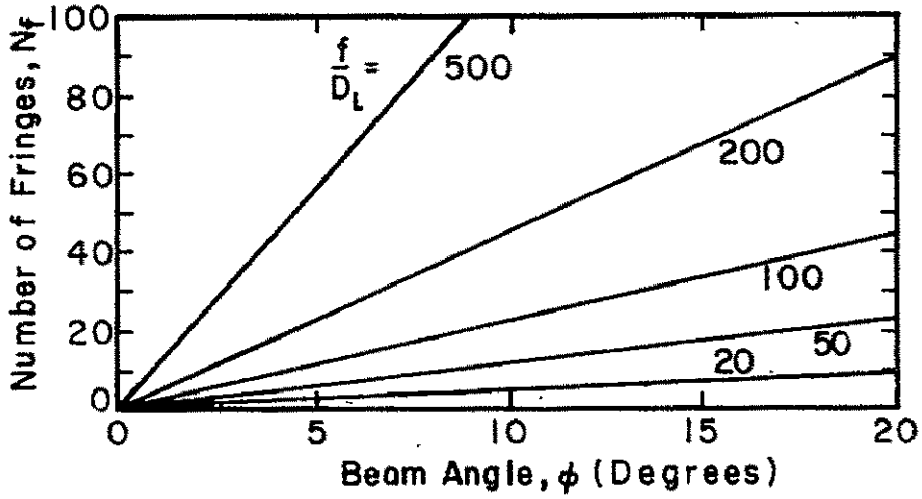

Figure 5b. Number of Fringes in Probe Volume as Function of Beam Crossing Angle.

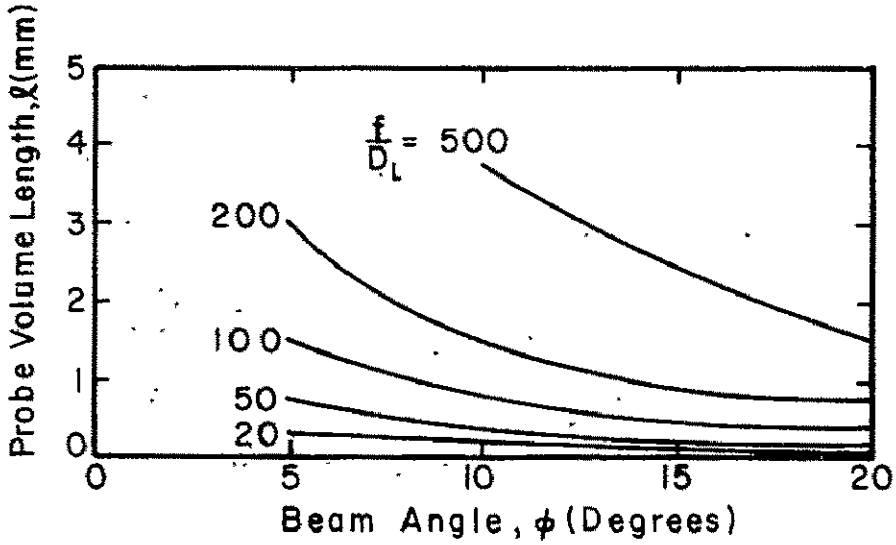

Figure 5c. Probe Volume Length as Function of Beam Crossing Angle.

The frequency processing equipment could be obtained either by constructing a "home-built" frequency counter or selecting a commercially available instrument. The latter was the more practical choice in terms of program time and cost constraints. The commercial system most readily available at the beginning of this program utilizes a time base frequency of 100 MHz, and requires 8 cycles of Doppler signal for period measurement. This unit also has a limit on the input frequency of about 100 MHz.

An analysis of the visibility* of particles in the probe volume (Reference 18) leads to the conclusion that the optimum ratio of particle diameter to fringe spacing is about 1/3. Then, for an average particle size of 0.75 μm, the minimum fringe spacing is about 2 μm.

From Figure 2, it is seen that the minimum passage size of interest is the depth of the impeller tip/diffuser entry region b_2. The flow in this region is essentially two-dimensional and in a plane perpendicular to the compressor axis. Thus, the passage must be probed with the axis of the input optics parallel to the compressor axis in order to map this two-dimensional velocity field. In order to measure the velocity profile across the depth b_2 of the diffuser channel, the probe volume length ℓ should be kept considerably smaller than b_2, say $\ell \sim b_2/4$.

*Visibility is a measure of the ratio of light scattered from a particle when it is in a light fringe compared to when it is centered in a dark fringe.

Finally, the limitations of the data acquisition electronics need to be considered in specifying the optics design.

A review of frequency counting methods shows a decrease in the accuracy of the measurement as the signal frequency approaches the time base frequency of the processor. The error derives from the need to count time base periods against an integral number of signal periods (or vice versa). This results in a digitizing error because a fraction of a period must always be missed. This basic frequency measurement uncertainty and the limitation on bandwidth of the available frequency processor dictates a limit to the maximum frequency, produced by a particle traversing the probe volume, of 80 MHz. However, this maximum frequency, at the highest expected flow velocity (400 m/s), implies a minimum fringe spacing of 5 μm. This is larger than the desired optimum fringe spacing of 2 μm discussed above. Also, from Figure 5a, it is seen that a crossing angle of about 6 degrees is needed, but that means a probe volume longer than desired if about 10 fringes are to be available for data processing by the processor unit ($f/D_L \simeq 100$ in Figures 5b and 5c).

Since the probe volume length was considered to be a major design constraint, it was decided to allow an upper frequency of 160 MHz, resulting in a shorter probe volume. But, this high frequency is well above the bandwidth of the processing electronics (100 MHz), and also results in count digitizing errors as high as 20% on individual velocity measurements. This problem was solved by incorporating a frequency divide-by-two circuit ahead of the processor, thereby shifting down to 80 MHz, the maximum frequency which must be counted. Of course in utilizing this divide-by-two, it must be recognized that a particle must traverse two fringes for each one that is counted by the frequency processor.

After considering all of these design trade-offs, the optical arrangement selected has:

$$\lambda = 514.5 \text{ nm}$$
$$\phi = 11 \text{ degrees}$$
$$f/D_L = 100$$

resulting in a probe volume having

$$D_A = 0.0655 \text{ mm}$$
$$\ell = 0.683 \text{ mm}$$
$$w = 0.0658$$

$$S_F = 2.68\ \mu m$$
$$N_F = 24$$
$$\Delta f_D/v_x = 0.373\ MHz/(m/s)$$

This design meets the major specifications and design constraints of probe volume size minimization, yet is compatible with available electronic processing instrumentation.

A remaining major specification is that the LV system be capable of acquiring velocity data for known and fixed positions of the impeller. This is accomplished by sampling the data acquisition system with a pulse synchronized from an impeller position indicator. By acquiring and storing data only for that impeller position, a velocity probability distribution (histogram) is built up which measures the velocity for repeated rotations of the impeller only when the impeller is at a known and fixed position.

There is a finite time associated with a particle traversing the probe volume and during this time the impeller is obviously still rotating. Figure 6 shows that this rotation is quite small (< 1% blade pitch) except at the very lowest particle velocities. In Figure 6, it is assumed that particles faster than 220 m/s must traverse 20 fringes, while those slower than 220 m/s need traverse only 10 fringes to obtain a valid period measurement from the frequency processor. Velocities greater than 220 m/s imply Doppler frequencies which must be divided to be processible, hence more total fringe crossings are needed, as discussed above.

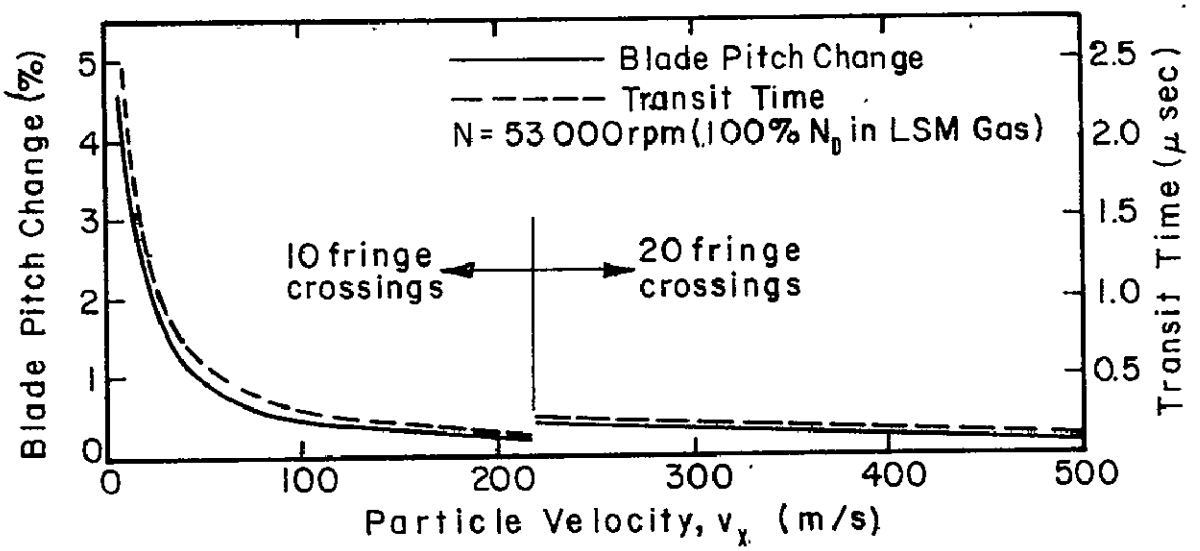

Figure 6. Impeller Rotation and Particle Transit Time as Function of Particle Velocity.

It may also be seen that the data sampling system should ideally have a variable "window" width so that for the very highest velocities better spatial resolution can be obtained.

From this review of the system specifications and design constraints, it is obvious that many trade-offs are needed in arriving at a laser velocimeter design system. The next section displays how these considerations have led to the final design.

DETAILED LV SYSTEM DESIGN

From the preliminary design considerations discussed in the previous section, a set of specifications evolved which were used to generate the detailed system design and to select optical, mechanical, and electronic equipment.

Optical System. A compact optical system was developed to fit within the existing compressor test facility. The back-scattering mode of signal reception is used for the inlet/inducer region and a back-reflected, forward-scattered mode for the diffuser region. Figure 7 shows an unfolded, two-dimensional view of the optical train. In order to position the probe volume anywhere within the compressor passages, part of the optical system was made traversable in three mutually perpendicular directions:

X - nominally parallel to compressor axis,

Y - perpendicular to the compressor axis in a horizontal plane,

Z - perpendicular to the compressor axis in a vertical plane.

The selected laser is of the argon ion type with a maximum output of about 1400 mW at 514.5 nm. The output beam diameter, D_i, is 1.5 mm at the $1/e^2$ relative intensity points, and has a divergence of 0.5 mrad.

The laser output passes through an acoustic-optic (AO) modulator. This device uses an acoustic wave propagating through a glass crystal to diffract the incoming laser beam, causing it to be diverted into and out of the optical beam path. By gating the acoustic wave on and off, data acquisition can be synchronized to the impeller position. Detailed specifications and the theory of operation of the modulator are contained in Appendix A. Because the angular separation between the diffracted and undiffracted beams is only of the order of 6×10^{-3} radian, it is necessary to provide an extension to the beam path to permit masking off of the unwanted, undiffracted beam.

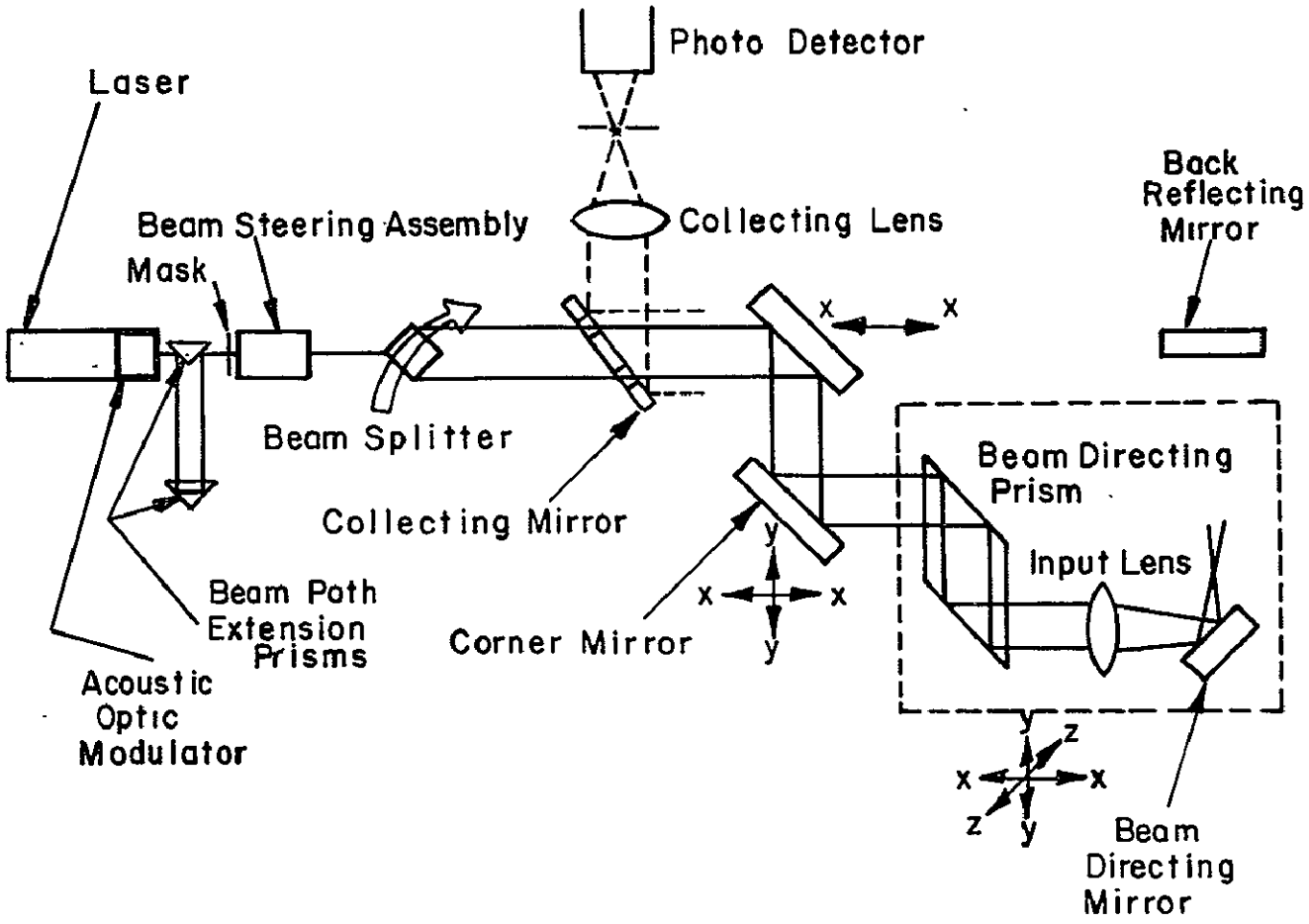

Figure 7. L.V Optical System – Unfolded View

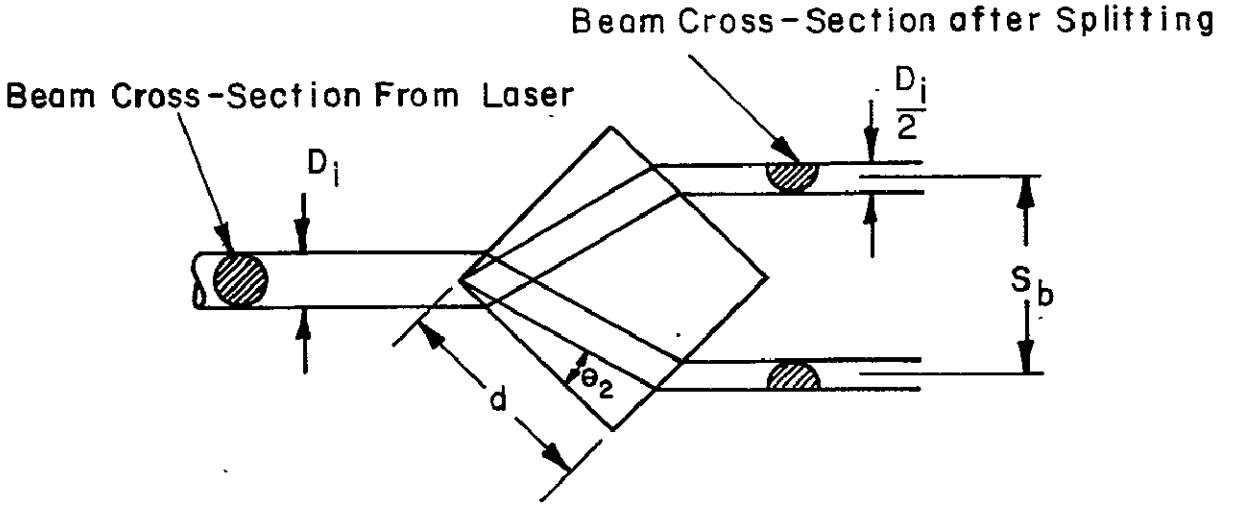

Figure 8. Beam Splitter Prism Configuration.

Immediately following the aperture or mask that is used to screen off the undiffracted beam is a beam steering assembly consisting of two mirrors. This steerer has adjustments to give horizontal and vertical displacement of the beam centerline as well as skewing of the beam relative to the laser axis.

The output from the beam steerer is directed to the edge of a beam splitter prism, Figure 8. Refraction of the beam at this edge results in two beams of semicircular cross section. This type of beam splitter was selected because it ensures that the outgoing beams will always be parallel, even in the event of severe mechanical vibrations at the splitter supports. If the prism is square with sides d and the input beam axis lies along a diagonal, as shown, the output beams are parallel to and centered about the input beam axis. The separation S_b of the output beams is:

$$S_b = \frac{2d}{\cos\theta_2} \sin\left(\frac{\pi}{4} - \theta_2\right) - D_i/2 \qquad (18)$$

where θ_2 is determined from,

$$\theta_2 = \sin^{-1}\left(\frac{N_1}{N_2} \sin\frac{\pi}{4}\right) \qquad (19)$$

N_1 and N_2 are the indexes of refraction for air and the prism glass at the appropriate wave length and d is the length of the side of the prism. In the present design, $S_b = 15.4$ mm, and $D_i/2 \sim 0.75$ mm. When the beam splitter is aligned with the input axis, a simple rotation of the splitter around the laser axis rotates the plane of the beams to any desired angle.

From the beam splitter, the input beams are projected to a plane, first surface reflector. Up to this point, the beams are parallel to the X-axis and all of the components are fixed relative to the compressor hardware. This first "corner" mirror redirects the beams parallel to the Y-axis and to a second mirror. This first mirror is mounted so that it traverses with motion in the X-axis, only. The second, first surface, "corner" mirror likewise is traversable, but it can be moved along both the X and Y-axes. Beams reflected from it are directed vertically upward and parallel to the Z-axis. At this point, the optical path enters a "periscope" assembly which protrudes into close proximity to the compressor hardware. This periscope assembly is traversable in all three coordinate planes.

In the head of the periscope, the beams enter a beam directing prism, which uses two internal reflections to direct the beams from the Z to the Y-axis. The parallel beams are next focused by the main input lens of 78.5 mm focal length. Following the lens is a small mirror which is used to direct the converging and focusing beams to either the inlet and inducer region or the impeller tip/diffuser entry region of the compressor (see Figure 2).

The radiation scattered from particles in the probe volume is focused by the input lens and directed back along the optical path to the collecting mirror which reflects the scattered light out of the main optical path toward the collecting telescope. This telescope contains a collecting lens which focuses the scattered light onto an adjustable aperture; the light which passes through the aperture falls onto the cathode of a photomultiplier tube.

For diffuser region measurements, a mirror is positioned on the diffuser backwall to reflect the forward scattered radiation back to the input lens. Also a mask is installed ahead of the collecting telescope to prevent the back reflected input beams from entering the photodetector.

Utilization of the forward scattered signal from the seed particles requires that the light collecting optics focus on the image of the probe volume "inside" the back reflecting diffuser wall, as shown in the sketch below. As the probe volume is traversed closer to the wall, the object-to-lens distance decreases. The opposite happens as the probe volume is moved away from the backwall; i.e., the distance from the input lens to the probe volume image increases.

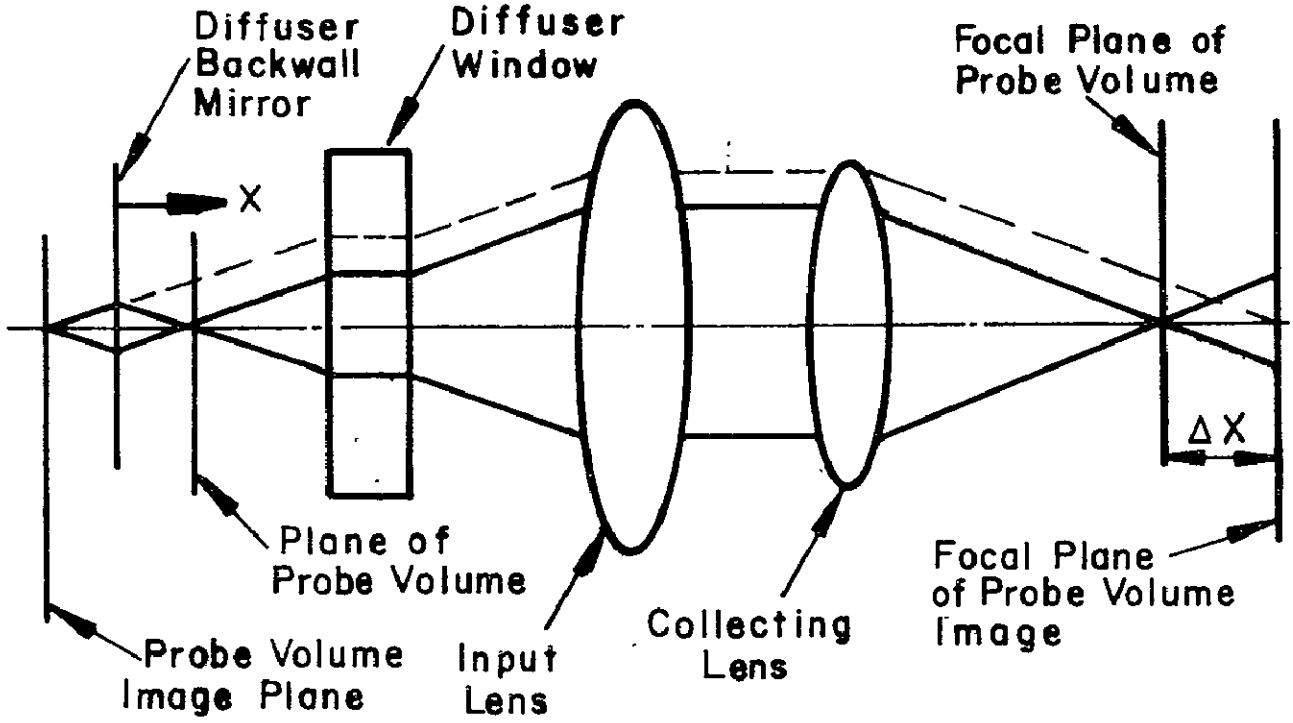

This change in object (i.e., probe volume image) to lens distance is equal to twice the change in the distance from the probe volume to the mirror backwall. When the probe volume is located at the backwall, the lens-to-object difference is equal to the lens focal length (≈ 80 mm). When the probe volume is traversed to the front diffuser wall, the lens-to-object distance is equal to the focal length plus twice the diffuser channel depth or about 86 mm. Because of these large changes in object location, the lens in the collecting telescope is made adjustable to focus the image of the probe volume onto the aperture. Figure 9 shows the relationship between the collecting lens position change and the probe volume position relative to the diffuser backwall. A collecting lens position change of zero should be interpreted to mean that the collecting optics are focused for the backscattered mode of operation.

Mechanical System. All of the optical components from the laser through the photomultiplier tube are mounted in a robust manner and are isolated from the mechanical vibrations which could be excited by the compressor or its drive system. A 25 mm thick steel base plate is used to tie all of the major elements to a seismic bed set in the laboratory floor. This bed consists of a 2 meter long by 1 meter wide by 1/2 meter deep slab of concrete resting on cork pads. The natural frequency of this system has been calculated to be ≈ 12 Hz. This is far below any driving frequencies from either the compressor or drive motor (> 50 Hz).

All of the traversable or rotatable components are rigidly tied to this bed plate, along with their actuators. The beam splitter is contained in a housing which is overhung from a shaft. Rotation of the splitter, to provide fringe patterns in two orthogonal planes, is done via a double-acting air cylinder. End stops are provided on the splitter housing to ensure that the measurement planes are truly orthogonal. The air cylinder is controlled from the main instrumentation console.

Traversing of the various optical elements is accomplished with a system of stacked sliding beds. These beds use a lead screw/captured nut system to provide relative motion of the slide to the bed. The sliding surfaces are machine ground with dovetail mating sections. Adjustable gibs are provided to ensure alignment of the slide to bed and to reduce play. In the present system, the X-axis bed is fixed to the ground plate, and the Y-axis bed is fixed to the X-axis slide. Then, using a right angle bracket, the Z-axis bed is attached to the Y-axis slide. Finally, the periscope assembly is attached to the Z-axis slide. Motion of the slides relative to their beds is provided by stepping motors coupled to the lead screws. These motors are controlled from the main console and may be operated in a variable speed "slewing" mode (0 to 10 mm/s) or in a "stepped" mode with each step being equivalent to approximately 0.0127 mm.

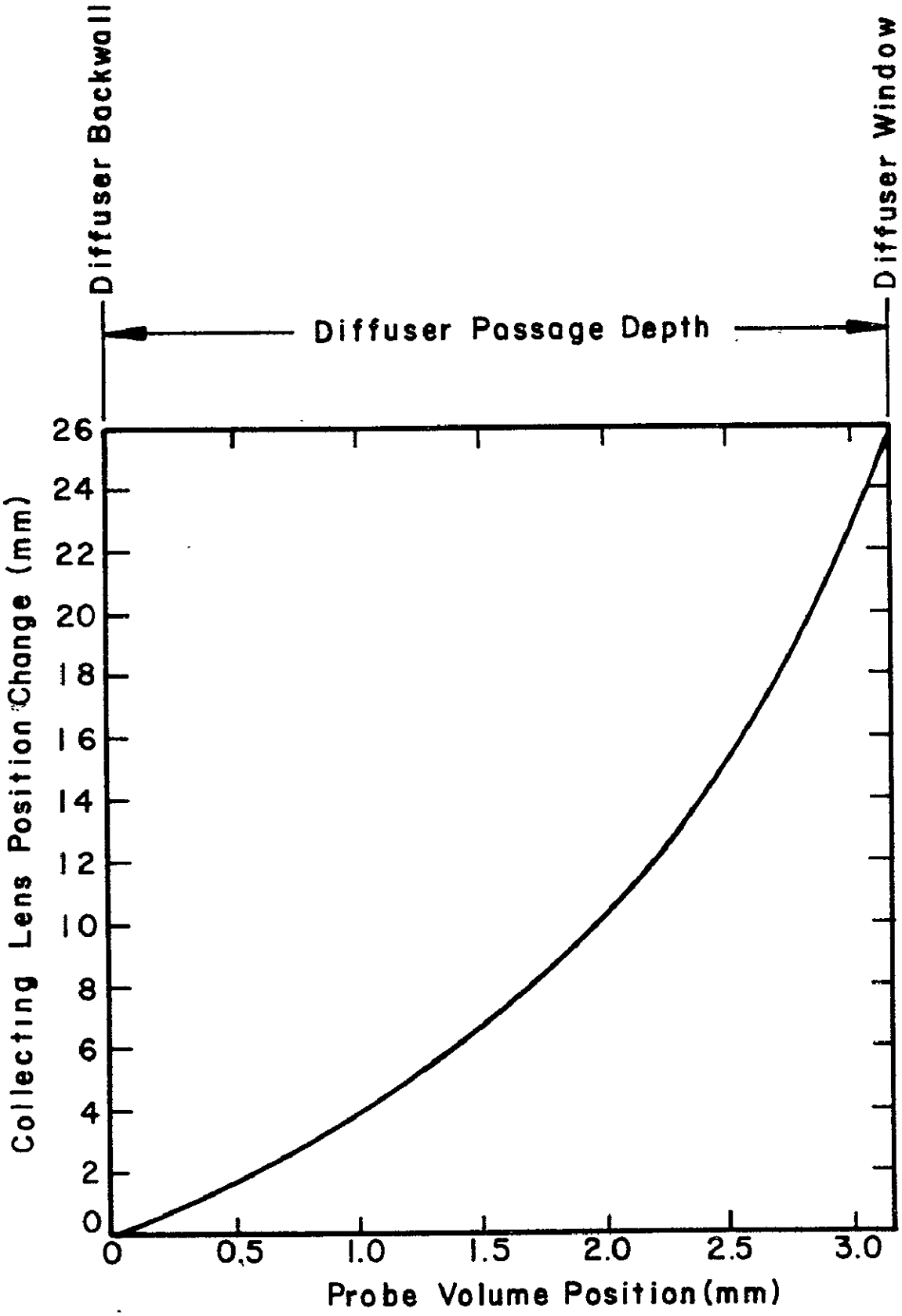

Figure 9. Collecting Lens Position Relative to Probe Volume Position for Diffuser Measurements

Slide position relative to the beds is measured with LVDT's (linear variable differential transformers) on each of the axes. Readout of the LVDT's is from a digital panel meter at the motor control panel. Use of the LVDT's eliminates position indication errors due to lead screw backlash or stepping motor count error. Each LVDT has a linear range of 50 mm, however not all of this is utilized due to the restricted space available for traversing the optics near the compressor. To prevent running this traversable mechanical assembly into the compressor hardware, and hence possible damage to optical or mechanical components, limit switches are placed at the extremes of the desired traversing range. Pneumatically-actuated locking screws are provided on each slide gib so that the beds may be securely fastened during data acquisition. These, too, are controlled from the main instrument panel.

The periscope which supports the beam directing prism, input lens and final directing mirror is made up of a length of hollow mechanical tubing 50 mm square with a 6.4 mm thick wall.

This entire mechanical system has been specifically designed to provide reliable positioning and robust support of the delicately aligned optical components and simple, accurate traversing of the probe volume relative to the compressor. Figure 10 is an isometric view of the complete optical/mechanical package.

Probe Volume Positioning. The optical system is traversed in order to make velocity measurements at various locations within the compressor. The LVDT position indicators do not read the probe volume position directly. They are set up to record displacements of each of the slides from some arbitrary fixed position in laboratory coordinates. It then remains to transform these position indicators of the slides to relate the probe volume position to the compressor coordinates. This is accomplished by utilizing the focused laser beams to locate the center of a "fiducial" mark whose position relative to the compressor is known.

The fiducial is a cross (+) whose arms are approximately 15 mm long. This cross is scribed into the compressor metal on a dark background at a known location and angle relative to a compressor feature (inducer inlet or diffuser vane leading edge). The approach is to locate two focusing beam spots on the plane of the fiducial (input optical axis essentially perpendicular to the plane of the fiducial), and then scan these spots around the fiducial such that each spot crosses each of the four arms. As a result of the scribing operation of the fiducial mark on a dark background, the fiducial arms reflect more light than does the surrounding background. By detecting this reflected light with a photocell, the intersection of an arm by a beam may be resolved very accurately. As each arm is intersected by each beam, the LVDT traverse positions are recorded. This same operation is then repeated for a slightly larger or smaller beam spot separ-

PART NO	DESCRIPTION
1	LASER
2	BEAM STEERING ASSEMBLY
3	BEAM SPLITTER PRISM
4	CORNER MIRRORS
5	BEAM DIRECTING PRISM
6	INPUT LENS
7	BEAM STEERING MIRROR
8	LIGHT COLLECTING MIRROR
9	LIGHT COLLECTING TELESCOPE
10	PHOTOMULTIPLIER TUBE
11	TRAVERSE DRIVE MOTORS
12	POSITION TRANSDUCER
13	TRAVERSING PERISCOPE
14	CENTRIFUGAL COMPRESSOR ASSEMBLY
15	A/O MODULATOR
16	BEAM PATH EXTENDER

ORIGINAL PAGE IS
OF POOR QUALITY

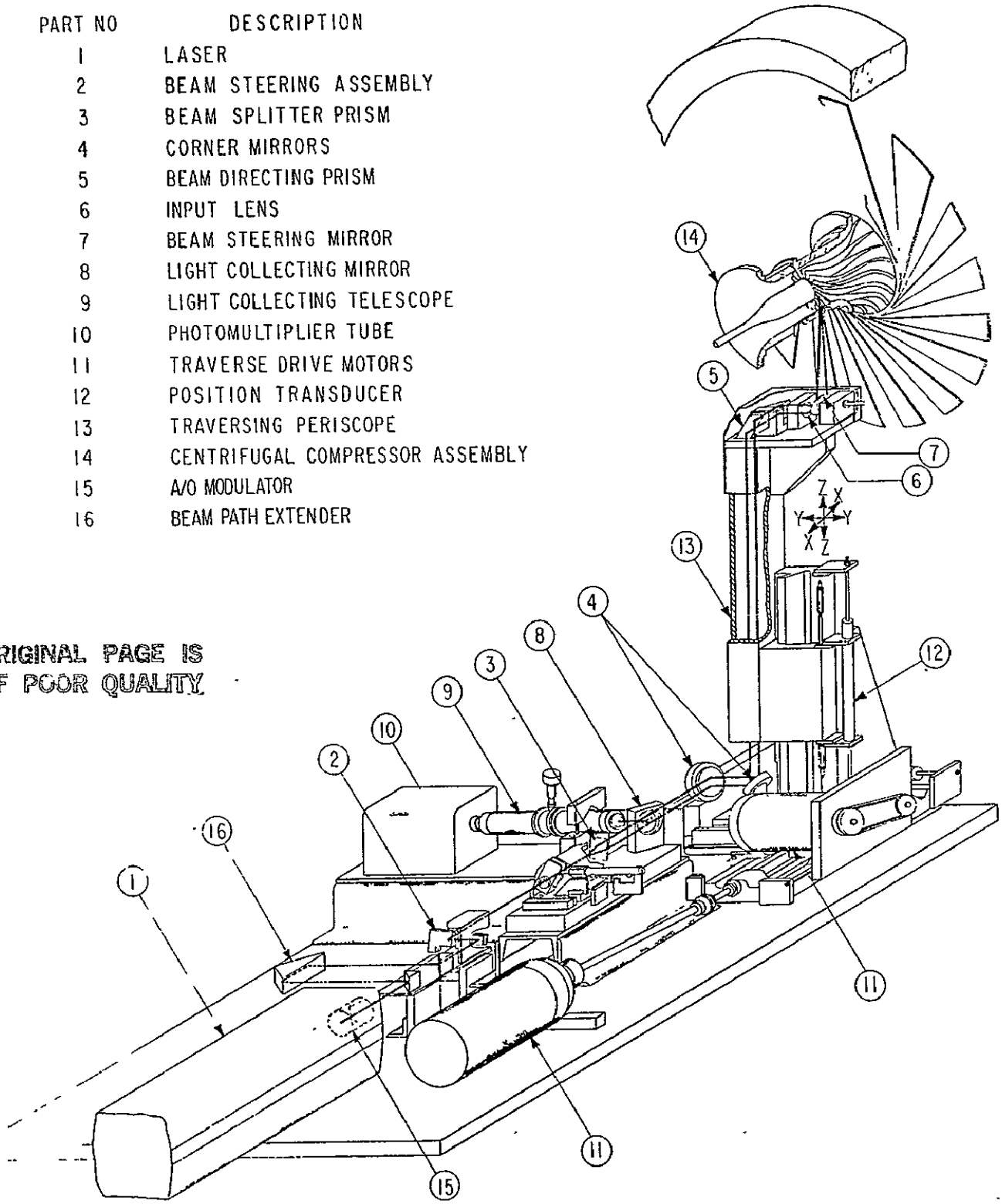

Figure 10. Isometric View of the Complete Optical Mechanical Package

ation on the fiducial plane. The result of these scans is a set of 16 (X, Y, Z) values which are fed to a computer program for calculation of the fiducial/probe volume center intersection coordinates. This same program is also used to generate a table of coordinates (in LVDT position indicator readings) used to place the probe volume at various measurement points of interest.

There are two fiducials used in this system. One is located on the inlet cover and is used to establish the probe volume relative to the inlet and inducer. The other is located on a diffuser vane and provides information for locating the probe in that region of the compressor. Theoretically, either fiducial should suffice to make the required measurements; however, we used this approach since the inlet and diffuser hardware are not pinned together during assembly. Therefore, small angular rotation (about the compressor axis) of the inlet cover relative to the diffusers could result, producing an error in positioning of the probe, if only one fiducial were used.

As in all of the other features of this system, control and readout of this fiducial scanning operation is performed remotely at the main console. This makes it unnecessary for operating personnel to be near the compressor while it is running.

Electronics System (Data Acquisition System). The electronic systems which detect, measure and process the LV signal are shown in Figure 11. The photomultiplier tube (PMT) is driven from a high voltage supply capable of delivering 10 mA at -2000 volts. Spectral response of the PMT is S-20 with a cathode sensitivity of 50 mA/W at 514.5 nm. Output from the PMT is taken to an instrumentation console from the test facility via an 8 meter length of coaxial cable. The signal is continuously monitored on an oscilloscope, and is parallel directed to either the Doppler frequency processor (DFP) or to the divide by two (÷2) electronics (the output from which is then fed to the DFP). Selection of the operating mode is done manually by changing interconnecting cables.

The LV must acquire velocity data for fixed impeller positions, with the actual acquisition time (width of the data "window") being variable and a function of the mean velocity. The data window position and width are set by a gate control system which uses a synchronous pulse from an optical blade position indicator as the primary control signal. This circuit provides a TTL (transistor-transistor logic) compatible pulse of desired duration (window width) which is fed to the acoustic/optic modulator driver and gates the RF signal to the crystal, thereby pulsing the laser beam in synchronism with the blade position. The resolution of the gate opening position is 0.1% of blade pitch, with window widths ranging from 60 ns to 6 ns (0.1% blade pitch to 100 blade pitches at 100% design speed).

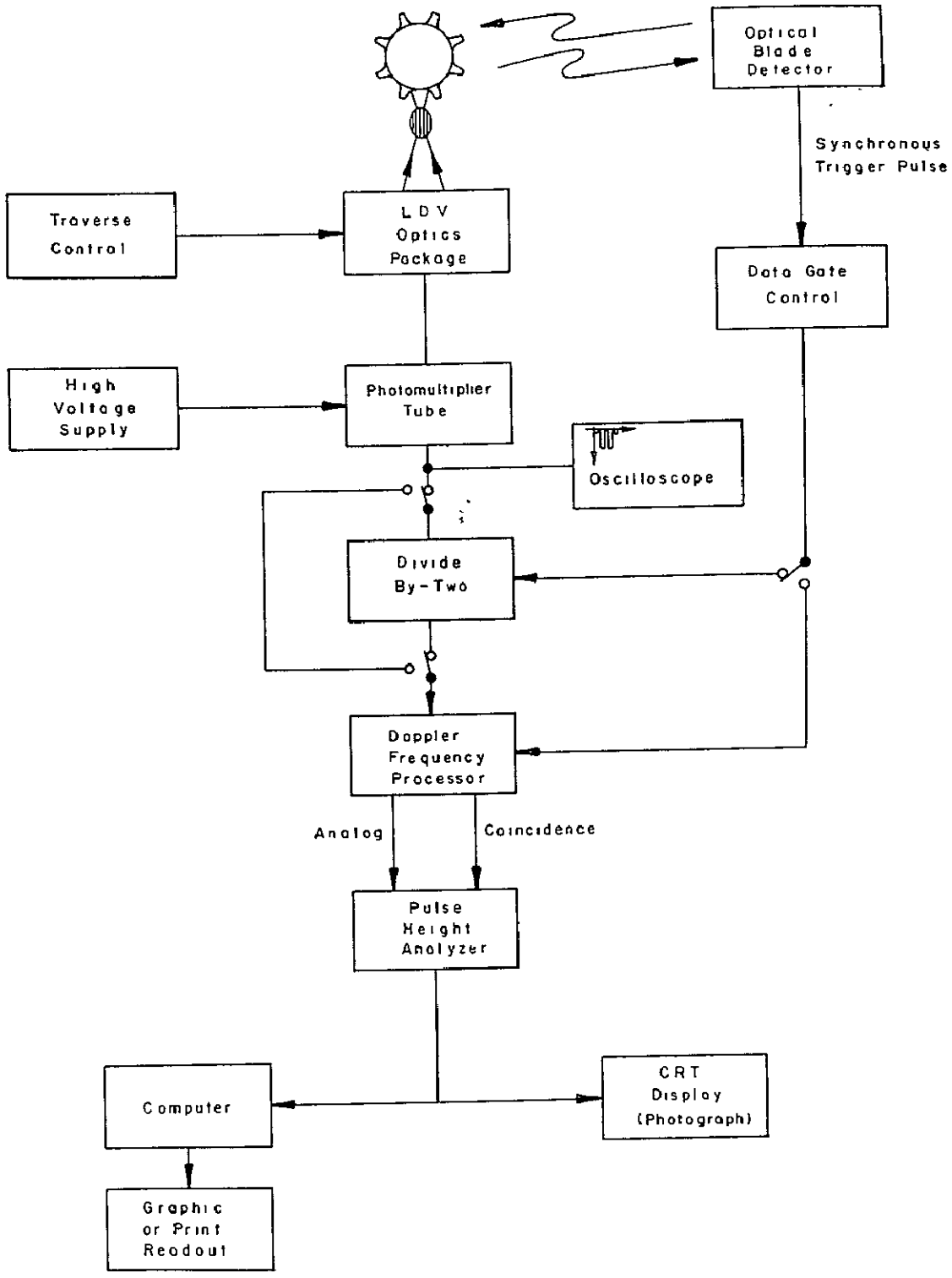

Figure 11. Electronics System

The control circuitry is designed to sample once per blade passage for each third impeller revolution. During the first revolution, the impeller speed is measured with a high frequency clock. The next impeller revolution is used to calculate (based on the measured wheel speed) the desired delay time before the gate is opened. The gate is actually opened and closed during the third revolution. Assuming one velocity measurement per gate opening and a gate opening for each blade channel (there are 19 blade channels in this particular impeller design), the maximum theoretical data rate is about 5700 Hz when operating in this fashion. The gate may also be operated to open only one time per wheel revolution, cutting the theoretical data rate to about 300 Hz. A more complete description of the gate control is presented in Appendix B.

The output from the frequency processor may be selected as a measure of either the time required to process eight Doppler cycles or its inverse, which is proportional to the velocity of a particle traversing the probe volume. This data is presented at the output terminals in both analog and TTL compatible digital form along with a coincidence pulse of about 1 μs duration. Appendix C contains a more detailed description of the divide-by-two electronics and the Doppler frequency processor.

The type of data acquisition system presented here is sometimes called the "individual realization method". That is, the velocity information is generated by individual particles traversing the probe volume. If the velocity field is unsteady, no single measurement can precisely describe the mean velocity. Thus, analysis must resort to statistical methods to obtain mean velocity and turbulence information. Reference 9 contains a good treatment of these methods for the individual realization laser velocimeter technique.

In order to record and store the velocity data of a point velocity measurement, a pulse height analyzer (PHA) is used to store each output pulse from the DFP. The PHA accepts the analog voltage signal and the coincidence pulse, and logs one count into an appropriate channel corresponding to the voltage (velocity) level. Using the PHA, a velocity probability distribution or histogram is built up. This histogram displays the number of counts versus channel number or velocity. The information is displayed on a CRT for real time analysis and is stored in the PHA memory for later output onto punched paper tape which is used for ultimate data reduction.

DATA ANALYSIS

Data Reduction. The basic data reduction procedure calculates a mean value and standard deviation of the distribution for each of the two measured orthogonal components of the total velocity vector at each measured point. The sample mean is defined as

$$\bar{U} = \frac{\sum_i n_i U_i}{\sum_i n_i} \tag{20}$$

and the sample standard deviation is

$$\sigma_s = \left[\frac{\sum_i n_i (U_i - \bar{U})^2}{(\sum_i n_i) - 1} \right]^{1/2} \tag{21}$$

where n_i is the number of occurrences at each velocity U_i.

Before the mean and standard deviation can be tabulated as velocity and RMS value of the fluctuation, respectively, the data must be treated to eliminate statistical biasing and distribution broadening.

The biasing comes about since more high velocity particles $(\bar{U} + u')$, where u' is the fluctuating component, cross the probe volume during the data acquisition time than do low velocity particles $(\bar{U} - u')$. Thus, the distribution tends to be biased toward the higher velocity. Reference 20 presents a good discussion of this biasing and describes a model to correct the distribution, assuming a one-dimensional flow. Their simplified model corrects the biased probability of occurrence of any velocity U_i by the ratio of $\bar{U}/U_i$. Here $\bar{U}$ is the biased sample mean, which approaches the true mean as the correction procedure is iterated in the data reduction program.

The probability distribution recorded from the individual LV measurements must also be corrected for broadening. There are several phenomena which tend to broaden the distribution:

1) turbulence (which is a property of the real flow),
2) statistical biasing,
3) velocity measurement inaccuracy,
4) velocity gradients in the probe volume,
5) particle Brownian motion, and
6) non-monochromaticity of the laser.

Only the first three of these are considered to be of significance in the present program.* Figure 12 displays these broadening terms in a graphical form. From the total probability distribution, we would like to be able to correct the distribution so that only the turbulence broadening contribution remains. This may be done by making some simplifying assumptions regarding the statistical biasing and the effect of measurement inaccuracy on the skewing of the distribution.

*Velocity gradient broadening may be important in the wall flow region of the diffuser and will be included in any subsequent analysis if found to be important.

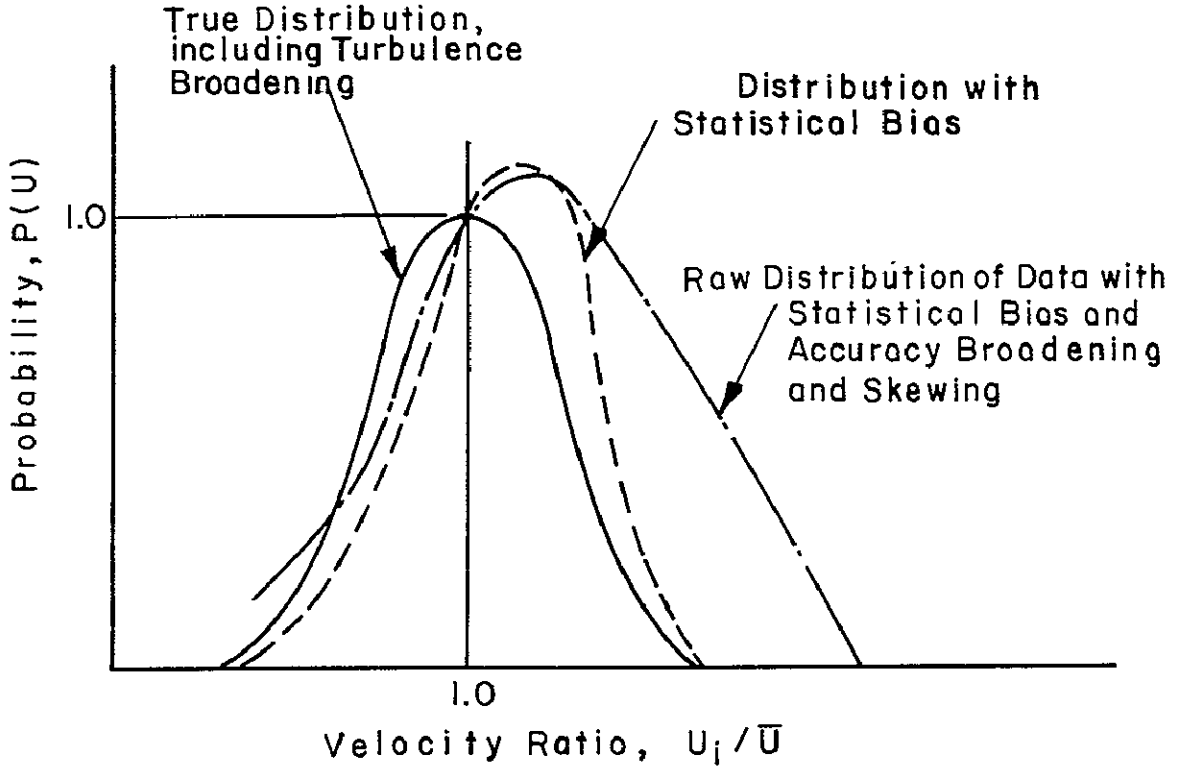

Figure 12. Probability Distributions Measured with Individual Realization LV System

Reference 20 shows that for a modified Gaussian probability distribution, the error in not accounting for statistical bias in the calculation of σ_s is small, except at very high levels of turbulence $\sqrt{(u')^2}/\bar{U} > 0.15$. In fact, for some cases, attempts to correct the biased distribution using the simple, one-dimensional model may yield estimates of $\sqrt{(u')^2}/U$ significantly greater than the true value.

The velocity measurement inaccuracy results from the digital nature of the frequency measurement.* Since the error in the measurement is directly proportional to the velocity, the velocity distribution becomes skewed to the high velocity side. The relative error is:

$$\sigma_m = \frac{1}{8} \frac{\Delta f_D}{f_C} \tag{22}$$

*Discussed in an earlier section on the design of the LV system.

The frequency processor has a clock frequency f_c of 100 MHz; thus the error is only 1.25% at $\Delta f_D = 10$ MHz, ranging to 10% at 80 MHz. If we ignore the skewing effect this error has on the distribution, it is possible to express the total broadening σ_{total} as a function of the turbulence broadening σ_t and σ_m:

$$\sigma_{total} = \left[(\sigma_t)^2 + (\sigma_m)^2\right]^{1/2} \tag{23}$$

This assumes that the measurement error is independent of the turbulence (i.e.; the effect of high levels of turbulence biasing the distribution is not important). Although not strictly true, this will at least allow a first order estimate of the turbulence level.

To summarize, the probability distribution is first corrected, using an iteration scheme, to find the unbiased mean velocity. Next, the total broadening σ_{total} is determined using the corrected mean velocity,

$$\sigma_{total\ c} = \left[\frac{\sum_i n_i (U_i - \bar{U}_c)^2}{(\sum_i n_i) - 1}\right]^{1/2} \tag{24}$$

where the subscript c denotes the corrected data. From the corrected mean velocity, the mean Doppler frequency is calculated, and the contribution to broadening from measurement inaccuracy is determined from Equation 22. Finally, the distribution broadening as a result of fluctuations of the mean velocity (turbulence) is obtained.

$$\sigma_{tc} = \sqrt{\frac{\overline{(u')^2}}{\bar{U}_c}} = \left[(\sigma_{total\ c})^2 - (\sigma_{mc})^2\right]^{1/2} \tag{25}$$

A final step of the data reduction procedure is then to relate the absolute velocity measurements made with the LV, in the laboratory coordinates, to relative velocities in the compressor coordinates. Figure 13 displays the vector addition to generate the total absolute velocity C from the two orthogonal vectors C_1 and C_2 measured with the LV. Also, the relative velocity W is shown as a function of C and u, the wheel speed.

Data Accuracy. There are three primary accuracy estimates important to the securing of velocity data in this program. These are the accuracy of positioning the probe volume within the compressor and the accuracy of measuring the magnitude and direction of the velocity vector.

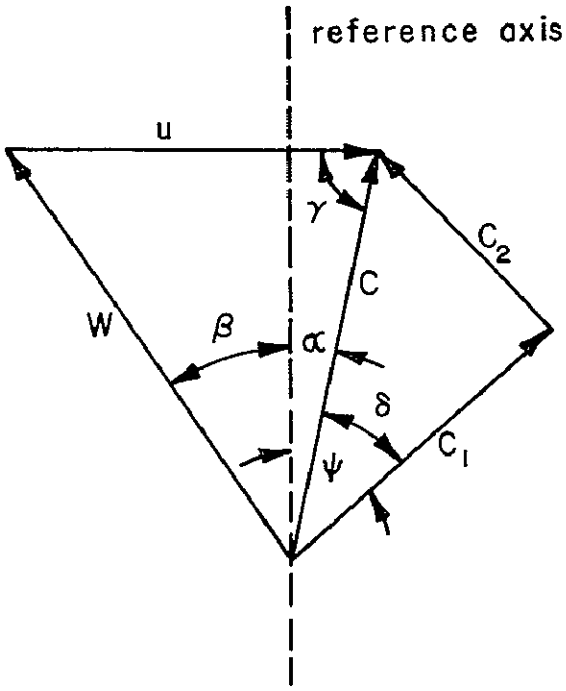

C_1 = absolute velocity vector measured with LV in beam orientation (1)

C_2 = absolute velocity vector measured with LV in beam orientation (2)

$C = (C_1^2 + C_2^2)^{\frac{1}{2}}$

N = rotational speed

r = radius from impeller axis

u = impeller velocity at $r = 2\pi rN$

W = relative velocity $= (u^2 + C^2 - 2uC\cos\gamma)^{\frac{1}{2}}$

α = absolute flow angle relative to axis $= \psi - \delta$

β = relative flow angle $= \tan^{-1}(u - C\sin\alpha)/(C\cos\alpha)$

$\gamma = \pi/2 - \alpha$

δ = absolute flow angle relative to $C_1 = \tan^{-1}(C_2/C_1)$

ψ = C_1 velocity measurement plane relative to reference axis, determined from fiducial scan.

Figure 13. Velocity Vector Addition and Nomenclature

Location of the probe volume within the compressor hardware may be resolved to ± 0.025 mm via the digital panel meter readout of slide position from the LVDT's. The position transducers are calibrated, and the maximum uncertainty (at 20:1 odds) of a curve fit through the position data is less than 0.075 mm. Thus the probable error in any LVDT reading is $[(0.025\ \text{mm})^2 + (0.075\ \text{mm})^2]^{1/2} = 0.08$ mm. The repeatability of the fiducial scanning technique, i.e., the ability of multiple trials to predict the intersection of the probe volume with the fiducial center, has been determined. In the plane transverse to the probe volume—the plane containing the fiducial—the predicted coordinates repeat to within ± 0.050 mm (6 trials). Along the optical axis—the direction containing the length ℓ of the probe—the repeatability is ± 0.127 mm. Thus, the maximum error in positioning of the probe volume is $[(0.080\ \text{mm})^2 + (0.127\ \text{mm})^2]^{1/2} = 0.15$ mm.

The accuracy in measurement of the magnitude of the velocity vector is a function of the number of individual realizations in the velocity histogram and the width of the probability distribution. Figure 14a, adapted from Reference 19, shows the number of data points required in a single sample in order that the mean be within a specified limit of the true mean. If each of the two components of the total velocity are measured to an uncertainty level ε, then the uncertainty in the magnitude of the total vector is $\sqrt{2}\varepsilon$. Reference 19 also shows that the number of counts needed for estimating the error in the sample standard deviation is a function only of the magnitude of the error. Figure 14b displays this error for a 95% confidence level.

Finally, an estimate of the error in determining the direction of the velocity vector is needed. The procedure for calculating the mean flow angle, with respect to some compressor coordinate system, involves first determining the flow direction with respect to the measurement planes of the probe volume. Angle δ in Figure 13 is the mean flow angle relative to the C_1 measurement plane.

$$\delta = \tan^{-1} \frac{C_2}{C_1} \tag{26}$$

Then, from the fiducial scanning operation, we extract the orientation of one of the beam planes with respect to the fiducial. Since the fiducials are very accurately located with respect to the compressor, we can transfer the beam plane orientation directly to compressor coordinates. The maximum error in relating the beam plane to the compressor is estimated to be ± 1 degree. This comes from the uncertainty in the fiducial scan and the initial fiducial scribing, producing values of

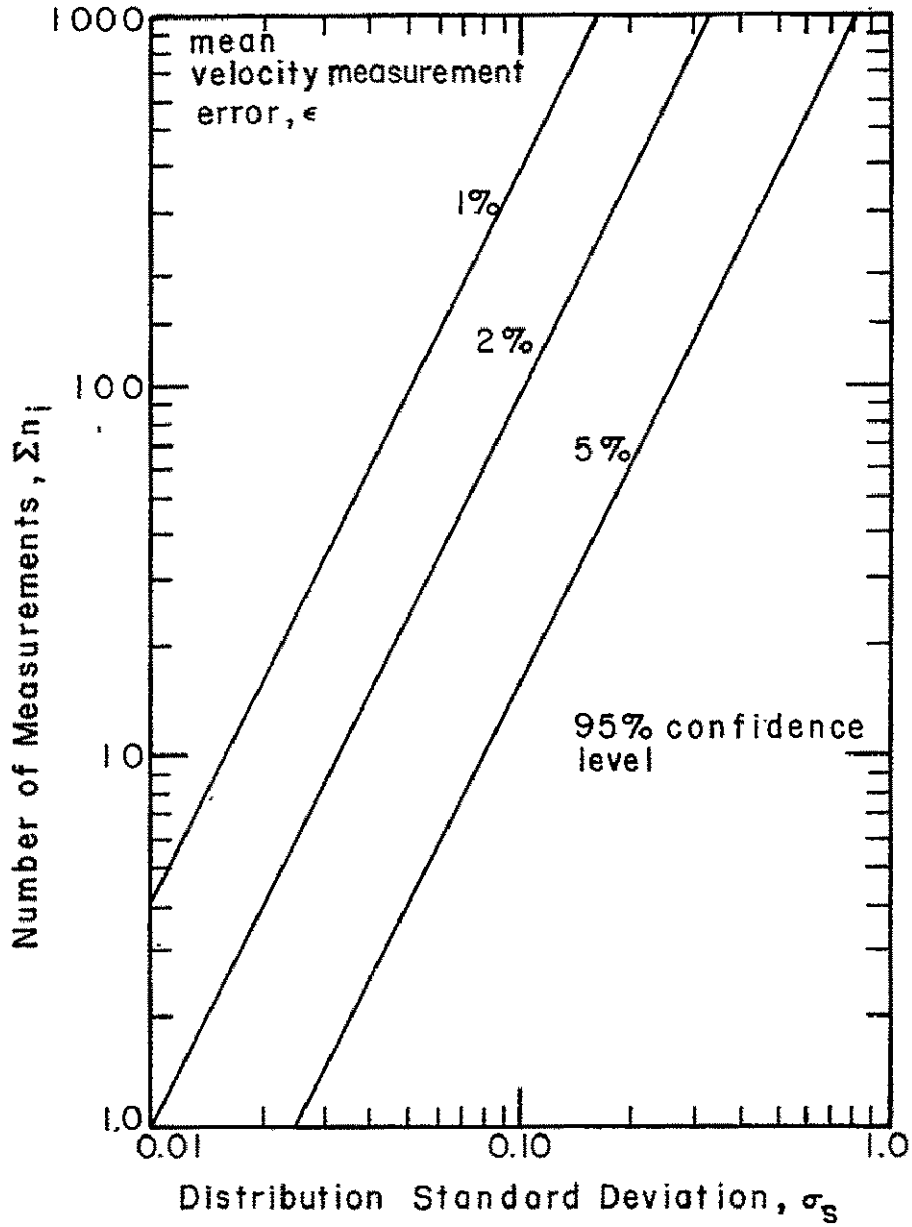

Figure 14a. Number of Measurements in Sample Required to Measure Mean Velocity to Specified Accuracy. (Adapted from Reference 19)

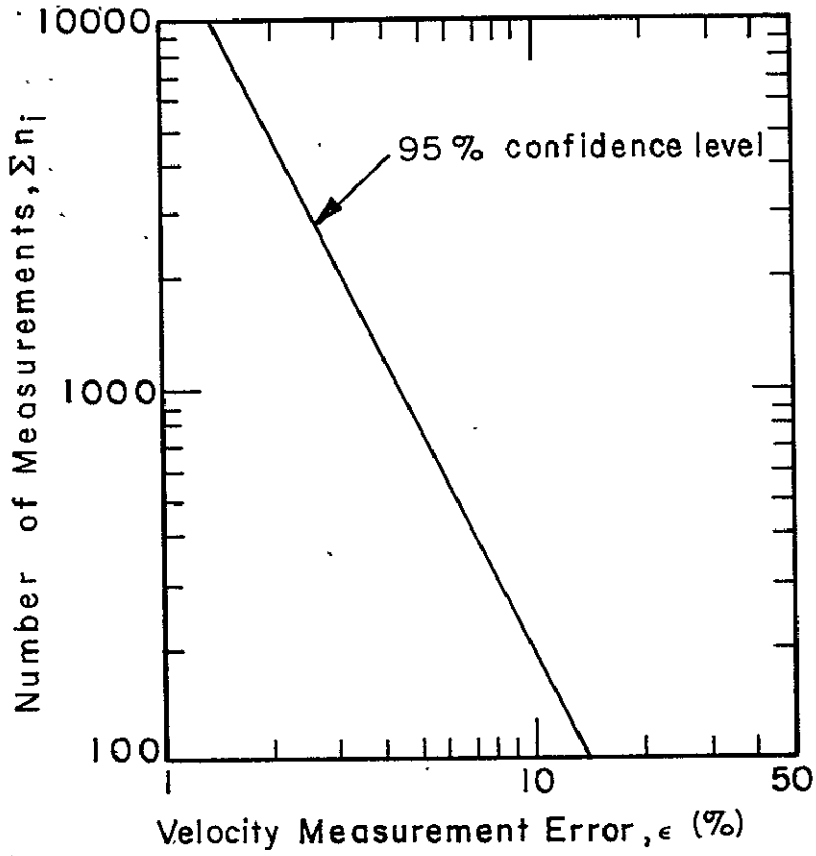

Figure 14 b. Number of Measurements in Sample Needed to Predict Standard Deviation. (Adapted from Reference 19)

approximately $\pm$ 0.7 degrees and $\pm$ 0.3 degrees, respectively. To this error must be added the error in δ calculation, resulting from errors in measurement of the C_1 and C_2 components. This error is a maximum when $\delta = 45$ degrees, $C_1 = C_2$. For a 2% error in each of C_1 and C_2, δ has an error of $\pm$ 0.9 degrees at 45 degrees; this increases to about 2 degrees for a 5% error in each velocity component, at $\delta = 45$ degrees. This relationship is plotted in Figure 15. The magnitude of the total angular error then is the vector sum of the 1 degree error in beam plane definition, plus the error related to the velocity magnitude measurement. For C_1 and C_2 at 2% of true, the total angular uncertainty is $\sqrt{(1)^2 + (0.9)^2} = 1.4$ degrees; for the 5% error case, this is 2.2 degrees.

There are two other significant error analyses which must also be considered. The first is referred to as the directional ambiguity of the present LV system. When a particle traverses the fringe pattern, it scatters light at a frequency proportional

to its velocity and inversely related to the fringe spacing; however, this information says nothing about the absolute direction of the particle; i.e., in which of the two possible directions does its vector lie along a normal to the fringes. There are optical methods (frequency shifting and use of polarized light) which can be used to negate this ambiguity, but they have not been included in this design. We must rely upon our knowledge of the flow and mass flow balances to deduce the absolute directions of each vector.

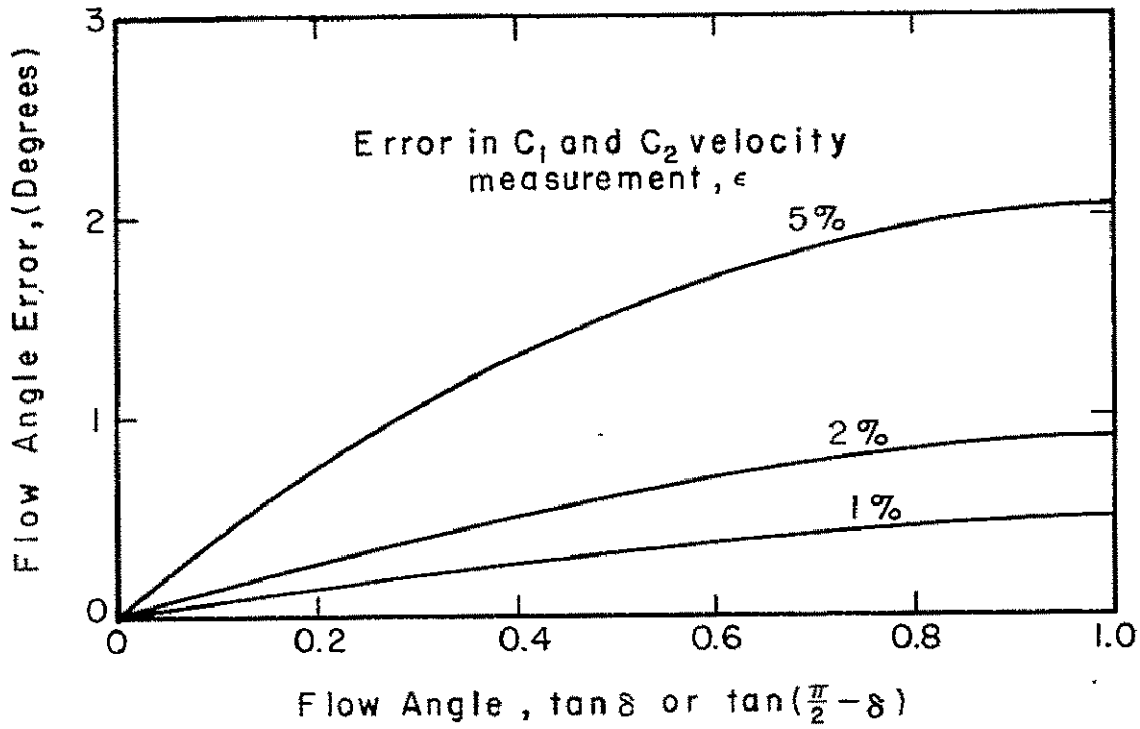

Figure 15. Error in Absolute Flow Angle as Function of Flow Angle.

The final error to be considered is that which results when one component of the total velocity vector lies nearly parallel to the fringe pattern. In such a case, the measured frequency is very low and there may be insufficient fringe crossings to provide even a valid signal. The geometry of this problem is presented below in a simplified form.

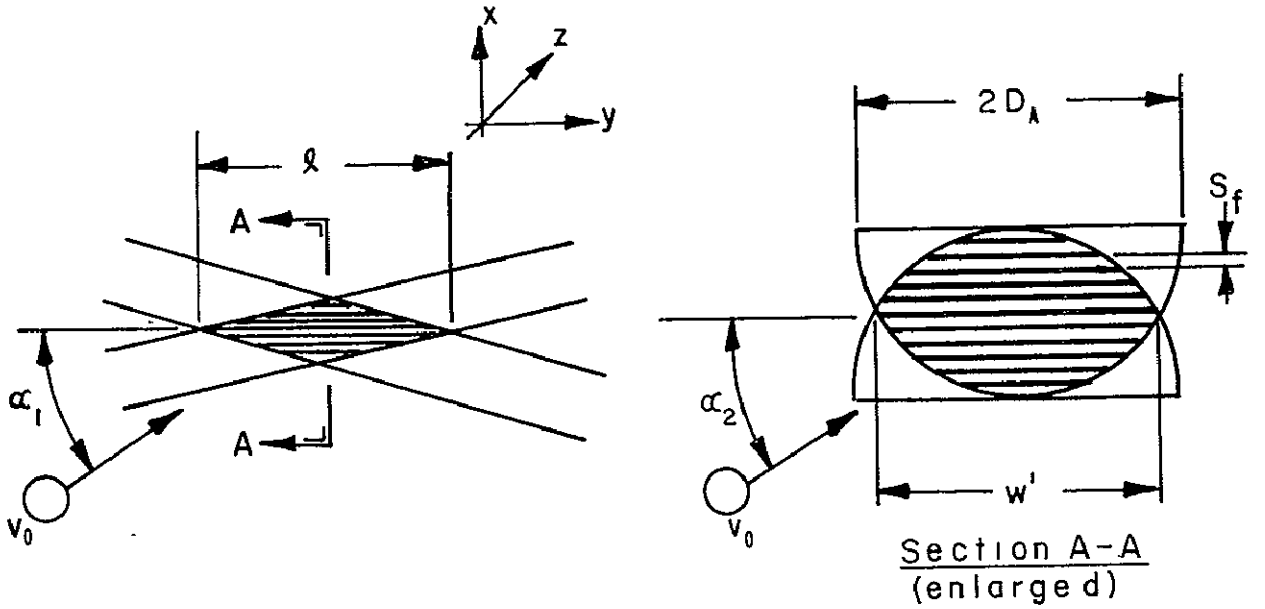

As shown in these sketches, there are two orientations of the total velocity vector v_o, which can result in insufficient crossings of fringes to generate a valid signal. In the first case v_o lies nearly parallel to the input optics axis. For the second, v_o is perpendicular to the input axis and nearly parallel to the fringe, as shown in the sectional view of the probe volume. For this LV system, the intersecting beam cross sections are semicircular, as a result of the method of beam splitting.

The minimum angles α_1 and α_2 that the vector can have with respect to the fringes, such that N fringes are crossed as the particle traverses the probe volume, can be calculated as follows: $\tan \alpha_1 = Ns_f/\ell$ and $\tan \alpha_2 = Ns_f/w'$. In each case, $N = 8$ fringes and $s_f = 2.68 \times 10^{-3}$ mm. The probe volume length $\ell = 0.68$ mm, and its width $w' = \sqrt{3}\, D_A = 0.113$ mm. Thus,

$$\alpha_1 = \tan^{-1}\left(\frac{8 \times 2.68 \times 10^{-3}}{0.68}\right) = 1.8 \text{ degrees} \tag{27}$$

and

$$\alpha_2 = \tan^{-1}\left(\frac{8 \times 2.68 \times 10^{-3}}{0.113}\right) = 10.7 \text{ degrees}$$

So, if the flow is closely aligned to the probe volume axis, $\alpha_1 < 2$ degrees, we will not be able to make valid frequency measurements. This situation is not expected to arise however, since the input optics axis will always be aligned perpendicular to the expected mean flow, i.e., radial in the axial flow portion of the impeller and axial in the radial flow discharge region. The second case, wherein v_o is perpendicular to the axis and nearly parallel to the fringes, is a more significant problem. Here, if $\alpha_2 < 11$ degrees, no velocity measurement v_x is possible. By rotating the fringe pattern 90 degrees, a second component v_z will be measured, but the total vector will be in error, 19% low in magnitude and $\pm$ 11 degrees in direction. This is recognized as a limitation of the present design, but it was felt to be a minimum trade-off in reducing the size of the probe volume. Measurement of a third v_o component $\pi/4$, with respect to the two orthogonal planes, would alleviate the problem. Thus far this ability has not been provided for in the present design, although the design can be easily modified to include this feature.

The next sections present the fabrication and assembly of the compressor and LV system, and the checkout and calibration of the LV in "bench-top" tests and in the compressor.

FABRICATION AND ASSEMBLY

COMPRESSOR HARDWARE

The test bed for the laser velocimeter is the 8:1 pressure ratio, 0191 kg/s mass flow, centrifugal compressor. This compressor was designed and fabricated under a companion program. Figures 16a, 16b, and 16c show the impeller, inlet cover, and the front diffuser plate with several installed diffuser vanes. Two sets of optical windows for the inlet and impeller tip regions, Figure 17, were also fabricated under the companion contract. These windows fit into the cutouts shown in Figures 16b and 16c. The diffuser window fits in flush with the diffuser front wall. The inducer window was made flat, and fits into the circular cross-section inlet with a slight recess at the edges (0.15 mm).

The assembled compressor "stack" is shown in Figure 18. The optical windows and their mounting cover plates are partially visible. The optical windows were fabricated to provide minimum clearance with the cover hardware. The diffuser window is clamped firmly to the tops of several diffuser vane islands, such that there is no leakage between window and vane. Silicone rubber O-rings are used to seal the windows and prevent leakage into or out of the compressor. Figure 19 is an overall view of the assembled test compressor and test facility, looking along the input drive shaft.

LV SYSTEM

Optical Train. All of the optical components used in this system are commercially available or may be fabricated by competent specialty houses. The beam splitter and beam directing prism were custom fabricated for this program. The input and collecting lens and the mirrors were commercially purchased items, except for the special coatings used to maximize the efficiency of the input and collecting elements. Table III lists each of the major items with comments regarding their characteristics.

Because of the inaccessibility of the optical system when assembled in the compressor rig, the mounts and supports for the optical elements were designed to require minimum maintenance to ensure alignment. With the exception of the beam steering assembly, all of the adjustable components are securely fastened to their respective mounting brackets once initial alignment is complete.

The optical system is aligned such that when the probe volume is traversed in any of the three principal coordinate directions the total transverse skew is less than 0.050 mm. This alignment is achieved by a procedure which utilizes a shift in the center of

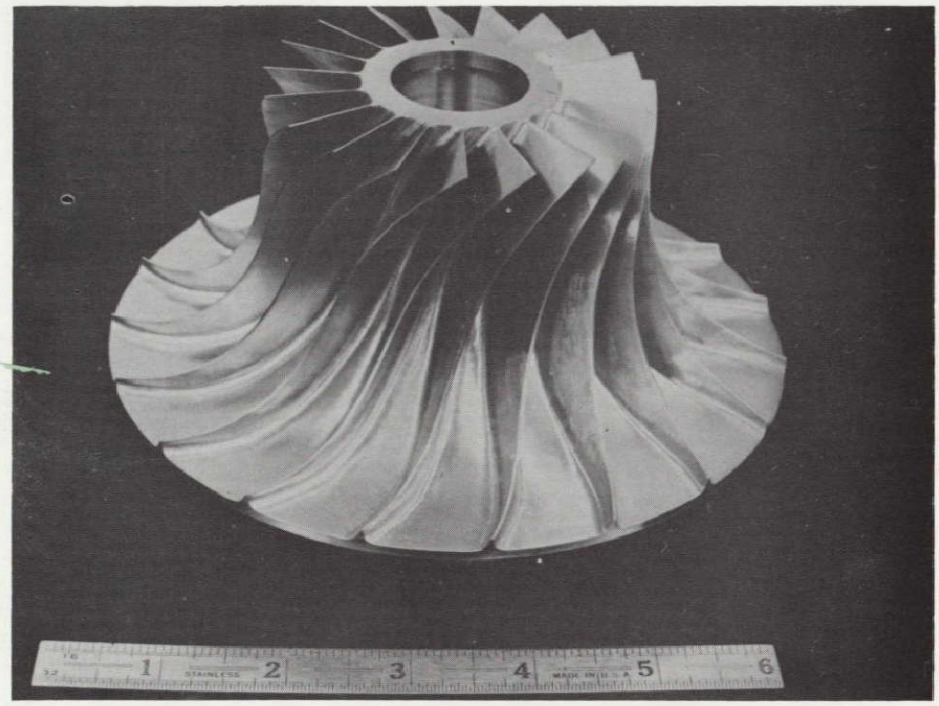

Figure 16a. 8:1 Pressure Ratio Impeller

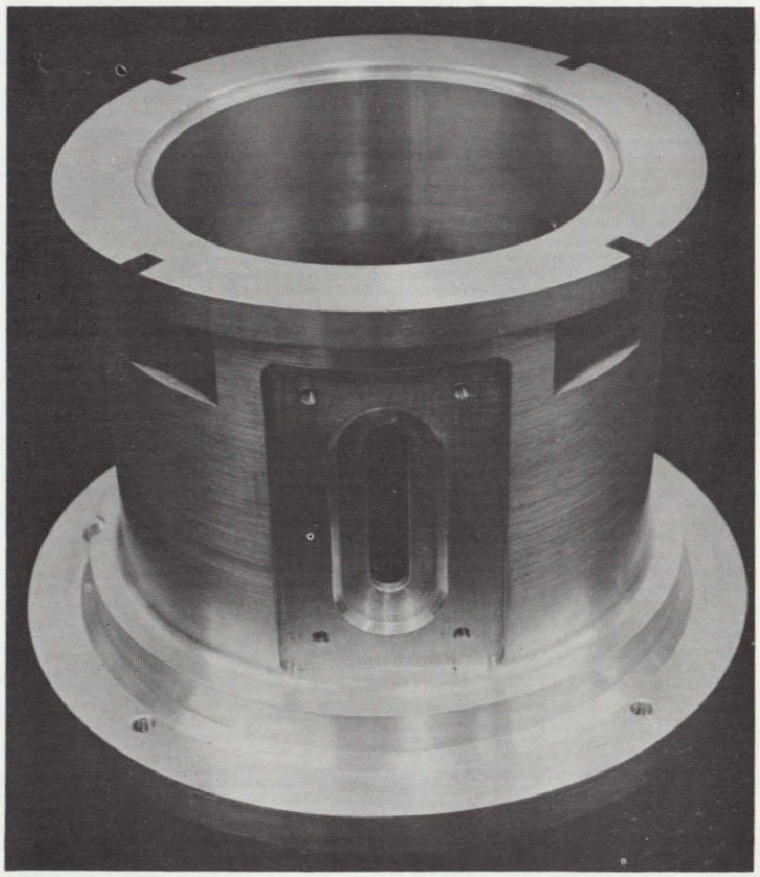

ORIGINAL PAGE IS
OF POOR QUALITY

Figure 16b. Inlet and Impeller Cover Showing Optical Window Opening

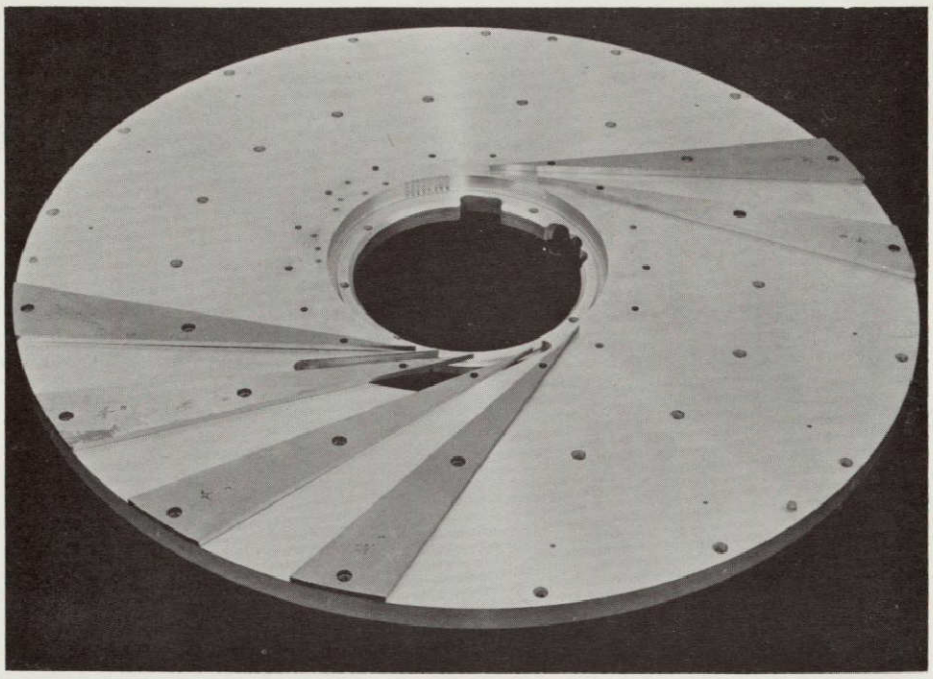

Figure 16c. Diffuser Front Plate Showing Optical Window Opening

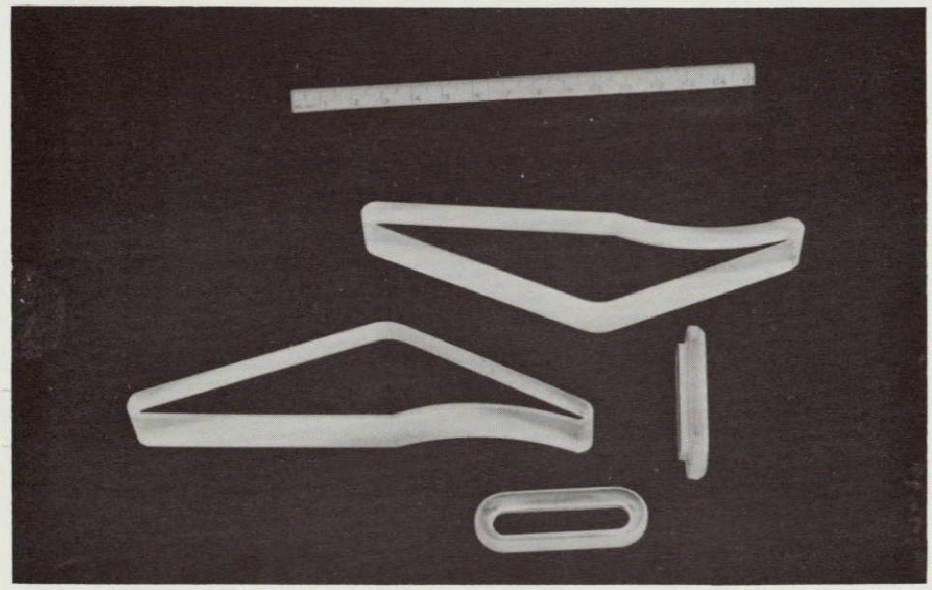

Figure 17. Inlet and Diffuser Optical Windows

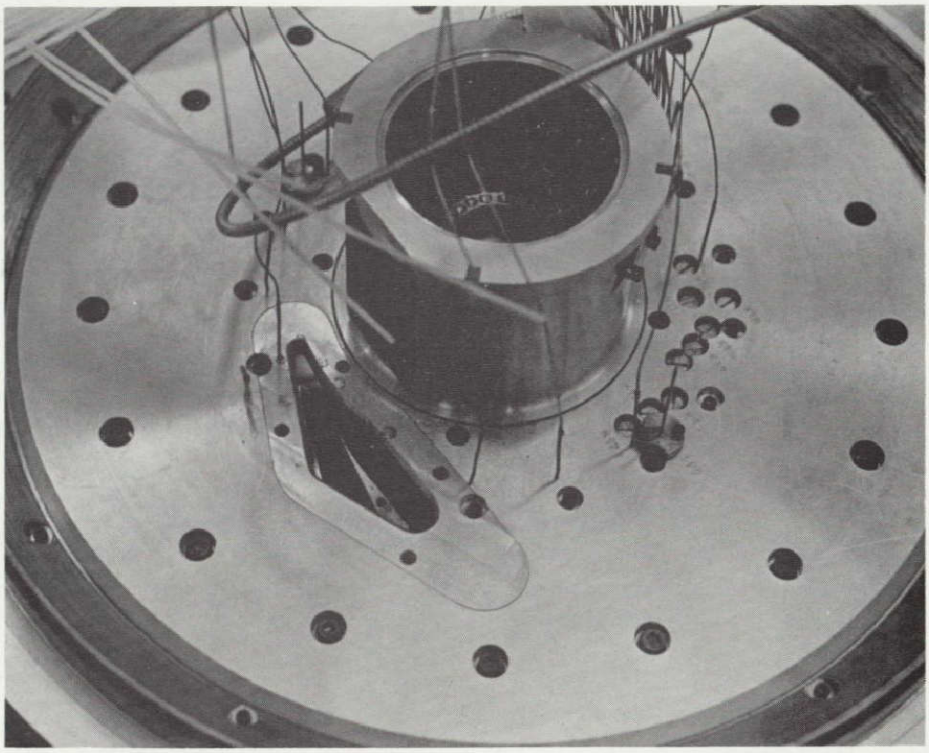

Figure 18. Assembled Compressor Hardware

ORIGINAL PAGE IS
OF POOR QUALITY

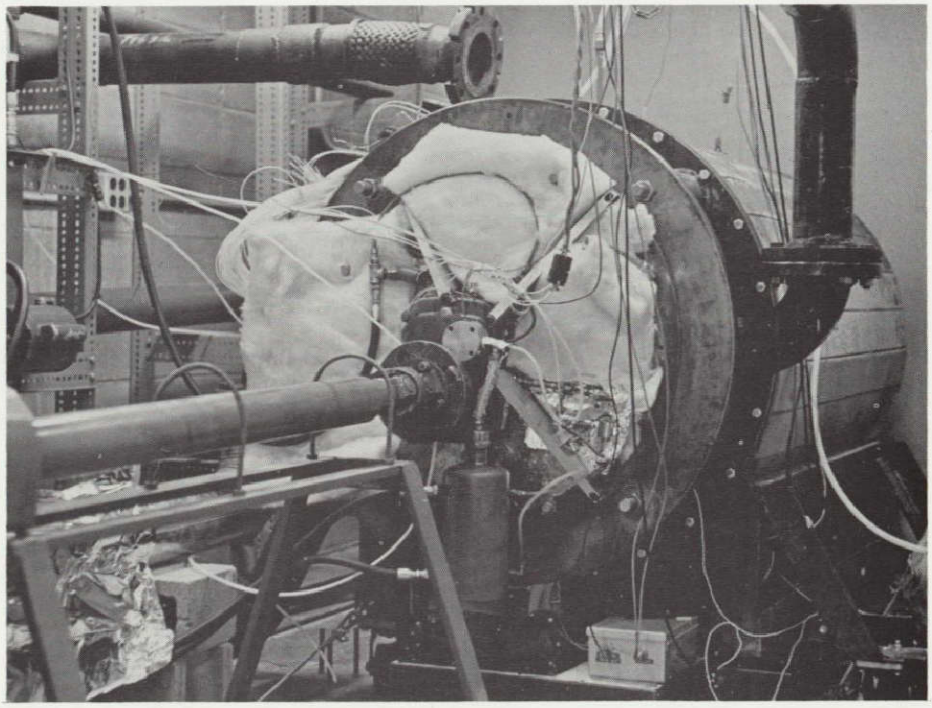

Figure 19. Assembled Compressor Test Facility

TABLE III. - MAJOR OPTICAL COMPONENTS	
Components	Remarks
Beam Steering Assembly	Used to align laser output with X-axis motion; two $\lambda/10$ first surface reflectors; total adjustment 20 mm linear and 6 degrees angular.
Beam Splitter Prism	Provides two parallel output beams 15.4 mm apart; UV grade fused silica; 24.1 mm x 24.1 mm x 12.7 mm thick; sides parallel and perpendicular to 5 arc seconds.
Beam Directing Mirrors (2)	Re-direct beams from beam splitter to traversing periscope; 50 mm dia. x 12.7 mm thick; $\lambda/20$ surface.
Beam Directing Prism	Provides two total internal reflections to direct and displace beams from vertical axis to horizontal; 25 mm cross section x 70 mm long; UV grade silica; angular tolerances better than 30 arc seconds.
Input Lens	Serves to focus input beams to form probe volume and collect scattered radiation; 78.5 mm focal length (measured); achromat; doublet.
Beam Steering Mirror	Used to direct probe volume to either inlet region or impeller exit region; 25 mm dia. x 6.35 mm thick; $\lambda/20$ surface.
Collecting Mirror	Directs collected scattered radiation from input axis to axis of photodetector; 35 mm dia. x 3 mm thick; $\lambda/4$ surface figure; provided with four holes to allow input beams (2 beam plane orientations) to pass through.
Collecting Lens	Serves to focus collected radiation onto aperture ahead of photomultiplier tube; 98 mm focal length x 25 mm dia.; achromat; doublet.

continued

TABLE III. - CONCLUDED	
Components	Remarks
Laser	Argon ion, operating in TEM_{oo} mode at 514.5 nm; with etalon; approximately 1 w peak power
Acoustic Optic Modulator	Used to divert laser beam into optical path; rise time < ns; angular separation 6×10^{-3} radian at 514.5 nm.
Optical Windows	Provide access to compressor hardware for input beams; inducer window 7.6 mm thick; diffuser window 17.8 mm thick; UV grade fused silica; $\lambda/20$ surface (Figure 17).

a diffraction pattern (formed by a pinhole illuminated with the laser beam) as the optical component being aligned is moved with the traverse mechanism, relative to the stationary input beam.

Mechanical Package. The section on design of the LV system discussed the mechanical system used to provide support for and traverse of the optical train. Figure 20 shows this completed package, assembled and installed on its seismic bed. The top of the bedplate is just below laboratory floor level to provide clearance for the inlet plenum, which is wheeled over the assembly for compressor operation.

The complete optical train is shielded from dirt contamination and possible damage by a cover shown in place in Figure 21. The traversing periscope, shown protruding out of the large flat box, is sealed to the box by a flexible rubber "boot". This boot seals the clearance gap needed for traversing without restricted motion in the three axes. The small opening on front of the periscope head provides the output path for the focused beams to explore the impeller tip/diffuser entry region. A similar hole on the top of the periscope looks into the inlet and inducer region.

Immediately behind the periscope is the inlet plenum for the compressor. The inlet bellmouth and centerbody are shown in place. The compressor inlet cover (Figure 16b) mates to the bellmouth and the completed compressor stack is attached to the four large stubs on the plenum.

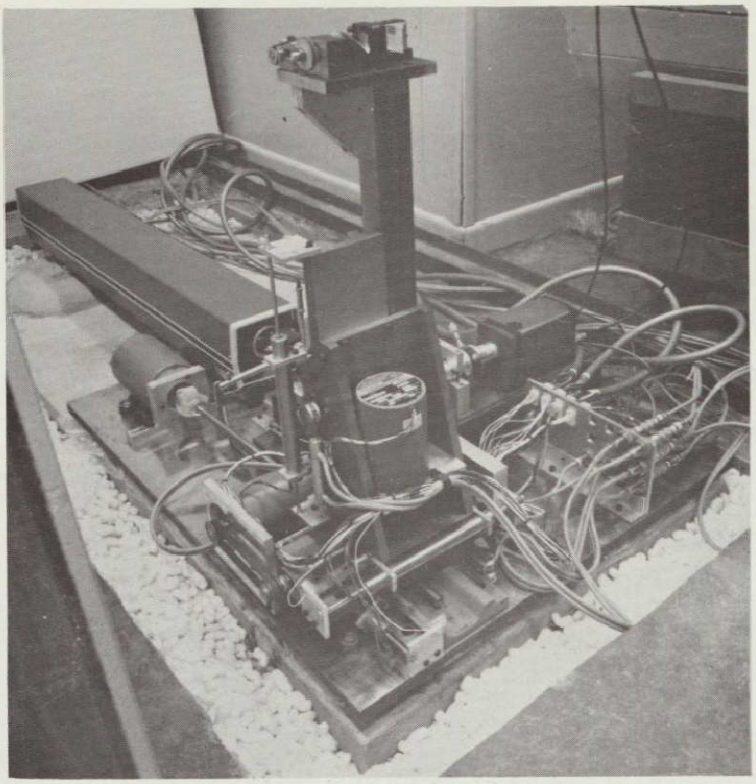

Figure 20. Assembled LV Hardware on Seismic Bed

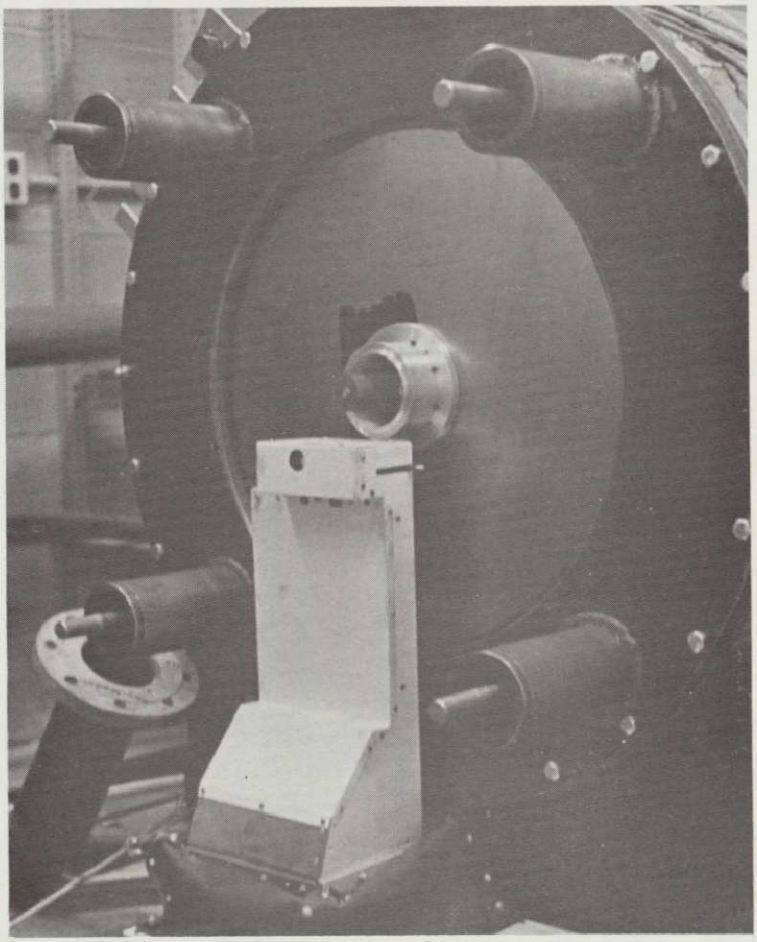

Figure 21. Assembled LV Hardware with Covers in Place

ORIGINAL PAGE IS
OF POOR QUALITY

A blower is used to keep the containment around the LV package pressurized slightly above ambient to minimize intrusion of dust, dirt, and oil, and to keep the entire LV package at uniform temperature.

Electronics Systems. The details of the design and operation of the gating electronics, the divide-by-two front end unit and the frequency processor are given in Appendices B and C. Figure 22 displays the complete control and data acquisition systems.

The laser power supply and control and monitoring oscilloscope are situated on the counter top to the right. Most of the major systems are mounted in the floor rack. Starting from the top, these are:

1) data gate control panel,
2) divide-by-two unit,
3) frequency processor,
4) pulse height analyzer,
5) XYZ traverse control panel,
6) high voltage supply for PMT, and
7) power supply console for stepping motors.

In addition to these components, the optical blade position indicator and A/O modulator electronics are located near the compressor.

All of these optical, mechanical and electronics systems have been checked out and tested in a wind tunnel facility and shown to be capable of measuring the range of velocities to be found in the compressor.

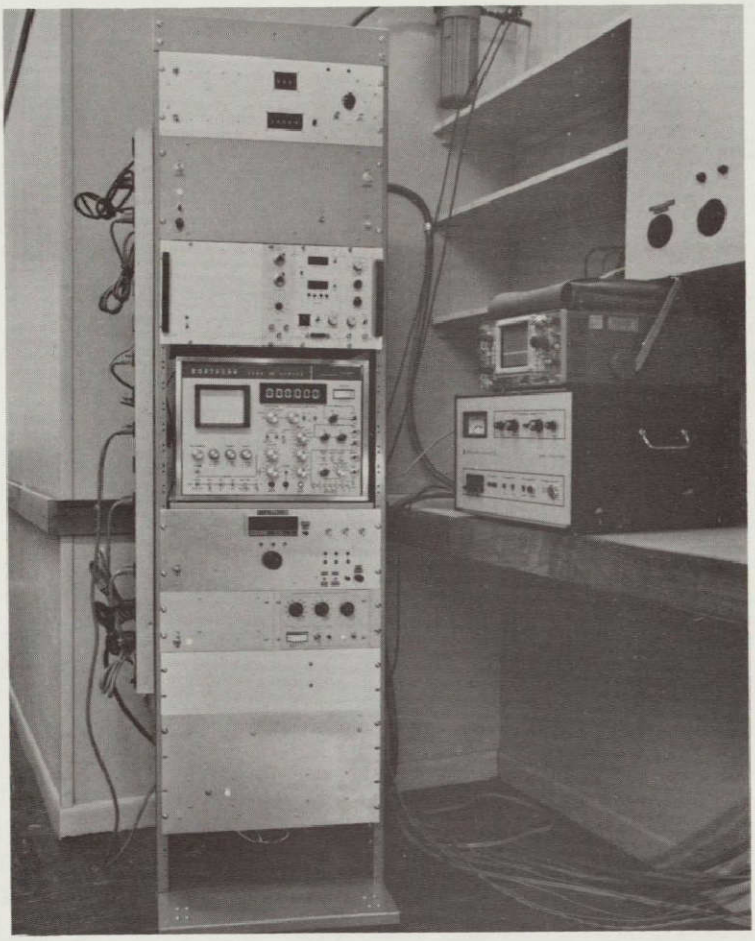

Figure 22. LV System Control and Data Aquisition Console

ORIGINAL PAGE IS
OF POOR QUALITY

INITIAL CALIBRATION TESTS

A series of calibration programs were executed to test out the optical, mechanical, and electronic subsystems, prior to installation in the compressor test facility.

Probe Volume Characteristics. One of the most important measurements needed is the fringe spacing dimension in the interference pattern. From Equation 12, the spacing S_f is a function only of the wave length λ and the crossing angle of the two input beams. If we assume that the spectral line from the laser is precisely known, then we need only determine the intersection angle ϕ. The intersection angle can be measured directly or may be calculated from the known focal length and input beam separation (Reference 21)

$$\phi = 2 \tan^{-1} \frac{S_b}{2f} \tag{28}$$

where S_b is the beam separation, calculated from Equation 18. The lens focal length f was measured by observing the rate at which two parallel input beams diverged beyond the focal point. The input beams were formed by illuminating a plate with two precisely located holes 20 mm apart with an expanded beam from the laser. Using this approach, the focal length has been calculated to be 78.5 mm, with a maximum uncertainty of $\pm$ 0.2 mm. The beam separation, calculated with the as-fabricated dimensions for the splitter and the nominal index of refraction for the glass, gives $S_b = 15.4$ mm. An estimate of the uncertainty on this calculation is $\pm$ 0.05 mm. The beam separation was also measured to be 15.4 mm but the uncertainty in the measurement is about $\pm$ 0.2 mm. Thus the beam intersection angle is 11.2 degrees with a probable error of $\pm$ 0.07 degree. Then, from Equation 12 we can calculate the fringe spacing at $\lambda = 514.5$ nm to be

$$S_f = \frac{514.5 \times 10^{-6}}{2 \times \sin \frac{11.2^\circ}{2}} = 0.002636 \text{ mm}$$

The uncertainty in the fringe spacing is directly proportional to the uncertainty in $\sin(\phi/2)$ since ϕ is assumed to be precisely known. This translates to an uncertainty in the velocity deduced from the measured frequency of $\pm$ 0.7%.

The final calculated probe volume characteristic dimensions are given in Table IV, along with other important characteristic dimensions of the LV system.

TABLE IV. - PROBE VOLUME AND SYSTEM CHARACTERISTIC PARAMETERS

Parameter	Description	Value
D_L	Laser beam diameter at input focusing lens, at the $1/e^2$ relative intensity points	0.875 mm
f	Focal length of input lens	78.5 ± 0.2 mm
f/D_L	"f/number" of input beam and lens	90
ϕ	Beam intersection angle	11.2 ± 0.07 degrees
D_A	Diameter of intersecting beams at focal point of lens	0.0588 mm
ℓ	Probe volume length, intersection length of two cylinders of diameter D_A, at angle ϕ	0.602 mm
w	Probe volume width	0.0581 mm
S_f	Spacing of fringes in probe volume	2.636 μm
N_f	Number of fringes in probe volume width w	22
$\Delta f_D/V_x$	Velocity to frequency conversion factor	0.379 ± 0.003 MHz/(m/s)
λ	Wave length of radiation from laser	514.5 nm
	Probe volume positioning uncertainty	± 0.15 mm and ± 1 degree

Position Indicator Calibration. The linear variable differential transformers (LVDT's) were calibrated for output voltage as a function of relative displacement of the slide and bed for each of the three traversing axes. This was done by coupling the LVDT's to their respective beds and by using the traverse controls and readout to displace the beds. The actual displacement (measured with precision calipers) was plotted as a function of LVDT reading, over the full-rated range of the transducers, 50 mm. The data were fitted to a third degree polynomial using a least-squares curve fitting routine. The maximum uncertainty on any of the transducers was $\pm$ 0.075 mm. A check was also made on repeatability of slide positioning, and this was found to be equivalent to the least count of the digital panel meter used for readout of the LVDT voltage, $\pm$ 0.025 mm.

Electronics Checkout. The main checkout task on the electronics system was to calibrate the doppler frequency processor (DFP) analog reading as a function of input frequency, and the pulse height analyzer channel number as a function of this analog level. These calibrations are shown in Figures 23a and 23b. The parameter n on these curves is the exponent displayed on the processor front panel. This exponent is not output in the analog signal and must be recorded separately for input to the data reduction procedure. The DFP analog display reading (shown in Figure 23a) is not utilized in any of the data reduction since it is only updated about once per second and displays the last valid measurement. It is used only as an indication that the processor is obtaining good, repetitive signals.

Following these preliminary checkouts, the LV system was set up to make measurements in a subsonic jet flow. This test bed was used to become familiar with the operation of the LV apparatus and to experiment with various seed materials and methods. Tests were also conducted to simulate conditions which would be encountered in the compressor, including probing across a 3 mm deep channel and through optical windows.

Free-Jet Tests. One of the first tests run was to measure the transverse velocity profiles in a freely expanding jet, and to compare the results with pitot-static and hot-wire anemometer measurements. The results are plotted as non-dimensionalized velocity U/U_m where U_m is the mass flow averaged velocity at the jet exit plane, as a function of radial position, z/R (Figure 24). As the measurement plane is moved further from the jet exit plane (y/D increasing), the velocity profile becomes more peaked as the jet core begins to dissipate via turbulent mixing.

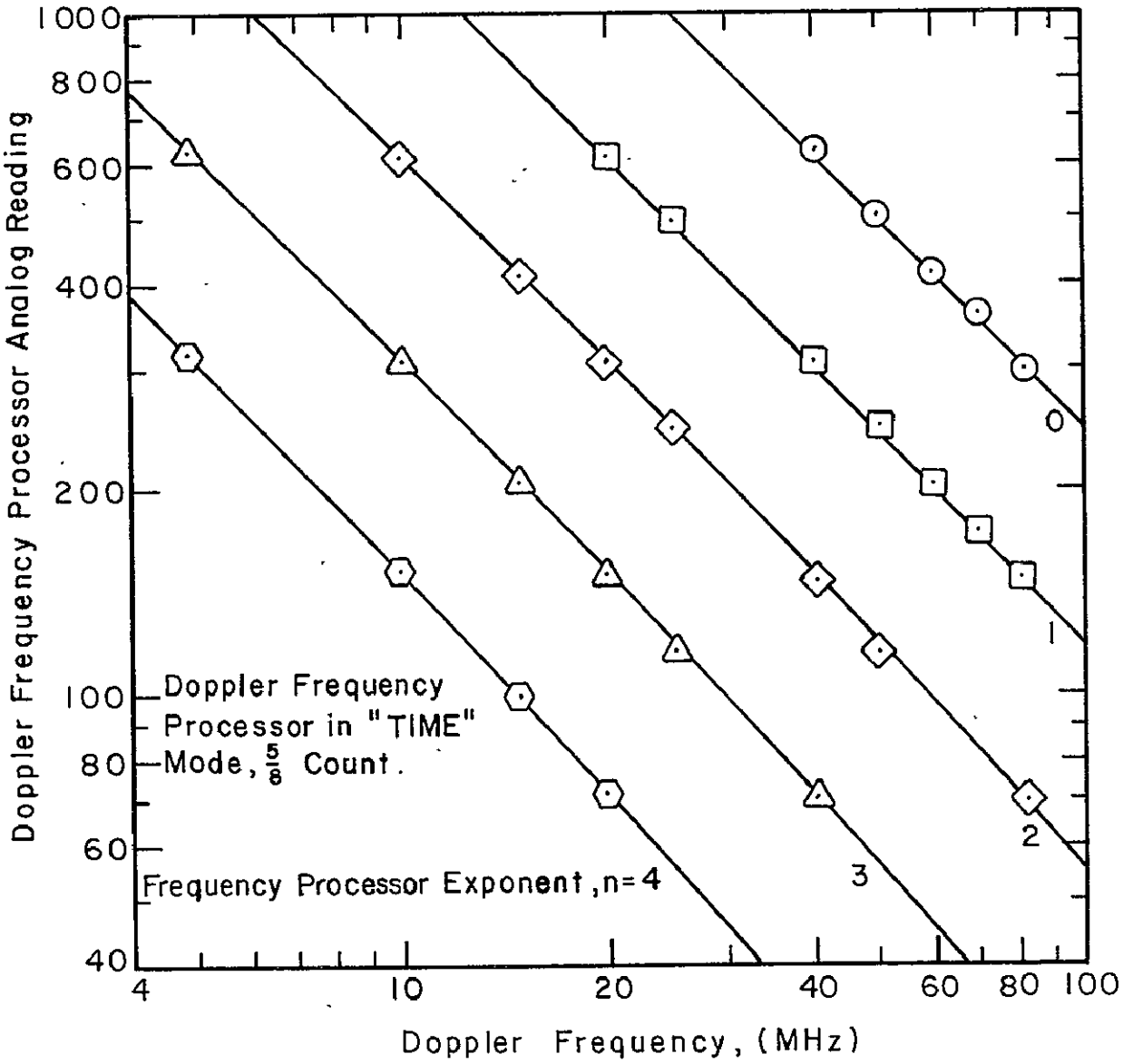

Figure 23 a. Doppler Frequency Processor Analog Display Reading as Function of Doppler Frequency.

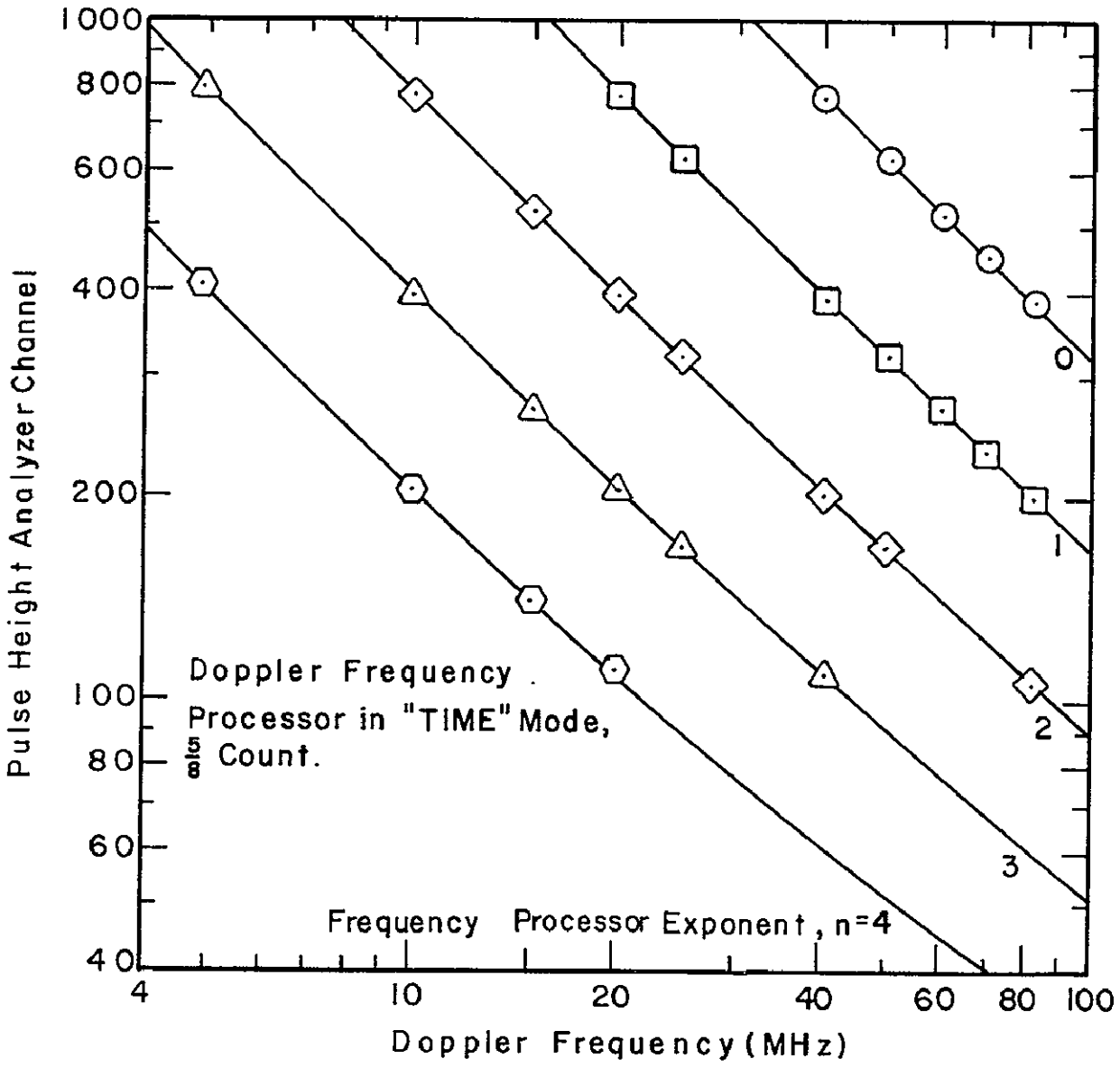

Figure 23b. Pulse Height Analyzer Channel Number as Function of Doppler Frequency.

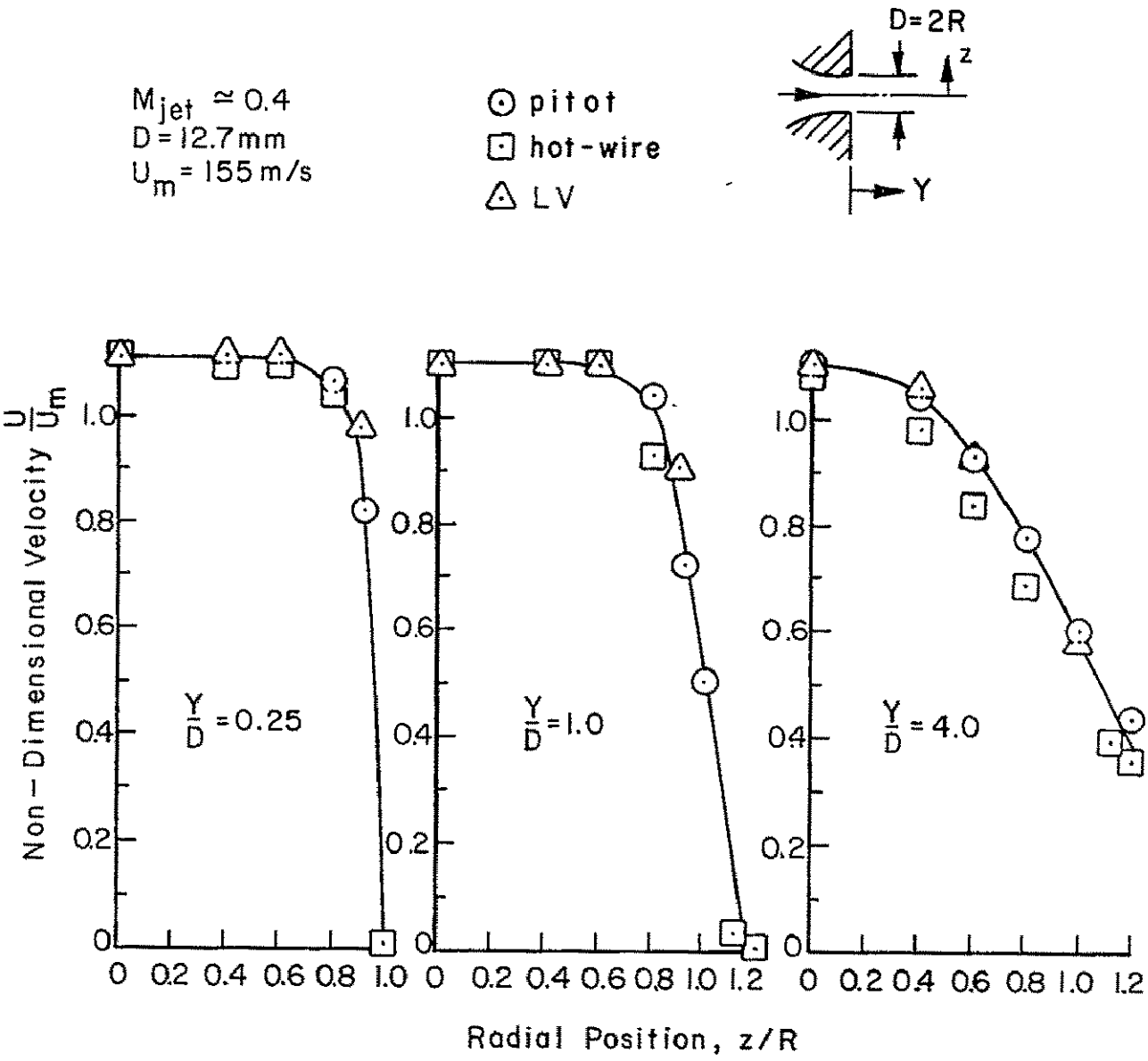

Figure 24. Non-Dimensional Velocity Profiles as Function of Axial and Radial Position in Jet.

The unsteady velocity component is shown in Figure 25, corresponding to the mean velocities in Figure 24. For the LV data, $\overline{(u')^2}$ was taken as the standard deviation of the velocity probability distribution, after having been treated as discussed in the Data Reduction section. In the case of the hot-wire data, the RMS value of the bridge output voltage was used as the fluctuation level.

To further verify the LV performance, a high velocity helium jet was set up. This facility was used to generate velocities to nearly 500 m/s from a jet 3.2 mm in diameter. The probe volume measuring plane was aligned approximately perpendicular to the jet axis to achieve the highest possible frequencies. The maximum frequency measured was 179 MHz, corresponding to a jet velocity of 475 m/s. The calculated velocity, assuming an isentropic core flow from the inlet plenum to the jet exit, was 490 m/s. This is about a 3% difference and may be partially accounted for in misalignment and displacement of the probe volume relative to the jet axis. Figure 26 compares the measured and calculated (isentropic conditions) jet velocities over a range of 100 to 500 m/s for air and helium jets. For the tests above about 200 m/s, the divide-by-two was used to shift the frequency range down to a level compatible with the frequency processor.

Seeding Tests. During the free-jet tests, experience was gained with various seed materials and seeding techniques amenable for application in a closed loop compressor facility.

The first material used was DOP oil (Di-octyl phthalate), dispersed from a battery of Laskin nozzles. The mass mean diameter from the generator is reported by the manufacturer to be around 0.8 μm. Experiments with this seed proved quite successful and the seeding rate was easily controlled.

Alternatives were tried such as silicone oil, dispersed with the same Laskin nozzles, and alumina (Al_2O_3) powder dispersed with fluidized beds and Laskin nozzles. The silicone oil produced essentially the same results as the DOP oil and was considered as a suitable substitute. The alumina, on the other hand, proved somewhat more difficult to disperse and did not produce as narrow a velocity probability distribution as the oils for the same flow situation. This was indicative of a wider distribution of particle sizes for the alumina, possibly due to poor dispersion of the powder particles. Based on these results, the DOP and Laskin nozzle system was the preferred method for seeding the compressor flow.

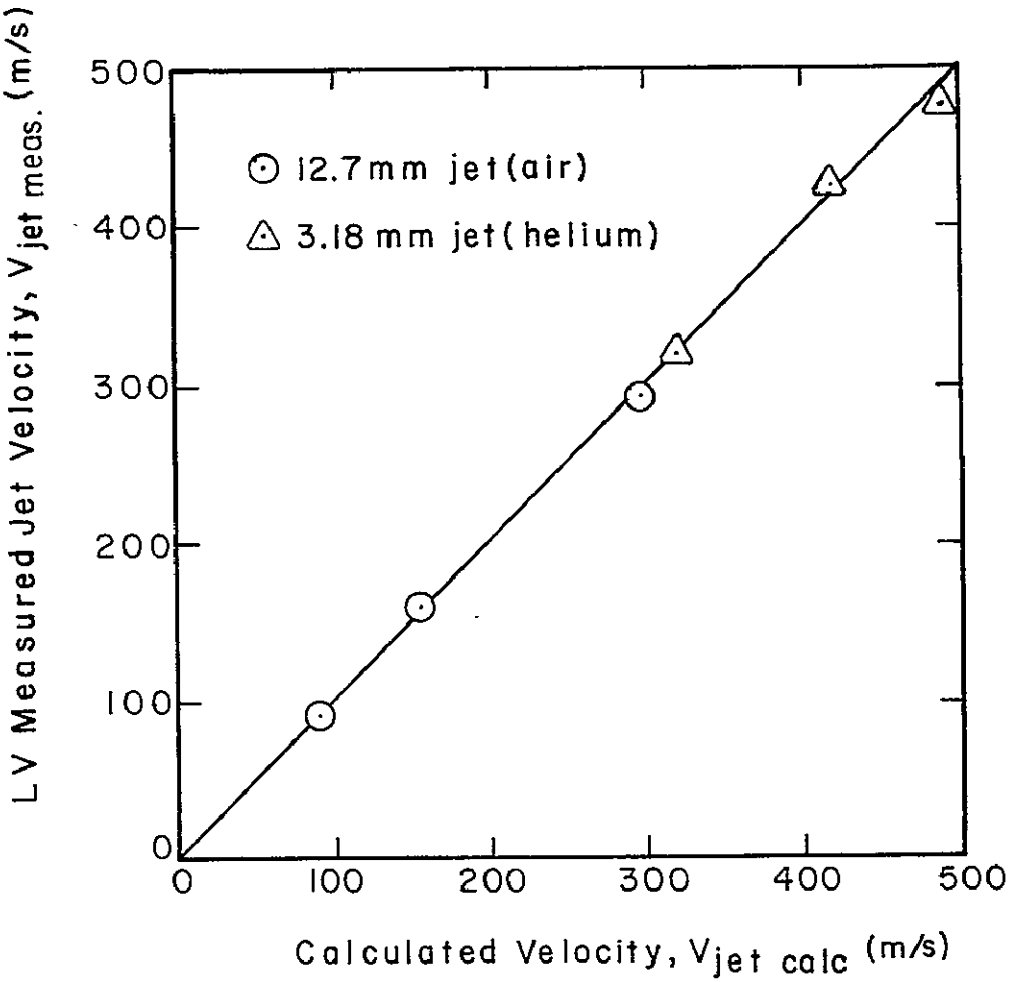

Figure 25. LV Measured Jet Velocity as Function of Calculated Velocity.

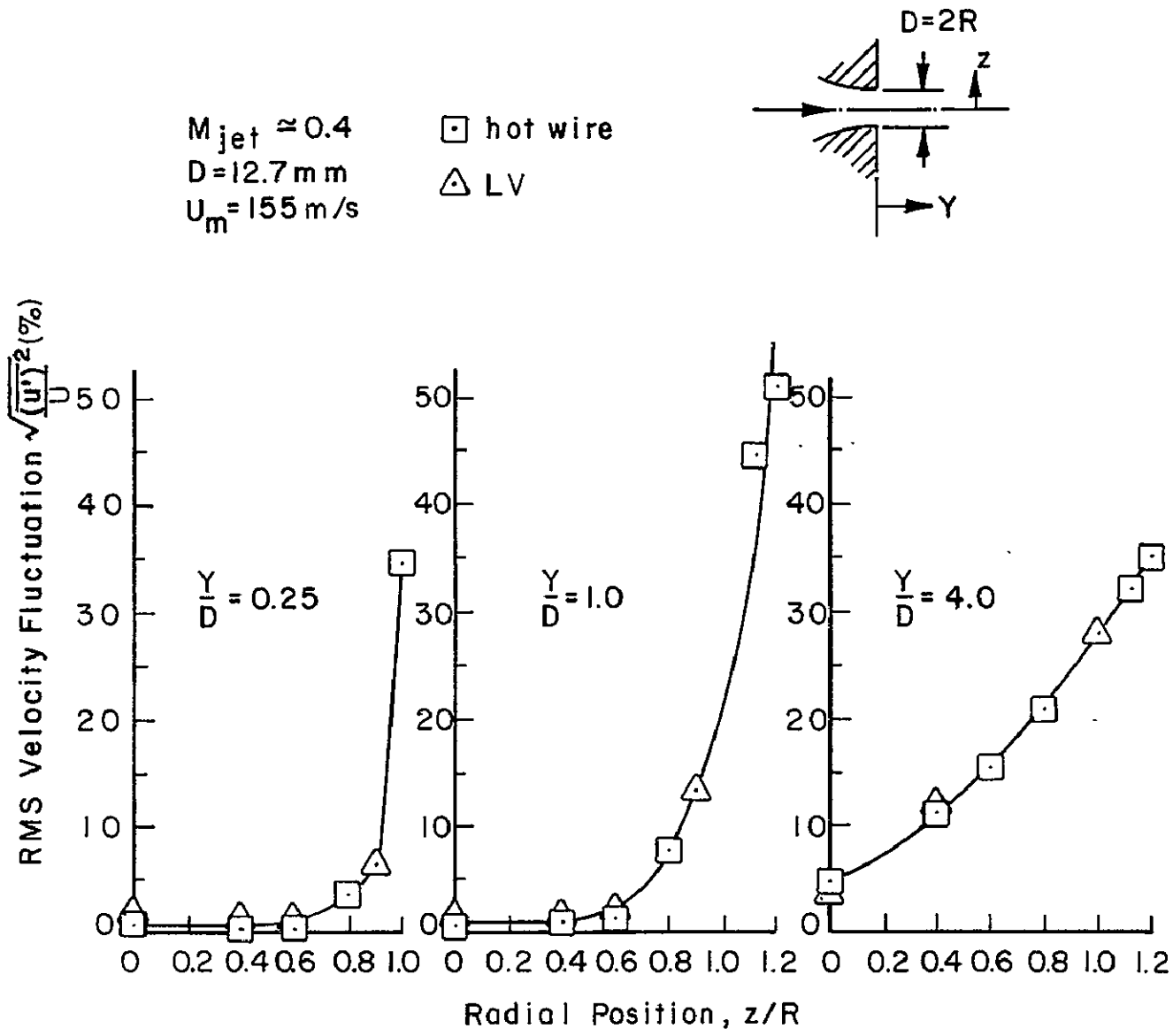

Figure 26. Turbulence Fluctuation in Jet as Function of Axial and Radial Position.

Special tests. Several special tests were set up in the free-jet facility to simulate conditions which might be found in the compressor. These tests all centered around making measurements in a shallow (3 mm) channel with the long dimension of the probe (0.60 mm) lying in this direction. This geometry duplicates that of the difficult to measure impeller tip/diffuser entry region of the compressor.

The first series of tests were to determine if any measurements could be made, or if the background radiation, reflected from the backwall, would completely swamp the signal. It was found that the normal aluminum plate backwall acted as a diffuse reflector and a low signal-to-noise ratio was attained. Special, non-reflective paints were tried, but the background noise still swamped the signal. Some signal was seen, but only at a low level. Signal amplification was tried, but the signal-to-noise ratio was generally too low for good frequency processing.

In order to combat the diffuse scatter from the backwall, a first surface reflector was substituted for the metal plate. Using this approach, the reflected beams coming from the backwall were masked off ahead of the photomultiplier. Improved signal quality was achieved, and at a processible level. However, over time the front window became contaminated with seed (oil or alumina powder) producing diffuse light scatter and the signal quality deteriorated.

Further experimentation with the reflective backwall led to attempts to utilize the forward-scattered radiation reflected backward to the optical train. These tests were quite successful resulting in signal amplitudes in excess of 500 mv at a laser input power of 100 mW and less; these levels being approximately an order of magnitude higher than similar conditions in backscatter operations. In addition, a high signal level and relatively low noise were maintained even with a light oil contamination on both the mirror and window. Attempts to use alumina in this application were not as rewarding. After a short period of operation, the alumina would coat both optical surfaces and degrade the signal.

These special tests concluded the preliminary checkout phase. The next task was to install the LV apparatus in the low speed modeling compressor test facility, and make velocity measurements in the compressor.

LV CHECKOUT USING THE COMPRESSOR

Following the installation and alignment of the LV in the compressor test facility, a series of checkout tests were conducted to prove the feasibility of velocity measurements in the compressor.

Seeding System Modification. The first of these tests included repeated measurements of velocities in the inlet duct, inducer, and diffuser regions. Only very limited success was achieved; low data rates and poor signal quality occurred after short periods of operation. Although the bench tests had indicated that a thin film of liquid on the optical windows did not seriously detract from the signal, in the compressor geometry the liquid film was sufficiently disturbed by the aerodynamics of the flow to make the use of a liquid seed material unsuitable for use in this test facility.

Having had some success with alumina in the earlier free jet tests, it was decided to try using this dry seed material. The main problem encountered was the inability to de-agglomerate and disperse the powder before injection to the inlet plenum. Also, it was found that injection into the inlet plenum resulted in a very uniform distribution of seed throughout the compressor inlet. This uniform distribution implied a need for a high total seed flow rate to achieve adequate seed density (number of particles per unit volume of gas) at the desired measurement location.

These observations eventually led to the use of a silica-coated, alumina particle for the seed, prepared by Micro Abrasives Corporation. The number mean diameter of the powder is about 0.75 μm. Dispersion of this seed is accomplished in a very simple fluidized bed, with an air-driven vibrator to prevent bed channeling. The transport fluid is LSM gas, taken from a high pressure point in the closed-loop test facility.

Injection of the seed is done by means of a lance in the plenum which is traversable in the circumferential direction to permit feeding the seed only at specified circumferential locations, Figure 27. The lance, support and rotating mechanism are located in the plenum where the throughflow velocities are expected to be less than 1 m/s, producing a minimum of disturbance to the inlet flow. Further, the flow rate of seeding gas is expected to be less than 0.1% of the compressor design of 1.17 kg/s of LSM gas.

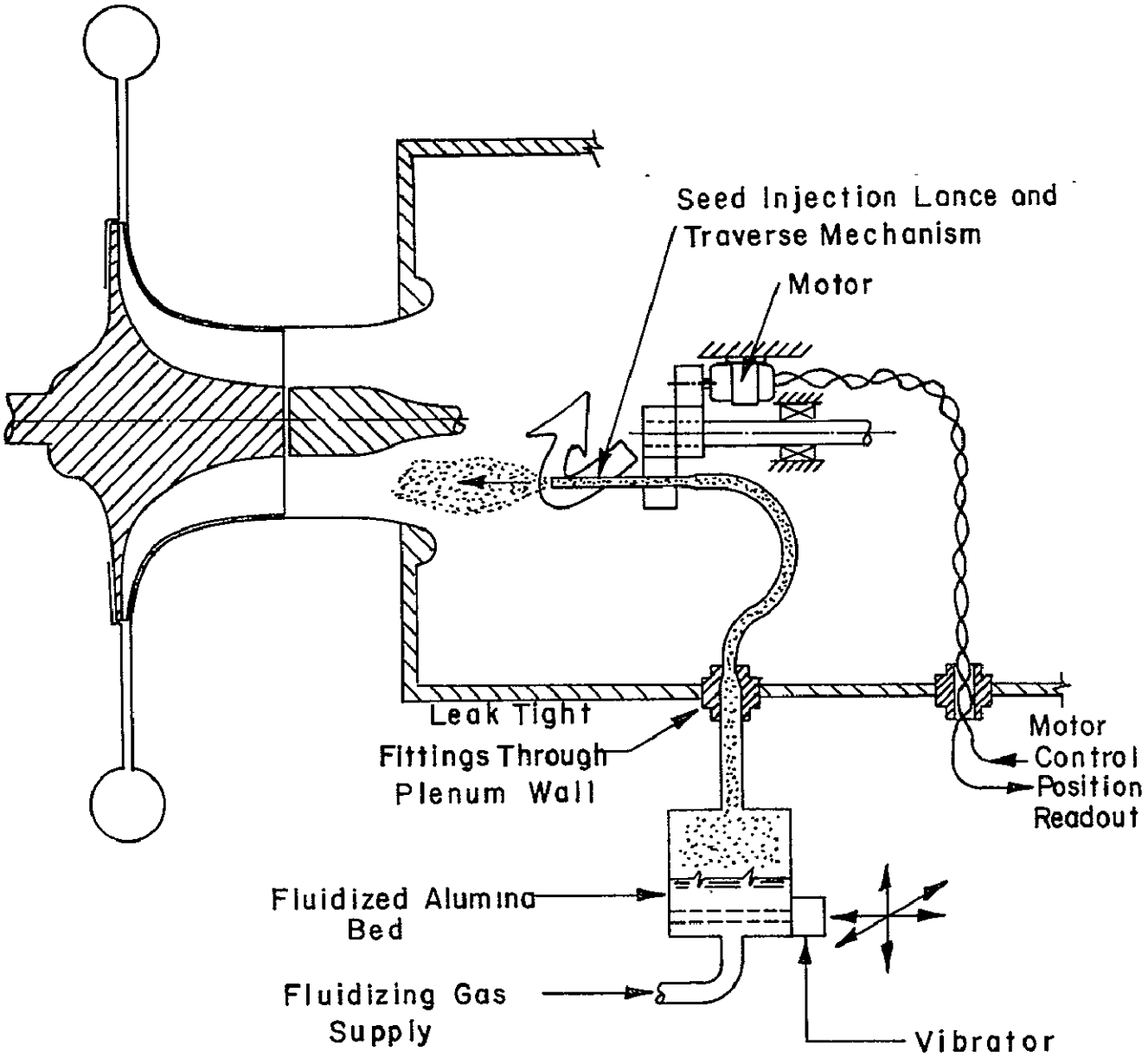

Figure 27. Compressor Plenum Seeding System

This improved seed dispersion method and seed injection technique were then used to make some velocity measurements within the inlet and inducer regions of the compressor. The results of these measurements are discussed in the section on LV data.

We believe the problem of poor signal quality in the diffuser was caused primarily by a high background noise relative to the signal. A solution to this problem was sought by utilizing the forward-scattered light from the probe volume and reflecting it from a first surface mirror on the diffuser channel backwall. This approach had been successfully developed in the free jet tests and some of the same concepts were adopted here. Details of this technique are presented in the section on optics design.

A chrome-plated brass plug, embedded in the diffuser backwall and flush with the surface, served as the first surface mirror. Using this plug mirror, LV measurements in the diffuser became possible. The technique produced a very high quality signal, even at low laser power. Data rates were higher than in the inlet/inducer region. The results of the limited measurements made in the diffuser region are summarized in the data section. After this initial success, a large mirror, covering the region from the impeller discharge radius out to one of the channel diffuser throats and spanning the diffuser passage width, was installed (Figure 28).

Using this mode to make measurements in the diffuser region the optical system is thus slightly modified from a pure backscatter mode of operation. In order to capture this forward-scattered/backward-reflected radiation, the collecting optics must focus on the virtual image of the probe volume "inside" the rear diffuser wall. This is accomplished by adjusting only the final collecting lens as discussed in the section on optical system design.

A major implication of this approach is that for the best signal-to-noise ratio the collecting lens should be refocused each time the probe volume is displaced axially in the diffuser channel depth. However, through experimentation it was found possible to maintain high data rates for a large displacement of the probe volume, $\sim$ 1.5 mm, which is approximately one-half of the channel depth, without readjustment of the collecting lens. Thus the approach used for taking data in the diffuser region was to fix the axial depth of the probe volume and make a complete survey of all the desired velocity locations in a radial plane.

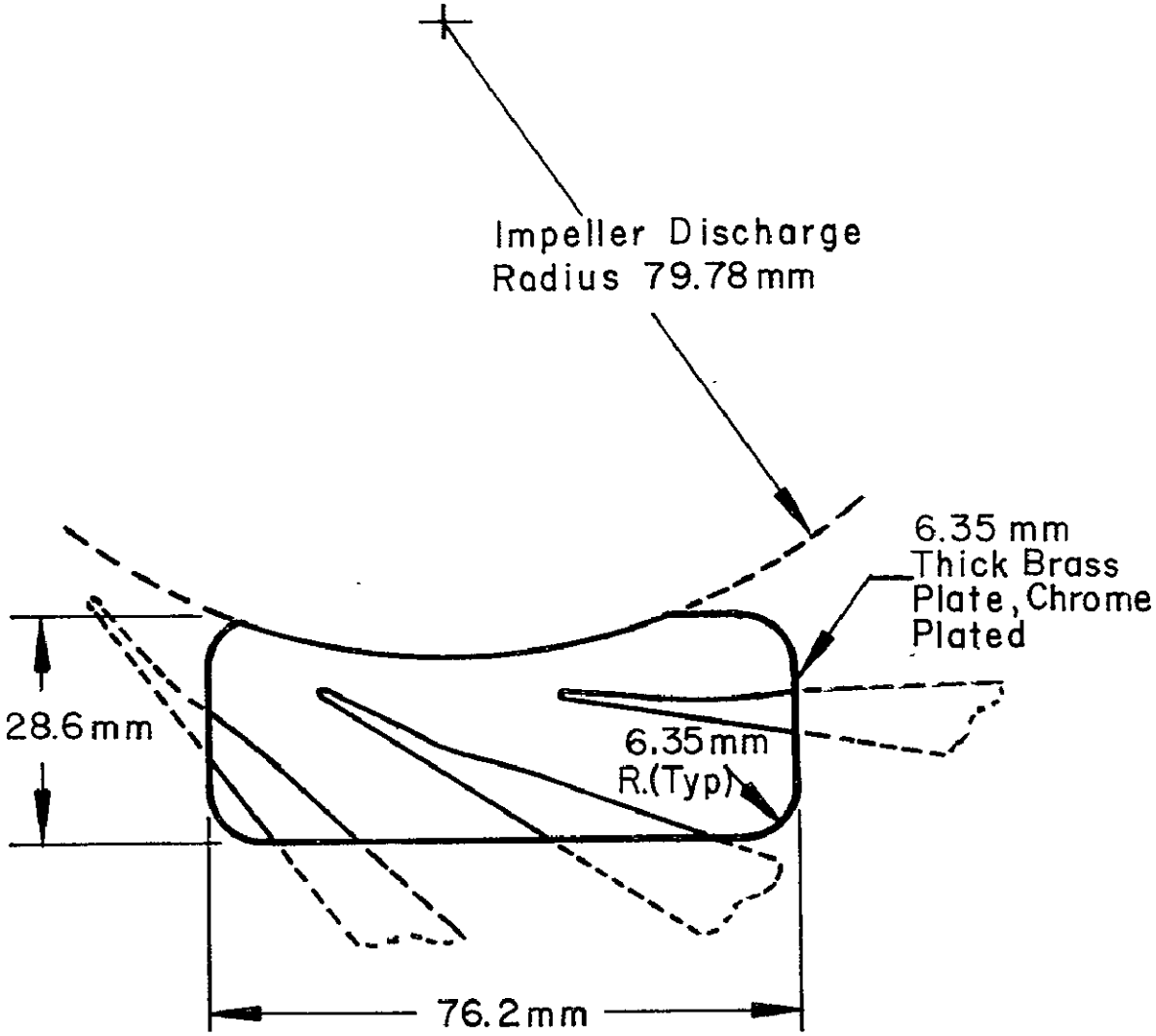

Figure 28. Diffuser Backwall Mirror

One other significant requirement for the use of this back-reflected mode of operation is that the reflecting mirror must be maintained perpendicular to the optical axis of the input beams. This implies that the entire diffuser backwall be aligned and maintained in an orientation perpendicular to the optical axis.

It was found during the development of the back-reflected mode of operation that for certain locations of the probe volume in the diffuser depth, the backward reflected portion of the input beams intersect the collecting mirror and reflect these beams as spots of light into the light collection telescope. This requires that a mask be placed ahead of the collecting lens to prevent these spots from reaching the photomultiplier tube and swamping the desired signal with noise.

Other Operating Experience. After these preliminary tests were completed, a modest test program was defined to measure velocity profiles in the inlet/inducer and in the impeller discharge region at several axial and radial planes, respectively. These results were to be the forerunner of a much larger scale test program to provide detailed velocity data for use in developing better design tools for the design and development of advanced centrifugal compressors. The objectives of this more modest program were to help develop estimates of the time and cost commitments required to provide realistic velocity data, and to develop methods for improved data acquisition rates whenever possible.

Repeated attempts to make velocity measurements were continually frustrated by operating problems:

- low and erratic data rates,
- dirty windows,
- optical system misalignments,
- component failures.

Details of these problems are discussed below.

The seeding system received considerable attention in attempts to obtain and maintain high seed densities which would lead to high data rates. It was found that the data rate obtained in free-jet tests with fresh seed in the fluidized bed were high, but after short periods of time, (order of one to several minutes of continued operation), the rate would rapidly decrease. Then, if the seed supply were turned off for approximately 10 to 15 minutes, the rate would recover, at least initially, to or near the initial value.

However, continued operation with the same seed material in the fluidized bed, even with on/off cycling, will eventually result in a continual decrease in seed rate as evidenced by a decrease in the validated data rate on the frequency processor.

These symptoms indicate several possible phenomena are taking place. The decay in the data rate following the initial turn-on is believed due to a depletion of the smallest particles, which in fact make up the greatest number of particles in the seed bed. Also, visual examination of the material in the seed bed indicates agglomeration of the particles, possibly due to electrostatic effects. The triboelectric charging of small particles in fluidized beds is a well known phenomenon, although little understood, and methods to eliminate the effect are not well defined. During long periods of operation, a film of particles collects upon the walls of the fluidized bed (an acrylic tube). If a grounded conductor is brought into contact with the outer wall of the bed, a large fraction of the particles are seen to "jump" away from the wall and fall to the bed. The recovery of the data rate following an "off" cycle is thought to be due to a partial deagglomeration of particles resulting from electrical charge leakage to ground.

The long-term degradation of seed rate (and hence data rate) is thought to be the result of an irreversibility in the agglomeration of seed material within the bed, and eventual depletion of those particles which can be transported out of the bed and can be used for obtaining a processible signal.

Means to circumvent this seeding problem were sought, and a modification to the seeding system and operation of the seeding system tried. The modification incorporates a bank of four identically constructed seed beds operating with two in parallel at any time. By running the two pairs of beds in a cyclic fashion, some of the problems discussed above are expected to be partially mitigated. The argument here is that two beds in parallel will give a higher seed density without increasing the gas through flow velocity, which would cause the large particles to be transported out of the bed and also must be matched to the seed lance flow to produce the correct velocity in the compressor inlet region. Also with the two sets of beds available for cyclic operation, the experience of recovered data rate following a short "off" period should be obtained.

Another seed system problem encountered was the build up of seed material within the flexible tubing leading from the seed "beds" to the injection system. A large fraction of the seed material transported from the bed becomes lodged on the walls of the tubing significantly reducing the amount of seed material which is actually injected at the compressor inlet.

This problem was minimized by eliminating unnecessary tubing and piping connections (abrupt area changes) and reducing the length of the remaining tubing to as short a length as possible.

Dirtying of the inducer and diffuser windows occurred under certain operating conditions. The inducer window would often show a band of collected seed material on its surface just ahead of the impeller inlet when the compressor was operated at an off-design condition. This is due to the presence of an inlet tip flow separation that causes backflow from the impeller inlet tip region and deposition of seed particles in the backflow recirculation zone. Evidence of this tip separation is also obtained from the impeller cover static pressure measurements whereby the pressure taps at and immediately ahead of the impeller lead edge indicate a static pressure higher than the inlet total pressure, at off-design conditions. Inducer backflow caused by the inducer tip separation is a well known phenomenon.

The diffuser window and the diffuser backwall mirror can become dirty with seed materials whenever lubricating oil from the high speed gearbox leaks past the shaft seal and drains onto the diffuser front and backwall surfaces. This leakage sometimes occurred during a surge cycle when the system pressure rapidly changed and a pressure imbalance existed across the shaft seal.

These two problems (one in the inducer and one in the diffuser) were corrected by establishing changes in operating procedures. The inducer window is kept clean by operating with seed material only when at flow rates which do not result in the inducer tip separation. In the case of the oil leakage, an improved drain system was provided to positively drain any oil (which does leak past the shaft seal) from out of the cavity behind the impeller; this prevents oil from finding its way into the diffuser region. By these methods, even after long periods (4 to 6 hours) of heavy seeding in the compressor, only a very thin film of material would build up on the windows. By conducting "benchtop" tests simulating these dirty window conditions, it was found that the thin film did not measurably affect the data rate in either the backscattered or back reflected modes of operation.

Some effort was put into testing a window washing scheme to be used in place in the compressor. The only alternative is to remove the windows regularly for cleaning and this results in a loss of modeling gas from the compressor facility and an interruption of several days for preparation of the test rig. This window washing scheme involved injection of a solvent

(we tried alcohol, several liquid freon compounds and acetone) upstream of the windows with the concept that solvent would loosen the particle-to-window bond and float the seed material out of the measurement region before the solvent evaporated. In practice the injection of the solvents seemed to have no discernable effect on window cleanliness. In fact, the only way we found to clean these windows was to remove them from the covers and wipe the dirt off with solvent moistened lint-free tissues. We have had insufficient operating experience to project the length of time or seeding conditions which will markedly reduce signal quality due to dirtying of the windows.

During the long course of attempts to make some basic velocity measurements in the compressor facility, several elements of the optical system required adjustment and realignment. Sometimes optics misalignment problems were not detected until considerable effort had been expended in seeking other answers to data acquisition problems. One major component problem has been the shifting of the compressor support hardware relative to the input beam axis resulting in a misalignment of the back reflecting mirror in the diffuser during diffuser measurements. This problem was at least partially solved by eliminating the strain producing piping elements connected to the compressor and providing additional support for the compressor assembly. One area that could not be thoroughly addressed was the possible thermal distortion of the diffuser backwall and mirror interface. Although there is no evidence to indicate that this does happen, it remains a concern for any future application of this LV system.

At one point in the program the beam splitter cube became loose in its mounting, resulting in a nonuniformity in the beam split (that was also nonrepeatable, thus making it difficult to find the problem). The solution was to add rubber padding to the mounting and an adhesive to better secure the cube in its holder.

One final optical system problem that may have been responsible for many of our problems in acquiring data in any of the gated or synchronized modes was the acoustic optic (A/O) modulator. Only at the very end of the test program was it discovered that the drive frequency for the modulator was not constant when the duty cycle of the gate signal applied to the A/O crystal was changed. For continuous gating, the RF signal to the A/O crystal was about 39.5 MHz, but when operated at a lower duty cycle, e.g., 5% blade pitch, the frequency would shift slowly to about 40 MHz. This change in RF frequency translates to a shift in beam position at the face of the splitter cube equivalent to approximately 20% of the beam radius. This translation causes a very nonuniform split between beams in the gated

mode, resulting in poor signal quality and an increase in the base noise due to stray radiation entering the collecting telescope. When this problem was discovered and pointed out to the manufacturer, they offered to repair the circuitry by replacing the LC oscillator with a crystal-control oscillator. This was done and the RF signal to the A/O modulator head was found to be constant at any duty cycle. However, there is still some deflection of the beam evident when switching from high to low duty cycles. After conferring with the manufacturer, we can only conclude that the high duty cycle is causing some thermal distortion to the crystal or its mounting structure. At this time the problem has not been resolved satisfactorily. It has in fact prevented the acquisition of LV data and must be solved if any future work is to be done using the gating approach.

At one time or another, during this program, most of the other major components in the data acquisition system have suffered failures. This point is mentioned only as a reminder that LV systems utilize many sophisticated optical and electronic devices which, even with normal use and maintenance, do fail. Some of the specific items and problems caused by component failure are mentioned below:

1. Laser:
   - cracked plasma tube on initial shipment
   - corroded cooling water connection on plasma tube causing power supply short and plasma tube damage
2. Pulse Height Analyzer:
   - defective gain control on the display
   - defective memory control circuit
3. Photomultiplier Tube:
   - failure of dynode chain
4. Acoustic Optic Modulator:
   - cracked acoustic crystal
   - short circuit in power supply
   - fluctuating RF power frequency
   - thermal distortion of acoustic crystal

In a related vein, there are certain elements in the optical system that if replaced would result in a better overall system, less susceptible to some of the problems encountered on this program. These are:

1. Beam Steering Mechanism. This device has not been a great problem as much as it is inconvenient to use. A more robust device, using a different approach on adjustment and pivoting could be incorporated.

2. Beam Splitting Prism. The edge type splitter requires too precise an alignment of the input beam and the defraction of the beam gives a somewhat distorted shape. This might be replaced with a Koester-type prism which uses internal reflection and coated surface to effect the split and is not subject to the problem of input beam alignment.

3. Beam Directing Prism. This prism produces a translation and rotation of the optical access in the periscope using internal reflections. However, the first surface reflections sometimes result in high noise levels reaching the photomultiplier tube. This device could be replaced with two mirrors set in a precisely machined support block.

4. Collecting Mirror. This mirror is now only 12.7 mm in diameter and it collects about 40% of the scattered radiation transmitted back from the input lens. A new mirror should be designed which collects a larger fraction of the available signal without interfering with the rotation of the input beams into any plane.

Finally, in the area of recommendations for modifications to this LV system, the data acquisition method could be improved. Instead of gating the laser to acquire data only for synchronous impeller positions, the approach should be to leave the laser on for the full impeller passage width and store all the velocity data whenever it occurs, along with a blade position signal. This approach will greatly reduce the total data acquisition time; however, it does require interfacing the output of the frequency processor with a minicomputer (or other computer backup) and possibly a buffered input device if high data rates are achieved.

The final section of this part of the report displays the limited LV data and contains our suggestions and recommendations for future applications of the LV apparatus in centrifugal compressor research work.

INDUCER AND DIFFUSER LV MEASUREMENTS

Test Data. The test program of limited scope and duration discussed above was undertaken to prove out the operation of all of the equipment under realistic compressor test conditions. Velocity measurements were made in the inlet/inducer region and in the diffuser entry region at compressor rotational speeds from 40 to 80% of design, in air and low-speed-of-sound modeling gas (30,000 to 43,000 RPM actual).

The data from the inlet region were acquired using the straight backscatter mode, while that from the diffuser entry region was taken with the back-reflected, forward-scatter mode of operation.

The results of these tests are shown in Figure 29, Parts a through r, as velocity histograms, photographed directly from the pulse height analyzer CRT display. The abscissa is a channel number (1024 full scale) corresponding to the time period for a velocity measurement (inversely proportional to velocity) while the ordinate shows the number of occurrences at each channel. Figures 29a through 29g are from the inlet/inducer tests, 29h through 29r are from the diffuser entry region tests. Tables V, VI, and VII provide a key to these data photographs, including pertinent probe volume location and data gating parameters.

Discussion. The velocity tabulated is based on the peak channel in the histograms shown, not from a calculated statistical average. For the data in Figures 29g and 29o, the mean velocity was also calculated via the data reduction program discussed in an earlier section of this report. In the case of Figure 29g, the corrected statistical mean velocity is 63.5 m/s, very close to the 64 m/s shown in Table V deduced from the peak channel reading. This seems reasonable since the RMS fluctuation is quite small (4.9 m/s) resulting in a very narrow velocity distribution (see Photo g in Figure 29).

On the other hand, the distribution in Figure 29o has a mean velocity of 90.5 m/s compared with the peak channel value of 101 m/s in Table VI as deduced from the peak channel reading. This large discrepancy is more easily understood by examining the actual distribution in Photo o of Figure 29. It can be seen that there is a second minor peak to the distribution which was not considered in the peak channel calculation, but which is included in the computer data reduction scheme that calculates the statistical average velocity. However, applying the data reduction program to data in the first quadrant of the histogram only, the statistical mean velocity is 103.9 m/s, much closer to the peak channel

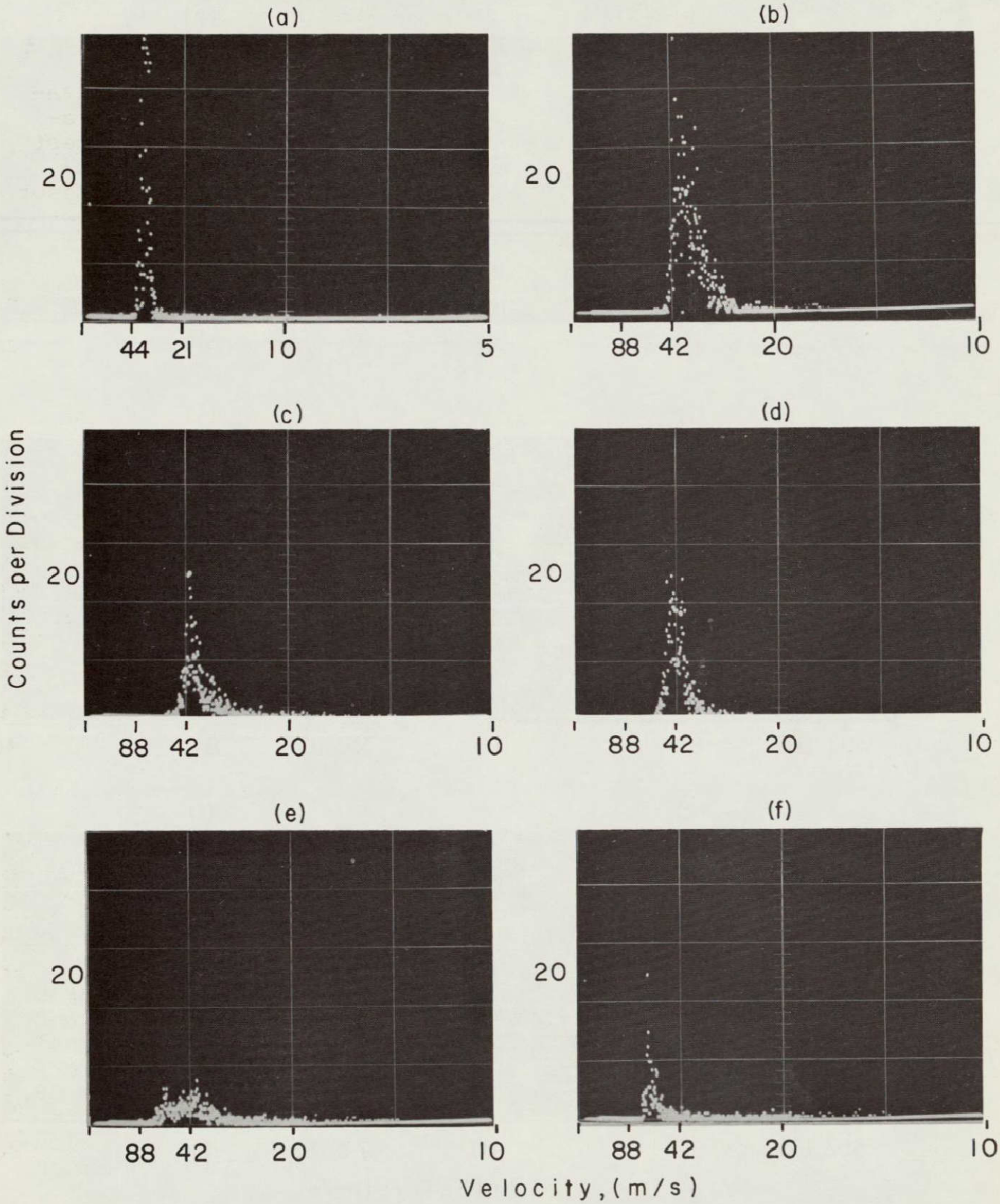

Figure 29. Velocity Histograms from Pulse Height Analyzer

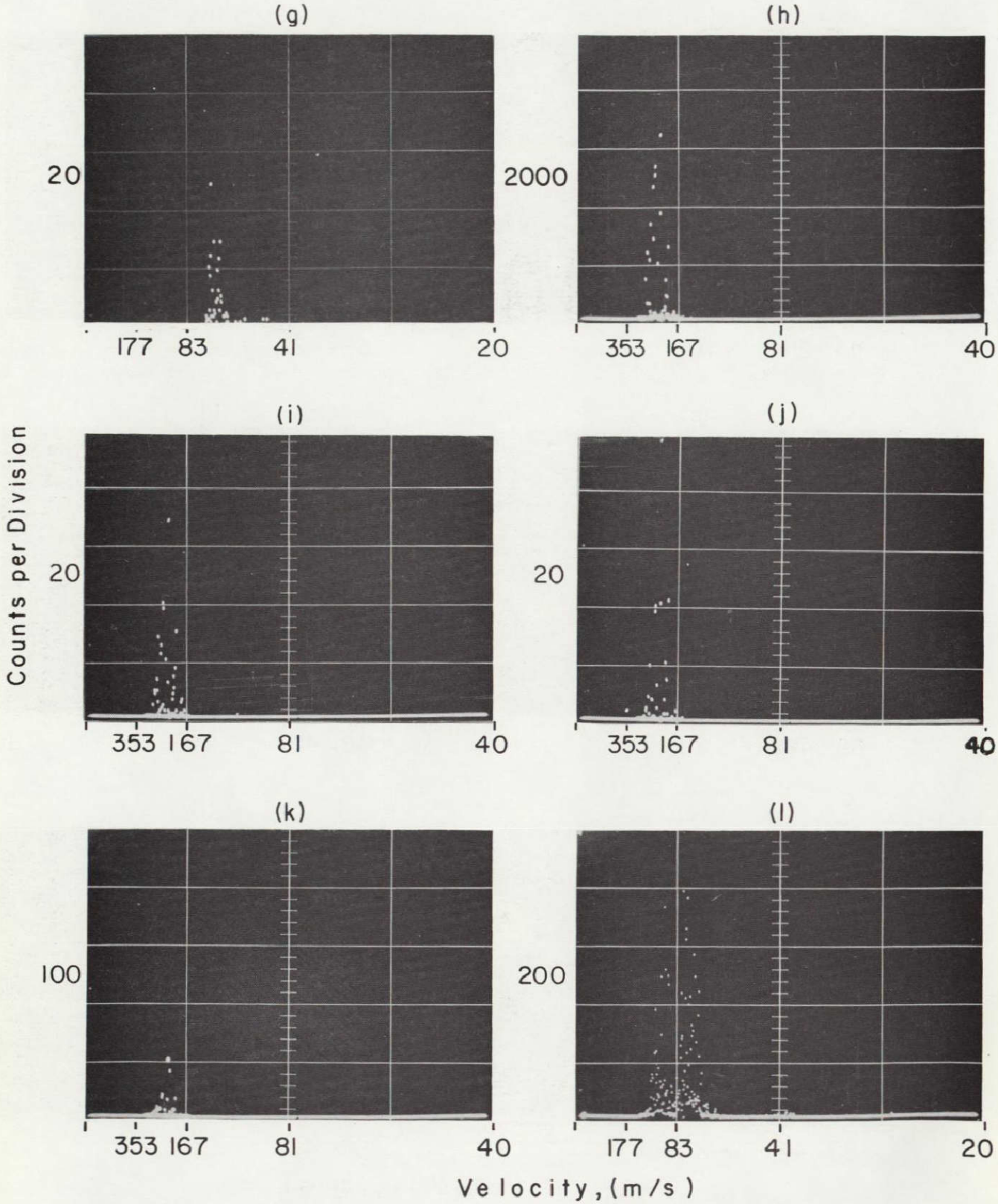

Figure 29. Velocity Histograms from Pulse Height Analyzer

ORIGINAL PAGE IS
OF POOR QUALITY

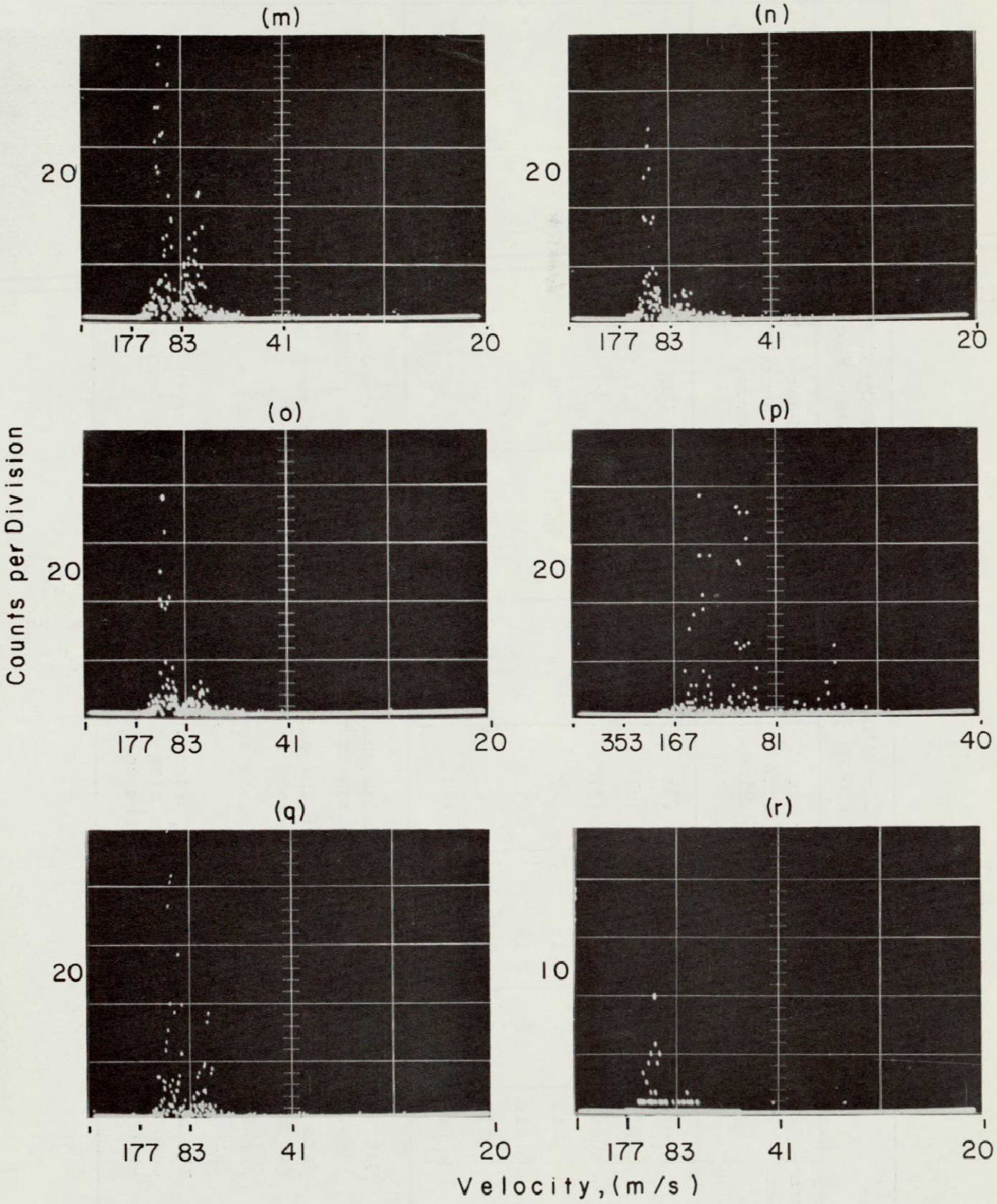

Figure 29. Velocity Histograms from Pulse Height Analyzer

TABLE V. - INLET/INDUCER LV MEASUREMENTS
(Reference: Pulse Height Analyzer Photos - Figure 29)

Figure Number	Gas	Speed (%N_D)	Gate[1] Position (%blade pitch)	Gate[2] Width (%blade pitch)	Measure-ment Plane[4]	Peak Channel Velocity (m/s)	Peak Channel Counts	Total Integrated Counts	Sample Time (seconds)
a	Air	40	NA	(3)	1	33.2	100	2938	39
b	Air	40	NA	(3)	1	36.1	100	3718	20
c	Air	40	NA	(3)	2	38.1	50	1536	356
d	Air	40	19	22	1	42.0	50	2071	172
e	Air	40	19	22	2	36.9	15	939	500
f	Air	40	32	22	1	60.3	50	634	248
g	Air	40	30	22	1	64.0	50	393	204

Notes:

(1) Gate position is the location at which the data acquisition is opened. For the inlet/inducer data, it is a percentage of blade pitch, following the blade suction surface.

(2) Gate width is the duration of the data gate. It is expressed as a percentage of blade pitch rotation for the inlet/inducer data.

(3) For indicated data sets, the data acquisition system was run in continuous mode, i.e., for a time-averaging mode.

(4) The measurement plane is the orientation of the probe volume with respect to the compressor hardware. The two planes '1' and '2' are mutually perpendicular and are each $\pm$ 45 degrees to the compressor centerline.

velocity of 101 m/s. The RMS fluctuation around this mean is 7.1 m/s, while for the whole distribution it is about 17 m/s.

A more detailed examination of Table VI and the corresponding velocity histograms shows a trend of decreasing amplitude of the second (lower velocity) peak as the gate width is reduced. This is especially true for the C_1 measurement, Figures 29ℓ, m, n, and o.

These double peaks are believed to be associated with the fluid dynamics of the flow in this region* and are the results of the time averaging of the velocity measurements in this region over a large percentage of the impeller blade pitch rotation. The data clearly show that as the gate width is reduced from a time-averaging mode to a minimum of 5.6% of impeller blade pitch change (rotation), less of the minor velocity peak is seen by the data storage system.

Table VII displays the deduced absolute and relative velocity measured ahead of and within the axial portion of the impeller.

Figure 30 shows the velocity vector diagram and the deduced velocity for a measurement point near the middle of the diffuser throat and approximately at mid-depth in the diffuser channel. The data indicated in Figure 30 are taken from Figures 29k and 29o which are for the LV beam positions 2 and 1, respectively. The gate position was at 50% of diffuser vane pitch as indicated in Figure 30. The gate width of 5% and other pertinent data for these photos are given in Table VI.

The direction of the C_2 vector is quite obvious; however, the C_1 vector could conceivably have either orientation shown because of directional ambiguity in the LV system. We believe that the solid line version is the correct direction for the C_1 vector. This direction is deduced from the fact that the 'dashed' C vector, shown in Figure 30, would provide too low a velocity component normal to the diffuser throat compared to the average velocity calculated from a mass flow continuity check at the conditions tested. While the solid vector implies a component directed along the channel centerline of approximately 218 m/s, which is slightly high compared to the calculated continuity velocity, this is not unreasonable considering

*The multiple peak histogram could be the result of an unmixed wake-jet flow pattern from the impeller blade passage passing through the diffuser inlet region. Any "explanation" of the double velocity peaks could be purely conjecture at this time and further measurements will be required to explain them in detail.

TABLE VI. - DIFFUSER REGION LV MEASUREMENTS
(Reference: Pulse Height Analyzer Photos - Figure 29)

Figure Number	Gas	Speed (%N_D)	Impeller Tip Velocity (m/s)	Gate[1] Position (% vane pitch)	Gate[2] Position (% vane pitch)	Measure-ment[4] Plane	Peak Channel Velocity (m/s)	Peak Channel Counts	Total Integrated Counts	Sample Time (s)
h	Air	40	251	NA	(3)	2	189	10,000	60,104	17
i	Air	40	251	50	50	2	189	100	522	25
j	Air	40	251	50	10	2	189	100	481	161
k	Air	40	251	50	5	2	193	100	457	224
l	Air	40	251	NA	(3)	1	73	1,000	20,982	92
m	Air	40	251	50	50	1	93	100	2,092	177
n	Air	40	251	50	10	1	101	100	913	184
o	Air	40	251	50	5	1	101	100	974	317
p	LSM	80	356	NA	(3)	1	115	100	1,297	25
q	LSM	65	285	NA	(3)	1	101	100	6,530	9
r	LSM	65	285	50	5	1	101	12	96	173

Notes:

(1) Gate position is location of impeller relative to diffuser lead edge at which data gate is opened. See Figure 30.

(2) Gate width is duration of data gate, expressed as a percentage of blade rotation relative to diffuser vane tips for the diffuser data.

(3) For indicated data sets, the data acquisition system was run in a continuous mode, i.e., a time-averaging mode.

(4) Measurement plane is the orientation of the probe volume with respect to the compressor. See Figure 30.

TABLE VII. - DEDUCED ABSOLUTE AND RELATIVE VELOCITIES FROM INDUCER LV MEASUREMENTS[1]

Figure Number	x[2] (mm)	R (% span from hub)	C_1 (m/s)	C_2 (m/s)	C (m/s)	α (deg)	u (m/s)	W (m/s)	β (deg)	M_{rel}[3]
a	-3.18	27	33.2	33.2[4]	46.9	0[4]	85.7	97.9	-61.3	0.28
b&c	0.00	20	36.1	38.1	52.5	-1.5	80.9	97.5	-57	0.28
d&e	0.99	20	42	36.9	56	3.6	80.9	95.2	-55.4	0.276

Notes:
(1) Reference: pulse height analyzer photos--Figures 29a through 29e and Table V.
(2) Axial location relative to inducer lead edge.
(3) Relative Mach number is defined here, based on inlet stagnation conditions.
(4) C_2 not measured, assumed same as C_1 for this data set, hence $\alpha = 0$.

TABLE VIII. - DEDUCED ABSOLUTE VELOCITIES FROM DIFFUSER LV MEASUREMENTS[1]

Figure Number	Gas	Speed (%N_D)	Gate[2] Position (% vane pitch)	Gate[3] Width (% vane pitch)	C_1 (m/s)	C_2 (m/s)	C (m/s)
m&i	Air	40	50	50	193	189	214
n&j	Air	40	50	10	101	189	214
o&k	Air	40	50	5	101	193	218

Notes:
(1) Reference: pulse height analyzer photos--Figures 29i through 29o and Table VI.
(2) Gate position is location of impeller relative to diffuser lead edge at which data gate is opened--see Figure 30.
(3) Gate width is duration of data gate, expressed as a percentage of blade rotation relative to diffuser vane pitch.

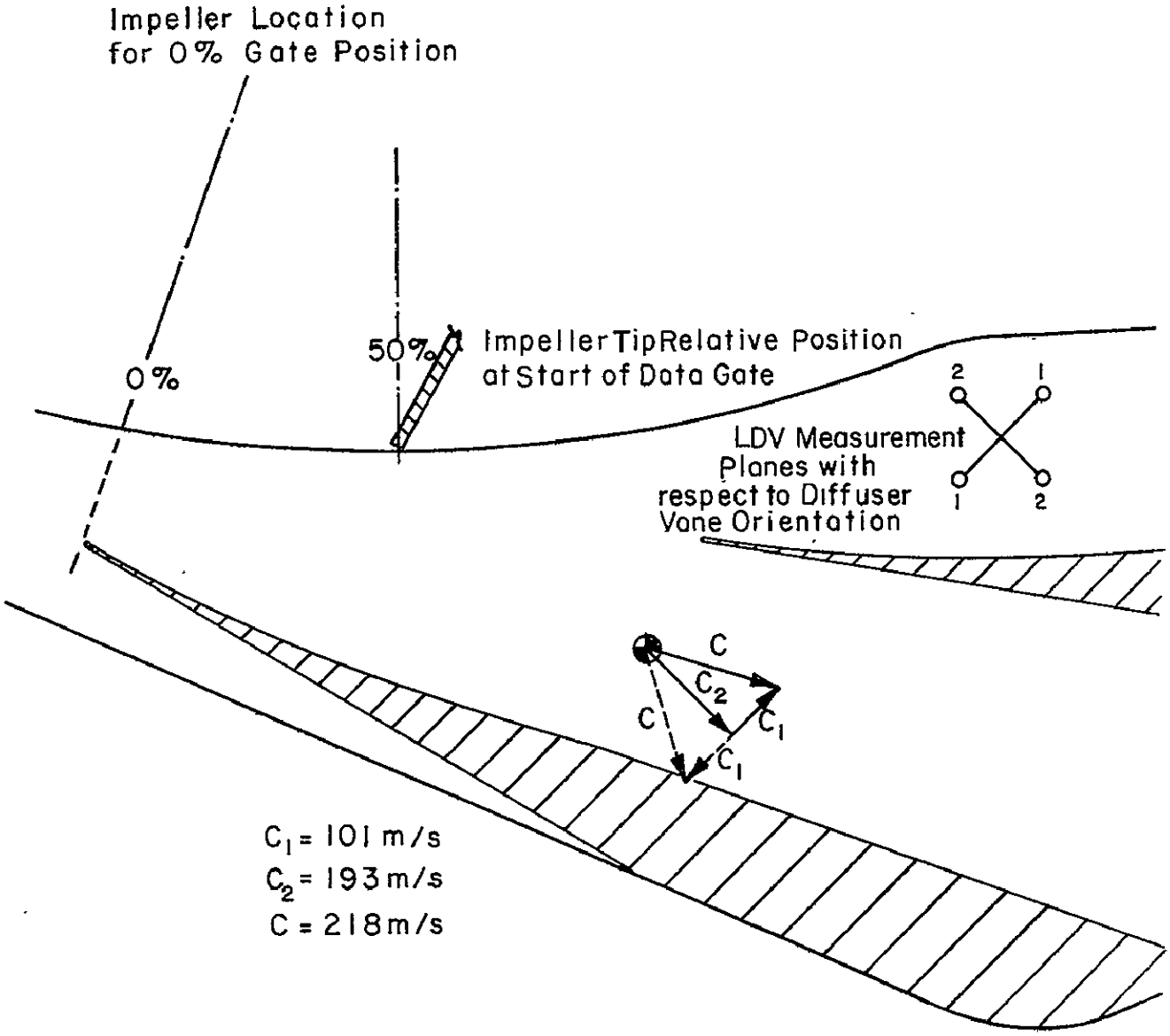

Figure 30. Velocity Vector Diagrams from Figure 29 Data.

the higher velocity expected near the center of the diffuser channel passage as the result of the large throat blockage under these operating conditions.

Table VIII shows the deduced velocity vector magnitude, for the three sets of data corresponding to the measurement volume location shown in Figure 30, for the three gate width values of 5, 10, and 50% shown in Table VI.

These data from this checkout program have verified the operation of the LV system under realistic compressor test conditions. However, further attempts to make detailed velocity field measurements, first in the impeller exit/diffuser entry region and later within the inducer at the 90% blade span location, did not meet with success. The primary causes for these frustrated measurements are laid to the problems of (1) long data acquisition times during gated LV operation caused by low seed rates, (2) maintenance of optical system alignment (particularly in the diffuser back-reflected mode), and (3) A/O modulator output beam drift during gated LV operation, as have been discussed in the previous section under "Other Operational Problems".

Because of the cost and lengthy times required to conduct these LV measurements with the present compressor hardware, it is recommended that a simpler experimental system be employed to overcome and check out the three basic problems mentioned above before any further LV tests are conducted with this LV system in either the present or other compressor hardware of a similar size and pressure ratio.

AERODYNAMIC TEST RESULTS

This section summarizes the vaned and vaneless diffuser tests of the 8:1 pressure ratio compressor stage designed as a workhorse compressor for LV studies. The details of the design and instrumentation for this compressor are given in Reference 14.

A summary of the stage design is given first. The performance data obtained from the stage for the vaneless and vaned diffuser tests are next presented. This section concludes with a presentation of the component (impeller and diffuser) performance and discussion and comment on the measured performance of the stage compared to design.

SUMMARY OF STAGE DESIGN

The stage is a presssure ratio = 8, 0.907 kg/sec (design point) vane island diffuser centrifugal compressor. The predicted efficiency, total-to-static, at the design point was 77%. A 12% choke-to-surge flow range was anticipated at 100% N_D. The design speed of the stage in air is 75,000 RPM. The stage has been tested under LSM modeling conditions where the design speed is approximately 52,500 RPM (actual design speed in LSM depends upon measured variations in LSM gas composition). Complete details of the stage design are given in Reference 14. The reader should refer to this report for stage geometry and instrumentation details. Several figures are included herein, however, to help make this discussion self-contained. These figures are:

Figure 31 - CDR2 Design Point Output (Design Predicted Performance - See Appendix D for Symbols)

Figure 32 - Relative Mach Number Distribution - (Cover Streamline Calculation With No Wake Flow)

Figure 33 - Nominal Impeller Geometric Coordinates

Figure 34 - Impeller Meridional View

Figure 35 - Compressor Inlet Geometry

Figure 36 - Vaned Diffuser Geometry, Build I

Figure 37 - Inlet Static Tap Locations

Figure 38 - Impeller Cover Static Tap Locations

Figure 39 - Table of Impeller Static Tap Locations

Figure 40 - Diffuser Pressure Static Tap and Kulite Locations

Figure 41 - Inlet and Impeller Semi-Conductor Transducer Locations

```
INPUT VALUES

P00= 101353.    P1= 79489.7     P2= 412297.     P4= 552067.
P04= 982482.    P5= 0           P05= 0          PCOL= 814678.
T00= 288.167    TCOL= 587.339   M= 0.907185     N= 7853.97
MW/M= 0.2       LC= 0           W4= 0.137709    B4= 3.2258 E-3
B1B=-56.3       B2B=-30.        ALPHT= 0        B2= 3.2258 E-3
PR= 8.03803     RSEP= 4.37159 E-2               RIH= 2.18567 E-2
R1T= 4.37159 E-2
R2= 0.079756    # BLADES= 19    # DIFF= 17

INDUCER TIP

TTREL= 288.104    PTREL= 101275.    MRELIT= 1.20425
CIT= 197.535    RCT= 0          WIT= 396.113
P1T= 79489.7    T1T= 268.638    M1T= 0.600541
B1T=-60.087     IT= 3.78702     U1T= 343.344
P10T= 101353.   INE= 0.256801

IMPELLER TIP

CT2J= 425.327   CM2J= 258.592   C2J= 497.682
C2W= 584.793    CM2W= 82.0991   CT2W= 579.002
W2W= 94.7998    W2J= 327.63     WT2W= 47.3999
P02J= 1.00093 E+6               MREL2J= 0.791727
T2J= 429.446    T02J= 549.882   M2J= 1.20477    U2= 626.402
P02W= 1.1338 E+6                M2W= 1.29959    E= 0.48093      P02MA=
 1.0275 E+6
T2W= 505.296    T02W= 668.388
MR= 1.52104     MRI= 3.1654     TN= 1.3208 E-3                  DR= 1.42649
WSEP= 277.683

STATES AFTER MIXING

T2*= 459.807    T02*= 573.823   T02**= 587.363
P2*= 444494.    P02*= 984057.
M2*= 1.13286    DP02= 43443.1
CT2*= 455.981   CM2*= 166.634   C2*= 485.475
T02**-TCOL= 2.43547 E-2
L= 2.73643

SIG*= 0.081522

WX= 305501.     WFC= 5699.      WFRD= 4749.17 WBF= 9424.5

DIFFUSER

P4= 552067.     M4= 0.950054    B= 0.114439
D*= 1.61833 E-4      CP2*4= 0.199371       M5= 0
CP4C= 0.610133 .                CPD= 0.68608
P04= 982482.    WL= 2.9189 E-3

EFFICIENCIES

DETSBF= 3.08494 E-2         DETSFC= 1.86546 E-2      DETSWL= 8.24335 E-4
DETSRD= 1.55455 E-2         DETSI= 0.135522
DETSD= 9.47526 E-2          DETSF= 3.42002 E-2
DETSIM= 2.23694 E-2         DETSIW= 4.81029 E-2
ETT= 0          ETS= 0.769726   ETT1= 0.864478
```

* Figure 31. Design Point CDR 2 Output.
(See Nomenclature in Appendix D)

ORIGINAL PAGE IS
OF POOR QUALITY

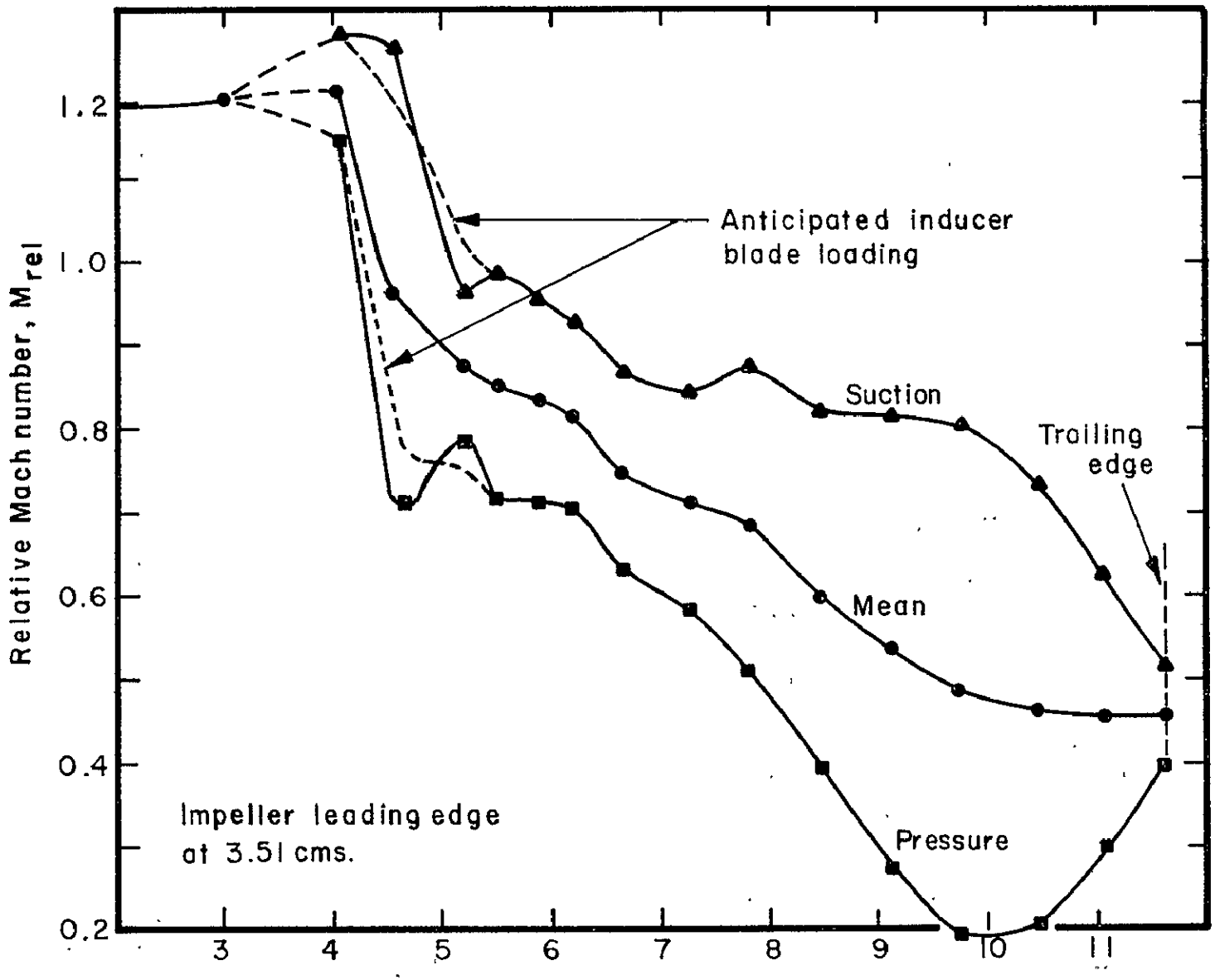

Figure 32 — Relative Mach Number Distribution—Cover Streamline

NOMINAL IMPELLER GEOMETRIC COORDINATES[1]									
Quasi-Orthogonal Number	Blade Angle, β (degrees)		Axial Distance, x (cms)		Radial Distance, r (cms)		Angular Location, θ (degrees)	Normal Thickness, t_n (cms)	
	cover	hub	cover	hub	cover	hub		cover	hub
4 (inlet)	-56.34	-36.70	0.	0.	4.3716	2.1858	0.	0.0152	0.0305
5	-54.24	-35.33	0.5080	0.5080	4.3716	2.2482	-9.2537	0.0610	0.1829
6	-43.33	-26.33	1.0160	1.0160	4.3716	2.3105	-16.9675	0.0610	0.2489
7	-37.18	-22.36	1.6510	1.6510	4.3716	2.3885	-24.0015	0.0610	0.3048
8	-30.25	-19.56	2.1755	2.1538	4.3859	2.4603	-28.6043	0.0610	0.3401
9	-24.78	-17.33	2.6708	2.5853	4.4294	2.5440	-31.9627	0.0610	0.3602
10	-19.94	-14.94	3.2841	3.0812	4.5345	2.6691	-35.2184	0.0610	0.3759
11	-17.21	-12.97	3.8417	3.5220	4.6954	2.8124	-37.6289	0.0610	0.3833
12	-16.03	-11.21	4.3413	3.9443	4.9142	2.9855	-39.5633	0.0610	0.3912
13	-16.11	- 9.06	4.8808	4.5064	5.2727	3.2892	-41.6539	0.0610	0.4013
14	-17.14	- 7.24	5.2419	5.0461	5.6300	3.6971	-43.2458	0.0610	0.4094
15	-18.40	- 5.99	5.4701	5.5383	5.9407	4.2394	-44.4685	0.0610	0.4163
16	-20.06	- 6.76	5.6607	6.0262	6.2889	5.1405	-45.7654	0.0510	0.4191
17	-22.13	-10.10	5.8128	6.2802	6.6756	6.1284	-47.1816	0.0610	0.4155
18	-25.55	-18.85	5.9541	6.3500	7.2527	7.1275	-49.3400	0.0610	0.3353
19	-30.00	-30.00	6.0262	6.3500	7.9756	7.9756	-52.2312	0.0610	0.2032

[1]Before correction on hub and shroud for inlet boundary layer growth.

Figure 33. Nominal Impeller Geometry Coordinates

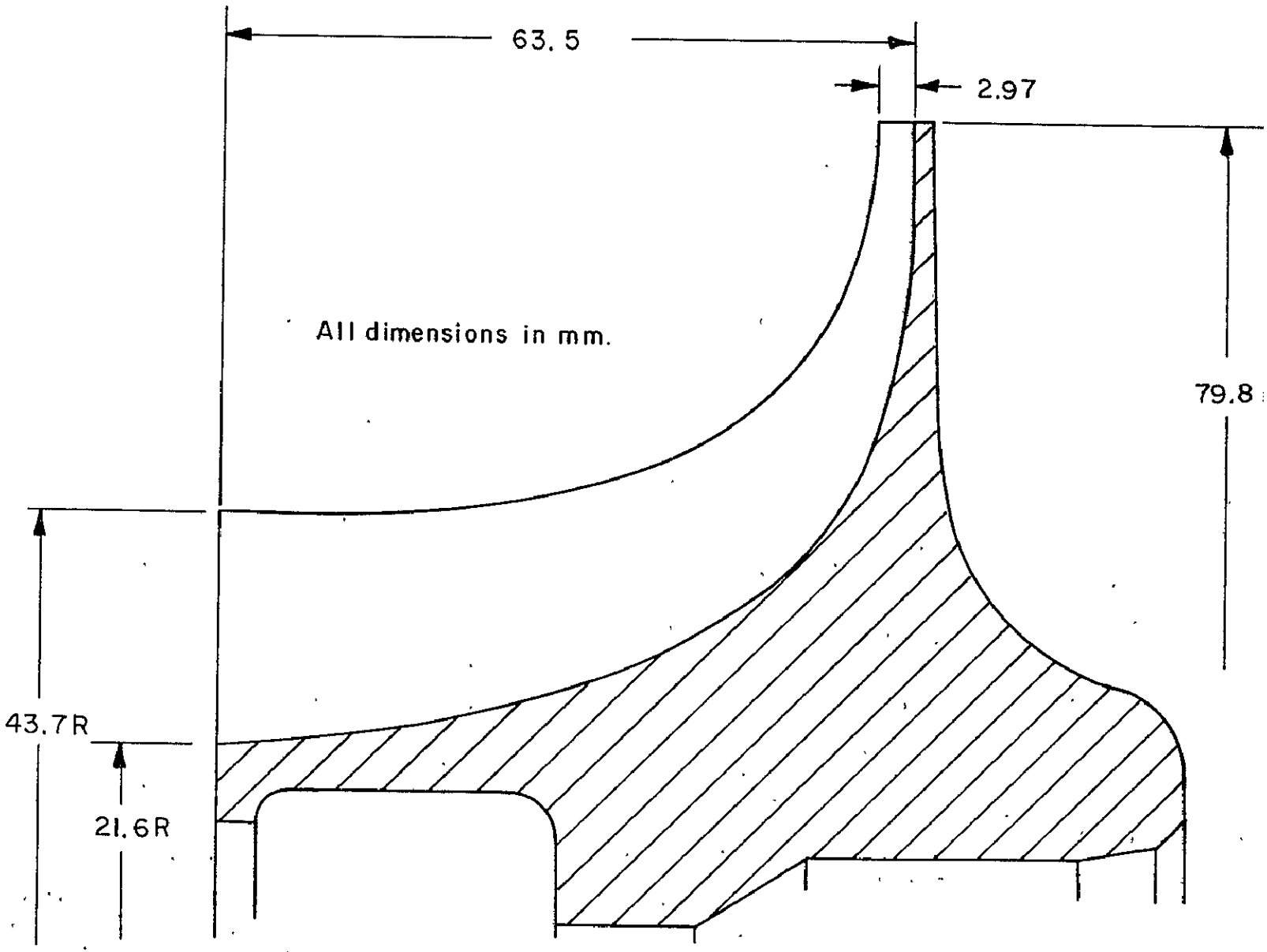

Figure 34- Meridional View of Impeller

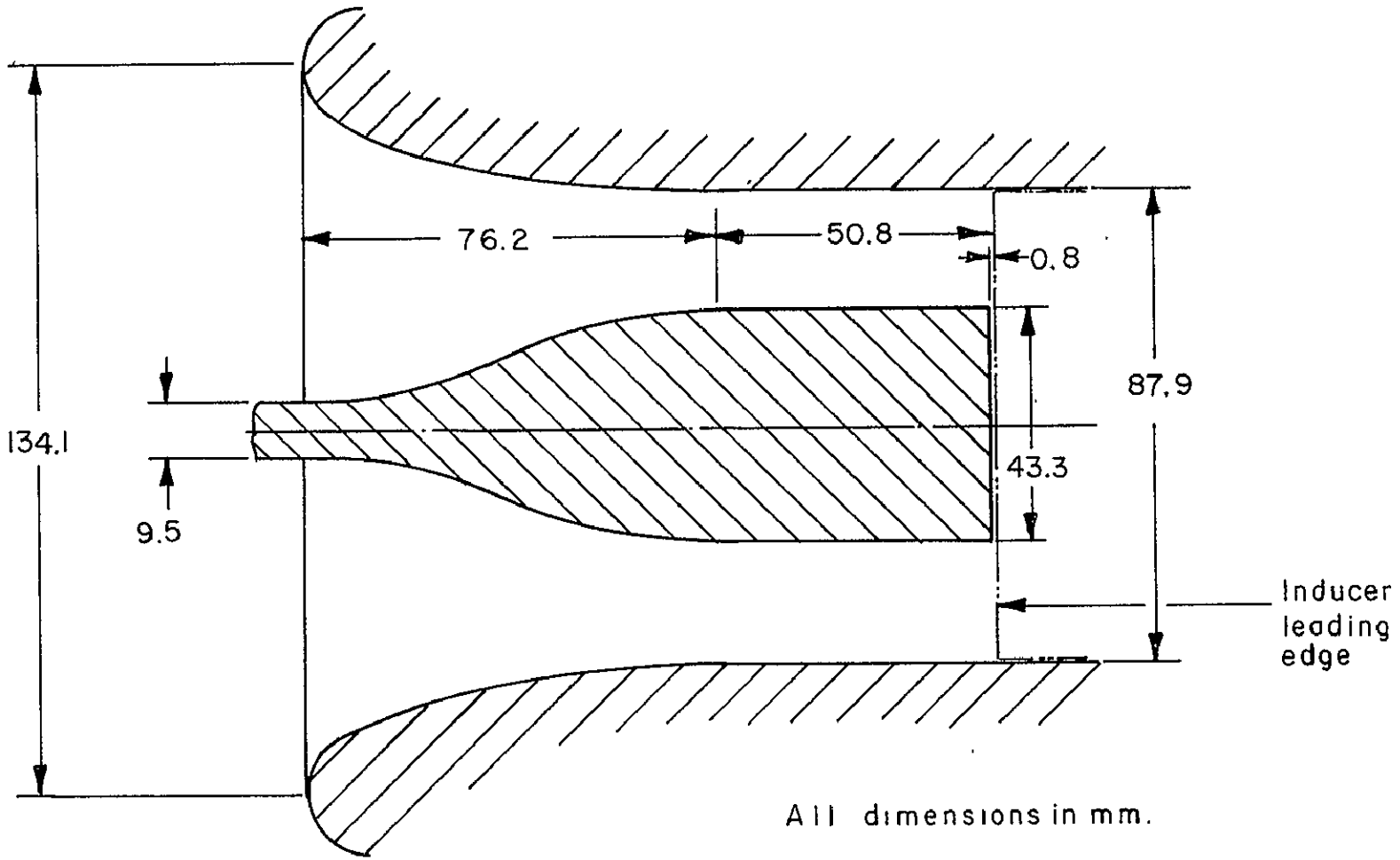

Figure35 – Compressor Inlet Geometry

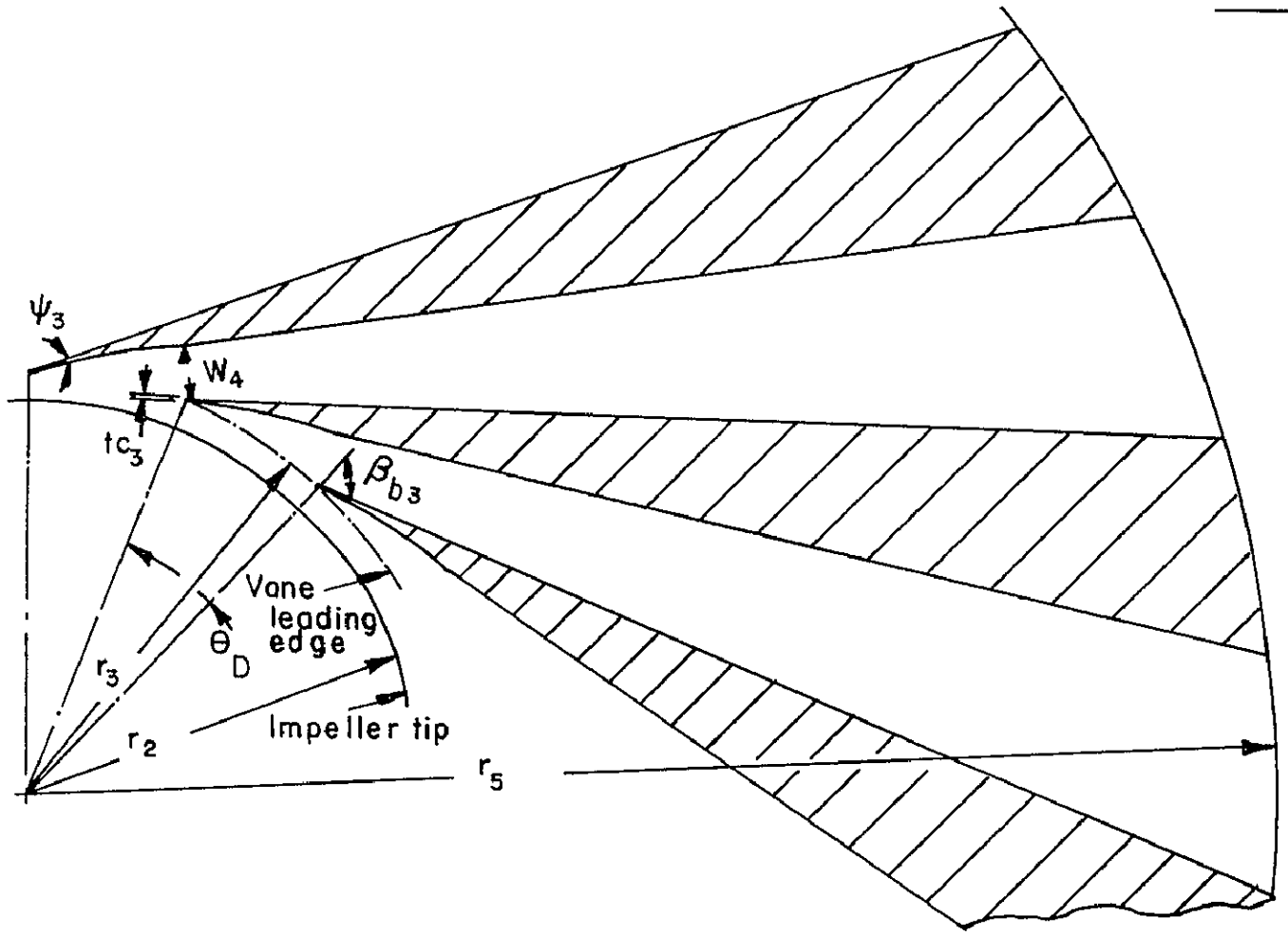

Diffuser parameters

$r_2 = 79.76$
$Z_D = 17$
$r_3 = 85.85$
$tc_3 = 0.254$
$\psi = 0°$
$\beta_{b3} = 70.04°$
$W_4 = 11.48$
$b_4 = 3.24$
$2\theta = 10°$
$L/W_4 = 17$
$r_5 = 254$
$\theta_D = 21.18°$

Circumferential plane divergence

All dimensions in mm.

Figure 36—Vaned Diffuser Geometry — Primary Design-Build I

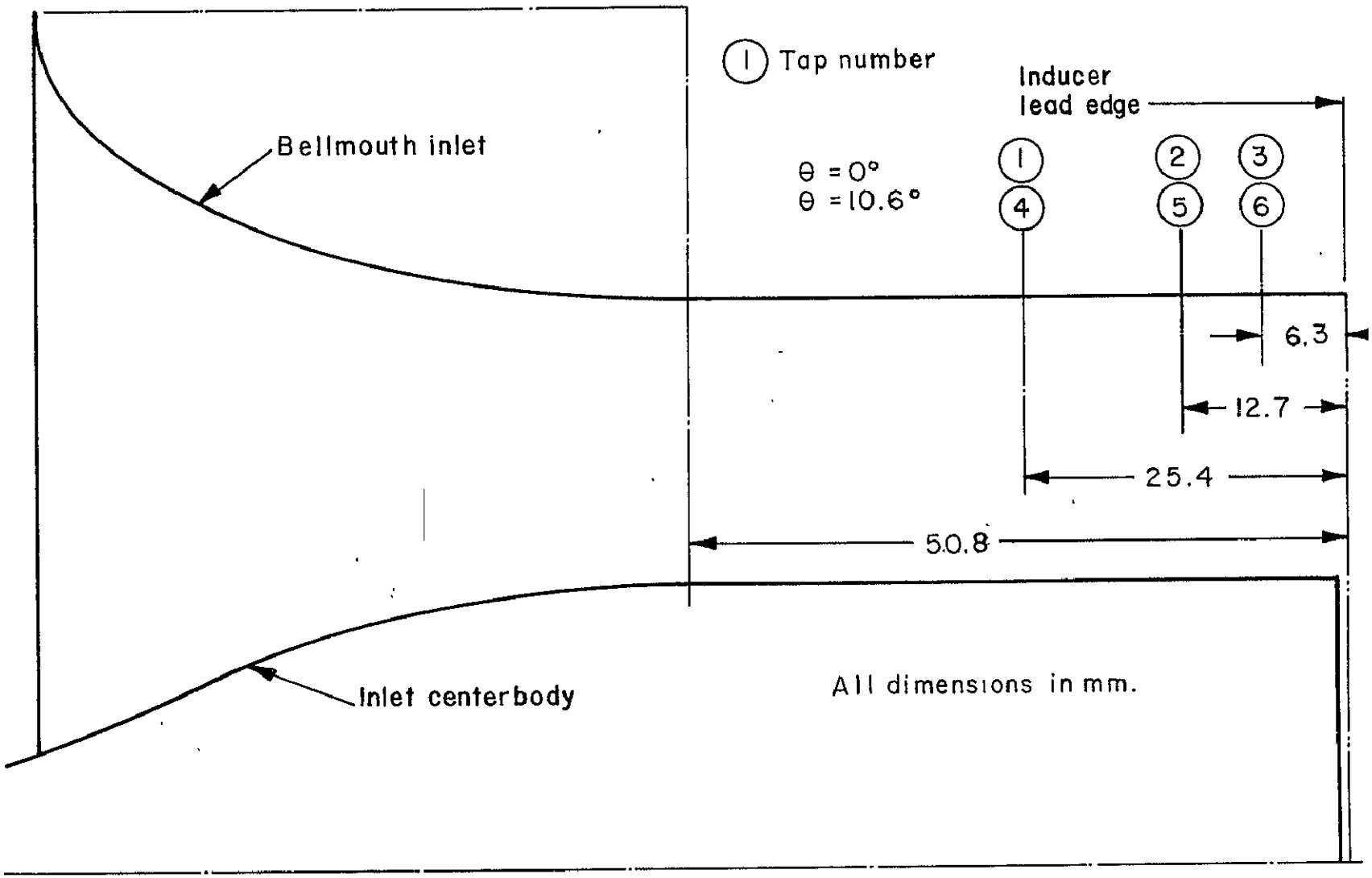

Figure 37–Inlet Static Tap Locations

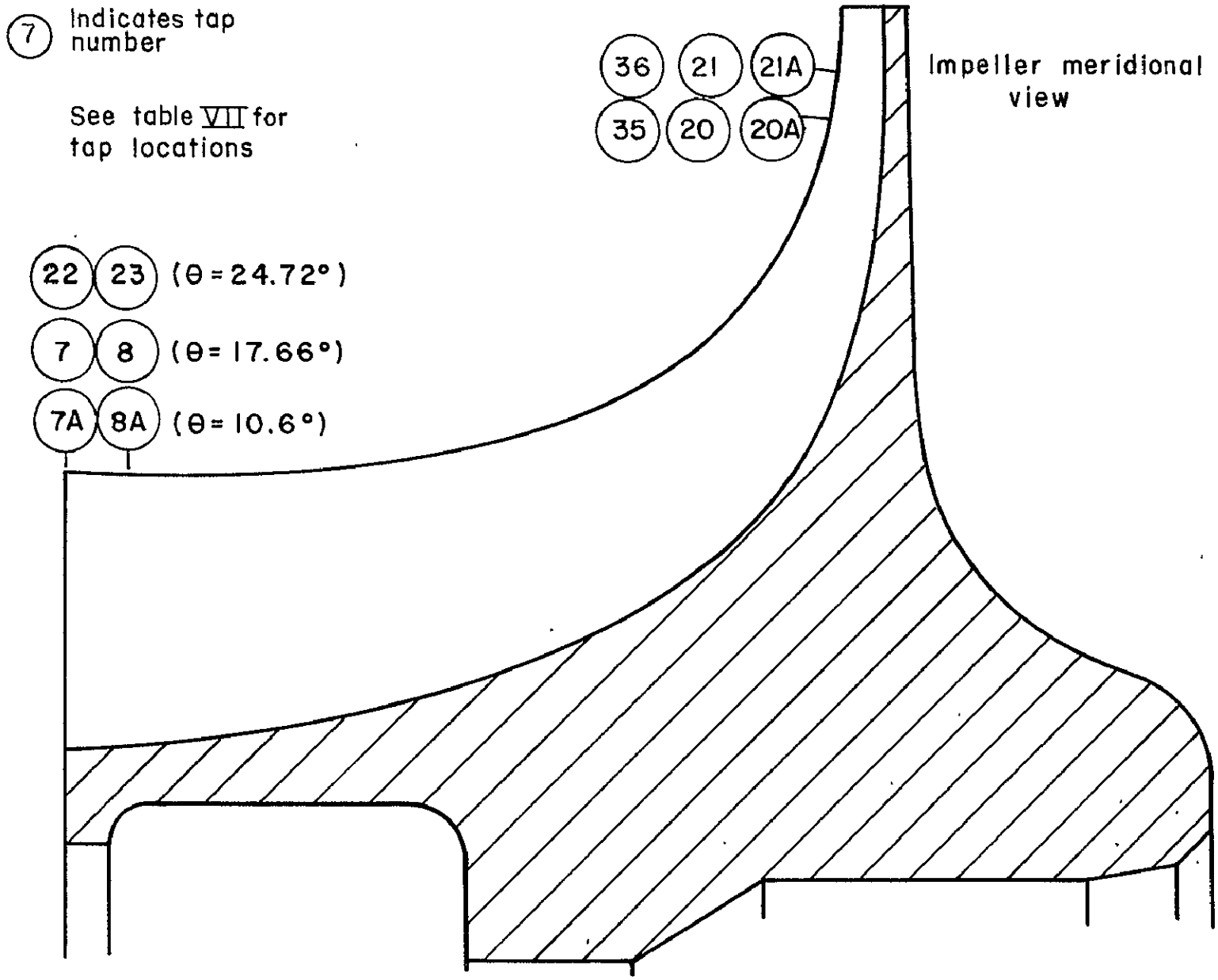

Figure 38—Impeller Cover Static Tap Locations

IMPELLER COVER STATIC TAP LOCATIONS			
Tap Number			Axial Distance, X (cms)	Radial Distance, r (cms)
7a	7	22		4.40
8a	8	23	0.51	4.40
9a	9	24	1.02	4.40
10a	10	25	1.65	4.40
11a	11	26	2.18	4.41
12a	12	27	2.67	4.45
13a	13	28	3.28	4.56
14a	14	29	3.84	4.72
15a	15	30	4.34	4.94
16a	16	31	4.88	5.30
17a	17	32	5.24	5.65
18a	18	33	5.47	5.97
19a	19	34	5.66	6.31
20a	20	35	5.81	6.70
21a	21	36	5.95	7.25
Taps 7a through 21a are located at = 10.6 deg.				
Taps 7 through 21 are located at = 17.66 deg.				
Taps 22 through 36 are located at = 24.72 deg.				

Figure 39. Impeller Cover Tap Locations

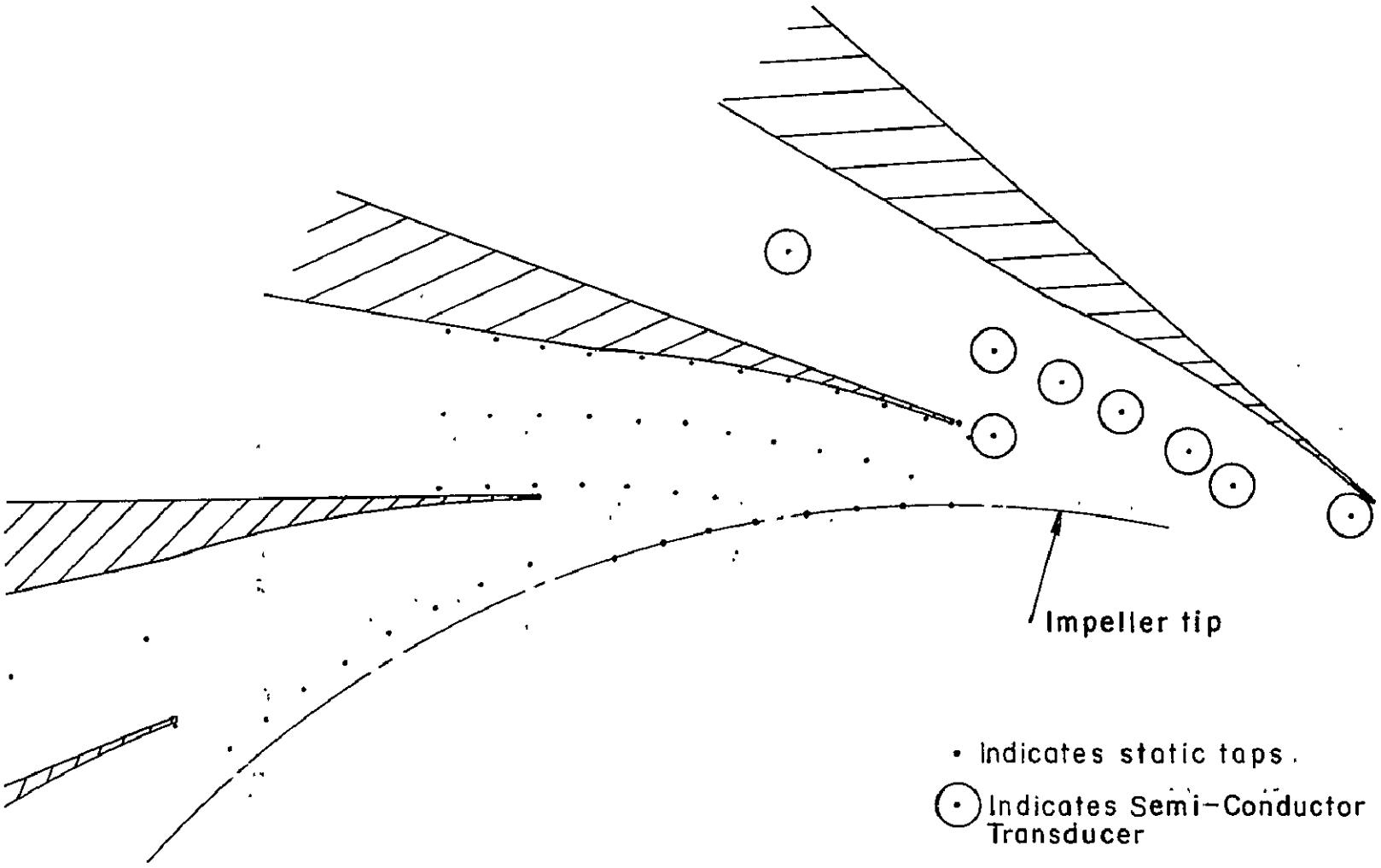

Figure 40- Pressure Static Taps and Semi-Conductor Transducer Locations in Diffuser inlet - Build I Diffuser

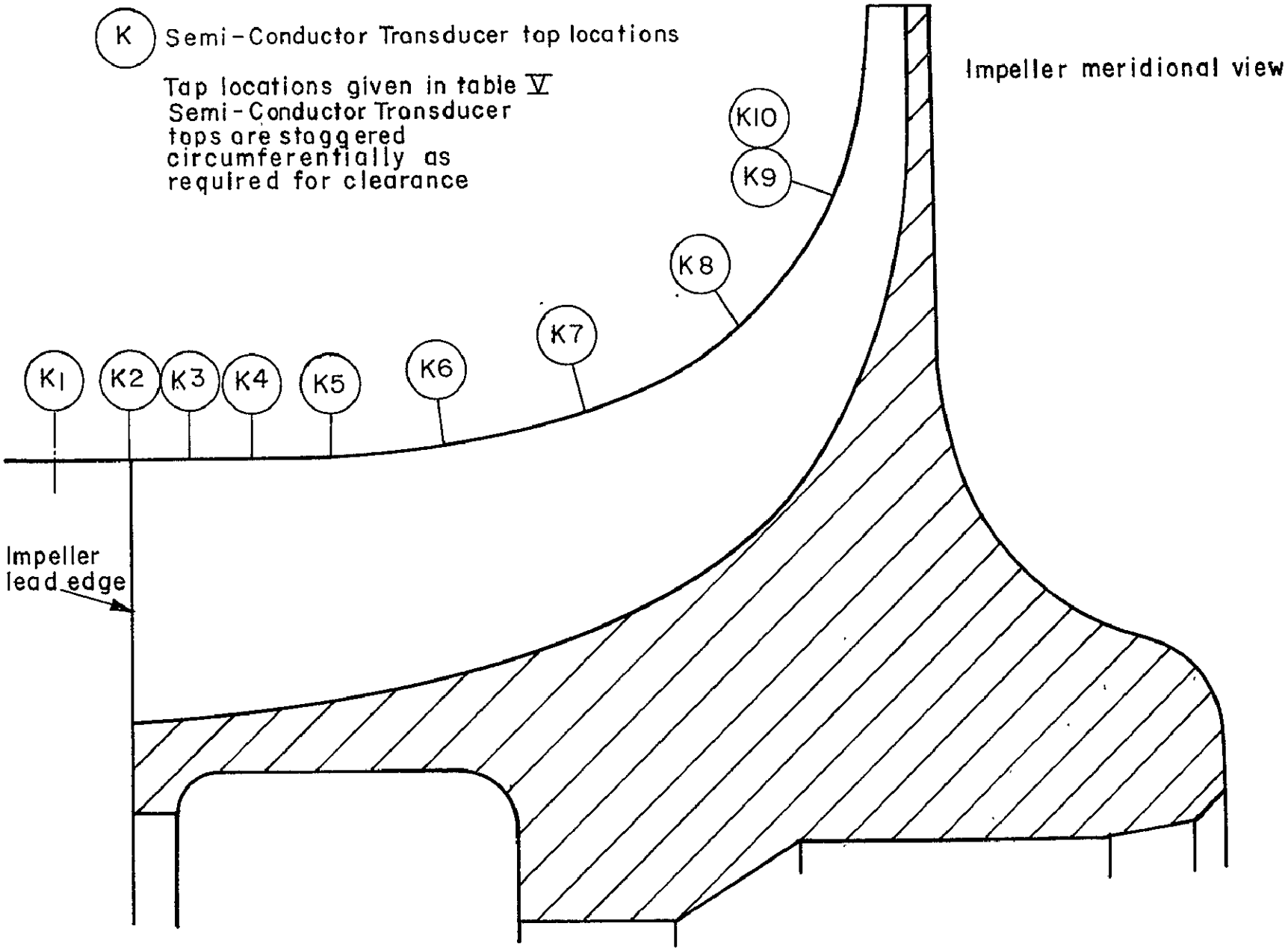

Figure 41-Inlet and Impeller Semi-Conductor Transducer Locations

The reader should consult Tables VII, IX, X, XI, and XII of Reference 14 for the exact locations of the static taps and Kulite taps on the impeller and shroud and in the diffuser.

SUMMARY OF OVERALL STAGE PERFORMANCE

The compressor has not met its design point performance. At 100% N_D (Tests 9.32-9.46), peak efficiency was 75.0% at surge. The pressure ratio also peaks at this same point, pr = 7.61 (Test 9.36). The performance at 50, 80, and 100% N_D for the vaned diffuser tests is shown in Figures 42 and 43. Choke flow was low, being approximately 0.898 kg/s at 100% N_D. Flow range choke-to-surge was thus only about 6.7% or about one-half the desired value. Figures 42 and 43 display the pressure ratio and efficiency vs. mass flow for the 100%, 80%, and 50% N_D data of Runs 6, 7, and 9.

Peak efficiency at 50% N_D was about 76% with a mass flow range of approximately 30%.

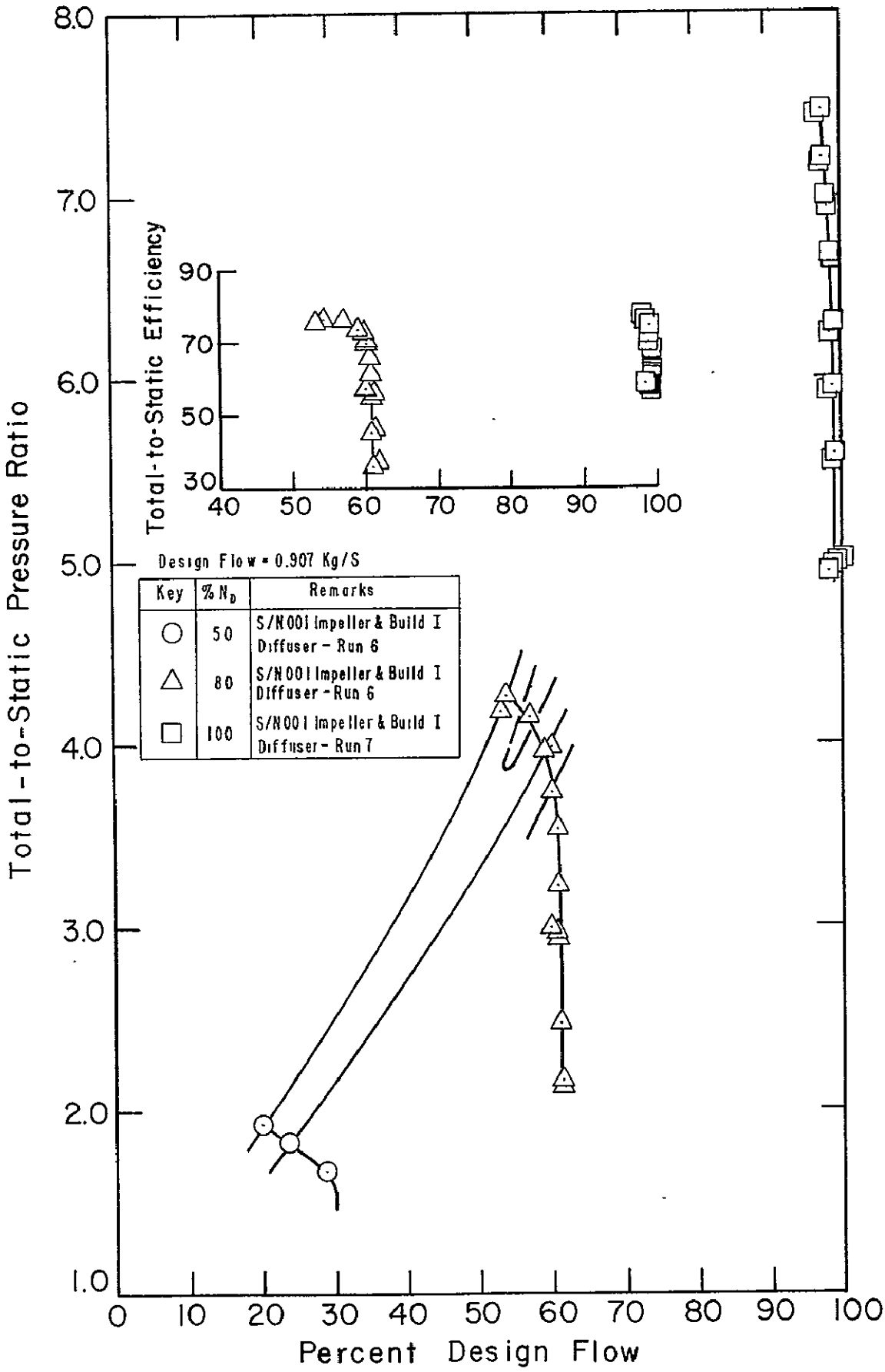

Figure 42. Stage Performance - Vaned Diffuser (Runs 6&7)

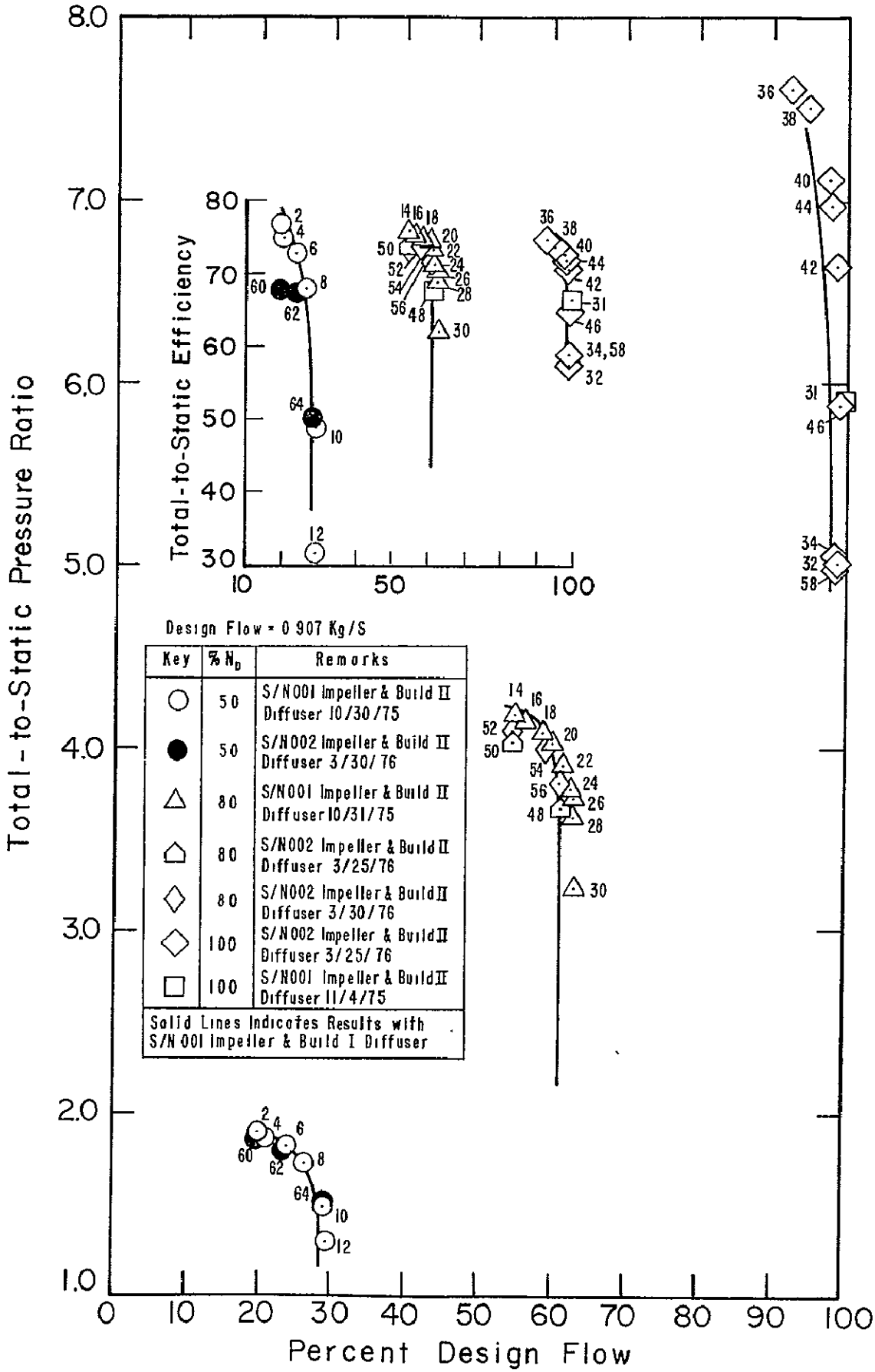

Figure 43. Stage Performance -Vaned Diffuser (Run 9)

SUMMARY OF VANED AND VANELESS DIFFUSER COMPRESSOR DATA

Stage Data. Test data are available for 50, 80, and 100% N_D for two vaned diffuser configurations. Tests have also been made for 50, 60, 70, 80, 90, and 100% N_D for a vaneless diffuser configuration. Both the vaned and vaneless diffuser configurations contain data at 100% speed for both a "high" and "low" Reynolds number (Reynolds number was reduced by a factor of 2), the latter obtained by using a low inlet plenum pressure.

Table IX summarizes the stage configuration by Run number.

All of the symbols used for the discussion of stage and component performance are defined in the listing of nomenclature given in Appendix D.

TABLE IX. - STAGE CONFIGURATION

Run No.	Configuration	Test No.	Description
6	Build I Diffuser with 0.010" tip clearance on S/N 001 Impeller	6.01- 6.16	50% N_D Vaned Diffuser
		6.20- 6.36	80% N_D Vaned Diffuser
		6.37- 6.56	100% N_D Vaned Diffuser, damaged diffuser optical window
7	Build I Diffuser but with aluminum diffuser window and S/N 001 Impeller	7.01 - 7.18	100% N_D Vaned Diffuser, 100% Reynolds number scaling
		7.19 - 7.29	100% N_D Vaned Diffuser, 50% Reynolds number scaling
8	0.010" Tip Clearance on Impeller S/N 001, no diffuser vanes, tie bolt blockage	8.01 - 8.100	50, 60, 70, 80, 90, and 100% N_D Vaneless Diffuser including Reynolds number scaling at 100% N_D
9	Build II Diffuser with 0.010" tip clearance, S/N 001 and S/N 002 Impeller	9.01 - 9.62	50, 80, 100% N_D Vaned Diffuser, 50% Reynolds number scaling

Two identical impeller masters were made for this program; these impellers are designated S/N 001 and S/N 002. Also, three diffuser configurations were designed and two of these configurations were built and tested; these two configurations tested are designated Diffuser Builds I and II. Build I is the vane island diffuser design described in the original design report (Reference 14). Build II is the modified diffuser configuration described earlier in this report, under "Hardware Development, Centrifugal Compressor Design".

Run 9 included testing with both impellers S/N 001 and S/N 002 for reasons described below. Chronologically the testing followed the order presented in Table IX. Run numbers 6 and 7 were performed with the Build I diffuser configuration and with impeller S/N 001. These tests are therefore for the initially designed vaned diffuser configuration and include stage and component performance data at 50, 80, and 100% N_D. All testing was done with Low Speed of Sound Modeling (LSM) with all data reduced to conditions equivalent to the following conditions in air:

inlet ambient temperature	228.15°K
inlet ambient pressure	101.43 kN/m^2

These conditions are referred to as 100% or "high" Reynolds number scaling.

In addition, for Run number 7 (Tests 7.19-7.29) at 100% N_D, tests were also run for conditions equivalent to the following conditions in air:

inlet ambient temperature	228.15°K
inlet ambient pressure	50.72 kN/m^2

These conditions are referred to as 50% or "low" Reynolds number scaling since the reduced inlet density reduced the Reynolds number for these test conditions.

Run number 8 was performed with a vaneless diffuser hardware configuration achieved by removing the vane island diffuser vanes from the Build I diffuser and appropriately modifying the hardware as follows.

The diffuser vane islands were removed and replaced with 12.7 mm diameter spacers at $r = 165.1$ mm and $r = 747.65$ mm (the tie-down bolts passed through the spacers). Tie-down bolts at $r = 101.6$ mm ($R = 1.27$) were necessary, but the diameter of these tie-down bolts was reduced to 2.16 mm. This diameter produced a blockage of only 5.4% at $R = 1.27$ for the 17 bolts used. A new diffuser window hold down frame was

fabricated and a solid window was used in place of the optical window. The "cold" impeller/cover clearance of 0.2 mm (0.254 mm hot)* was maintained. Semi-conductor transducers were installed at two locations, near the inducer lead edge (x = 10.2 mm) and at approximately the 80% meridional distance (K4 and K10 Kulite locations). Impeller cover time-averaged static pressures were measured out to R = 1.02 and total pressure measurements were made with the p_{o4} probes in the same locations and orientation as used for the vaned diffuser tests. The diffuser depth was kept the same as for the vaned diffuser configuration; i.e., $b_4 = 3.74$ mm.

Run number 9 was undertaken with the redesigned diffuser Build II. These tests were started with the S/N 001 impeller and tests were run at 50% N_D (9.01-9.12), 80% N_D (9.14-9.30), and at 100% N_D (9.32) where only one test point was obtained at 100% N_D with the S/N 001 impeller because the impeller (and impeller shroud) was damaged when a main shaft bearing failed on the high speed shaft assembly.

Because the S/N 001 impeller was damaged beyond repair, the Run 9 tests were then continued with the S/N 002 impeller and a new impeller shroud. As will appear obvious from the data displayed later in this section, there is a small but measurable difference in the performance of impellers S/N 001 and S/N 002, and hence also a difference in stage performance with these two impellers used with the Build II diffuser. This is attributed to the mechanical rub of the S/N 002 impeller inducer into the shroud when it was not properly balanced. Some of the inducer blade tips were slightly bent during the rub and then straightened by a technician using hand tools.

Included in this section are figures and tables giving:

1) selected impeller cover relative Mach number and static pressure distributions for the 100% N_D vaned diffuser tests,
2) selected impeller cover relative Mach number and static pressure distributions for the 100% N_D vaneless diffuser tests, and
3) diffuser wall static pressure distributions measured for the 100% N_D vaned diffuser tests.

*Estimated from the proximity sensor calibration corrected for temperature changes between "cold" and "hot" running conditions.

Appendix D gives the data reduction (CDR2) computer output displays for the 50%, 80%, and 100% N_D vaned diffuser tests and the 50%, 80%, 90%, and 100% N_D vaneless diffuser tests.

For this impeller shroud data, a computer program calculates the local static pressure to total inlet pressure ratio deduced from the time-average static pressure measurements and then calculates DR, W, and M_{rel} at each static tap location.

In the CDR2 outputs, there are sometimes two outputs for a given test run shown. In these cases, a second calculation was made with the slip factor (σ) adjusted to bring to zero the negative backflow losses indicated on the regular CDR2 output. These rerun cases have been marked "ZBF" (zero backflow) in their headings. While we have no assurance that there may not be some backflow in these cases, we know of no reason why there should be a negative backflow.

Appendix D gives a listing of the CDR output nomenclature.

Figure 42 displays the total-to-static overall pressure ratio vs. mass flow for all tests of Runs number 6 and 7. Figure 43 shows similar data for all of the Run 9 tests. These figures provide an easy key to the location of particular data points with respect to choke and surge at a given speed for all of the tests in Runs 6, 7, and 9.

IMPELLER PERFORMANCE DATA

The various figures displaying the impeller and diffuser performance data are briefly described next. More detailed technical comment on the data is given under the section 'Discussion'.

Impeller alone performance in terms of MR_2 vs. MR_{2i} is shown in Figure 44 for all of the speeds 50% through 100% of design speed. Data were taken from the vaneless diffuser tests of Run 8. Also shown on this figure is the "design point" predicted performance.

Figure 45 shows the Run 9 impeller data plotted together with the 50%, 80%, and 100% N_D data of Figure 44.

Table X lists the impeller tip incidence i_{1t} and inlet tip relative Mach number $M_{rel\,1t}$ for all of the vaned and vaneless tests at 100% N_D. Incidence has been calculated from the impeller rotational speed and the upstream axial velocity

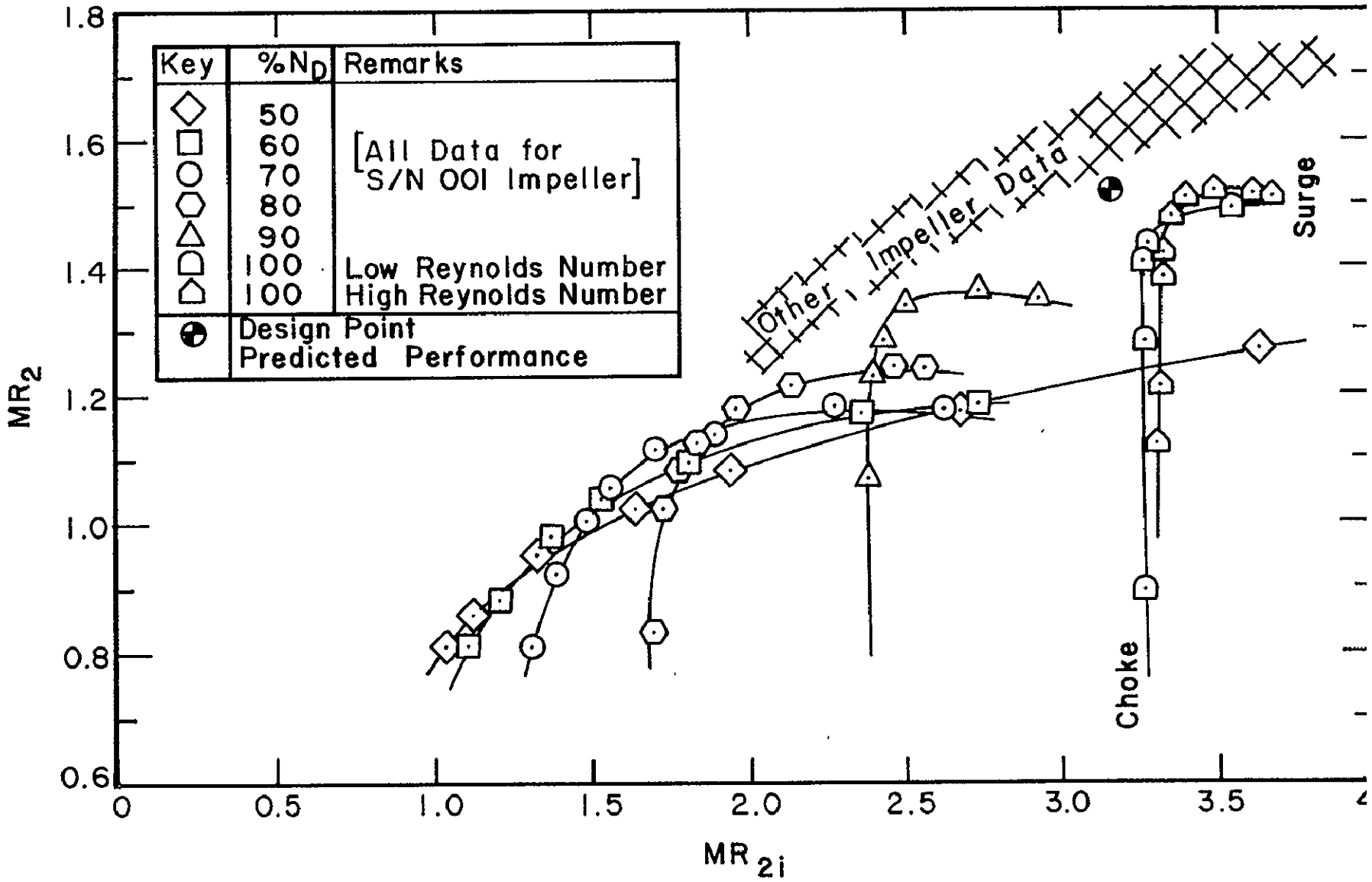

Figure 44. Impeller Performance - MR_2 vs. MR_{2i} (Vaneless Diffuser Test)

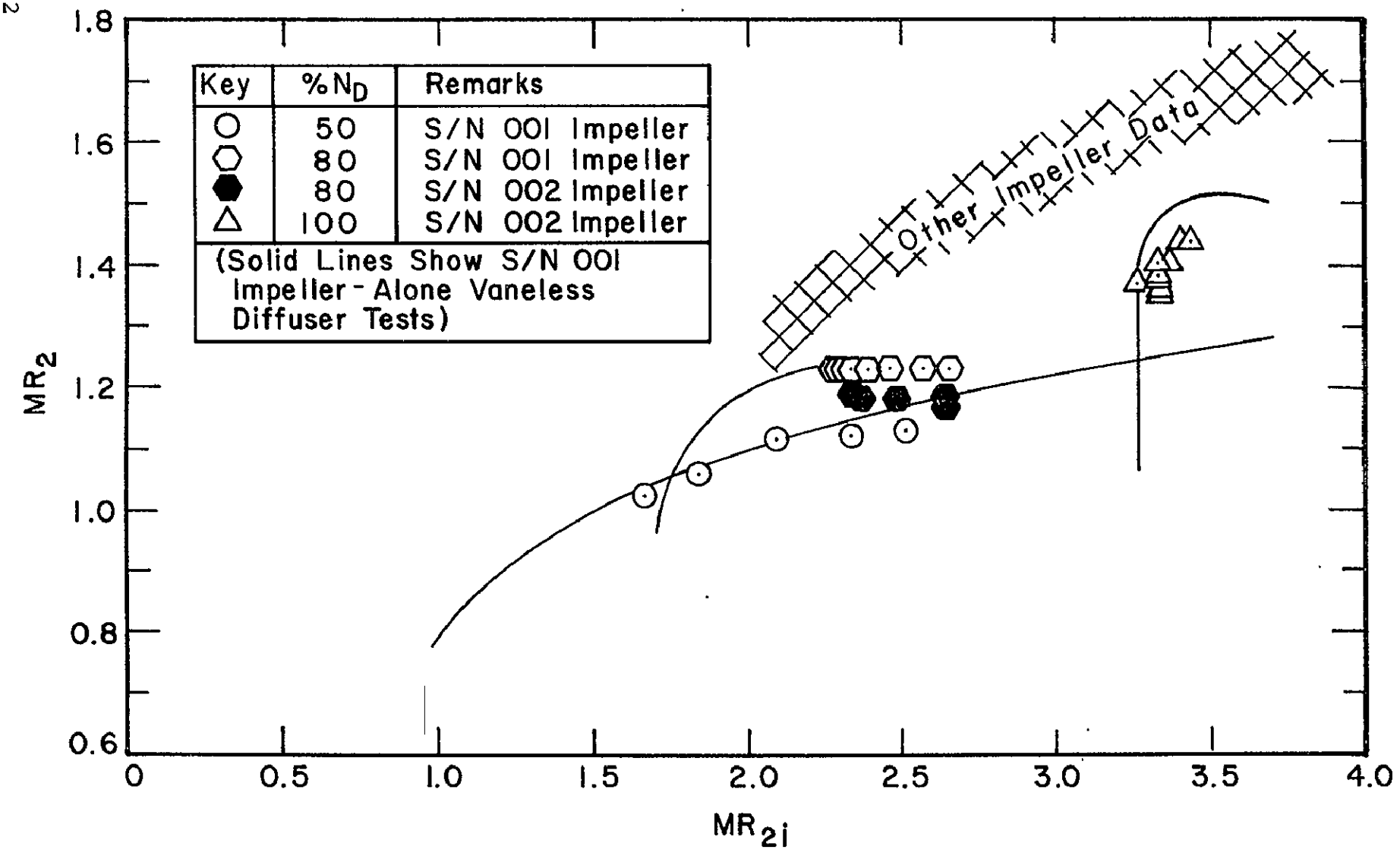

Figure 45. Impeller Performance - MR_2 vs. MR_{2i} (Vaned Diffuser Test)

TABLE X. - IMPELLER INCIDENCE VERSUS INLET TIP RELATIVE MACH NUMBER - VANED AND VANELESS TESTS AT 100% N_D

Test	Mass Flow (kg/s)	$M_{rel\ lt}$	i_{lt} (degrees)
7.20	0.821	1.16	7.1
7.22	0.825	1.18	5.8
7.24	0.865	1.19	5.3
7.27	0.870	1.19	5.2
7.28	0.871	1.20	4.58
8.74	0.783	1.14	8.5
8.76	0.896	1.24	2.1
8.76 mass ave	0.896	1.19	5.3
8.78	0.900	1.24	1.8
8.80	0.905	1.25	1.5
8.82	0.902	1.24	1.7
8.84	0.908	1.25	1.4
8.86 mass ave	0.772	1.13	9.9
8.86	0.772	1.15	8.2
8.88	0.799	1.17	6.6
8.90	0.829	1.18	5.6
8.92 mass ave	0.857	1.17	6.9
8.92	0.857	1.19	4.6
8.94	0.887	1.22	3.4
8.96	0.909	1.26	1.4
8.98	0.909	1.26	1.5
8.100	0.909	1.26	1.5
9.32	0.896	1.25	1.6
9.34	0.895	1.24	1.9
9.36	0.837	1.18	5.7
9.38	0.860	1.21	4.0
9.40	0.885	1.22	3.1
9.42	0.894	1.24	2.3
9.44	0.888	1.23	2.7
9.46	0.898	1.24	1.9
9.58	0.893	1.24	1.8

ORIGINAL PAGE IS OF POOR QUALITY

based upon shroud static pressure measured just upstream of the inducer (pressure tap #2 in Figure 37) for all cases listed, except for those listed as 'mass average'. The 'mass average' incidence was calculated using an upstream approach axial velocity obtained from the measured mass flow rate assuming a uniform axial velocity profile in the flow approaching the inducer.

Figure 46 shows the tip incidence versus mass flow for the vaned and vaneless data at 100% N_D.

For the vaneless, and vaned data, we have Kulite photographs of the inducer blade-to-blade pressure loading. These photographs have been used to compare apparent stall or choke effects in the inducer, as indicated by the characteristic of the static pressure signal, with the incidence listed in Table X and with the incidence data plotted in Figure 46.

Impeller static pressure ratio (static pressure ratioed to $p_{ref} = 101.353\ kN/m^2$), relative velocity, and relative Mach number distributions for the 100% speed high Reynolds number tests (Runs No. 7, 8, and 9) are shown in Figures 47 through 54.

The calculated impeller discharge mixed out stagnation pressure p_{o2*} as a function of mass flow rate for the vaneless diffuser tests is shown in Figure 55. The "design point" $p_{o2*} = 983.5\ kN/m^2$ at 100% of design speed is shown on this figure.

p_{o2*} versus mass flow for the vaned diffuser tests at 50%, 80%, and 100% N_D, for Runs 6, 7, and 9, is shown in Figure 56.

Measured, stagnation pressures p_{o4} versus mass flow for the vaneless diffuser tests are shown in Figure 57. The same measurements for the vaned diffuser tests are shown in Figure 58. For the vaneless diffuser tests, the total pressure probes are located in the same diffuser locations as were used for the vaned diffuser tests. The flow direction orientation of the total pressure probes are also the same. For the vaned diffuser tests, the probes are located along the centerline of the diverging vaned diffuser passage with the total pressure hole midway between the shroud and hub walls of the diffuser. The probe is oriented with the pressure tap aligned with the diffuser passage centerline. The measurements shown are taken from an average of the three total pressure probe readings.

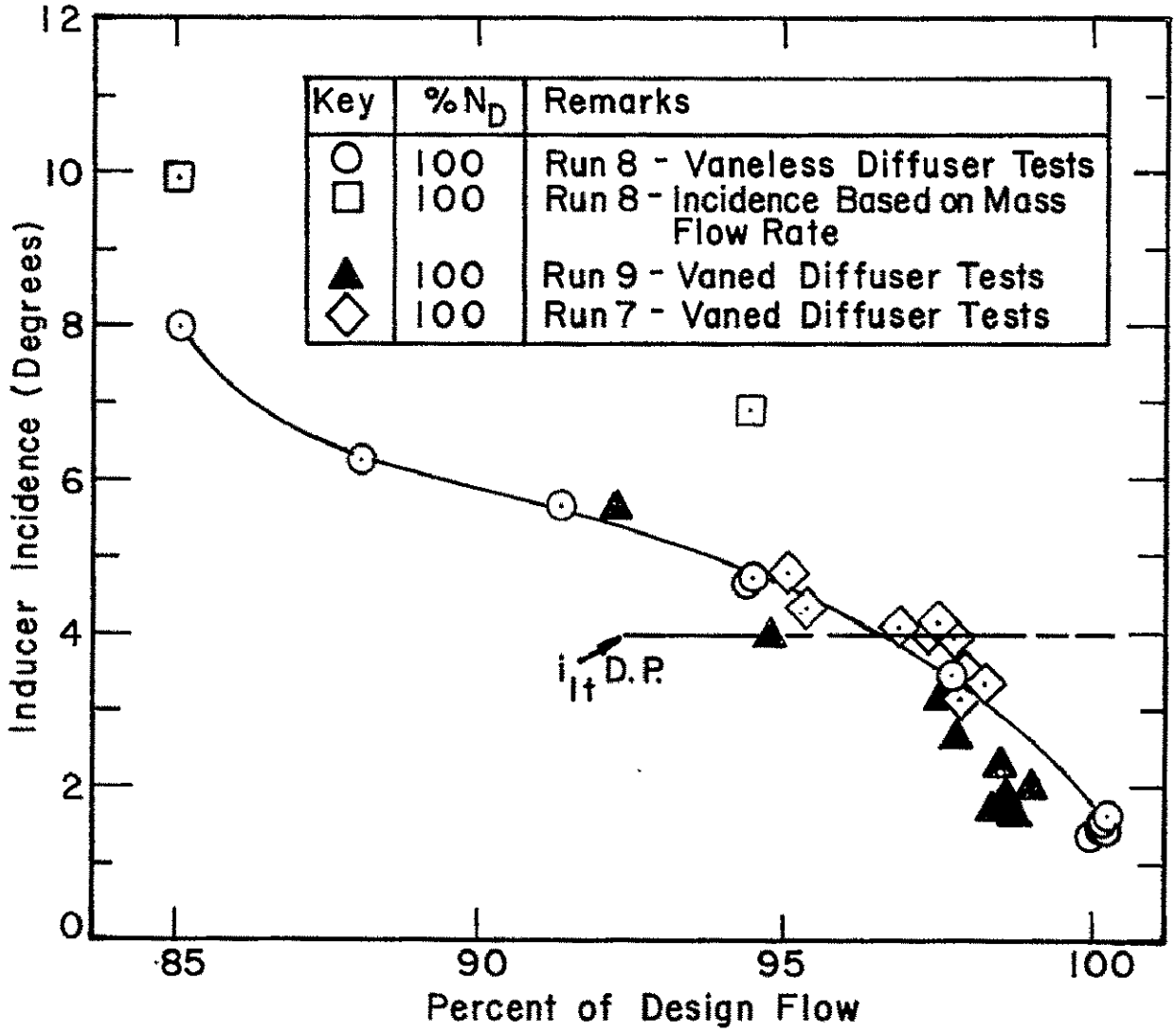

Figure 46. Inducer Incidence vs. Flow Rate at 100% N_D

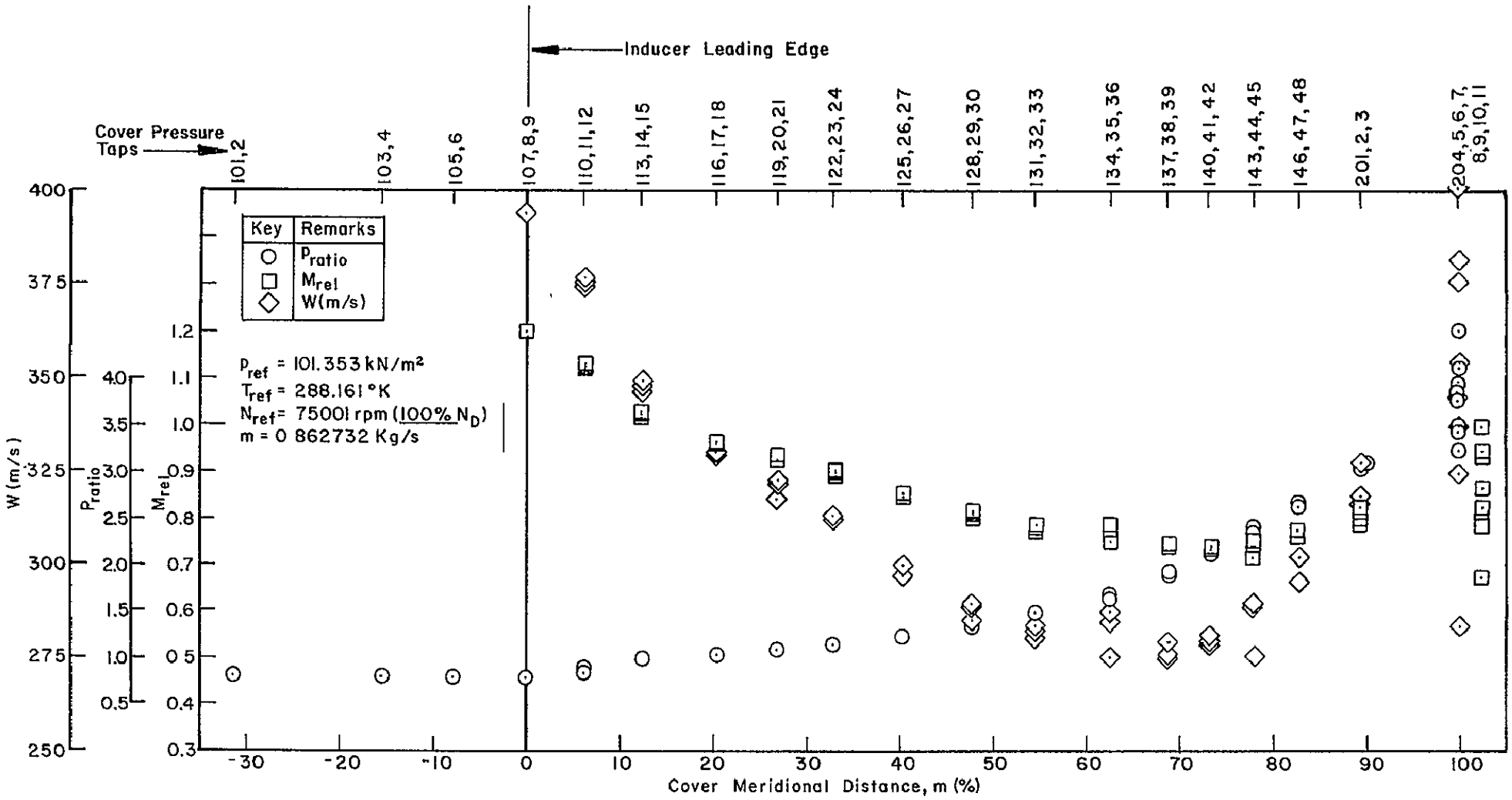

Figure 47. Distribution of Cover Static Pressure Ratio, Relative Mach Number, and Relative Velocity vs Cover Meridional Distance — Run 7 (Test 7.11) Vaned Diffuser Tests at 100% N_D, Near Surge

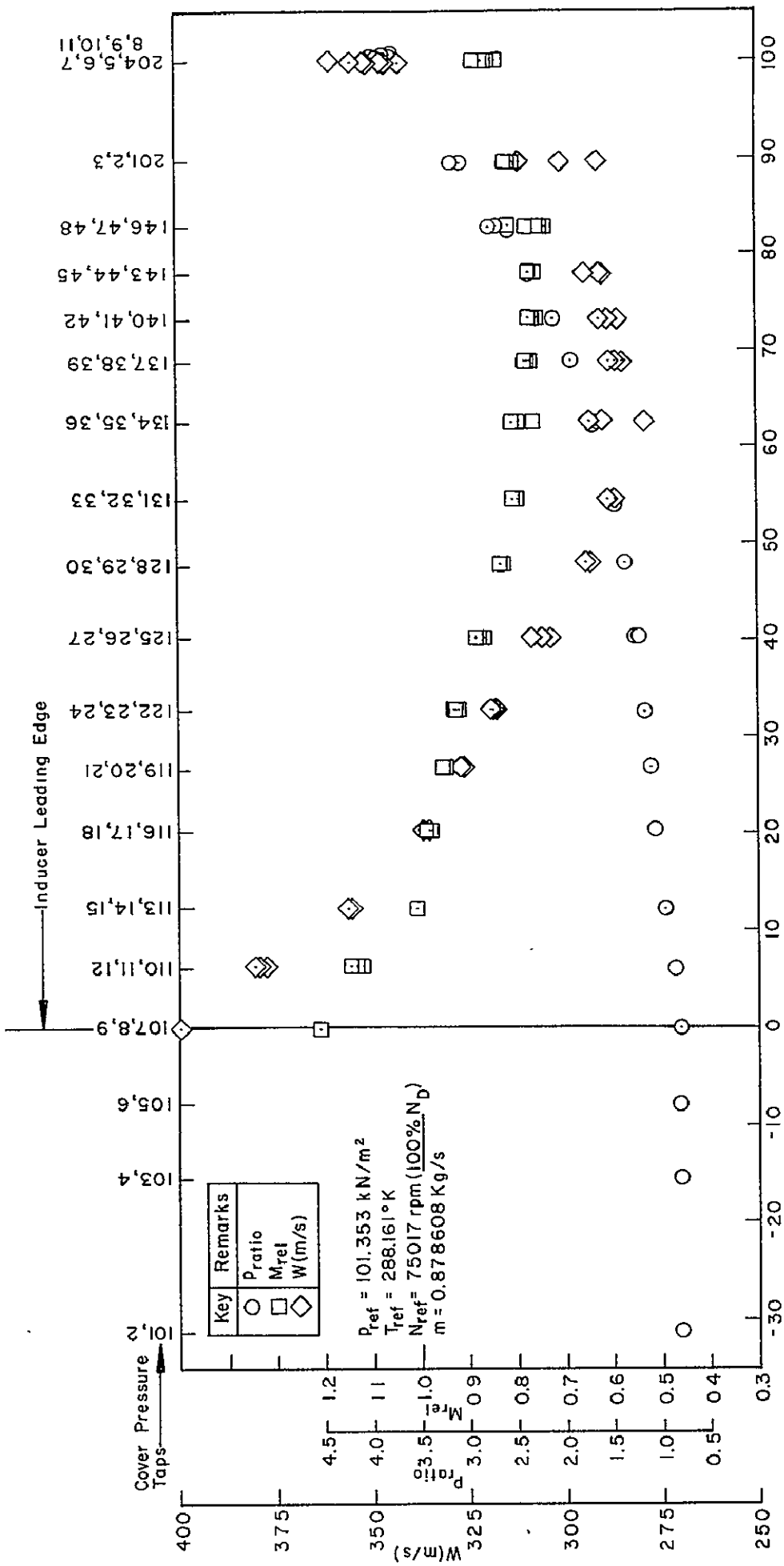

Figure 48. Distribution of Cover Static Pressure Ratio, Relative Mach Number, and Relative Velocity vs. Cover Meridional Distance — Run 7 (Test 7.13) Vaned Diffuser Tests at 100% N_D—

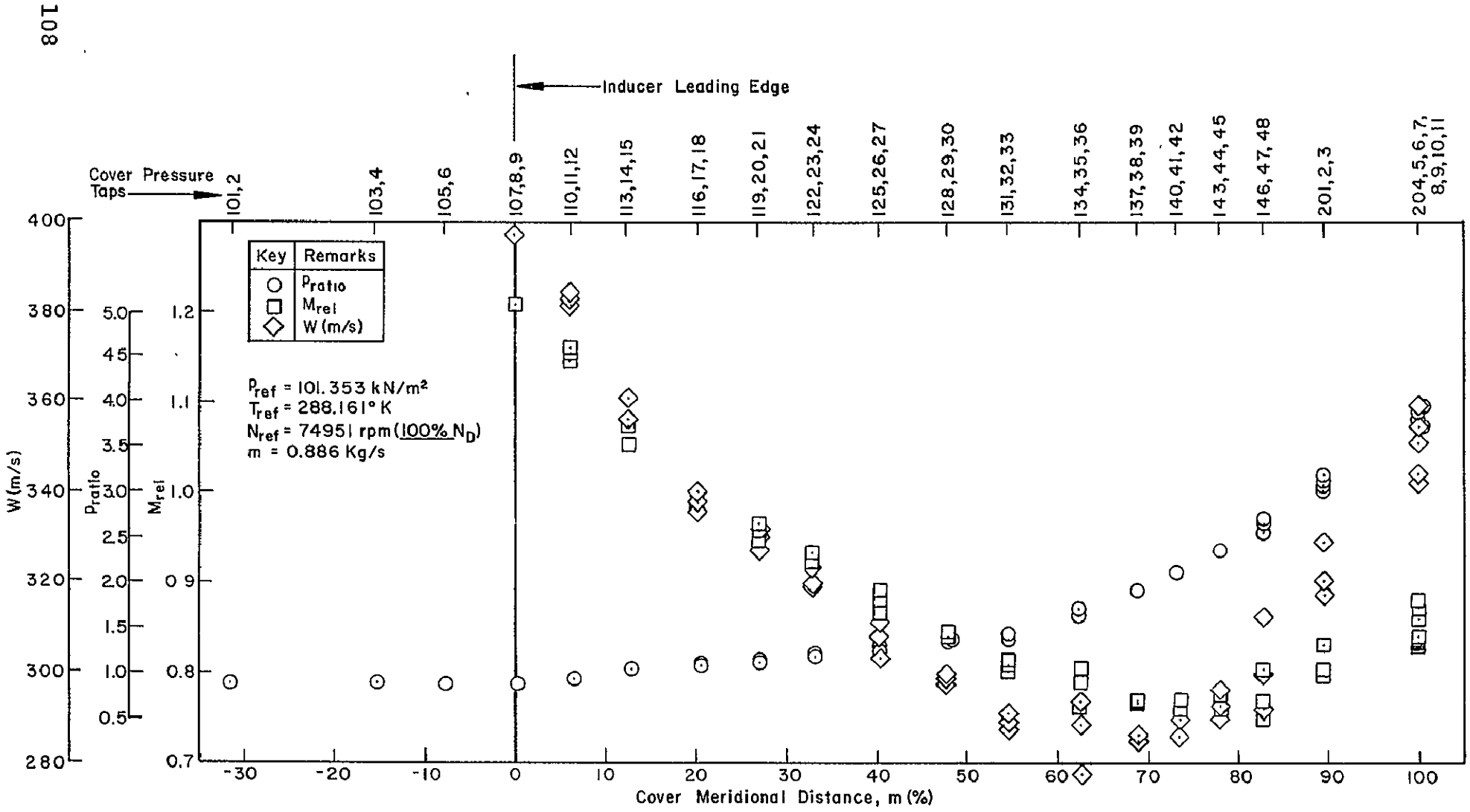

Figure 49. Distribution of Cover Static Pressure Ratio, Relative Mach Number, and Relative Velocity vs. Cover Meridional Distance — Run 7 (Test 7.17) Vaned Diffuser Tests at 100% N_D, Near Choke

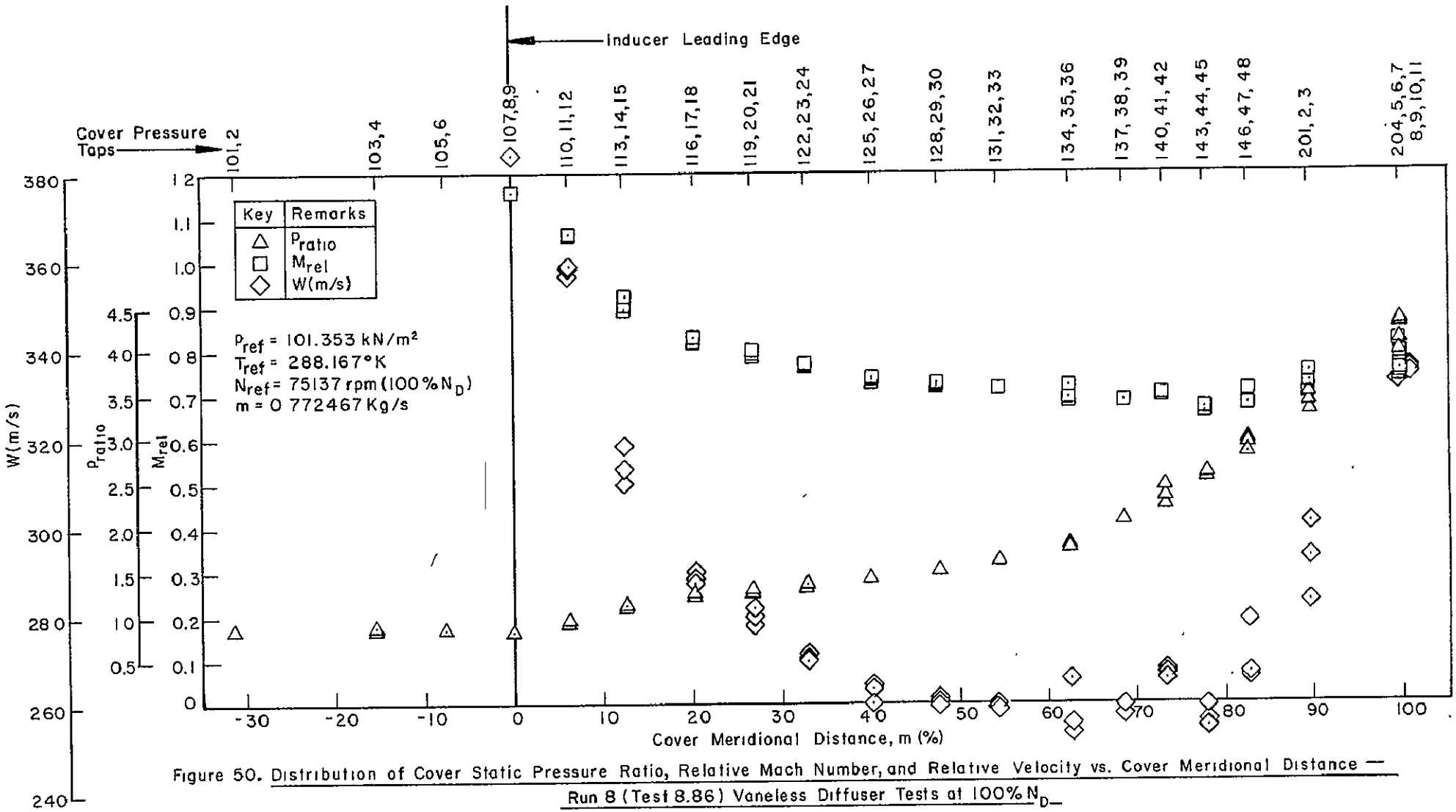

Figure 50. Distribution of Cover Static Pressure Ratio, Relative Mach Number, and Relative Velocity vs. Cover Meridional Distance — Run 8 (Test 8.86) Vaneless Diffuser Tests at 100% N_D

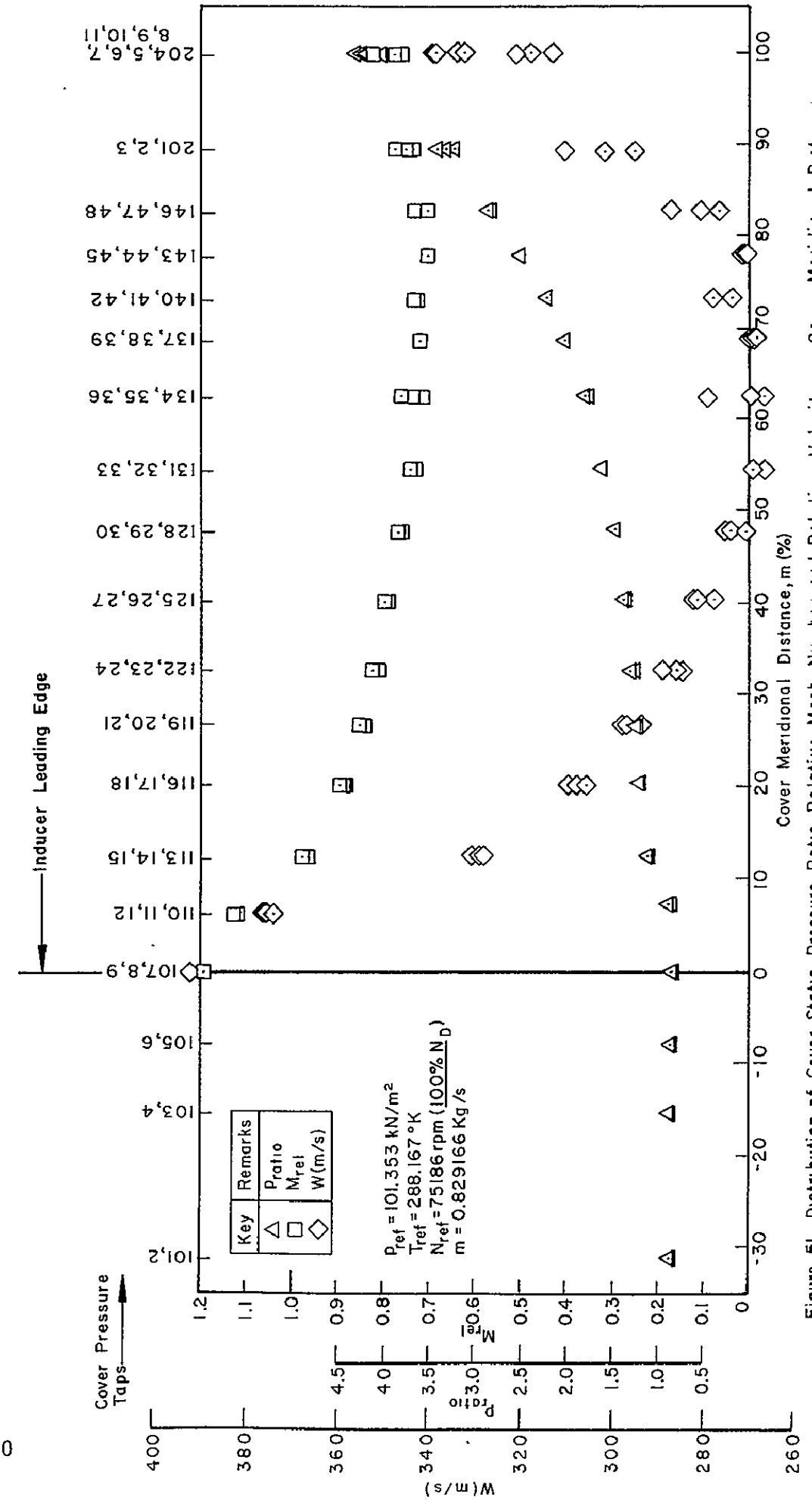

Figure 51. Distribution of Cover Static Pressure Ratio, Relative Mach Number, and Relative Velocity vs Cover Meridional Distance — Run 8 (Test 8 90) Vaneless Diffuser Tests at 100% N_D

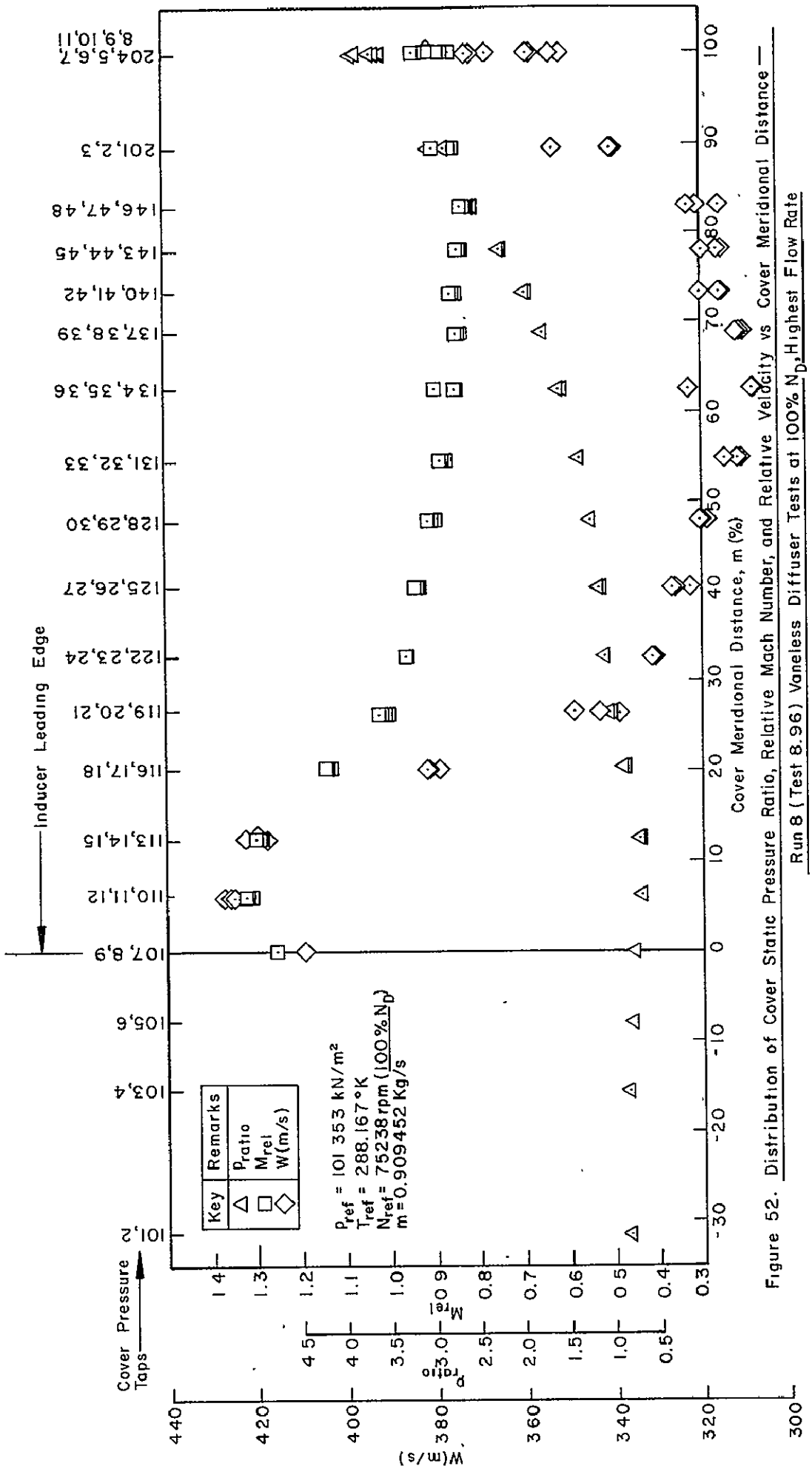

Figure 52. Distribution of Cover Static Pressure Ratio, Relative Mach Number, and Relative Velocity vs Cover Meridional Distance — Run 8 (Test 8.96) Vaneless Diffuser Tests at 100% N_D, Highest Flow Rate

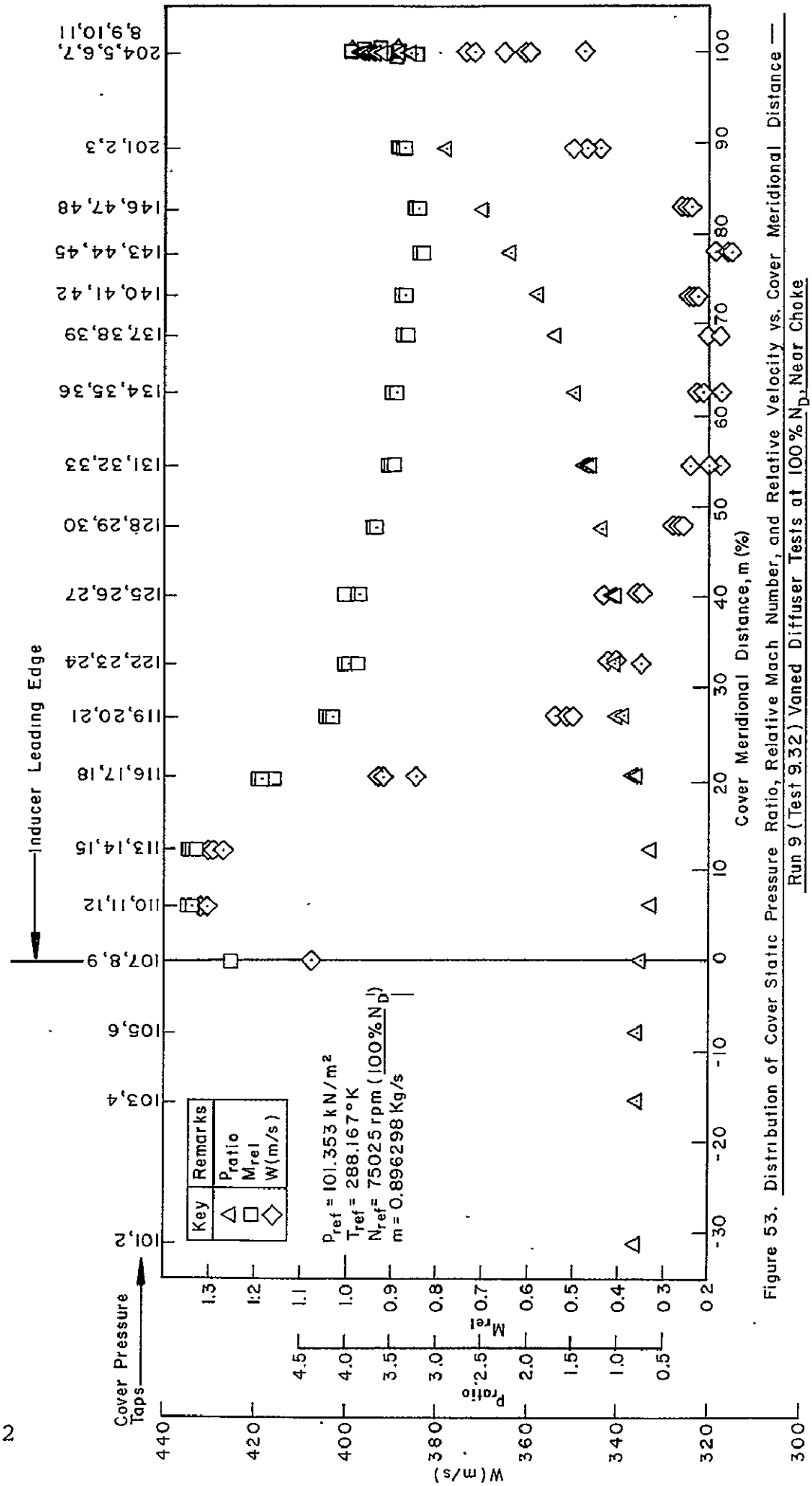

Figure 53. Distribution of Cover Static Pressure Ratio, Relative Mach Number, and Relative Velocity vs. Cover Meridional Distance — Run 9 (Test 9.32) Vaned Diffuser Tests at 100% N_D, Near Choke

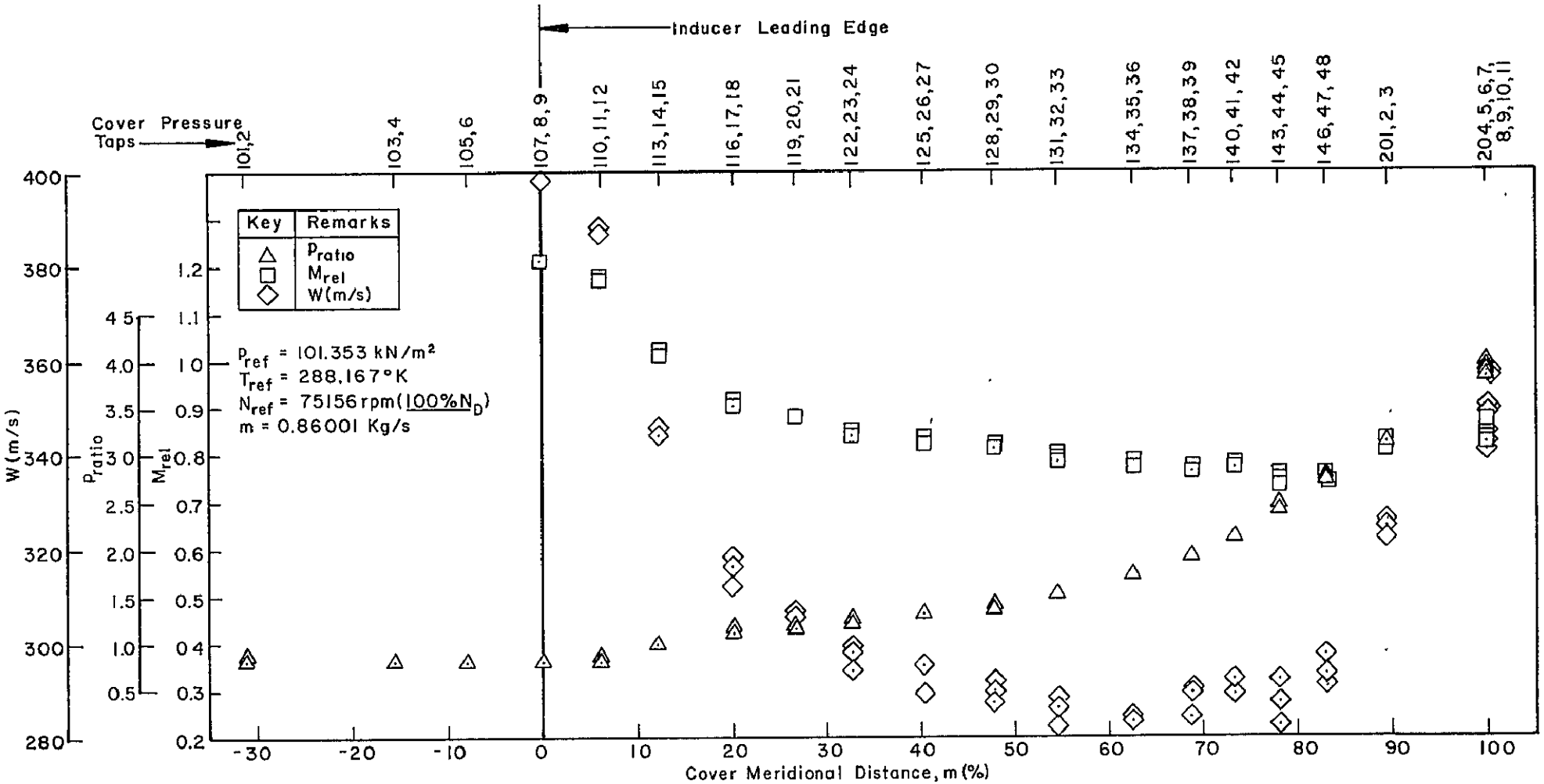

Figure 54. Distribution of Cover Static Pressure Ratio, Relative Mach Number, and Relative Velocity vs. Cover Meridional Distance — Run 9 (Test 9.38) Vaned Diffuser Tests at 100%N_D, Near Surge

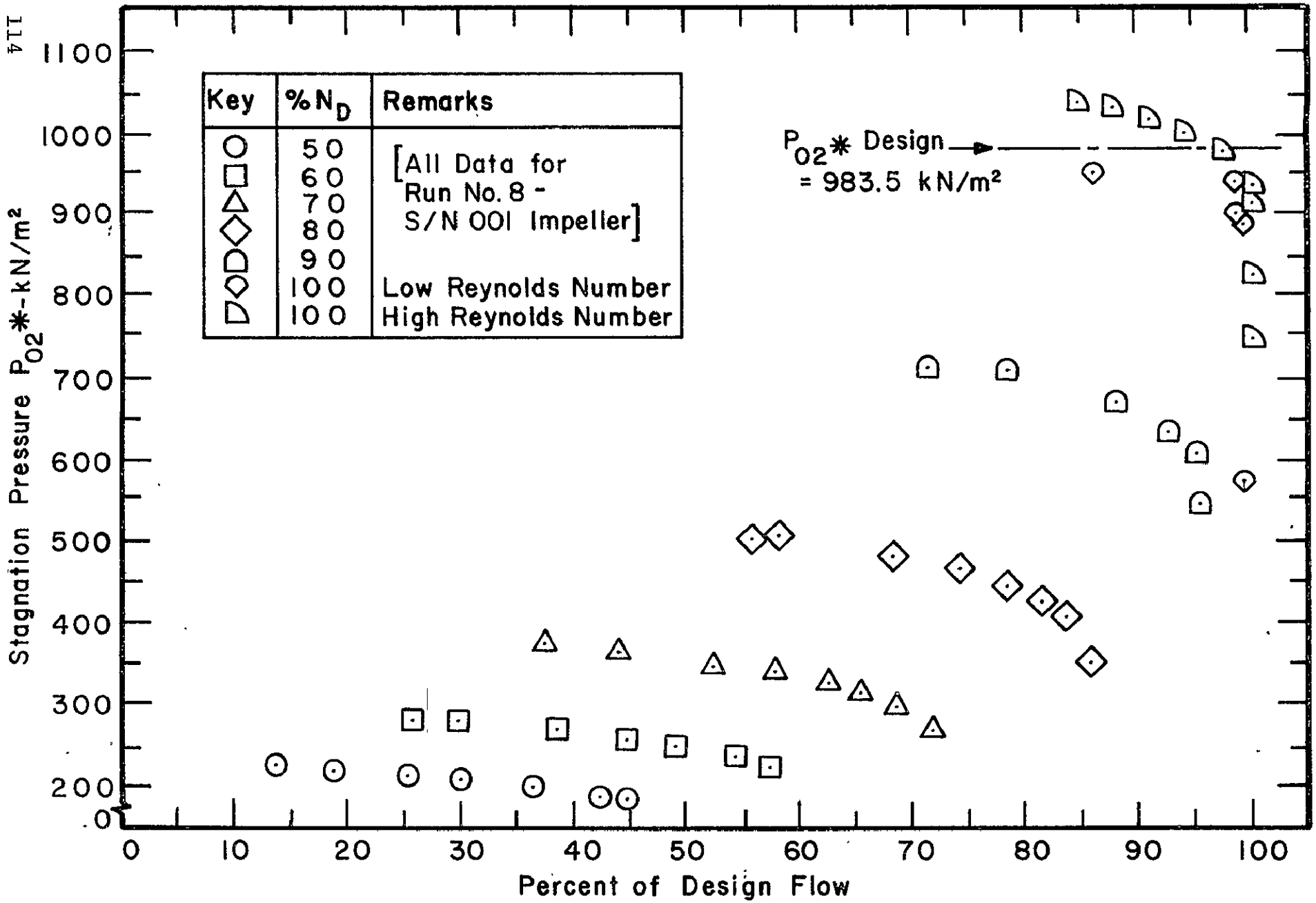

Figure 55: Mixed-Out Stagnation Pressure P_{02}* vs. Flow Rate - Vaneless Diffuser Tests

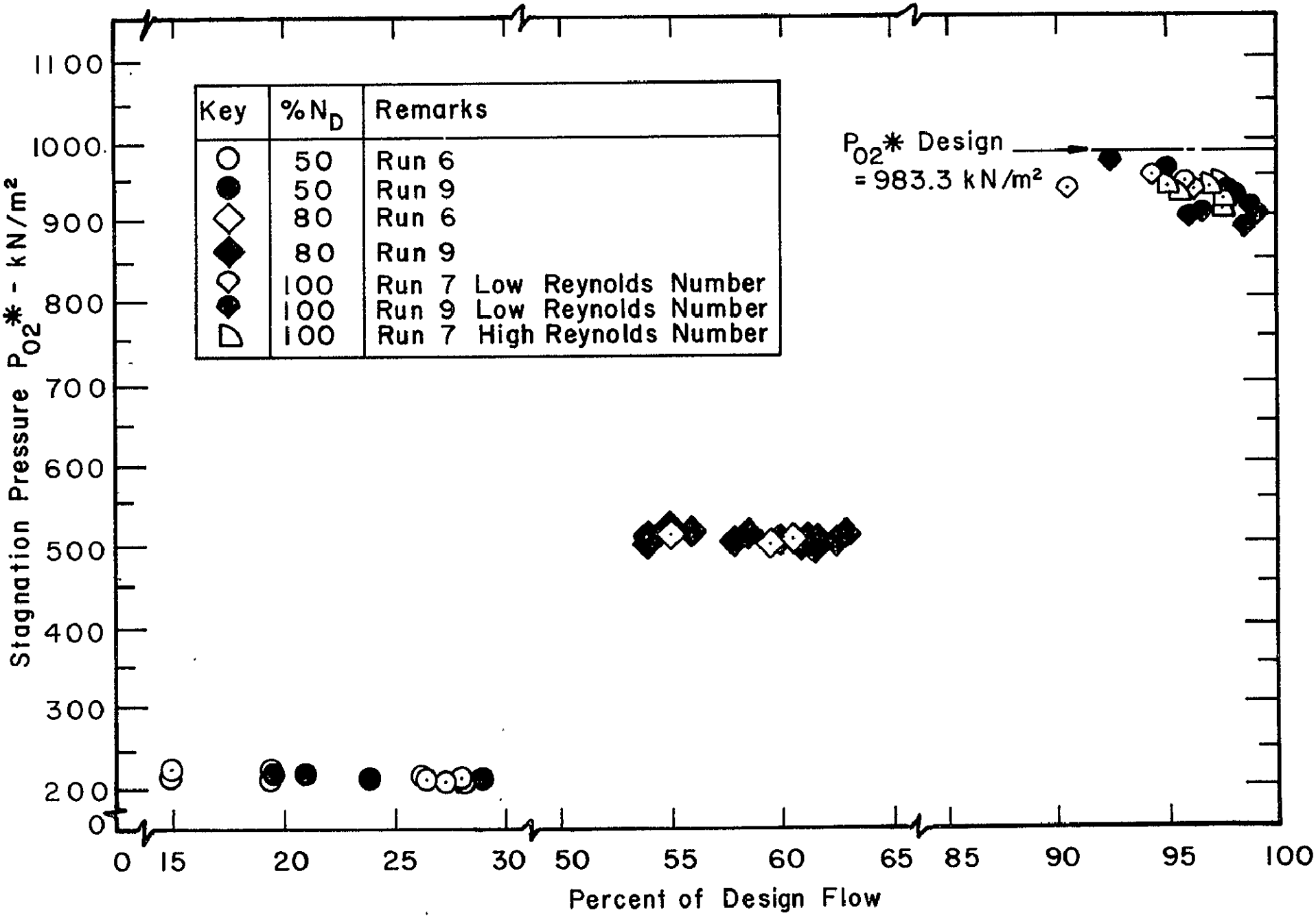

Figure 56. Mixed-Out Stagnation Pressure P_{02}* vs. Flow Rate - Vaned Diffuser Tests

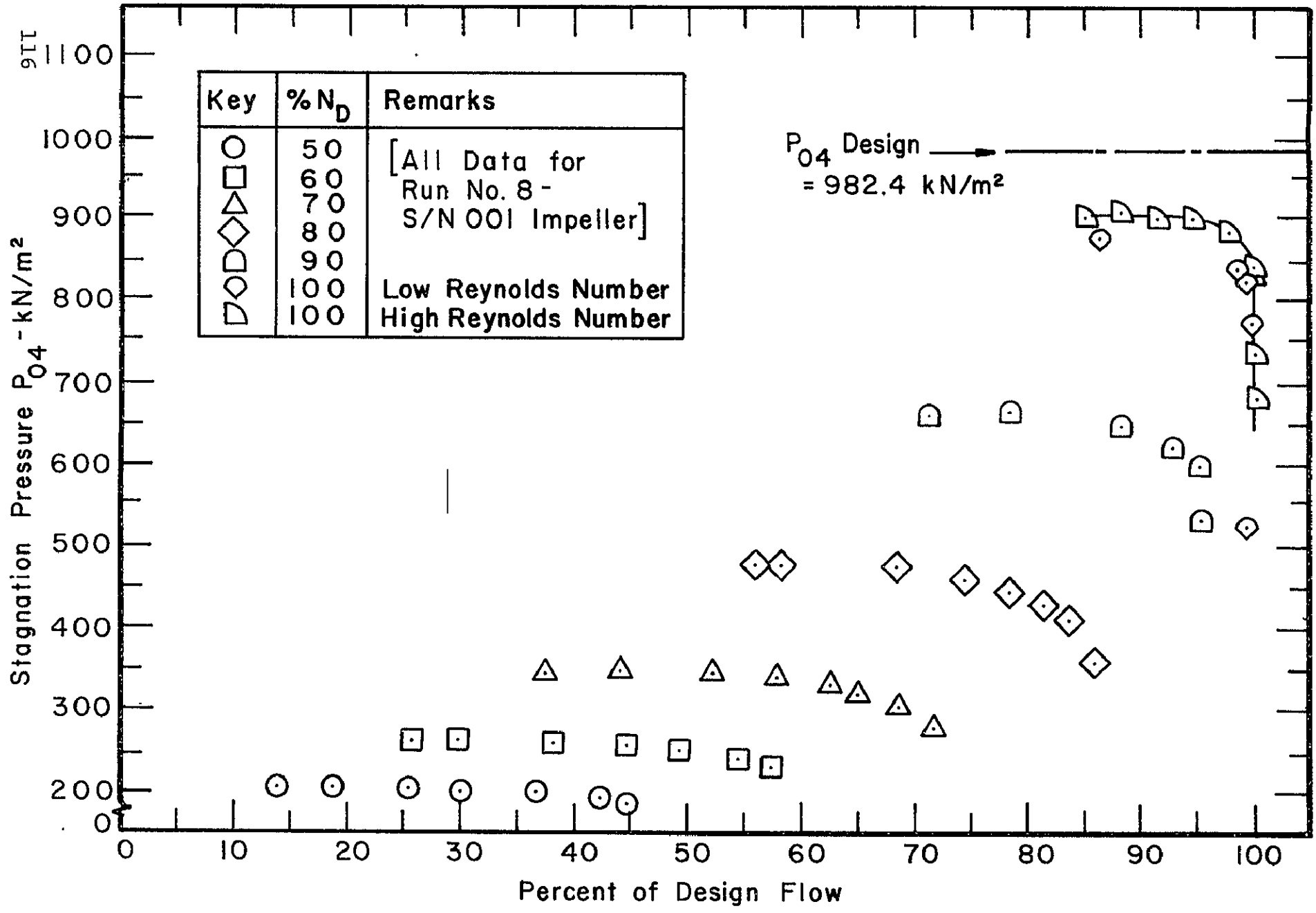

Figure 57. Measured Diffuser Stagnation Pressure P_{04} - Vaneless Diffuser Tests

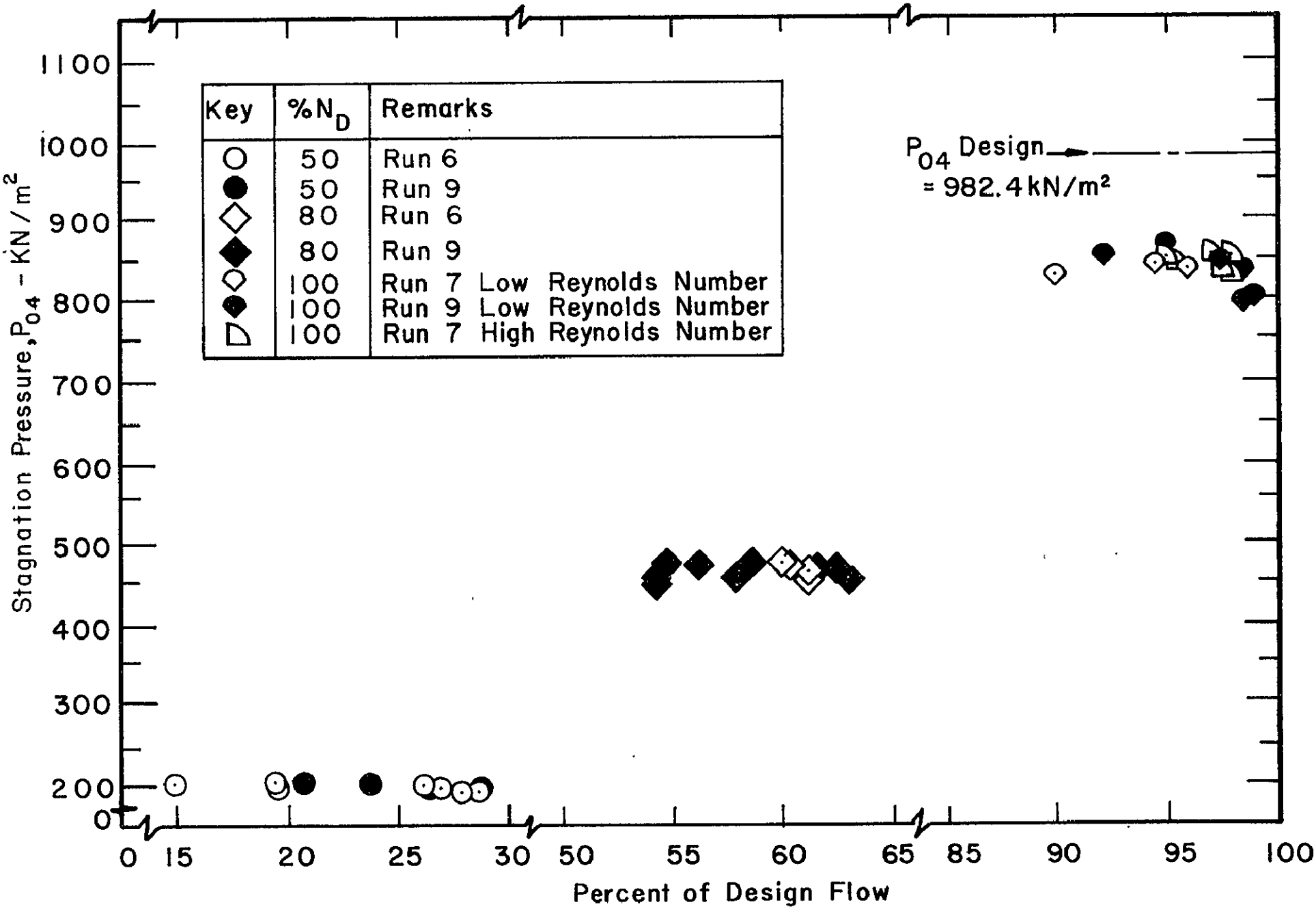

Figure 58. Measured Diffuser Stagnation Pressure P_{04} - Vaned Diffuser Tests

The aligned setting angle of these probes (measured from the radial direction) is 65° at a radius ratio R = 1.207 (referenced to the impeller tip exit radius). Calibration of these total pressure probes in a free jet at M = 1.0 showed an essentially flat response to ± 15° angles either side of the aligned position. The calculated, mixed-out, impeller exit, flow angle for the vaneless tests deviates from the probe angle, reaching about 8° difference at the lowest vaneless flows tested at 100% N_D. At the highest flows, the deviation is approximately 1° at the 100% N_D conditions. Therefore, it is not expected that there is any significant probe error in reading p_{o4} by these techniques for the vaneless diffuser tests for the range of flows tested.

Figure 59 shows the impeller efficiency η_{TTI} and decrements in total-to-static efficiency for the internal wake (η_{IW}), discharge mixing (η_{DM}), and total skin friction (η_{SF}) for the 100% N_D vaneless diffuser data (Run No. 8 - high Reynolds number). For this data, backflow losses have been set at zero by adjustment of the impeller slip factor σ.

Figure 60 shows the variation of the impeller exit wake flow fraction ε and the Mach numbers M2* and $M_{rel\ lt}$ versus the mass flow for the same data.

Impeller data for the 100% N_D vaned diffuser configurations are shown in Figure 61. Figure 61 gives the total-to-static stage efficiency losses attributable to internal wake losses ($\Delta\eta_{IW}$), total skin friction ($\Delta\eta_{SF}$), total impeller ($\Delta\eta_I$), discharge mixing ($\Delta\eta_{DM}$), and impeller/diffuser backflow ($\Delta\eta_{BF}$). Figure 62 presents the wake fraction ε and M2 and $M_{rel\ lt}$ vs. mass flow rate.

DIFFUSER DATA

Figure 63 shows the pressure recovery performance of the diffuser as deduced from the measured p_{o4} pressures. C_{pD} is based upon the "calculated" 2* values of static and total pressure taken from the CDR data reduction output. C_{p2*-4} and C_{p4-c} are based upon the measured p_{o4} values and by setting $p_4 = 0.528\ p_{o4}$; i.e., assuming, for all of the Run 7 data, that the diffuser channel is choked. The reasons for this latter assumption are explained later.

Figure 64 gives C_{p4-c} as a function of B_4 for the 100% N_D vaned diffuser data where the Run No. 7 data have been adjusted for $p_4 = 0.528\ p_{o4}$ where required. Also shown on this figure is the laboratory channel diffuser performance data for the channel diffuser configuration.

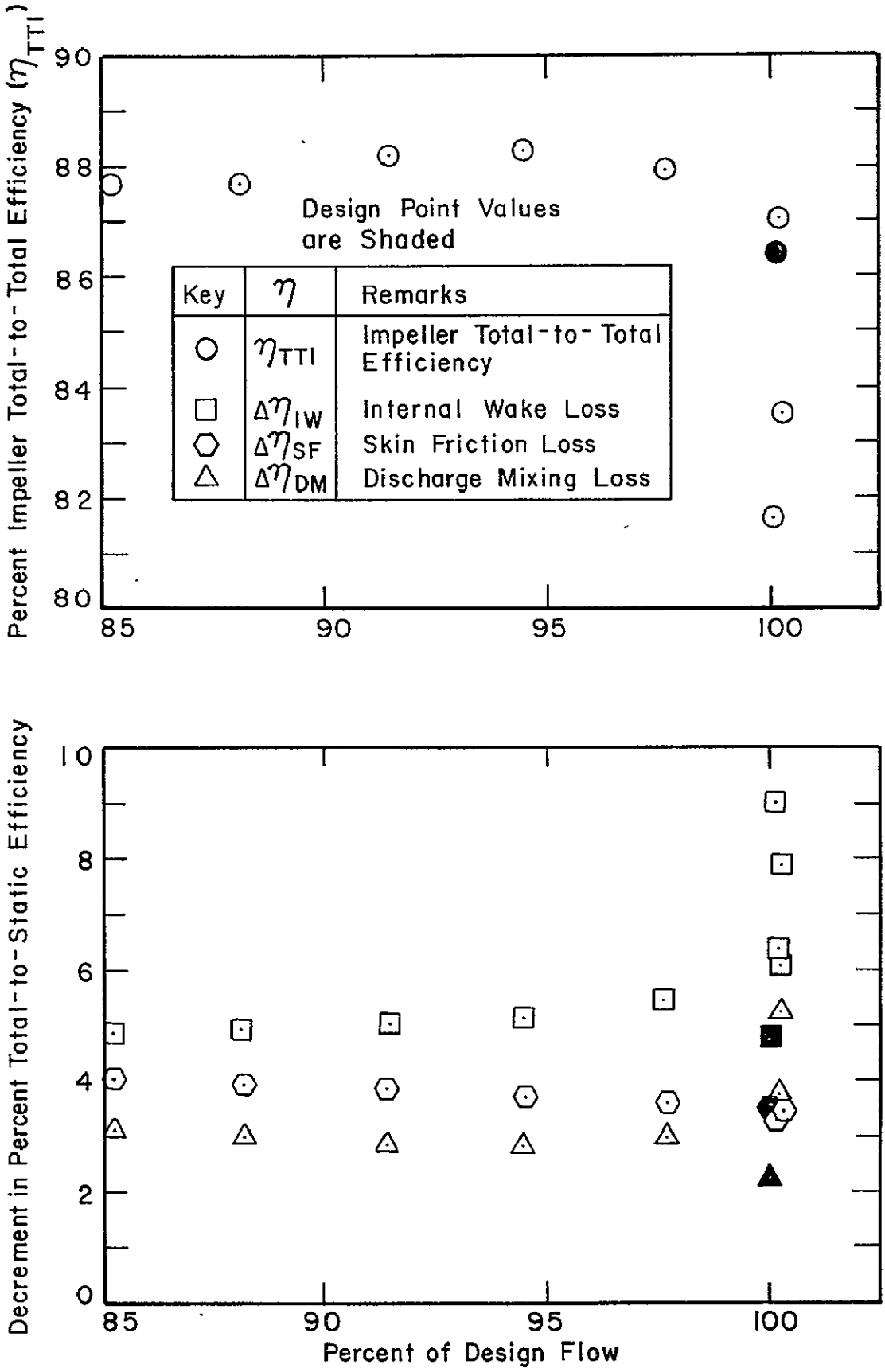

Figure 59. Impeller Efficiency Performance vs. Mass Flow Rate — Vaneless Diffuser Tests at 100% N_D

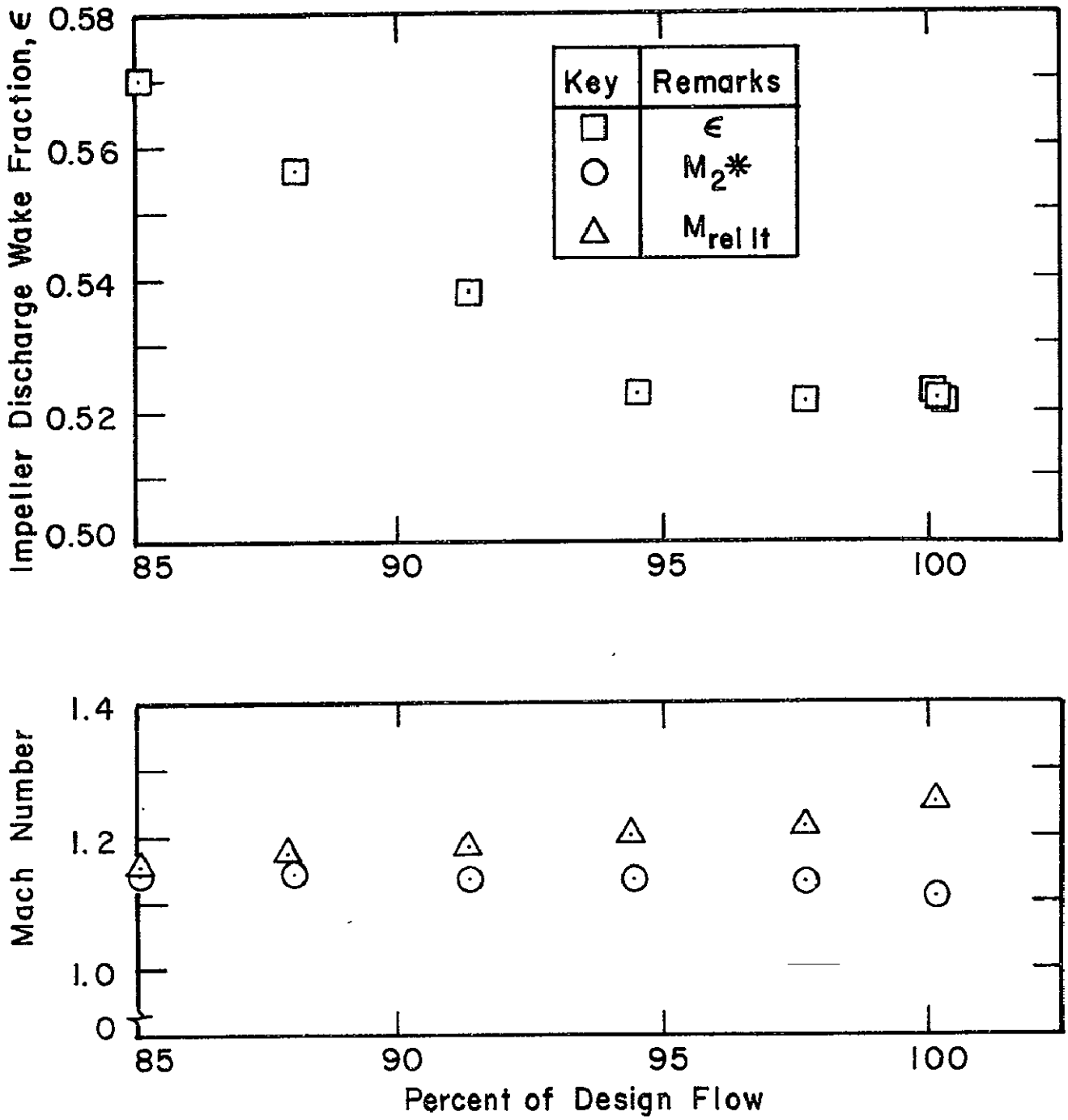

FIGURE 60. ϵ, M_2^*, $M_{rel\ It}$ vs. Mass Flow Rate — Vaneless Diffuser Tests at 100% N_D

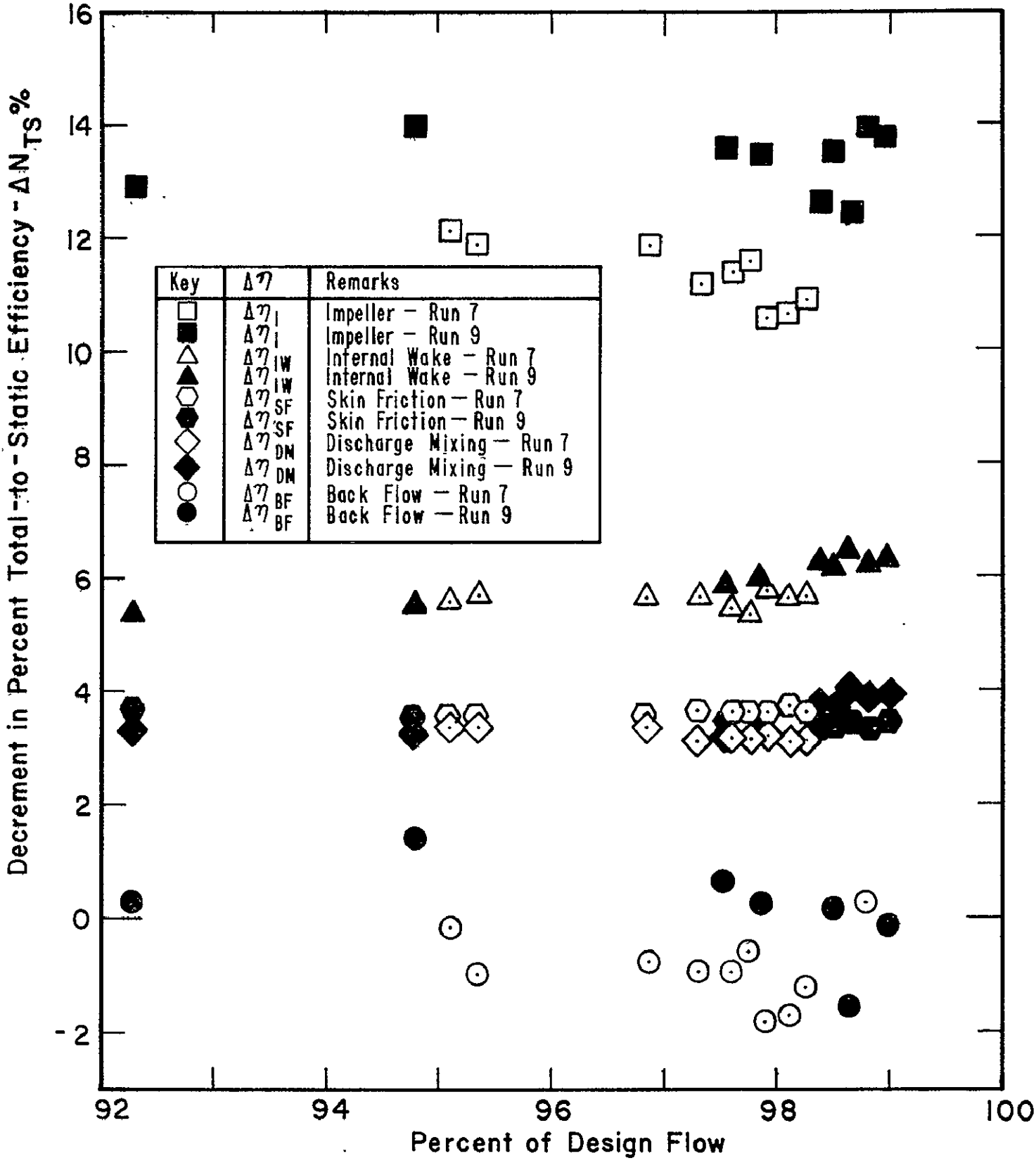

Figure 61. Impeller Efficiency Performance vs. Mass Flow Rate — Vaned Diffuser Tests at 100% N_D—

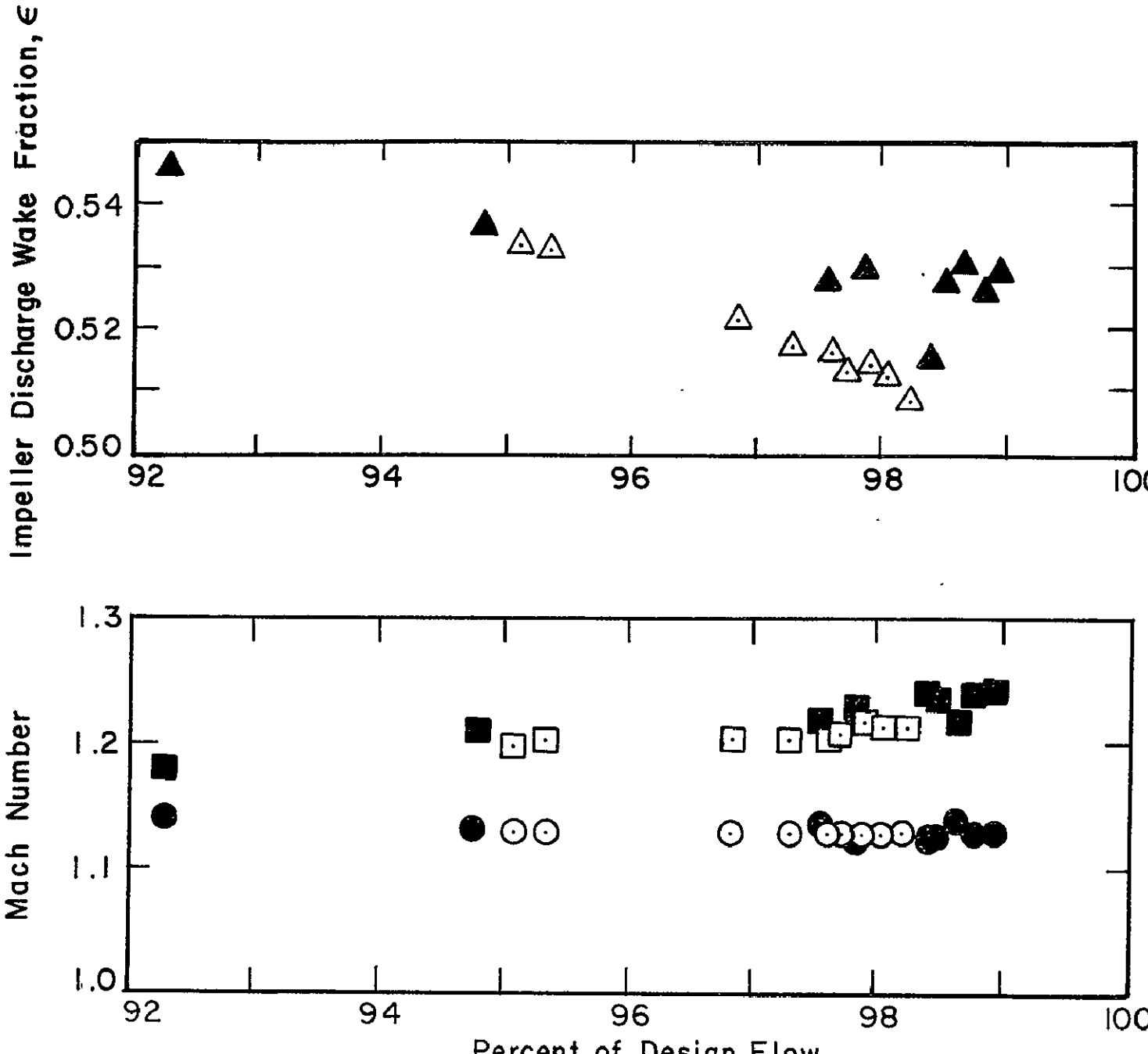

Figure 62. ϵ, M_2^*, $M_{rel\ lt}$ vs. Mass Flow Rate — Vaned Diffuser Tests at 100% N_D

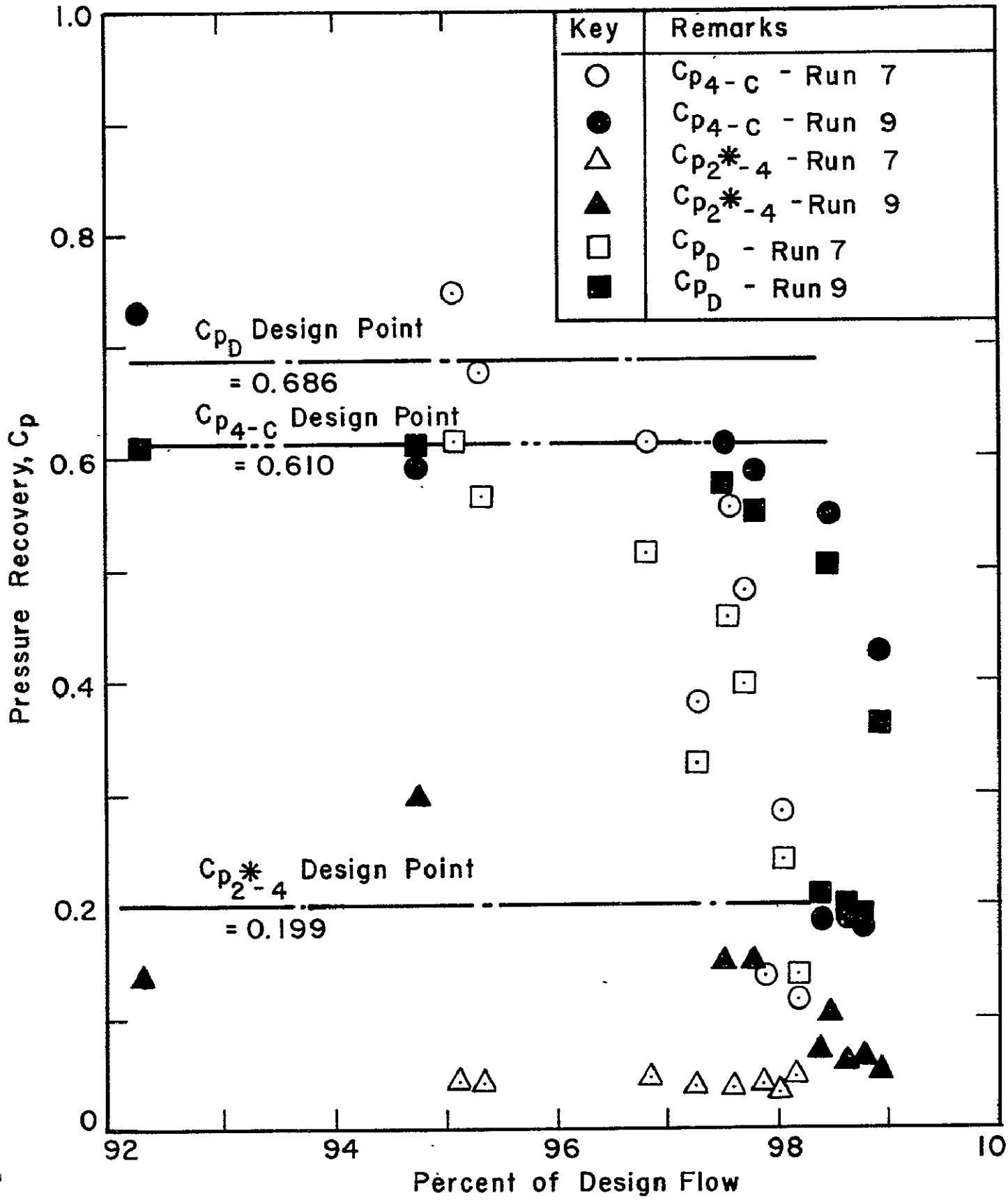

Figure 63. Diffuser Pressure Recovery Performance vs. Mass Flow Rate — 100 % N_D —

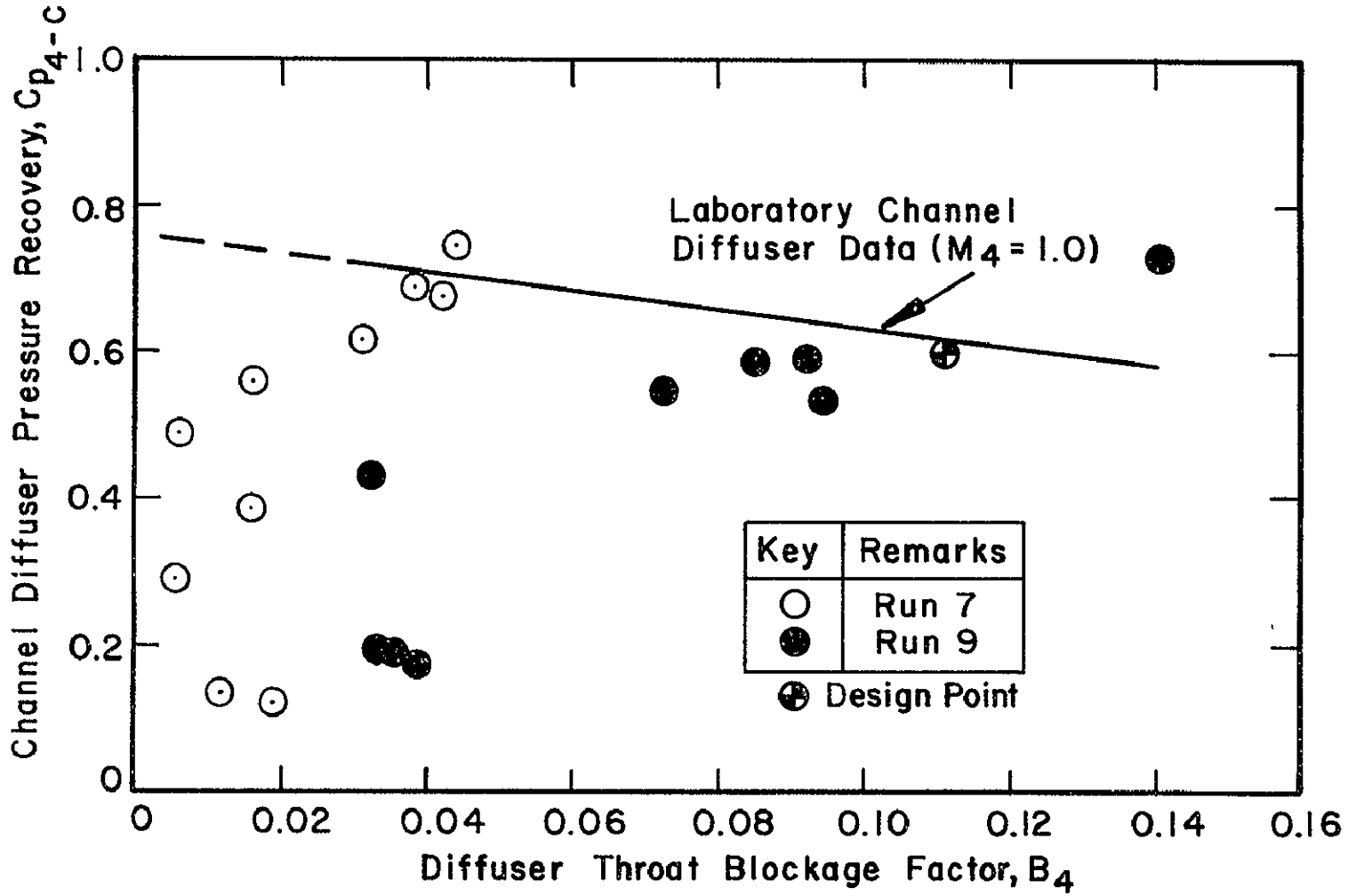

Figure 64 Channel Diffuser Pressure Recovery, $C_{p_{4-c}}$ vs. Diffuser Throat Blockage, B_4 - 100% N_D

Figure 65 shows B_4 vs. C_{p2^*-4} as a function of B_4 for the 100% N_D data where again the data of Run No. 7 are adjusted for $p_4 = 0.528\ p_{o4}$.

Figure 66 shows the decrements in total-to-static efficiency caused by the diffuser performance ($\Delta\eta_D$) and by the impeller exit to channel diffuser throat stagnation pressure loss ($\Delta\eta_{2^*-4}$) as a function of mass flow for the $p_4 = 0.528\ p_{o4}$, Run No. 7, 100% N_D data and the 100% N_D data of Run. No. 9.

The high blockage factor data shown in Figure 64 are for flow points near to surge. Shown on Figure 64 is the expected design point performance for the channel diffuser based upon the laboratory channel diffuser data for $M_4 = 1.0$ (and at other high subsonic throat Mach numbers). The data for both Runs 7 and 9, shown in this figure for 100% N_D, both have the high blockage factor, near-to-surge data clustered about the laboratory channel data. The low blockage factor data for each run are for choked diffuser conditions where the channel diffuser is supercritical with a shock in the diverging channel diffuser; hence the channel diffuser performance rapidly falls off from the laboratory data under these conditions. The static pressure data clearly illustrating the shock in diffuser operation is presented in the next section.

Figure 65, which shows the same data points as given in Figure 64, illustrates how the crucial channel diffuser throat blockage factor is dependent upon the calculated pressure coefficient C_{p2^*-4}. Also shown on Figure 65 is the correlation that was used during the diffuser design. While there is a lot of scatter in the data, it seems clear from this plot that the 'design correlation' curve is not applicable to this stage. Since the throat blockage factor is quite well defined by the stage measurements (mass flow rate, channel throat geometry, and measured total and static pressures), most of the uncertainty in the data shown in Figure 65 lies primarily in the calculation of C_{p2^*-4}. C_{p2^*-4} depends upon a calculated value of p_{o2^*} since there were no measurements made of stagnation pressure at (or near to) the impeller exit. The major uncertainty in understanding the performance of the stage lies in determining the actual value of p_{o2^*} produced by the impeller flow into the diffuser. Do large stagnation pressure losses exist in the vaneless/semi-vaneless space of the diffuser or does the impeller not produce as high an exit stagnation pressure p_{o2^*} as is calculated from the measured exit pressure p_{2^*}? The discussion given in the next section addresses this question.

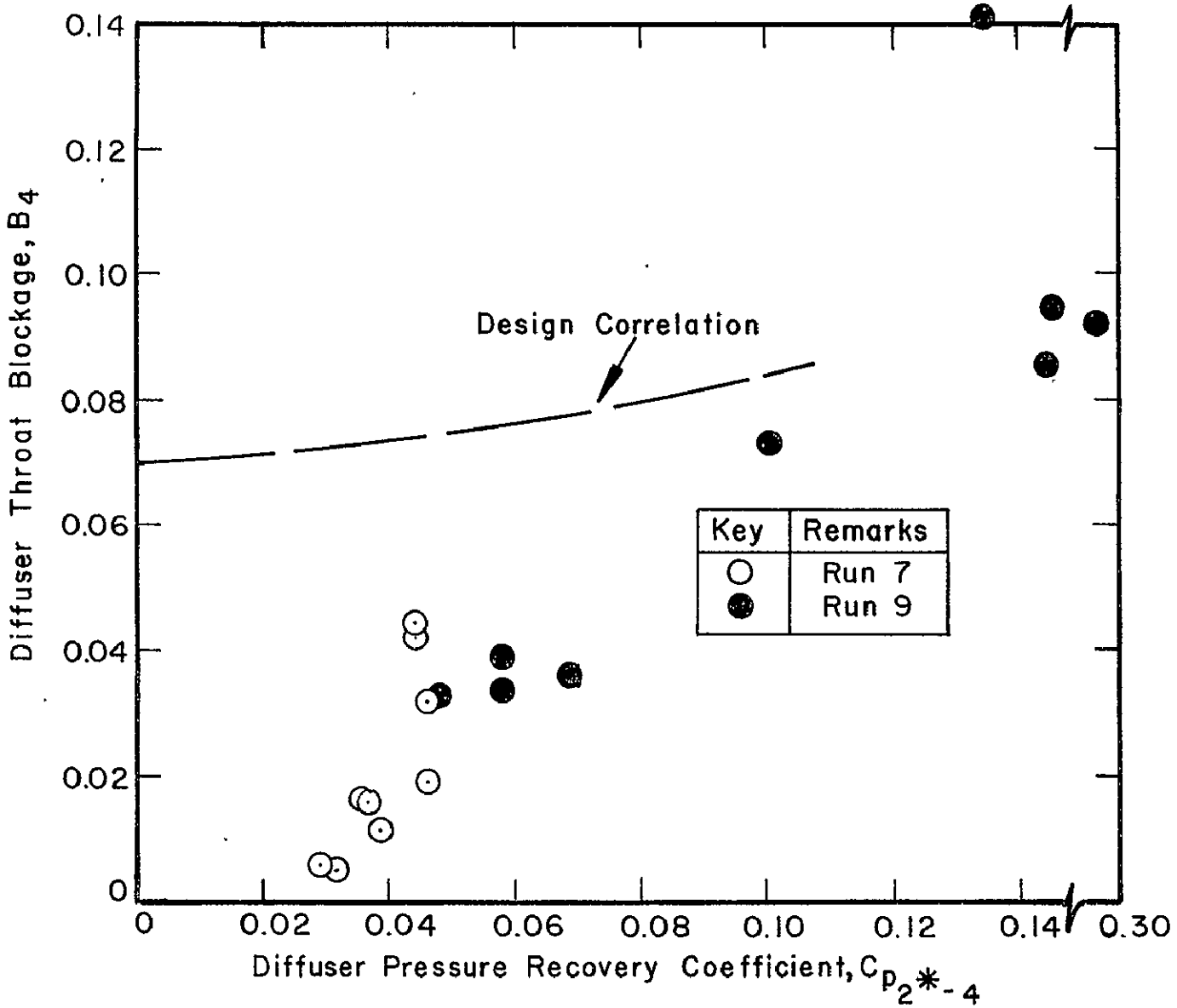

Figure 65. Diffuser Throat Blockage, B_4, vs. Diffuser Pressure Recovery Coefficient, $C_{p_2}*_{-4}$

$\frac{100\%N_D}{}$

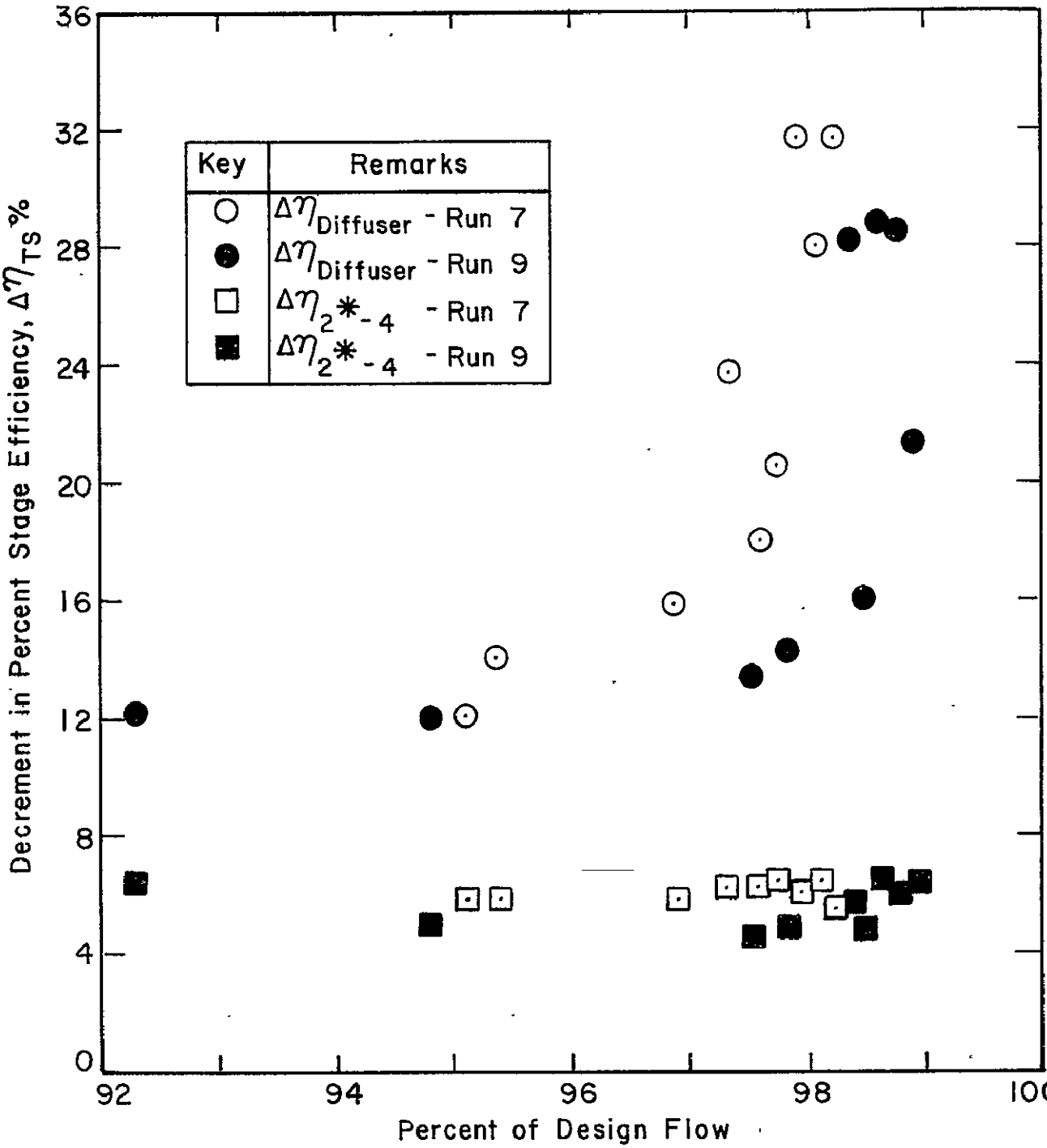

Figure 66. Diffuser Decrements in Stage Efficiency (Total-to-Static)-100 % N_D-

DISCUSSION

OVERALL STAGE PERFORMANCE

Stage performance for the vaned diffuser geometry appeared adequate up to 80% N_D (90% N_D performance was not measured for the vaned geometry). At 80% N_D, range was marginally satisfactory (12.3% choked-surge) and the peak efficiency appeared to be away from the surge line (see Figure 42). The peak efficiency was measured to be at 76% (75.99%). It was thus thought (after taking the 80% N_D data) that an efficiency "island" would appear in the 80%, 90%, and 100% speed range, and the performance would be close to the target design efficiency of 77%. Range would also be adequate (order of 10-12%) if the same choke-to-surge margin as for the 80% N_D data held up to 100% N_D.

Such was not the case, however (Figures 42 and 43). Efficiency fell short (a bit below 77% instead of the design 77% for the Run 7 data and 75% for the Run 9 data), range was short (2.5% to 3% choke-to-surge margin for the Run 7 data and 6.8% for the Run 9 data), and the stage choked prematurely (approximately 0.889 kg/s for the Run 7 data and 0.898 for the Run 9 data instead of the design intent of greater than 0.907 kg/s). Examination of the component performance of the impeller and diffuser leads us to believe that the impeller, while not a stellar performer, is performing adequately and that the main problem lies in the diffuser performance. Table XI summarizes the stage performance with the vaned diffuser.

TABLE XI. - VANED DIFFUSER PERFORMANCE TEST RESULTS, 100% N_D

	Build I/SN 001 Measured	Build II/SN 002 Measured	Design Intent
pr_{TS}	7.46	7.61	8.0
η_{TS}	75.4%*	75.0%	77%
m_{choke} (kg/s)	0.889	0.898	0.952
m_{surge} (kg/s)	0.863	0.837	0.838
$\frac{m_{choke} - m_{surge}}{m_{choke}}$	0.029	0.068	0.12

*76.7% η_{TS} was measured at 50% Reynolds number scaling at $m_{surge} = 0.82$ kg/s.

Examination of the MR_2/MR_{2i} data from the vaned tests shows that at stage choke the impeller inducer was not choked. Examination of the diffuser cover pressure data (Figures 67, 68, and 69) for the Build I diffuser clearly demonstrates that at stage choke the diffuser channel throat was choked with a shock located in the diverging portion of the channel diffuser. The reason for the very short flow range at 100% speed was not so obvious.

The vaneless diffuser performance tests were then run to confirm that the impeller operated satisfactorily and to attempt to provide better data for a redesign of the diffuser (Build II). The diffuser redesign was made to (1) increase the channel diffuser throat flow area sufficient to bring the diffuser choke flow higher than the choke flow of the impeller of 0.907 kg/s and, (2) to make other minor alterations that would lead toward improved flow range.

Examination of the static pressure field in the diffuser for the Build II configuration (Run 9 data) shows that choke was still brought on by the diffuser channels before the impeller inducer chokes.

The impeller and diffuser component performance are discussed separately next.

IMPELLER COMPONENT PERFORMANCE

The overall impeller performance in terms of MR_2 vs. MR_{2i} taken from the vaneless diffuser tests (Run No. 8 - Figure 44) shows that the impeller achieved very close to the desired diffusion (MR_2) but at slightly lower flow rates than the "design point" flow rate of 0.907 kg/s. The set of constant speed line curves on Figure 44 for 50% through 100% N_D followed the trend of other impeller data we have seen. However, they do fall below the "correlation" band shown in this figure.

For other high pressure ratio, good performing, high $M_{rel\ lt}$ impellers, the peaks of the curves rise from low values, for choke flow, up into the correlation band on Figure 44 as flow is reduced from choke. An examination of these data, however, shows that although these impellers have transonic $M_{rel\ lt}$ inducers, the relative Mach numbers are close to sonic or slightly below. It appears to be characteristic of higher relative Mach number inducers, i.e., $M_{rel\ lt} = 1.2 - 1.4$, that Mach number effects on the suction surface reduce the attainable diffusion of the impeller to somewhat below the correlation band of Figure 44. This impeller seems to follow this trend. The lower speed data (up to about 80% N_D) blend

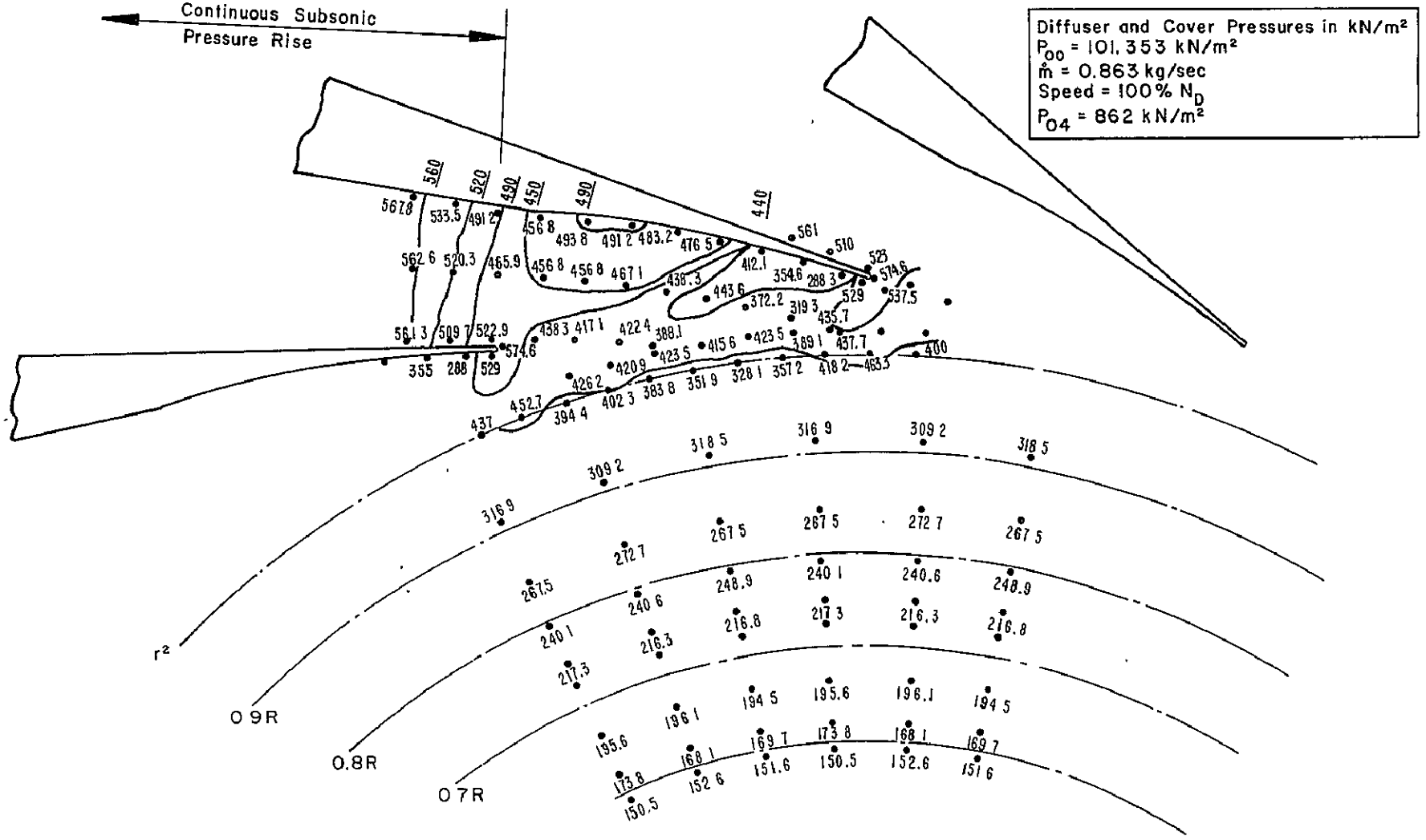

Figure 67. Diffuser & Cover Static Pressure Distribution and Isobars – Run 7 (Test 7.11)
Vaned Diffuser Test at 100% N_D Near to Surge

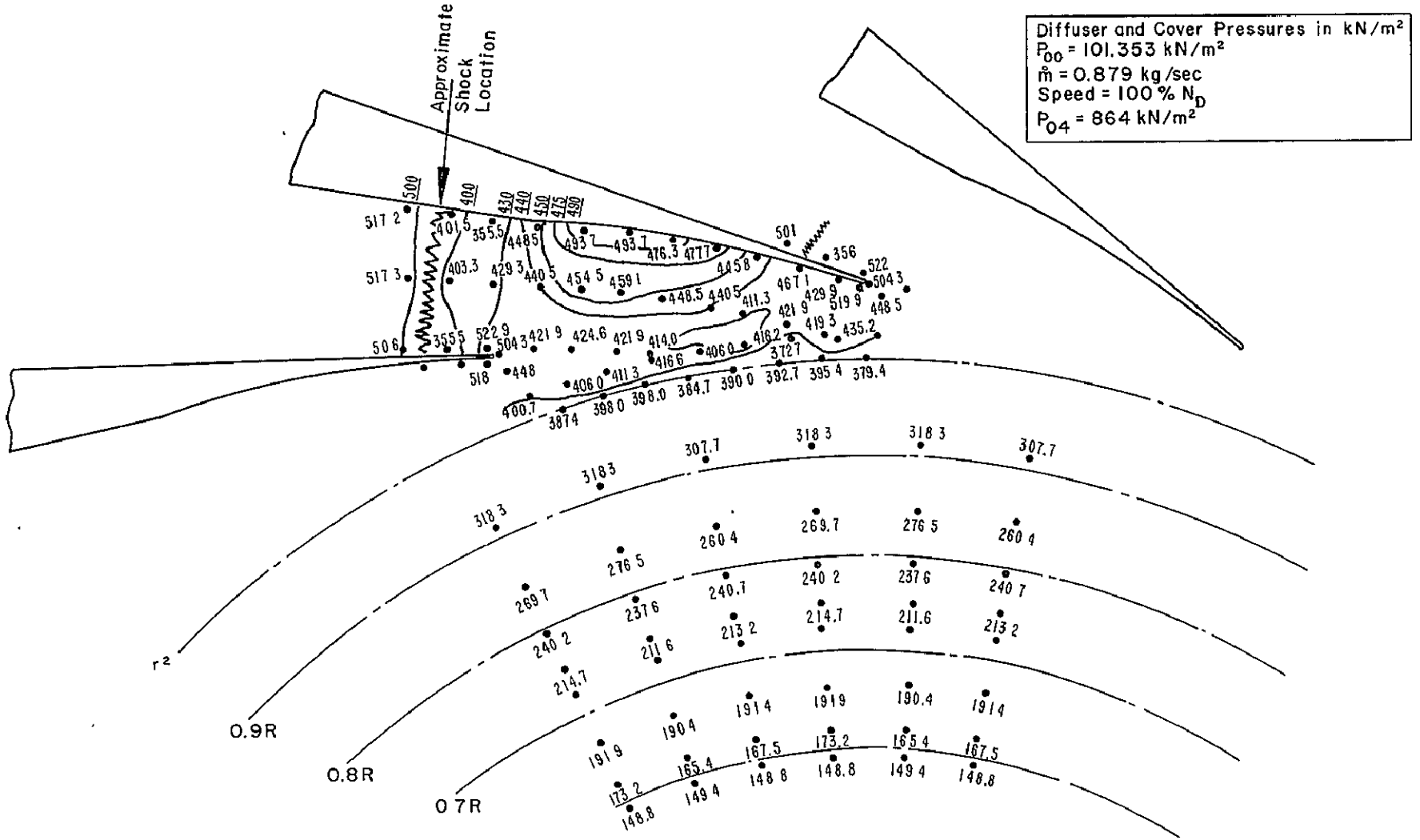

Figure 68. Diffuser & Cover Static Pressure Distribution and Isobars — Run 7 (Test 7.13)
Vaned Diffuser Tests at 100 % N_D Choked Flow

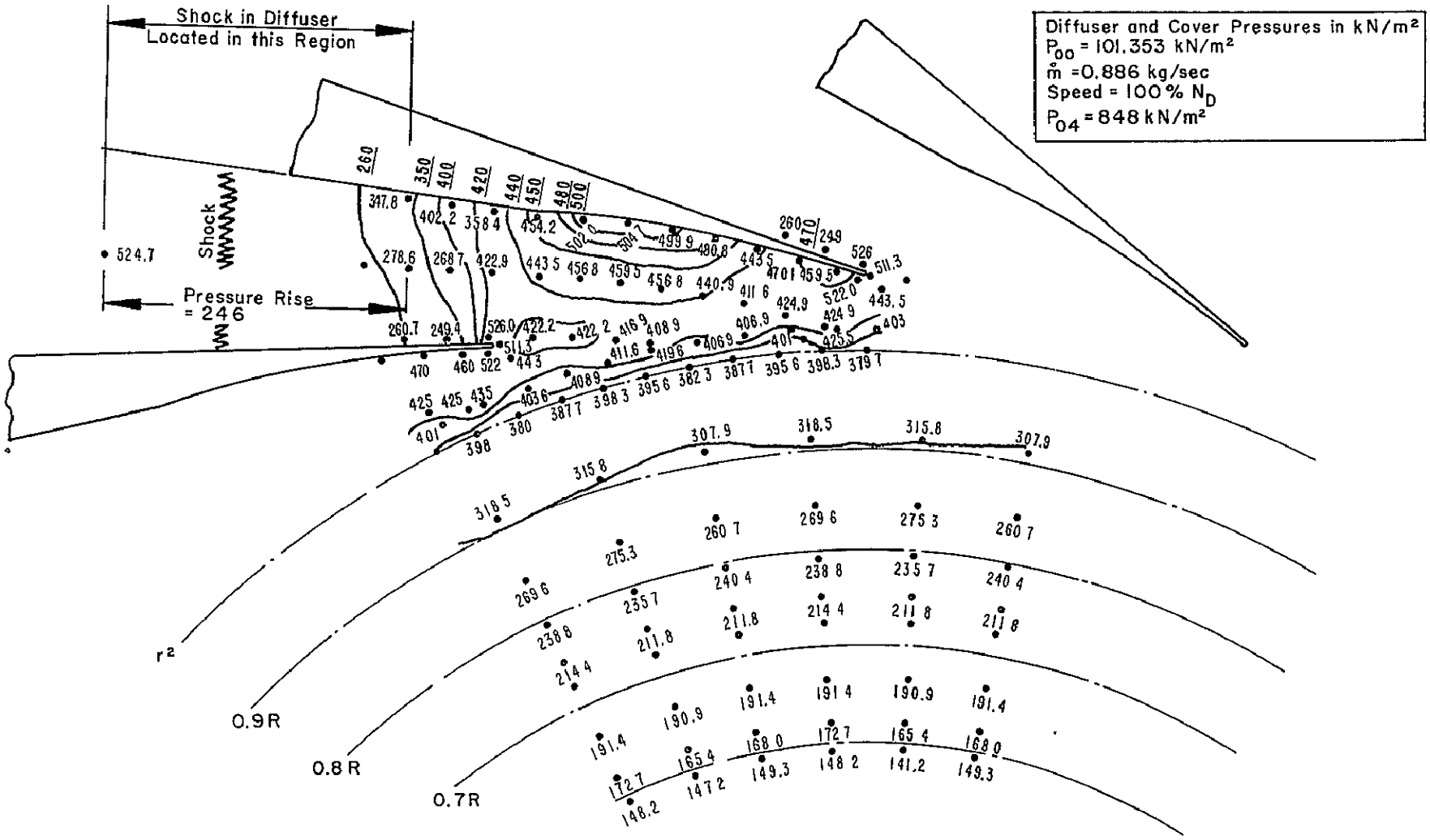

Figure 69. Diffuser & Cover Static Pressure Distribution and Isobars — Run 7 (Test 7.17) Vaned Diffuser Tests at 100% N_D

in very closely to the bottom line of the correlation band while the 80%, 90%, and 100% N_D speed line data demonstrate a continual "dropping away" from the lower values of this correlation.

Figure 44 also shows that the low Reynolds number 100% speed data did not achieve as much diffusion as the high Reynolds number data. Remember that Reynolds number differs by a factor of 2 between these two cases.

Figure 45 (impeller data for the vaned diffuser tests) shows that all of the SN 002 impeller data fall below that for the SN 001 impeller. However, all of the SN 002 data are also at the low Reynolds number scaling while the SN 001 data shown on this figure are at high Reynolds number. From Figure 44, as discussed above, a portion of the performance decrease in Figure 45 is associated with Reynolds number scaling, but it also seems clear that the SN 002 impeller did not perform as well as the SN 001 impeller.

Examination of the impeller cover pressure data (Figures 47-54) shows that the impeller probably is separated from about 40% meridional distance to the tip.* Figure 50, line 8.86, indicates separation at a slightly earlier position in the impeller (at approximately 30% meridional distance). This is probably due to inducer incidence effects. For line 8.86, the incidence is positive and approximately 8 degrees. Figure 52, line 8.96, shows data for the case where the impeller is somewhat into choke. The relative Mach number rises, in this case, after the impeller lead edge, in contrast to the other distributions at this speed. And even though separation seems to occur slightly downstream of the 40% meridional distance, the relative Mach number only diffuses to approximately 0.9 at the impeller exit.

These impeller cover distributions for the vaneless diffuser data are almost the same as the distributions shown in Figures 47-49 for the 100% vaned diffuser data when referred to in the same mass flow rate.

Table X and Figure 46 show that the design point incidence of about 4 degrees was actually obtained at a lower mass flow rate than the "design point" flow of 0.907 kg/s. This seems to be verified by the Kulite data from the inducer (see Figure 75) where at 3.5 degrees incidence (Figure 75b) the blade-to-blade loading is relatively consistent compared to that at 8 degrees incidence (Figure 75b).

*This argument is based upon a constant M_{rel} line which meets the "unloaded blade" M_{rel} at the impeller exit at $r = r_2$.

The inducer was designed using a one-dimensional mass average calculation that takes into account meridional distortion of the flow streamlines approaching the inducer resulting from blade blockage and the hub ramp. Both of the mass average incidence data points on Figure 46 are approximately 2 degrees above the curve through the incidence data deduced from the inlet static pressure. Thus a curve drawn through the mass average incidence data (the dashed curve in Figure 46) would come close to the design point incidence of 4 degrees at 100% N_D. The mass average incidence calculation method is essentially the same as used in the design analysis. The lower incidence values deduced from the measured static pressures ahead of the inducer in the inlet duct indicate a greater distortion in the flow approaching the inducer than was assumed in the design calculations.

We now look at the impeller exit conditions. Figure 55 shows that the calculated (i.e., deduced) stagnation pressure p_{o2*} is very close to the design value of 983 kN/m^2 at the mass flow corresponding to the design point incidence of 4 degrees on the impeller inducer tip. Lower mass flows produce a higher p_{o2*} than "design". At the original design point mass flow of 0.907 kg/s, the stagnation presssure p_{o2*} falls to about 945 kN/m^2, i.e., about 38 kN/m^2 below the design point value.

Figure 56 for the vaned diffuser tests shows that at 100% N_D the calculated p_{o2*} values are lower than those for the vaneless data, being about 945 kN/m^2 at the 4 degree incidence flow rate ($\sim$ 97% of design flow rate).

A major discrepancy in stagnation pressure data appears, however, when the p_{o2*} values, which are deduced on the basis of measured impeller tip exit pressure p_2, are compared with the measured stagnation pressure from the p_{o4} probes located in the diffuser throat. Figure 57, for the vaneless diffuser test data, shows p_{o4} reaching maximum values of approximately 900 kN/m^2 (at 85% to 95% of design flow). At 97% of design flow rate, which corresponds to the 4 degree incidence flow rate, the deduced p_{o2*} for the same vaneless tests is approximately 983 kN/m^2 (the p_{o2*} design value - see Figure 55) and still continuing to increase as flow rate is reduced. Thus there appears a decrement in stagnation pressure of $\sim$ 10% between the p_{o4} measured value and the calculated p_{o2*} at the 95% of design flow point, and this decrement becomes even larger as flow rate is reduced.

Measured p_{o4} pressure for the 100% vaned data, shown in Figure 58, displays a measured value of about 863 kN/m^2 at the 4 degree incidence flow point. At this flow rate, there is thus a decrement of about 82 kN/m^2 below the calculated p_{o2*} value for the vaned data (see Figure 56) and also a decrement

of about 20 kN/m^2 lower than the corresponding p_{o4} measurement in the vaneless diffuser configuration.

This mismatch between the design calculated value of stagnation pressure at the impeller exit (state 2*) and that actually measured at the diffuser throat (state 4) is the primary reason for the mismatch in vaned diffuser choke flow at the 100% speed line. The diffuser design calculations assumed only a small stagnation pressure loss (a normal shock stagnation pressure loss) between p_{o2*} after mixing and the throat core value of stagnation pressure p_{o4}.

An interesting comparison is to be made between Figures 55 and 57, which display the measured p_{o4} values for the vaneless data. These data show almost no discrepancy between p_{o2*} and p_{o4} measured up to 80% N_D (for most of the flow range along a constant speed line, the foregoing is true; only at the lower flows does a pressure discrepancy appear which only amounts to about 14-28 kN/m^2 at the lowest flow point for each speed line, respectively). However, for the 90% and 100% speed line data, a major difference shows up between the impeller tip calculated p_{o2*} and the measured throat values of stagnation pressure p_{o4}. This discrepancy is glaringly obvious at the 100% speed situation. At 100% speed, the difference in stagnation pressure at the 4 degree incidence flow point is about 97 kN/m^2, but becomes increasingly worse as the impeller is run to low flow rates. At 85% of design flow, there is a 138 kN/m^2 decrease in stagnation pressure between 2* and 4.

A comparison between Figures 57 and 58, which display the measured p_{o4} values for the vaned and vaneless diffuser tests, shows the behavior as discussed above for speeds up to 80% N_D. That is, the measured p_{o4} values for the vaned data agree very well with the vaneless p_{o4} values at the same mass flow rates. Further, these values are in almost exact agreement with the vaneless p_{o2*} values.

Whatever is the cause of this stagnation pressure loss (Δp_{o2*-4}), at the higher speeds, we believe it is associated with some high transonic Mach number effect at the impeller exit. It is hard to see how the tie-bolt blockage can account for this stagnation pressure loss in the vaneless diffuser tests, since the blockage caused by the first row of bolt circles located at a radius ratio of 1.27 is only 5.4%. The key to greatly increasing diffuser component performance at the high pressure ratio Mach number conditions for this stage will be to explain the cause and to devise methods to reduce the large stagnation pressure loss between the impeller tip and the flow through the diffuser throats. It will be necessary to verify with survey probes near the impeller exit that the calculated values of total pressure (p_{o2*}) are representative of the actual pressure in the flow.

Finally, Figure 59 shows the measured impeller performance in terms of impeller total-to-total and total-to-static efficiency loss mechanisms. Shown on this figure are the "design point" values (indicated by the shaded symbols). The impeller performance with the vaneless diffuser exceeds the "design point" performance at less than 100% design flow rate. In particular, if the mass flow point corresponding to optimum incidence onto the inducer (the 4 degree incidence flow rate) is examined, the internal wake, skin friction, and discharge mixing losses are within one point of the design values. Backflow loss is very close to zero. The impeller total-to-total efficiency is higher than design for the vaneless diffuser test, i.e., $\eta_{TTI} \simeq 88\%$. At higher mass flows, the internal wake and discharge mixing losses increase slightly and drop the impeller efficiency for the vaneless diffuser test to about 87%.

Figure 61 shows the same type of data taken for the vaned diffuser tests (Runs No. 7 and 9). This figure shows the impeller internal loss mechanisms to agree within one point of those shown for the vaneless tests at the same mass flows. The decrement in impeller efficiency $\Delta\eta_I$ varies between 12% and 14% with the lower values corresponding to the Run No. 7 data for diffuser Build I. Thus the Run No. 7 data show an impeller total-to-total efficiency close to 88% (the same as that indicated by the vaneless diffuser performance shown in Figure 59) while the Run No. 9 data, using the Build II diffuser, show an impeller total-to-total efficiency closer to the design value of 86%. Some of the backflow loss data for both Runs 7 and 9 indicated a "negative" backflow loss. These values were brought to zero by adjusting slightly the magnitude of slip factor in the calculations. In all cases these adjustments were small, the adjustment decreasing slightly the overall impeller efficiency while having almost no effect on internal wake, skin friction and discharge mixing loss.

Figures 60 and 62 show that the impeller discharge wake fraction ε and the mixed-out impeller discharge Mach number M_2^*, using the wake/jet flow model, are calculated to be essentially identical for both the vaned and vaneless tests. The Run No. 7 data in Figure 62 show a slightly lower wake fraction and discharge Mach number than the data for Run No. 9 at the highest flow rates. This may be a real effect, caused by the differences in diffuser builds between these two series of tests, or the small differences may be attributable to the accuracy of determining an average impeller exit static pressure from the measurements made at the impeller exit with the vaned diffuser geometries.

Impeller Component Summary. An overall summary of the impeller performance is that it meets design specifications, but does so at a mass flow rate about 3% below design intent.

Impeller efficiency is slightly higher than "design" by about 1.5% for the vaneless diffuser tests and equal to the design value for the vaned diffuser tests. Impeller choke is just slightly higher than design flow (0.907 kg/s). It would be desirable to redesign the diffuser to obtain a much improved range-to-surge (surge at lower flows) and to shift to a "new design point" mass flow on the order of 97% of the present design flow. This mass flow would provide for optimum incidence onto the inducer lead edge at the tip.

DIFFUSER COMPONENT PERFORMANCE

From the discussions above, it is obvious that the vaned diffusers, both Builds I and II, choke prematurely. This is caused by a stagnation pressure at the diffuser throat which is much smaller than the design value.

Figure 63 shows the components of diffuser pressure recovery, C_{pD}, C_{p4-c} and C_{p2^*-4} for the vaned diffuser data at 100% N_D. The data plotted for Run 7 are from the CDR output, setting $p_4 = 0.528\, p_{o4}$ measured. The reason for plotting the data this way was that from the diffuser cover static pressure contours (discussed below) it was obvious that the diffuser throat was close to choke for mass flows of 0.88 kg/s (97% of design flow) and above. The standard CDR2 output accepts the p_4 measured value as "accurate" and adjusts p_{o4} downward if the values of measured p_4 and p_{o4} indicate the diffuser channel has a Mach number higher than unity. Because the diffuser was choking at these mass flows and it is difficult to accurately locate the aerodynamic throat in the diffuser, it seemed more reasonable to believe the stagnation pressure measurement of p_{o4} and adjust p_4 to agree with choked values of C_{p4-c}.

The stagnation pressure probes are located just downstream of the diffuser throat and any loss in stagnation pressure as a result of shock effects is expected to be small (less than 2% for Mach numbers up to 1.3); the stagnation pressure values were not corrected for any shock effects.

It is apparent that at 97% of design flow (and greater), the overall diffuser recovery C_{pD} is significantly below the design value of 0.686. There is a difference of about 18 points in overall pressure recovery (at this mass flow) between the design point value and the measured value for the Run No. 7 data, and about 10 points difference for the Run No. 9 data. Figure 66 shows that there is about 12 to 16 points in overall stage efficiency loss accountable to the diffuser recovery at 97% of design flow.

Figure 63 also shows, even with the data scatter present, that the straight channel recovery values C_{p4-c} rise appreciably as the mass flow rate is reduced. At the lower mass flow rates, the recovery of the straight channel is equal to or greater than the "laboratory" straight channel data, based upon the actual measured values of p_4 and p_{o4}. At the higher flow rates approaching choke, the channel recovery deteriorates rapidly. An explanation is found from an examination of the static pressure isobars measured on the shroud cover of the diffuser (see Figures 67 to 71). The diffuser flow at mass flows approaching and into choke is actually "supercritical" with the diffuser channel choked and a shock located downstream in the diverging portion of the channel. The downstream shock is destroying the subsonic channel diffuser recovery. As the mass flow is reduced, the diffuser channel finally unchokes, and the channel recovery "rises" to the laboratory indicated values for the blockages measured. The observed variation in mass flow at "choked conditions", i.e., from about 0.880 kg/s (97% of design flow) to the maximum value of 0.889 kg/s for Run 7, could be due to slight area changes caused by boundary layer changes in the diffuser throat; we have seen such a choked flow mass flow increase before.

Thus for the low mass flow rates of Runs No. 9 and 7, 100% N_D data, the channel diffuser performance is close to design intent but the overall diffuser recovery is low by about 10 points for Run 7 and about 8 points for Run 9. This is the result of the large stagnation pressure loss that appears to occur between 2* and 4; this loss was not allowed for in the stage design. The reduction in peak stage efficiency due to this loss is about 5 percentage points (Figure 66). This loss, moreover, has produced a lower overall stage pressure ratio than design intent. Thus we are once again faced with the problem of explaining the unaccountable stagnation pressure loss Δp_{o2*-4}. Bear in mind that this loss is also observed in the vaneless tests for the higher speeds.

Stage Surge. What causes the stage to surge? Figures 67 68, and 69 show the Build I diffuser shroud pressure measurements for the vaned 100% N_D data of Run 7. Figures 70 and 71 show similar data for the Build II diffuser data of Run 9. Drawn on these figures are pressure contours (isobars) for the three mass flows. Careful examination of the diffuser pressure distributions shows that Tests 7.13, 7.17, and 9.32 (Figures 68, 69, and 71, respectively,) have shocks located in the channel diffuser. These cases are operating at mass flows where the diffuser is choked and a relatively strong shock sits in the diverging portion of the channel. Tests 7.11 and 9.38, on the other hand, show a continual pressure rise

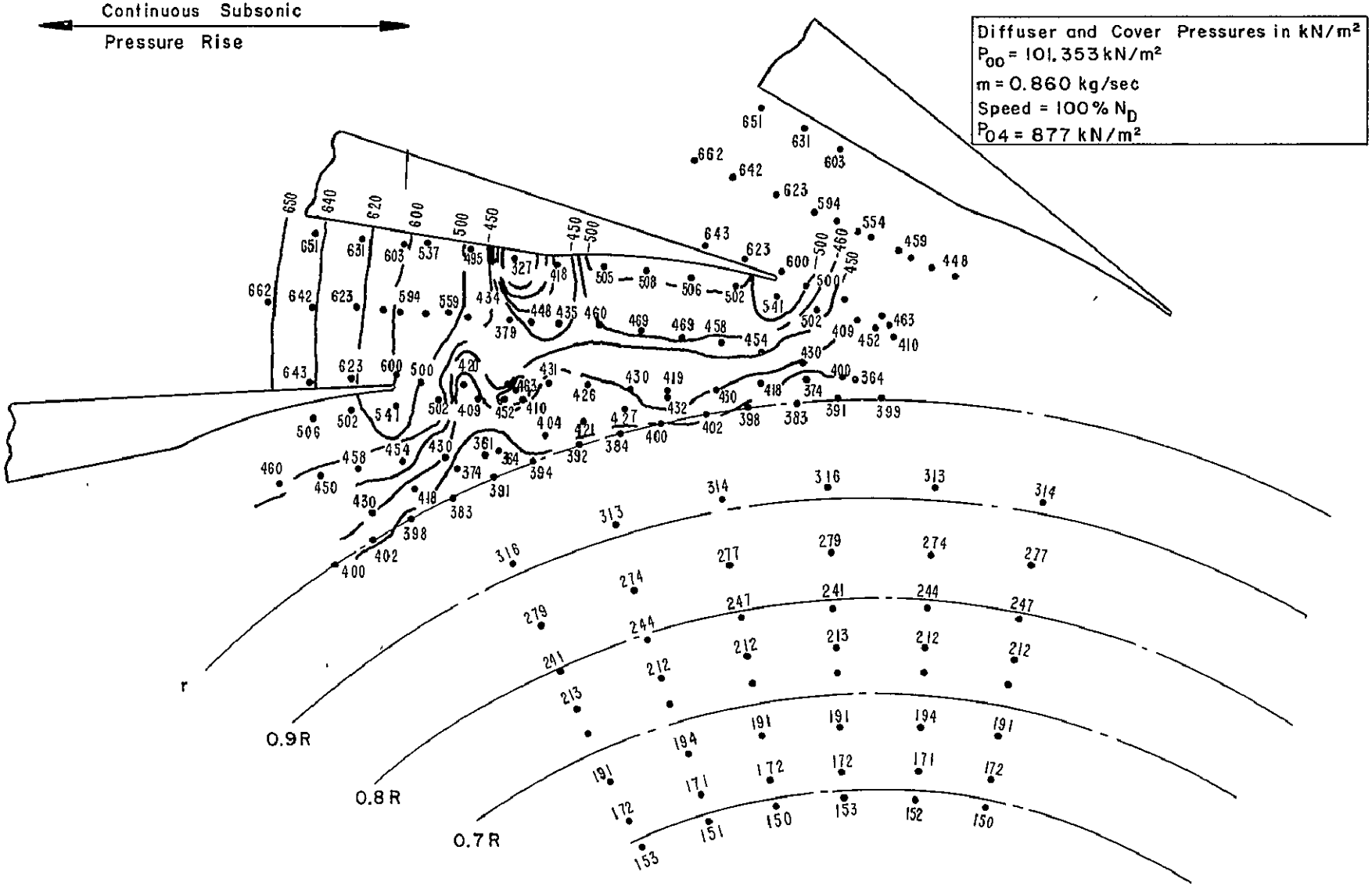

Figure 70. Diffuser & Cover Static Pressure Distribution and Isobars - Run 9 (Test 9.38)
Vaned Diffuser Test at 100% N_D Near to Surge - Build II Diffuser

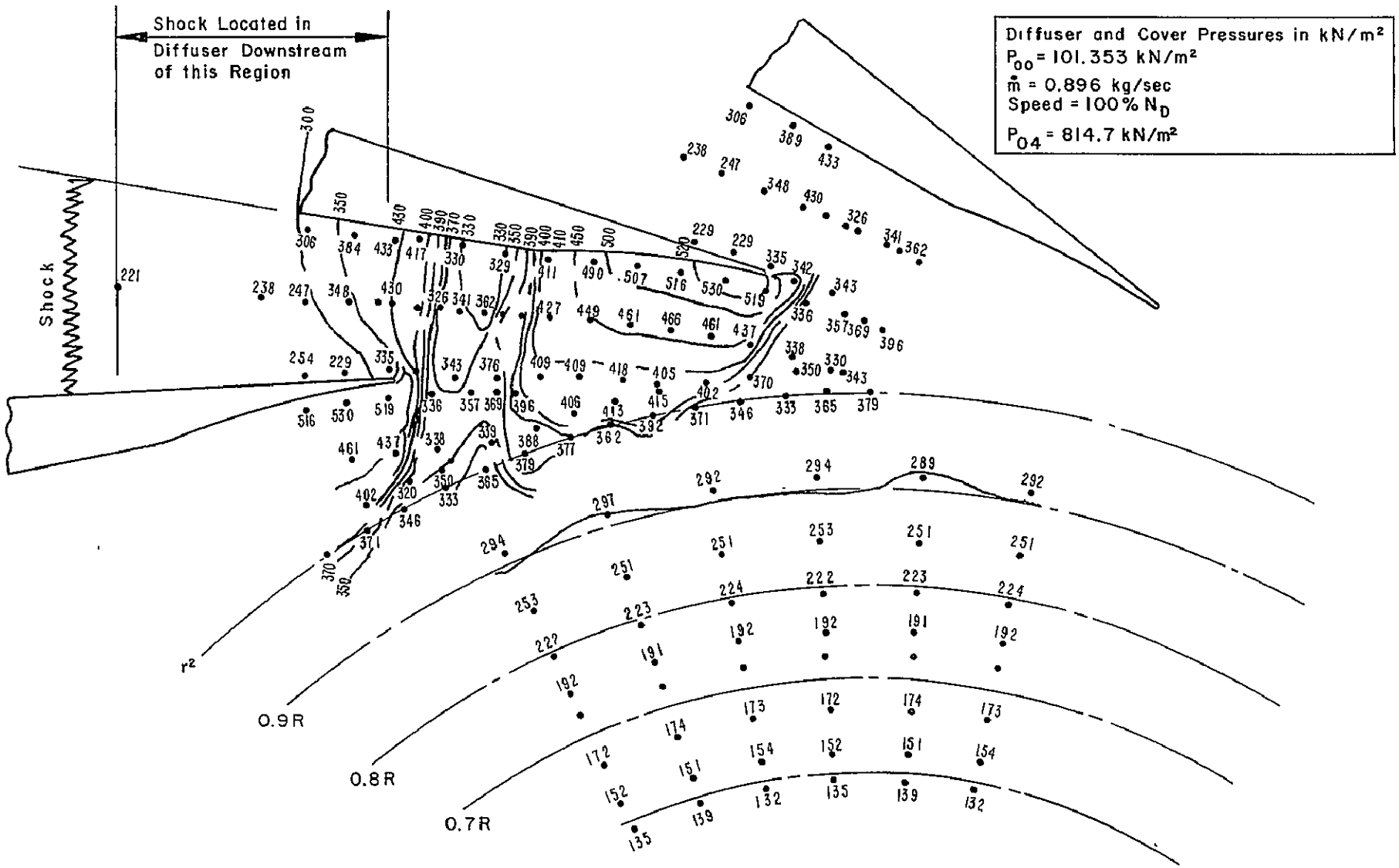

Figure 71. Diffuser & Cover Static Pressure Distribution and Isobars – Run 9 (Test 9.32)
Vaned Diffuser Test at 100% N_D at Choke Flow – Build II Diffuser

of the flow through the diffuser from upstream of the throat. Based upon the "measured" p_{o4} values, the static pressure corresponding to M = 1.0 for these lines is about 455 kN/m^2 for the Test 7.11 and 463 kN/m^2 for Test 9.38. These values give an idea of about where in the pressure field of the diffuser the Mach number = 1.0.

Similar data show the same results for the 80% vaned diffuser performance of Run 6. (This data is not presented.)

Examination of these pressure contour figures shows that for both the 80% and 100% N_D cases, and for flow near or at surge, a rapid and strong acceleration occurs at slightly supersonic speed (assuming the stagnation pressure in the flow is that measured by the p_{o4} probes). This expansion produces a maximum supersonic Mach number on the suction surface (corresponding to the measured minimum pressure values) as shown below. (Actually the maximum Mach number may well be slightly higher than these values since the pressure taps are spaced at finite intervals apart.)

Speed Line	80% N_D	100% N_D
p_{min} (kN/m^2)	184	288
M_{max}	1.25	1.35

The static pressure thus rises, in both cases, quite rapidly (apparently through a shock) as the flow proceeds along the suction surface. The pressure rise associated with these levels of Mach number is "typical" of shock/boundary layer interaction values known to induce turbulent boundary layer separation at these Reynolds numbers. (For example, in the channel diffuser, under supercritical flow, when the shock Mach number approaches 1.2 to 1.3, the diffuser boundary layer separates and pressure recovery deteriorates.)

Plots showing this Mach number distribution (deduced from the static pressure distribution assuming the stagnation pressure equals p_{o4} measured) are shown in Figures 72 and 73 [Runs 7.11 and 7.13 (Figure 72) and Runs 6.24 and 6.29 for the 80% speed data (Figure 73)]. These 80% and 100% N_D pressure data for the Build I diffuser strongly suggest that the expansion and rapid acceleration around the vane's lead edge is associated with the occurrence of "positive" incidence of the flow onto the vane lead edge. This is deduced from the location of the indicated maximum static pressure (stagnation point location) on the vane tip. If this is true, a small decrease in flow will cause a more positive incidence on the vane, leading to stronger expansions, thereby increasing the

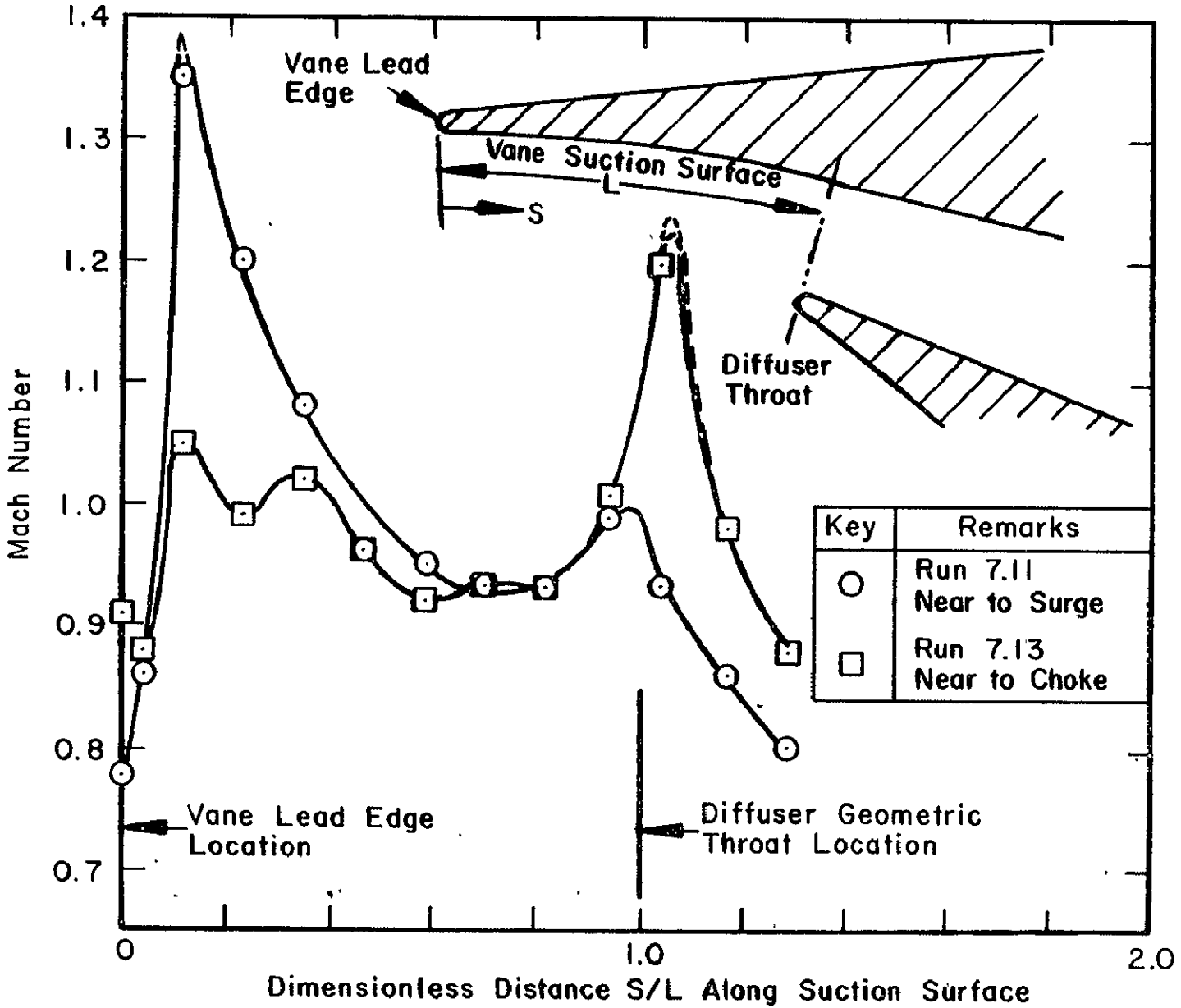

Figure 72. Mach Number Distribution Along Diffuser Vane Suction Surface — 100% N_D, Build I Diffuser

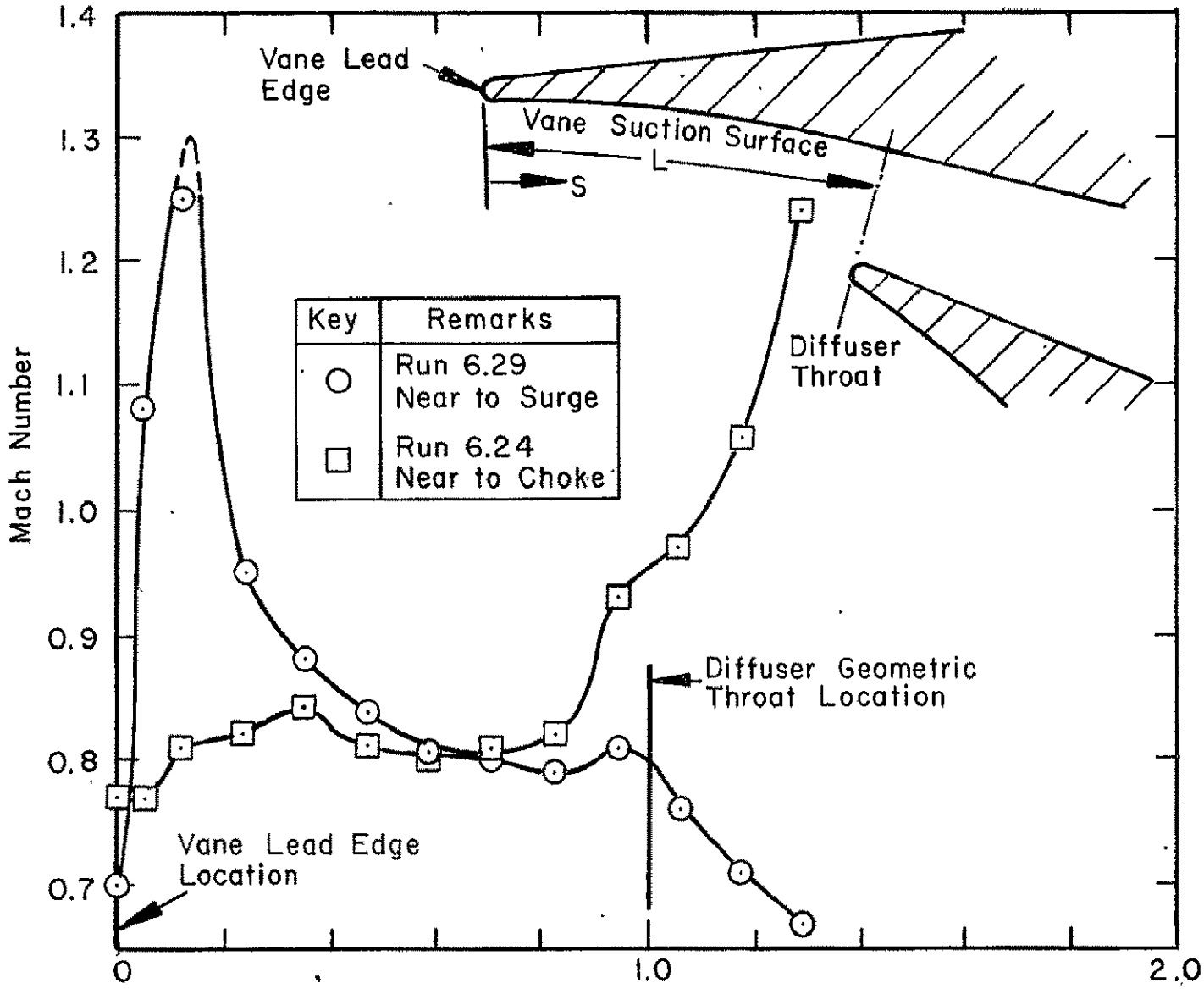

Figure 7.3. Mach Number Distribution Along Diffuser Vane Suction Surface — 80 % N_D, Build I Diffuser

maximum Mach number immediately after the vane lead edge on the suction surface. The suction surface boundary layer will be required to negotiate an even larger pressure rise along the vane suction surface. If the Mach number is sufficiently high, this "shock/boundary layer interaction" leads to suction surface boundary layer separation. We can then hypothesize that the separated flow is swallowed by the channel diffuser as it flows along the vane suction surface; a rapid decrease in channel diffuser pressure recovery then results which may be the initial event leading to surge.

Similar data are plotted in Figure 74 for the Run 9 Build II diffuser data at 100% N_D. Shown on this figure are the Mach number distributions for Run 9.32 (choke - Figure 71) and Run 9.38 (near to surge - Figure 70). For both choke and near surge flow rates for this Build II diffuser configuration, the sudden acceleration of the flow around the diffuser vane lead edge, seen in the Build I data, has been eliminated but now there is a rapid rise in Mach number along the vane suction surface immediately ahead of the channel diffuser throat. From the data available, it appears that the expansion of the flow occurs where the log-spiral portion of the vane suction surface joins the two-dimensional portion of the channel diffuser. This point is a remnant of the Build I diffuser vanes that were modified to make the Build II diffuser. The Mach number and hence the strength of the resultant shock pressure rise, as the flow attempts to match the subsonic pressure rise of the channel diffuser, increases as the flow is reduced toward surge. From this evidence, the same arguments applied above to the Build I diffuser apply also to the new flow acceleration location found in the Build II diffuser. This occurs in spite of the fact that the Build II diffuser has successfully eliminated the rapid acceleration around the vane lead edge by rotating the vanes 2 degrees toward tangential and placing the vane lead edge at an increased radius ratio. One suspects that a Build II diffuser design that successfully eliminated the "bump" between the log-spiral and the channel diffuser portion of the vane suction surface would be able to achieve a larger range to surge than has been observed in the Run 9 tests.

Summary of Diffuser Performance Behavior. A substantial loss in stagnation pressure occurs between the impeller mixed-out conditions, 2*, and the diffuser throat region. This stagnation pressure loss is substantial at 100% N_D and below. This loss accounts for a decrement of 5 points in overall stage efficiency and is responsible for the early choke of the channel diffuser at 100% N_D. The channel diffuser, when

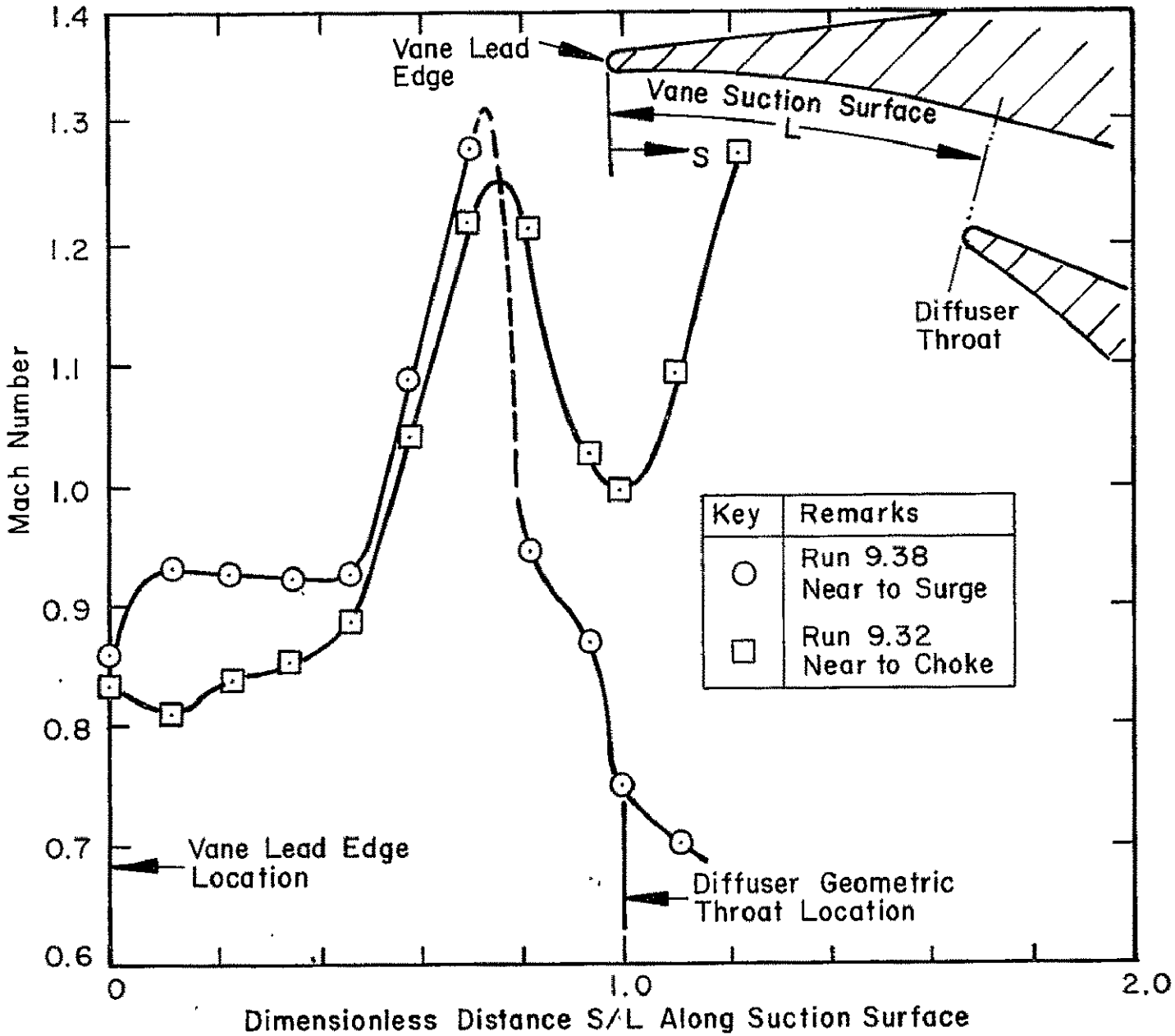

Figure 74. Mach Number Distribution Along Diffuser Vane Suction Surface — 100% N_D, Build II Diffuser

analyzed using the static pressure data measured on the shroud cover, shows choked flow when the channel recovery C_{p4-c} begins to deteriorate. These choking conditions produce a shock located in the diverging portion of the channel diffuser. The shock is responsible for the substantial deterioration in channel diffuser pressure recovery for these mass flows. The cover static pressure data show a Mach number ahead of the normal shock on the channel pressure surface in the channel diffuser of at least 1.2 (and probably slightly higher).

At mass flows approaching surge, the channel diffuser unchokes and the actual static pressure and blockage measurements show that the channel diffuser performance is indeed very close to the laboratory measured channel diffuser performance for this geometry and blockage.

The vaned diffuser has a very narrow choke to surge margin (only 2.5% to 3% for Run 7 and 6% to 7% for Run 9). The reason for the surge of the vaned diffuser is really not known. However, analysis of the pressure distribution along the vane suction surface for the Build I diffuser shows that the increasing angle of the flow measured to radial at decreasing mass flow produces a "positive" incidence onto the vane lead edge. This "positive" incidence leads to rapid acceleration around the vane lead edge and an increase in local Mach number on the vane suction surface. The Mach numbers measured approach values of at least 1.3 to 1.4 near the surge point. The shocks and consequent rapid pressure rise following these Mach number levels are high enough to separate the vane suction surface boundary layer under these conditions. The Build II diffuser had a lower Mach number at the vane lead edge and the vanes were rotated 2 degrees toward tangential. This eliminated the large acceleration around the leading edge due to flow incidence (see Figure 74), but a large acceleration and subsequent deceleration did occur at the transition on the suction surface from the log-spiral to the two-dimensional channel diffuser. This acceleration and deceleration could be responsible for boundary layer separation near the channel diffuser throat as the flow immediately downstream of this location is required to match the subsonic pressure rise of the channel diffuser. This series of events leading to separation could be the precursor to subsequent stage surge. We postulate that reorienting the diffuser vanes so that the zero incidence setting angle is even more towards tangential and reconfiguring the suction surface will delay, to substantially lower mass flows, the onset of the observed "positive" incidence and the suction surface acceleration.

The interpretation of the data results is subject to some uncertainty because of the measured change in impeller performance between the Build I and Build II diffuser tests. The comparison made earlier between Figures 44 and 45 shows that both

the change in Reynolds number and the impeller change (SN 001 to SN 002 impeller) between Runs 7 and 9 reduced the impeller diffusion. Therefore, both the impeller exit stagnation pressure and impeller exit flow angle may have been changed between the Build I and Build II tests (neither of these parameters could be measured directly). Interestingly, the measured stagnation pressure in the vaned diffuser throat, p_{o4} shown in Figure 58, has about the same value for the high Reynolds number Run 7 data as for the low Reynolds number Run 9 data. The comments above, postulating reorientation of the diffuser vanes, etc., are made assuming that the impeller exit flow angle and stagnation pressure changes, that may have occurred between the Runs 7 and 9 vaned diffuser tests, were small in overall impact on diffuser range and performance compared to the effect of the design changes made to the diffuser. It would have been preferable to test the Build II diffuser design with the original high Reynolds number SN 001 impeller, but this was not to be.

An unexplicable result is the magnitude of calculated stagnation pressure loss for the 100% speed data (and for the 90% N_D data for the vaneless diffuser). Note that this type of loss is observed for the parallel wall, vaneless diffuser configuration, as well as for the vaned diffuser geometry.

TIME-DEPENDENT PRESSURE DATA

Time-dependent pressure recordings were made in the inducer, radial portion of the impeller and at the throat of the channel diffusers. In addition, for the vaneless test, data were also taken close to the impeller exit on the front cover.

The same type of data for the 100% N_D tests of Run 8 (vaneless) for the inducer and impeller are shown in Figure 75. The upper trace is location K4 (Figure 41) and the lower trace is the K10 position (Figure 41) at R = 0.8. The deflection factor for the upper trace is 9.25 kN/m^2 and 53.1 kN/m^2 for the lower trace.

Figure 75a is Run 8.86 which is close to surge (m = 0.772 kg/s and incidence = 8 degrees). Exposure of the photo is at 1/30 s so that a number of multiple sweeps appear in this photograph. Figure 75b is the same test point but a single sweep (different time scale than Figure 75a). The blade loading in the inducer (upper trace) at K4 position for Figure 75b is erratic as can be seen from the single sweep photo. Blade loading between the pressure and suction surfaces varies in Figure 75b from about 6.5 kN/m^2 to 16.6 kN/m^2. The impeller trace at R = 0.8 for Figure 75b is more consistent, varying between 85 kN/m^2 to 132 kN/m^2. The axial progenitor blade from which this inducer blade was designed (see Reference 14) would indicate the inducer to be on the verge of separation at this flow incidence.

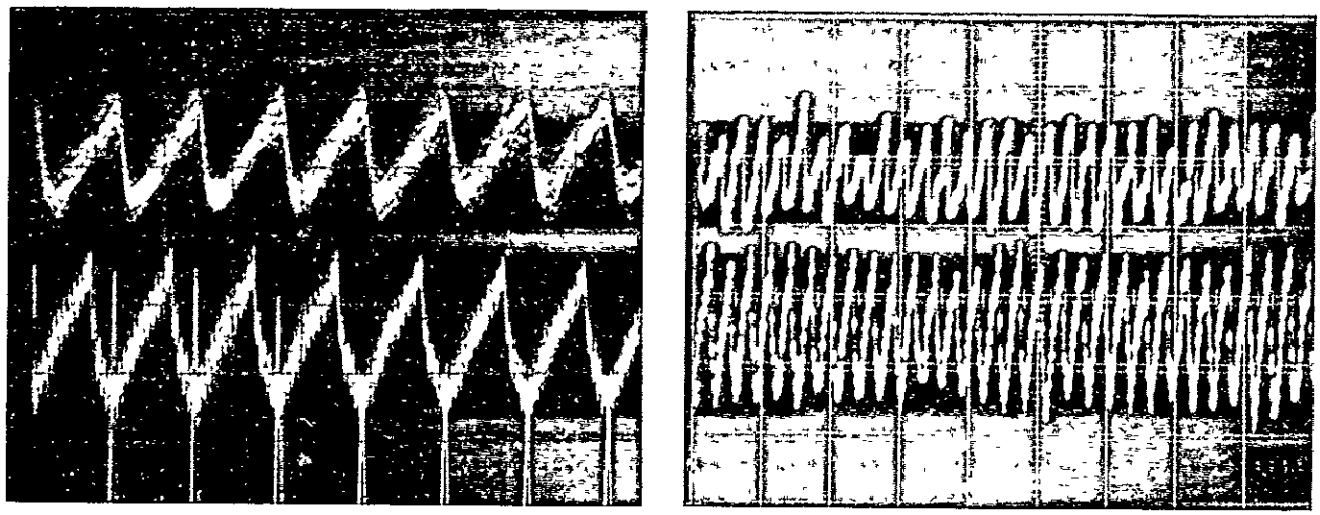

(a) (b)

	Upper Trace	Lower Trace
Probe Location	X = 10.2 mm	R = 0.8
Trace Sensitivity	9.3 KN/m^2 per division	53 KN/m^2 per division

Figure 75. Unsteady, Time-Dependent Pressure Transducer Traces - Run 8, 100 % N_D Vaneless Diffuser Tests - High Reynolds Number

ORIGINAL PAGE IS
OF POOR QUALITY

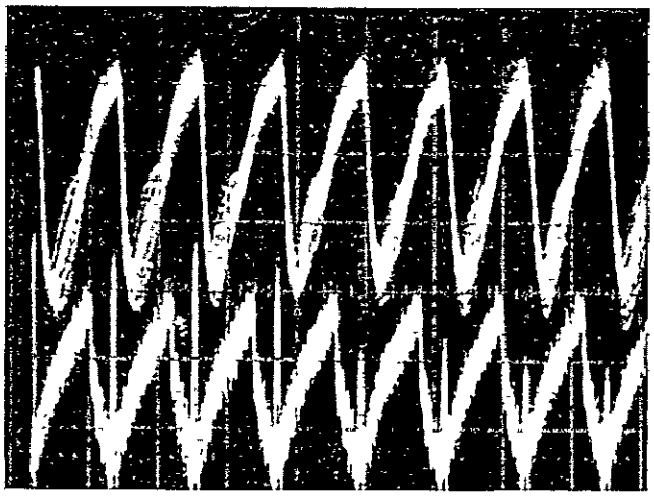

(c)

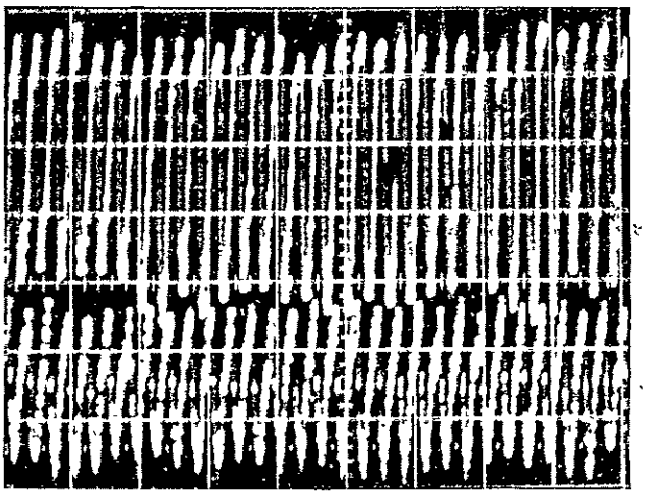

(d)

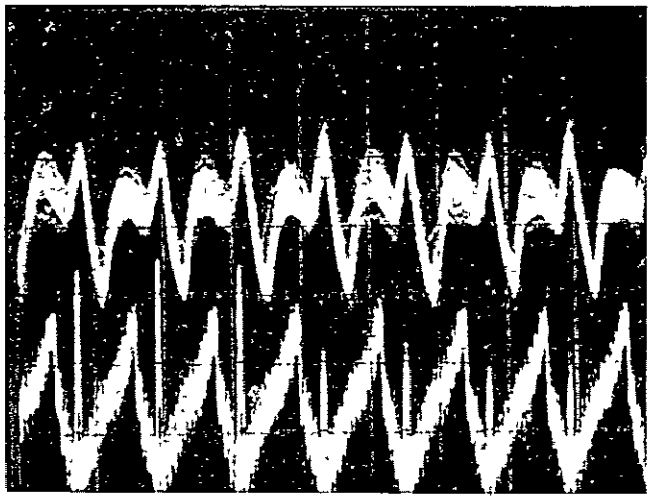

(e)

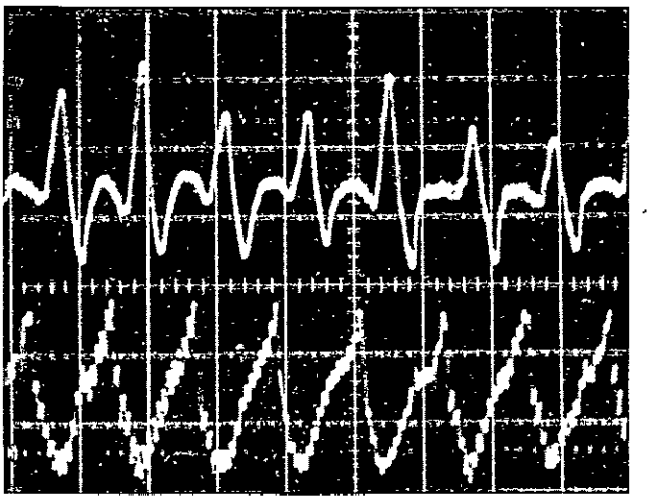

(f)

Figure 75 (continued)

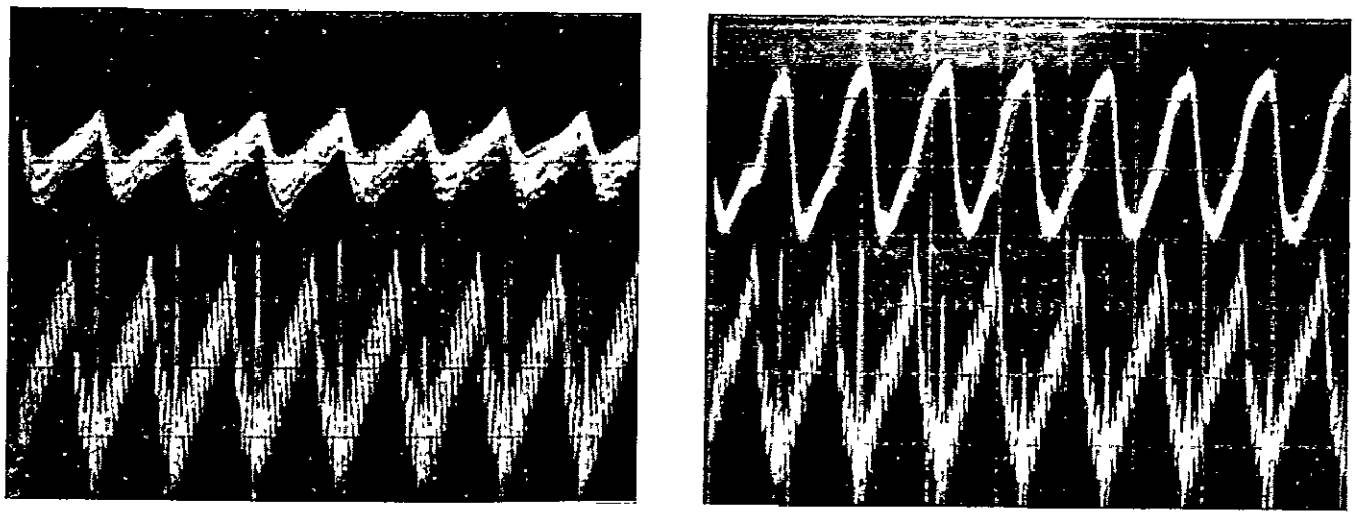

(a) (b)

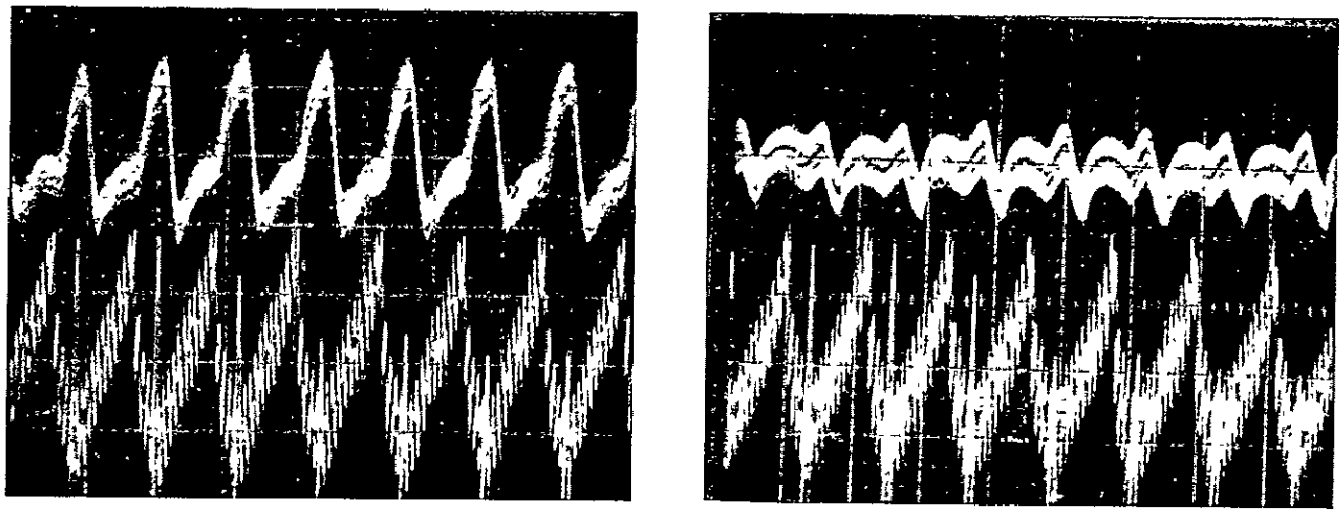

(c) (d)

	Upper Trace	
Probe Location	X = 10.2 mm	R = 0.8
Trace Sensitivity	9.3 KN/m^2 per division	21.3 KN/m^2 per division

Figure 76. Unsteady, Time-Dependent Pressure Transducer Traces-Run 8, 100% N_D Vaneless Diffuser Tests—Low Reynolds Number

At a higher flow rate close to the design point incidence shown in Figures 75c and 75d, the inducer loading is appreciably higher (about 30 kN/m^2 on the average). The loading is much more constant as evident from the single sweep photo of 75d. These data are for test 8.94 (m = 0.887 kg/s and incidence = 3.5 degrees). This incidence condition is very close to the design point incidence of 4 degrees. The blade loading at R = 0.8 for Figure 75c is about the same as for Figures 75a and b, perhaps slightly less. In the inducer, the pressure rises almost linearly with blade pitch on each blade passage with only a slight variation in loading and perhaps a small amount of flattening of the pressure trace close to the pressure surface.

Figures 75e and f show the same transducer trace locations for the impeller in choke. A major alteration of the inducer trace is obvious, caused by the choked flow condition at the inducer tip. The K4 trace flattens near to the middle of the blade passage and the average blade loading at this location is significantly reduced from that shown in Figure 75c. However, the blade trace and average loading at R = 0.8 is much the same as was observed at the lower flows of Figures 75a and 75c.

The vaned diffuser tests of Runs 7 and 9 experienced stage choke at flow rates just slightly above the conditions displayed by Figures 75c and d. It is clear that the stage choke (impeller plus vaned diffuser stage) is caused by choking of the diffuser. At stage choke the impeller inducer has not yet experienced any appreciable choking behavior.

All of the data shown in Figure 75 are for the SN 001 impeller at the "high" Reynolds number condition (p_{oo} = 101.4 kN/m^2).

The data shown in Figure 76 are similar data but for the low Reynolds number condition, p_{oo} = 50.7 kN/m^2. Figure 76a is for Test 8.74 at m = 0.785 kg/s and incidence = 8.5 degrees. The inducer loading is erratic and the blade is believed to be at or above stall incidence.

Figure 76b is Test 8.76 where m = 0.896 and is very close to the diffuser choke flow point for the Build II diffuser conditions found in Run 9. The pressure loading for each channel in the inducer is nearly identical and does not vary from channel-to-channel as it does near stall.

Figures 76c and d show the data traces as the inducer is pushed into choke condition. The same type of pressure trace distortion is observed in the inducer trace as was seen at the higher Reynolds number conditions of Figure 75. Figure 76d is for the impeller deep into choke.

Table XII lists the test number, mass flow and incidence conditions for the traces of Figures 75 and 76.

Figures 77 are photos of data traces made with the pressure transducers located near the channel diffuser throat (see Figure 40). These data are for Run 9 at 80% N_D. Similar traces were not made at 100% N_D. Figure 77a shows an oscillation in the channel diffuser throat pressure of about 46 kN/m^2 at a frequency of approximately 80 Hz. This photo is for Test 9.20 where conditions are just above the "knee" of the pressure ratio/mass flow curve (Figure 43). As the flow is brought progressively closer to the surge condition, the amplitude of this p_4 pressure oscillation grows. This is displayed in Figures 77b and c which are for Tests 9.18 and 9.16, respectively. Figure 77c is at a presssure ratio of 4.18 and conditions are at incipient surge.

TABLE XII. - CONDITIONS FOR UNSTEADY PRESSURE TRACES OF FIGURES 75 AND 76

Figure No.	Test No.	Mass Flow Rate (kg/s)	Incidence (degrees)	Plenum Pressure (kN/m^2)
75a, b	8.86	0.772	8.0	101.4
75c, d	8.94	0.887	3.5	101.4
75e, f	8.98	0.909	1.5	101.4
76a	8.74	0.785	8.5	50.7
76b	8.76	0.896	2.1	50.7
76c	8.78	0.901	1.8	50.7
76d	8.80	0.905	1.54	50.7

For Figure 77c, the flow condition near to surge, the amplitude of the pressure oscillation is approximately 78 kN/m^2 peak-to-peak. This assumes an oscillation of 38 kN/m^2 about a mean value of p_4. The measured stagnation pressure for this test was approximately 478 kN/m^2 and the average throat pressure was 331 kN/m^2. This implies a surge Mach number at the throat of approximately $M_{4\ surge} = 0.74$. If we assume that p_{o4} is not changing with time, the above minimum and maximum oscillating values of p_4 imply the following oscillating variation of throat Mach number:

$$p_{4\ average} = 331\ kN/m^2$$
$$p_{o4\ average} = 478\ kN/m^2$$
$$M_{4\ average} = 0.74$$
$$p_{4\ maximum} = 370\ kN/m^2$$
$$M_{4\ minimum} = 0.62$$

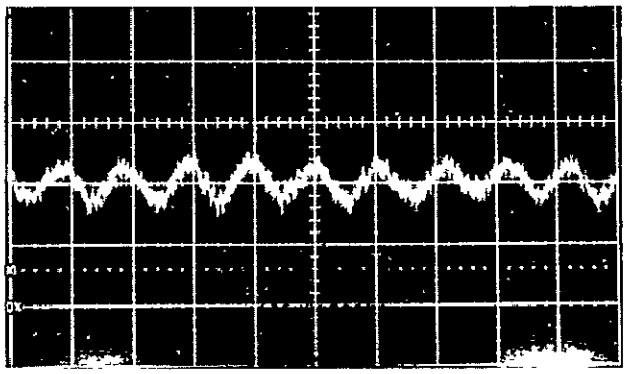

(a) pr = 4.06

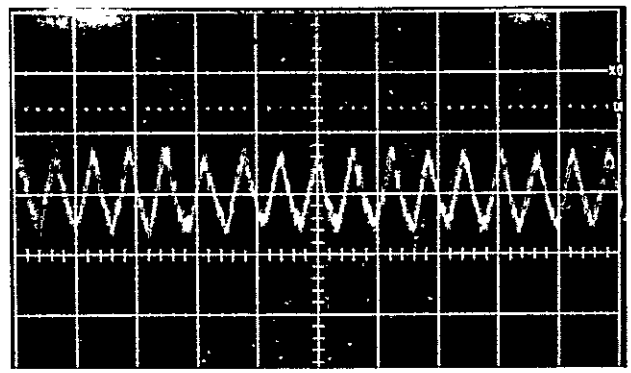

(b) pr = 4.1

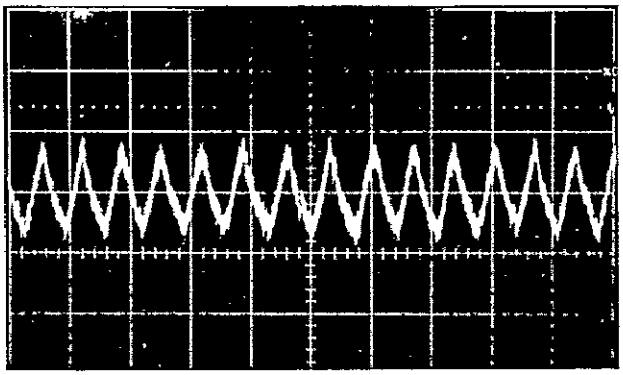

(c) pr = 4.18
Incipient
Surge

Scale Factors

46.2 kN/m^2 per division
10 ms/division - Figure (a)
20 ms/division - Figures (b)&(c)

Photo	Test No.	Mass Flow (kg/s)
(a)	9.20	0.545
(b)	9.18	0.532
(c)	9.16	0.511

ORIGINAL PAGE IS
OF POOR QUALITY

Figure 77. Time Unsteady Pressure Measurements at the Build II Channel Diffuser Throat – 80% N_D

$$p_{4\ \text{minimum}} = 292\ \text{kN/m}^2$$
$$M_{4\ \text{maximum}} = 0.87$$

These oscillations in throat pressure are believed to be of the same type and nature as have been reported to occur in other high pressure ratio stages, e.g., References 22 and 23. The implication is that the mass flow rate through the diffuser channel is also oscillating in synchronism with the pressure trace; i.e., the mass flow rate is periodically unsteady. From the measurements made on this stage we do not know the true nature and cause of the observed throat pressure oscillations. For the high pressure ratio stages studied in References 22 and 23, rotating stall in the diffuser was eliminated as the cause of the periodic throat pressure oscillations. In fact, in Reference 22 it was concluded, from hot-wire measurements made in the inlet to the stage, that the stage mass flow did fluctuate in synchronism with the throat pressure oscillations.

If a periodic unsteady flow rate is considered characteristic of this stage at high pressure ratio near to surge, then the stage flow rate oscillation should be reflected in the dynamic static pressure recordings made in the inducer because of periodic variation in the inducer incidence. This cannot be checked with the existing inducer data since inducer traces, which presumably would indicate a periodic variation of blade-to-blade loading, in synchronism with the diffuser oscillations, were always taken at high sweep rates. These high sweep rates, for which approximately 10 blade passings are recorded, thus correspond to only about 1/20th of a single diffuser oscillation at 80 Hz, and therefore the blade loadings would appear about constant anyway.

There remains a final possibility that the impeller is producing an unsteady pressure rise into the diffuser while the flow rate remains essentially constant. For this to occur would require a periodic vibration in the static and stagnation pressure produced by the impeller. While we do not have data to document this characteristic for the present impeller operating with the vaned diffuser geometries, Reference 22 did document that for the throat pressure oscillations observed for that stage, the stagnation and static pressure rise produced by the impeller were constant.

Measurements to document further the time dependent pressure and flow characteristics of this stage during the precursor period prior to surge would appear desirable.

CONCLUSIONS

This report describes the analysis, design, and procedural efforts of an experimental program to adopt laser velocimeter techniques to the aerodynamic investigation of the flow through a small, high speed, high pressure ratio centrifugal compressor.

In part the program has been successful:

1) The laser velocimeter equipment designed can make velocity measurements in high velocity flows and in close proximity to solid surfaces.

2) The aerodynamic study of the 8:1 pr compressor using detailed time-average and time-dependent pressure measurements has revealed useful information about the fluid dynamic performance of the centrifugal stage components.

However, the program has not been successful:

3) in making the detailed aerodynamic measurements of the compressor impeller and diffuser velocity fields, and

4) demonstrating the feasibility of using this equipment as a reasonably cost effective and practical experimental tool for the routine study and improvement of small, high speed, high performance turbomachinery.

LASER VELOCIMETER EQUIPMENT

The important characteristics of the velocimeter design which are of interest to its application to small turbomachinery are as follows:

The LV instrumentation has been optimized to permit the measurement of instantaneous velocities up to approximately 500 m/s, measured in absolute coordinates. The LV equipment accomplishes the velocity measurement with a non-contact process. One of the most important motivations for using the laser velocimeter in compressor aerodynamic studies is that the non-contact process does not disrupt the flow. This is believed important in small compressors since even the use of the smallest probes used for conventional measurements in this type of hardware have been shown to seriously disrupt the aerodynamic performance of the machine. Also the ability to make measurements of velocities within the rotating impeller for this class of pressure ratio compressors is not possible with any other technique.

The optics design has established a measuring volume that is an ellipsoid of revolution with a minor diameter (width) of approximately 0.06 mm. This small probe volume necessitates the use of small seed material on the order of 0.75 μm number mean diameter required to accurately measure the flow velocity.

In the inlet and approach flow regions of the compressor, where the velocity components are primarily axial or tangential, the laser beams are oriented such that the probe volume "length" is approximately in the radial direction. The probe volume "width" dimension is approximately oriented in the direction of the flow and therefore produces good resolution of the flow velocity field. In the radial diffuser flow region of the compressor, the laser beam orientation places the probe volume "length" across the flow from cover to hub wall while the probe volume minor diameter or "width" lies in the flow direction or radial plane. Since the diffuser depth is shallow, the long "length" dimension of the probe volume affects the velocity field resolution from cover to hub wall. However, even in the present compressor design where the diffuser passage depth is only 3.22 mm, it should be possible to obtain about four distinct non-overlapping velocity measurement regions between the front cover and rear hub walls.

The mechanical system design has been configured so that the probe volume can be positioned accurately relative to the compressor hardware. Electronic strobing equipment has been designed and fabricated to permit repeated measurements of the flow velocity at any fixed point within the flow regions described above and at a fixed position relative to the rotating impeller. The strobing system allows for a minimum of less than 0.5% of blade pitch rotation of the impeller for a single velocity realization using the 19-bladed impeller, rotating at 53,000 rpm. Measurement times required for a single velocity realization are approximately 0.1 μs at 200 m/s and approximately 0.08 μs at 500 m/s.

The output of repeated LV measurements at a point permits the development of a histogram of the flow velocity vector located relative to the rotating impeller. Analysis of this histogram developed over time then allows the calculation of the mean velocity of the flow at this point, assuming that the flow is steady or periodic at the blade passing frequency relative to the rotating impeller. Statistical analysis of the histogram also permits evaluation of some properties of the unsteady and fluctuating flow.

While some measurements have been made within the diffuser and impeller inlet regions of the 8:1 pr compressor, sufficient measurements to obtain the details of the velocity fields in

these regions have not been successfully accomplished to date. The depletion of seed particles in the LV probe volume with time and unstable operation of the acoustic (A/O) modulator during gated operation of the LV system appear to be the causes of the inability to obtain LV measured data.

Although the seed particle rates drop to low values after prolonged operation of the LV system, this does not seem to be the primary cause of the problems experienced in obtaining LV data to date. The misalignment of the optical system caused by drifting of the A/O modulator, on the other hand, completely prohibits the acquisition of LV data during gated operation and is a problem that has only recently been uncovered.

COMPRESSOR AERODYNAMIC PERFORMANCE

The time-average temperature and pressure measurements and the time-dependent pressure measurements made on the 8:1 pr stage have revealed the following:

The compressor impeller appears to meet its design point characteristics of pressure ratio and efficiency but at a flow rate lower than design. Using the calculated incidence values at the inducer blade tip, the flow rate at which good performance is obtained agrees with the flow rate at which design incidence β_{1t} is actually obtained; unsteady, time-dependent pressure transducer measurements verify these flow rate/incidence measurements. The efficiency and pressure ratio measurements are based upon the static pressure p_2 measured at the impeller exit which is used to calculate the mixed-out impeller exit total pressure p_{o2*}.

The vaned diffuser (Build II) performance does not meet design specifications. The diffuser pressure recovery C_{pD} is low by approximately 8 points, compared to the design point recovery of 68.8%, when based upon the calculated p_{o2*} mixed-out stagnation pressure. The channel portion of the diffuser appears to attain the proper pressure recovery at the lower flow rates near to surge, based upon the measured values of throat static and total pressures and diffuser flow blockage factors. At higher flow rates, the diffuser chokes and goes supercritical with a shock located in the diverging portion of the diffuser which destroys the diffuser recovery. Although the impeller inducer chokes at a flow rate just slightly higher than the original design flow rate of 0.907 kg/s, stage choke is brought on by the choking of the diffuser.

Overall stage total-to-static efficiency at 100% N_D is 75% compared to design intent of 77% (see Figure 78 which is a repeat of Figure 43). The low efficiency appears attributable

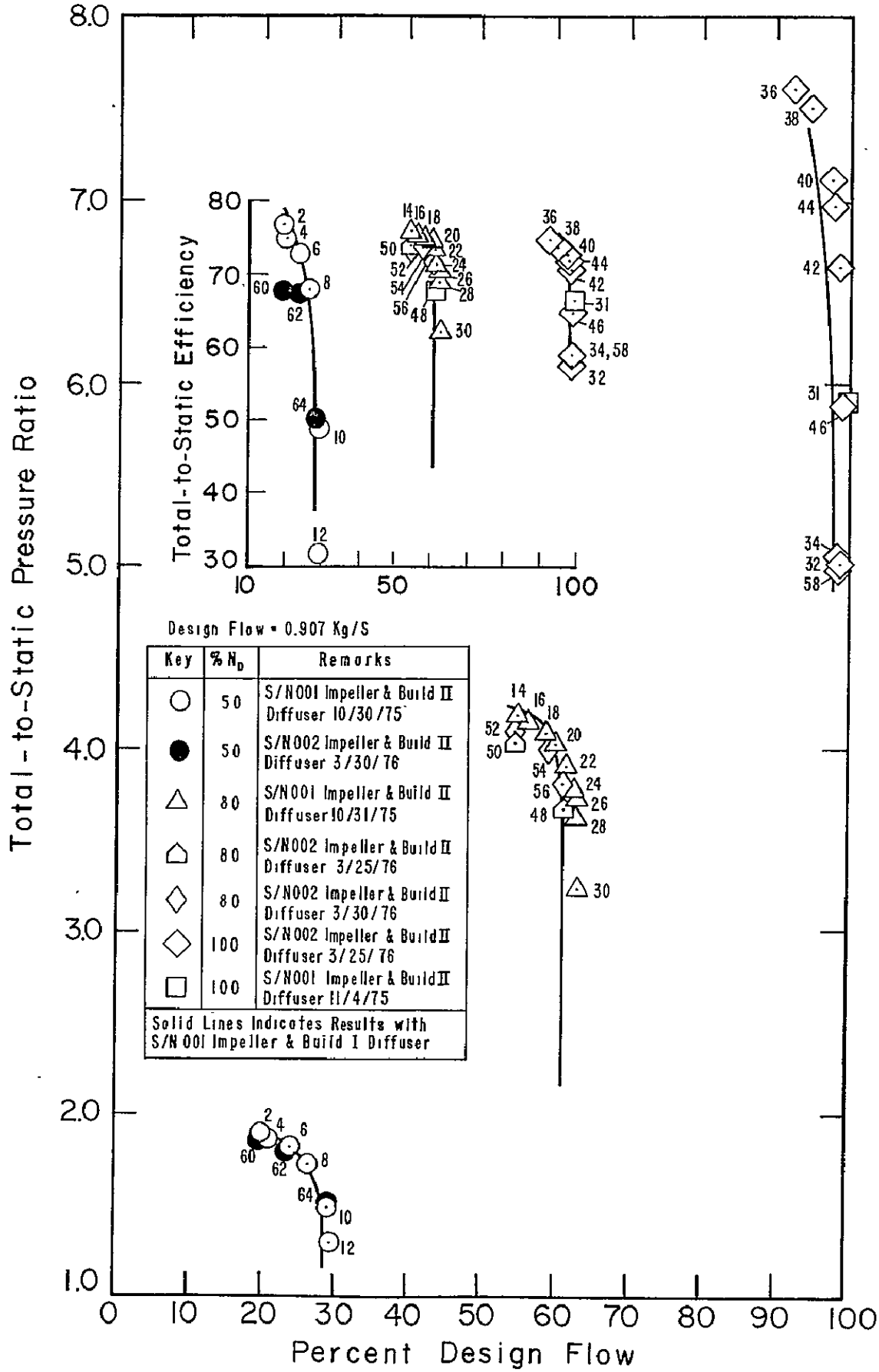

Figure 78. Stage Performance - Vaned Diffuser (Run 9)

to the loss in stagnation pressure between the calculated value at impeller exit and the measured value at the diffuser throat. Similar vaneless/semivaneless stagnation pressure loss has been observed in other high pressure ratio, vaned centrifugal stages and is believed connected with the transonic impeller exit mixing conditions. A similar stagnation pressure loss was also measured between the impeller exit and p_{o4} measurement in the vaneless diffuser tests; this fact may indicate that the loss process is basic to the impeller exit mixing out process or that p_{o2*} is improperly calculated using the impeller exit static pressure. There is no evidence, however, for a fundamental error in the calculation of p_{o2*} based either on fluid dynamic principles or the evidence in the literature on jet/wake mixing. Additional measurements using total pressure probes at smaller radius ratios approaching closer to the impeller exit are needed to resolve this question.

Flow range from choke-to-surge was lower than design intent (6.8% compared to design of 12% with the Build II diffuser configuration). The diffuser chokes at a lower flow rate than design. Near surge, measurements of the pressure field in the semi-vaneless space reveal strong shocks standing on the vane suction surface just upstream of the diffuser throat; the strength of these shocks appears sufficient to induce boundary layer separation at flow rates approaching the surge flow rate. It is hypothesized that separation induced by such shocks could be the initiator of deep surge. Future efforts should be directed at establishing diffuser designs for this stage that provide sufficient flow range to choke flow conditions and eliminateor mitigate the high Mach number accelerations and shocks on the vane suction surface in an attempt to extend flow range to surge.

Finally, unsteady, time-dependent, pressure measurements at the location of the diffuser throat at 80% N_D reveal strong, large amplitude, constant frequency, pressure oscillations as the stage flow approaches surge. These pressure oscillations are similar to and believed to be of the same type and nature as have been observed in other high pressure ratio stages and reported in the open literature. It is believed that these precusor pressure oscillations possibly may be connected with (1) simultaneous flow rate oscillations throughout the entire stage, or (2) with an unsteady pressure rise produced by the impeller into the diffuser, or (3) with rotating stall in the diffuser and, in any event, are strongly connected with time-dependent, unsteady flow phenomena that are fundamental to the onset of stage surge in high pressure ratio centrifugal machines. These oscillations and other unsteady flow behavior need to be further explored and understood to provide a better basis for understanding and eventually extending surge range.

APPENDIX A

ACOUSTO-OPTIC MODULATOR DESCRIPTION

The Acousto-Optic modulation system includes an electronics cabinet and a Bragg angle glass cell. The electronics delivers a 40 MHz signal to an electrical gate which is operated on by the input gating signal from the data gate control panel. The acousto optical head is designed to be mounted to the Spectra-Physics laser with a threaded adaptor. The output RF signal from the modulator is launched into the glass interaction medium by an array of transducers bonded to the glass block. An alignment knob varies the "tilt" angle of the block to the laser output so that the condition necessary for Bragg angle diffraction is satisfied. When the laser output is properly aligned to the grating produced by the ultrasonic vibrations, light is diffracted into the first order. The amount of light diffracted to that position is dependent upon the amplitude of the ultrasonic wave. The angular separation between the undiffracted beam and the diffracted beam is proportional to the wave length of the radiation, the ultrasonic wave frequency and inversely proportional to the acoustic velocity in the medium. The diffracted beam is aligned to an external aperture which then absorbs the undiffracted beam.

Specifications. Below are a set of abbreviated specifications for the acousto-optic modulation system used in this program.

Name of Parameter	Brief Description of Parameter
Bandwidth	dc to 3.5 MHz based on a beam diameter of 0.8 mm at the $1/e^2$ points
Rise Time	200 ns for a beam diameter of 1.5 mm at $1/e^2$ points
Extension Ratio	10,000 to 1
Diffraction Efficiency	85% at 633 nm
Dynamic Efficiency	80%
Input Impedance	50 ohms
Carrier Frequency	40 MHz
Carrier Power	2 watts (maximum)
Diffraction Angle	6 mrad at 514.5 nm

APPENDIX B

DATA GATE CONTROL - THEORY OF OPERATION

General Description. The data gate control (DGC) generates gate pulses of known delay and duration for the purpose of strobing data into and out of the data acquisition electronics. A trigger pulse is generated from an optical blade position indicator for each revolution of the impeller. Using this trigger as a synchronization pulse, the wheel speed is measured for one full revolution (CYCLE 1). During the next revolution (CYCLE 2), the calculated speed is multiplied by the desired gate delay. On the third revolution (CYCLE 3), the gate is opened for a predetermined width after the initial delay. Figure B-1 is a functional block diagram of the operation of the system.

Trigger Detection. Blade passage is sensed by an optical method. Light directed down a bifurcated fiber optic scanner is reflected by a passing blade tip and detected by a high speed photofet. This analog signal is applied to a high speed comparator, which is used as a line driver between the remote optical detector box and the gate control panel (approximately 8 meter separation).

Cycle Control Circuitry. A second comparator terminates the transmission line from the detector box to a single line digital pulse. These digital pulses are applied to a mode three counter which enables and/or disables the 3 CYCLES of the gate control in their proper sequence. When the mode control switch on the front panel is in the "CONT" position, the data gate is always enabled and the trigger pulses are inhibited from the cycle control counter. Returning the mode control to "1" or "100" reinitializes the cycle control counter and enables the digital trigger.

CYCLE 1 - Compressor Speed. The compressor speed is measured by a 16 bit counter which is enabled by the first digital trigger pulse (start CYCLE 1) and disabled by the arrival of the next trigger pulse (start CYCLE 2; stop CYCLE 1). The counter's clock is a 17 MHz crystal controlled oscillator with a frequency stability of 0.001% (0°C to 50°C).

The CYCLE 1 counter will overflow at 2^{16} (65536) counts, therefore a compressor speed below about 15,500 RPM will cause this overflow. If this does occur, a front panel light is energized and CYCLE 3 is inhibited keeping the data gate closed until the overflow condition is eliminated.

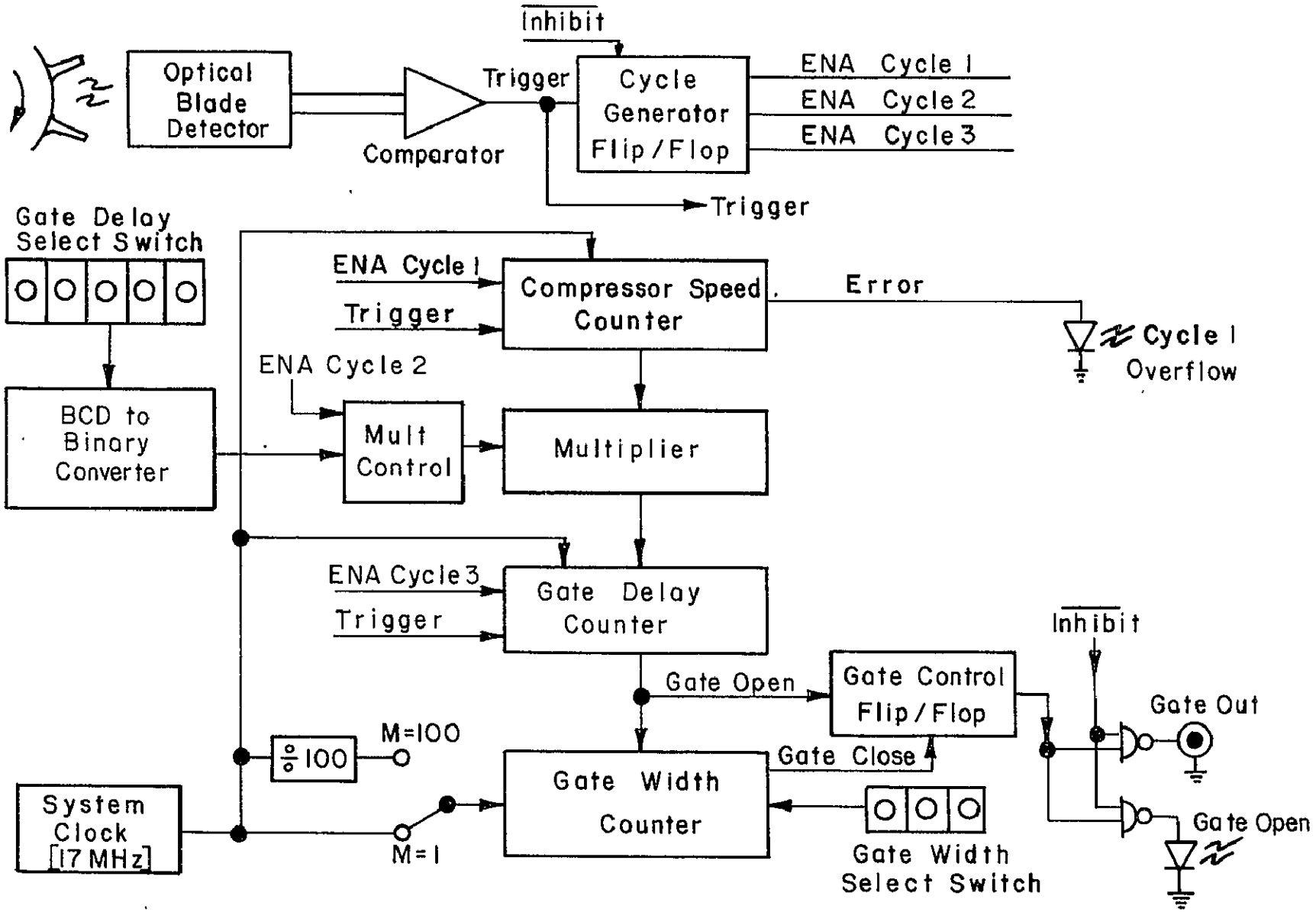

Figure B-1. Data Gate Control Circuitry

CYCLE 2 - Gate Delay. CYCLE 2 is initiated at the completion of CYCLE 1. The 16 bit binary number in CYCLE 1 counter is transferred to CYCLE 2 where it is digitally multiplied by a 16 bit number representing the fraction of a cycle the gate is to be delayed. Only the most significant 16 bits of the product are saved and transferred to CYCLE 3. The product transfer occurs at the completion of the multiplication routine and before the end of CYCLE 2.

The fraction of cycle 16 bit number is entered by means of five thumbwheel switches on the front panel. The switches are direct reading and internal circuitry converts the selected decimal number (in percent of cycle delay) to its fractional binary equivalent. This conversion routine must be manually enabled each time a new delay time is selected or on power up. A front panel switches is used to accomplish this.

CYCLE 3 - Gate Operation. The arrival of a third trigger pulse ends CYCLE 2 and starts CYCLE 3. A 16 bit counter preset during CYCLE 2 with the multiplication product is enabled, and counts at the 17 MHz rate. Carryout of the 16 bit counter causes a gate flip/flop to toggle (GATE OPEN). The output of the gate flip/flop is buffered and connected to the GATE OUT jack. This carryout also enables the three decade gate width BCD (binary coded decimal) counter which has been preset. Presetting is accomplished by thumbwheel switches on the front panel. The dials are direct reading in 17 MHz clock pulses. Thus, the pulse width will be the setting times 58.82 ns times M, where M is 1 or 100 depending on the mode control setting. When M = 1, the gate width is adjustable from 58.82 ns to 58.76 μs. Setting M = 100 causes the 17 MHz clock to be divided by 100 before being applied to the 3 decade BCD counter. In this mode, gate width is adjustable from 5.88 μs to 5.88 ms.

The gate will not be closed by the ending of CYCLE 3, but will only close on the carryout of the BCD gate width counter. The cycle control circuitry will proceed to CYCLE 1 and then CYCLE 2. If the gate is still open, it will proceed through a dummy CYCLE 3.

Modifications. The data gaté control circuitry has been modified to permit gating for each blade passage during CYCLE 3 instead of once during CYCLE 3. If the selected gate width is greater than the blade pitch, only the first gate, following the initial delay, will be enabled. The logic then follows the same procedure as the original scheme. It is possible to select either the original "once per three" operating mode or the new "once per passage per three" from a front panel switch.

Power Supplies. Logic power is supplied by a 5 volt, 5 ampere, modular supply. The comparator is supplied by an encapsulated ± 15 volt source.

APPENDIX C

DESCRIPTION OF DIVIDE-BY-TWO AND DOPPLER FREQUENCY PROCESSOR

DIVIDE-BY-TWO (÷2)

The function of this module is to reduce the maximum detected Doppler frequencies to a level which may be processed by the Doppler frequency processor (DFP). In practice, the ÷2 is selected manually, or not, depending on the mean Doppler frequencies observed on the oscilloscope. If the frequency is above about 80 MHz, the ÷2 is directly coupled to the output of the photomultiplier tube (50 ohm impedance matched) and the divided output is sent to the DFP (also through a 50 ohm match).

Figure C-1 shows a block diagram of this circuit. The high frequency signal is first stripped of its pedestal with a 10 MHz high-pass filter. The zero centered signal is then applied to an in-house assembled, three-stage amplifier and then to a level shifter which makes the DC level compatible with the emitter-coupled logic (ECL) divide-by-two flip/flop. Finally, the divided signal is level shifted, buffered and sent through a 50 ohm match for frequency measurement.

Output from this ÷2 may be controlled by the data gate control (Appendix A). Alternatively, an internal gate may be applied, allowing "continuous" signal output; then the DFP is controlled by the data gate circuitry.

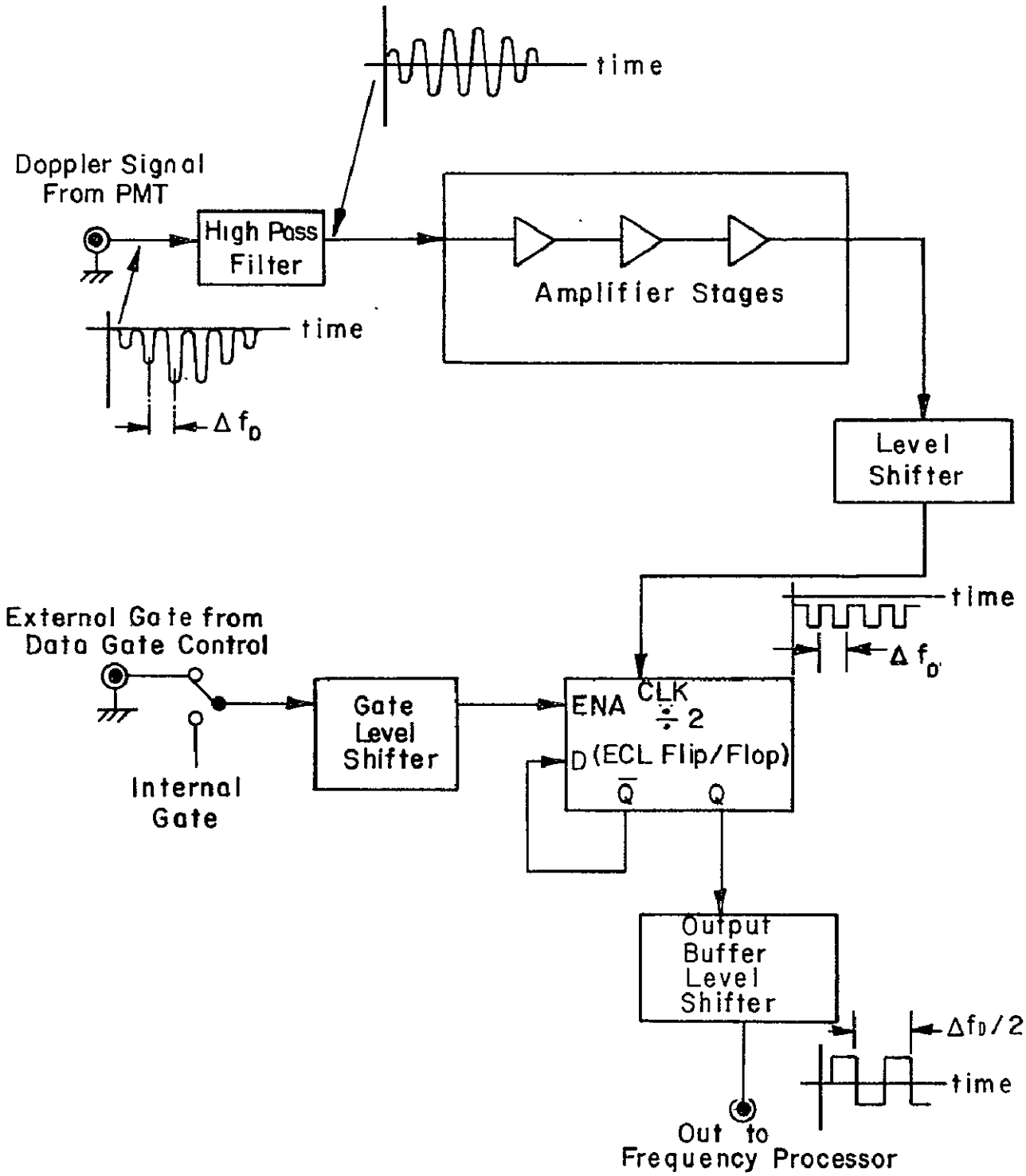

Figure C-1. Divide-by-Two Circuit Diagram

DOPPLER FREQUENCY PROCESSOR

(text adapted from manufacturer's manual)

The Doppler frequency processor (DFP) consists of two major components:

1) front end detection module (FED), and
2) logic and output display module (LOD).

The front end module accepts a Doppler burst from the photomultiplier or divide-by-two and produces a TTL compatible square wave pulse train corresponding to the passage of a particle by adjacent interference fringes.

The logic and output display module measures the passage time for the completion of a preset number of square wave cycles to occur (5/8 or 10/16) and outputs either this time directly or its inverse (the Doppler frequency). In addition, the data is validated by comparing the measured times to complete five pulses and eight pulses (alternatively ten and sixteen pulses may be selected).

OVERALL SPECIFICATIONS

The system provides analog and digital output of Doppler frequency or its inverse for individual particles at a maximum rate of 1 MHz. The doppler frequency range is from 1 kHz to 100 MHz. The instantaneous accuracy of the system (single particle measurement) is 1% up to 8 MHz and drops to 10% at 80 MHz.

Average readings are accurate to 1%. The LOD module incorporates two separate counters which measure the particle passage time for 5 and 8 interference fringes. If these times differ by more than a preset amount, the measurement is ignored. A multi-position switch is used to set the comparison threshold, with the error allowed being up to 10 bits, set in one bit increments. The scale is selected automatically by the LOD module. Readings which are out of range are ignored to eliminate the possibility of including saturated values. An output is provided to signal the user when the data is valid. In addition, two displays are provided for direct visual output of average velocity or time, and error or data rate. The FED module removes the pedestal from the Doppler burst and limits the resulting signal, providing a square wave output compatible with the LOD module.

Description of Operation - FED Module. The Doppler burst presented at the input is passed through a high-pass filter to remove the superimposed lower frequency pedestal waveform which acts as an envelope to the Doppler burst signature. It is then amplified and the resulting signal is then electronically limited about the zero crossing point (subject to the hysteresis added to eliminate switching of the Schmitt trigger due to noise).

Prior to the high pass filtering, the amplified Doppler burst is passed through a buffer amplifier and presented to a comparator to determine if it exceeds a preset threshold height. If the threshold is exceeded, the overload output is driven to ground indicating to the LOD that the data being processed should be ignored.

Description of Operation - LOD Module. The LOD module consists of two timers, validation circuitry and control logic. It is entirely digital with the exception of a portion of the auto range circuitry. Normally a burst of TTL level pulses corresponding to the Doppler burst is presented at the input. At the occurrence of the first pulse, a 100 MHz clock is gated to two counters. When 5 pulses have occurred, the first counter is stopped, after 8 the second counter is stopped.

Each counter consists of 20 bits; however, only 8 bits are selected depending on the scale setting. When the counters are stopped, the 8 bits from each counter are compared to determine if they are in the proper 5 to 8 ratio. The allowable error is set by a front panel adjustment. If the allowable error is exceeded, the data is ignored, the counters are reset and the input circuit is enabled to begin another reading. If the readings are validated (within set error limits), the output (10 bits) from the eight pulse counter is strobed into a storage register.

These data are then presented, along with the scale, to a digital output located on the rear panel. In addition, they are converted to an analog signal. When the D/A converter has settled, the data ready line, which was brought to the high state as the data was strobed to the storage register, is lowered indicating the data are valid. The analog signal is passed through a divider to convert the time measurement to frequency. Either time or frequency may then be selected at the front panel. The selected signal is low-pass filtered and the voltage level is displayed on the front panel in conjunction with the appropriate exponent.

Each time data are taken, the result of the comparison is stored. The result of the last 1,000 samples is stored to yield the percent of signals which are being validated.

At any time prior to data validation, a negative signal on the reset inputs will cause the data to be ignored; the counters will be reset and the input circuitry will be enabled for the next measurement.

In the data rate mode, the number of validated readings occurring during a one-second interval are calculated and displayed on the front panel. The display covers two ranges, 9.99 kHz full scale and 999 kHz full scale. The range is automatically determined and the reading is directly in kHz.

Modifications. During the course of working with the DFP several modifications were made to improve its operation. One of these was to provide a new FED module with an input amplifier (Gain = 10 or 1) and improved high-pass and low-pass filters. The second modification was in the discrimination logic to permit processing of Doppler signals based on the sequence of zero and threshold level crossings, rather than only a 5/8 comparison.

APPENDIX D

D-1. LV INSTRUMENTATION SYMBOLS AND NOMENCLATURE

b_2 = impeller tip depth

C = absolute velocity

C_1 = absolute velocity vector measured with LV in orientation (1)

C_2 = absolute velocity vector measured with LV in orientation (2)

C_{2J} = jet absolute velocity at impeller tip

C_{2w} = wake absolute velocity at impeller tip

C_{2*} = mixed out absolute velocity

C_4 = absolute velocity at diffuser throat

C_{x1} = absolute velocity at impeller inlet, axial

c = speed of light

D_A = Airy diameter of focused laser beam

D_i = laser beam diameter at beam splitter

D_L = laser beam diameter at focusing lens

d = length of side of beam splitter prism

f = frequency or focal length, in context

f_a = sum frequency of beam a

f_b = sum frequency of beam b

f_c = clock frequency

Δf_D = differential Doppler frequency

f_L = frequency of laser radiation

f_{sc} = scattering frequency

ℓ = probe volume length

N = impeller rotational speed or number, in context

N_f = number of fringes in probe volume

N_1 = index of refraction

N_2 = index of refraction

n_i = number of occurrences

$P(X)$ = probability of occurrence of argument

r = radius

r_{1h} = impeller inlet hub radius

r_{1t} = impeller inlet tip radius

r_2 = impeller discharge tip radius

r_3 = diffuser vane island tip radius

S_b = spacing between beam at beam splitter

S_f = fringe spacing

U_i = i^{th} velocity in a distribution

U_m = mass averaged velocity

$\bar{U}$ = mean velocity in a distribution

u = impeller velocity

u' = fluctuating component of U_i

V_{jet} = velocity of jet

v_o = velocity of particle in probe volume

W = fluid velocity relative to rotating impeller

W_4 = diffuser throat width

w = probe volume width

w' = probe volume width transverse to plane of measurement

X = nominally parallel to compressor axis

Y = perpendicular to the axis in a horizontal plane

Z = perpendicular to the axis in a vertical plane

α = absolute flow angle relative to axis

β = relative flow angle

γ = angle between total absolute vector and impeller direction

δ = angle between C_1 vector and total absolute velocity

ε = measurement error

θ_2 = diffraction angle in beam splitter

λ = wave length of radiation

σ_m = frequency processor probable error

σ_s = sample standard deviation

σ_t = turbulence level of histogram

ϕ = total included angle between input beams

ψ = angle between beam bisector and detector or C_1 velocity vector relative to compressor reference axis, in context

Subscripts

1a, 1b = direction vectors relative to scattering particle

c = corrected value

total = total velocity probability distribution broadening

x = axial direction

D-2. CREARE CENTRIFUGAL COMPRESSOR MODEL NOMENCLATURE AND CDR2 INPUT/OUTPUT NOMENCLATURE

A — flow area (normal to mean velocity vector, specifically defined)

A_{eff} — effective area = "one dimensional" cross-sectional flow are

A_{geom} — geometrical cross-sectional area

AR_i — impeller passage geometrical area ratio (inlet to outlet)

AR_{equiv} — equivalent impeller one dimensional flow area ratio

AS_4 — channel diffuser throat aspect ratio (b/W for radial-plane divergence; W/b for meridional-plane divergence)

a — acceleration

a — speed of sound

B — boundary layer blockage:

$$B \equiv 1 - \frac{A_{effective}}{A_{geometrical}}$$

b — meridional depth of passage (normal to mean meridional velocity component)

BF — blockage factor:

$$B_F \equiv \frac{A_{effective}}{A_{geometrical}}$$

C — absolute velocity (relative to a Newtonian frame, e.g., compressor casing)

c_f — wall friction coefficient:

$$c_f \equiv \frac{\tau}{\rho W^2/2g_o}$$

where:

W is measured relative to subject wall

C_p pressure recovery coefficient:

$$C_p = \frac{p - p_{ref}}{(p_o - p)_{ref}}$$

where:
measuring and reference states and stations must be specifically defined

c_p specific heat at constant pressure

C_R torque coefficient, friction

DR diffusion ratio:

$$DR = (W_1/W_{sep})_t$$

E energy

E_L impeller effectiveness: MR_2/MR_{2i}

F force

g_o proportionality constant in Newton's Second Law

$$F = Ma/g_o$$

H boundary layer shape factor = δ^*/θ

H_i boundary layer shape factor for incompressible flow before transformation to compressible flow

h static enthalpy/unit mass

h_o stagnation enthalpy/unit mass

h_T total enthalpy/unit mass (in a coordinate system rotating in Newtonian space in absence of electricity, magnetism, gravity and capillarity):

$$h_T = h + \frac{w^2 - u^2}{2g_o J}$$

i incidence angle of flow onto blades:

$$(i = \beta_b - \beta)$$

J constant = 1: (778 ft-lb_f/Btu)

k ratio of specific heats

L diffuser centerline length (from throat to exit plane)

LP impeller load parameter:
$$LP = r_2\Omega/W_{2Z_i}$$

ℓ length of channel diffuser throat, see Figure 3

M Mach number

M mass

m distance along specified meridional trajectory (often streamline of potential solution)

m mass flow rate

MR_2 Mach number ratio $= M_{rel\ 1t}/M_{rel\ 2j}$

MR_{2i} $M_{rel\ 1t}/M_{rel\ 2i}$

$M_{rel\ 2i}$ ideal impeller discharge relative Mach number for a given impeller geometry, m and N and for isentropic internal flow; discharge blockage β_2 = only blade metal blockage, uniform discharge state and $\beta_2 = \beta_{b2}$ mean line

N shaft speed

N_s specific speed
$$N_s = \frac{N\sqrt{Q_o}}{(\Delta h_o)^{3/4}}$$
where:
N = radians/s: (rpm)
Q_o = inlet flow = $m\rho_{oo}$ in m^3/s: (ft^3/s)
Δh_o = ideal stage enthalpy rise in joules/kg: $ft\text{-}lb_f/lb_m$

p static pressure

p_o stagnation pressure

pr pressure ratio
$$pr = p/p_{oo}$$

p_t total pressure; a rotating coordinate property defined by (for perfect gas):

$$\frac{p_T}{p_{oo}} = \left(\frac{T_T}{T_{oo}}\right)^{\frac{k}{k-1}}$$

q dynamic pressure:

$$q = \frac{1}{2g_o}\rho C^2$$

Q heat

R radius ratio, r/r_2

R gas constant

°C, °K degrees

r radius

r radial coordinate (see Figure 1)

S distance between impeller blades:

$$S = 2\pi r/Z$$

SP stability parameter: $SP = (\partial pr/\partial m)/pr$

s entropy/unit mass

T static pressure

T_o stagnation temperature

T_T total temperature (defined by h_T and c_p for a perfect gas)

t blade thickness (in direction specified)

t_b blade (metal) thickness

u impeller (metal) velocity

W diffuser throat width (in radial plane)

W relative velocity (in coordinate system rotating steadily in Newtonian space)

W_x total shaft work per unit mass of fluid

W_{xi} work input to impeller per unit mass of fluid

V_s slip velocity:

$$V_s = C_{m2} \tan \beta_{b2} - W_{\theta 2}$$

x axial coordinate (see Figure 1)

Z number of blades

α absolute flow angle (see Figure 1)

β relative flow angle (see Figure 1)

γ pitch angle in meridional plane (see Figure 1)

δ^* boundary layer displacement thickness

ε wake width

ε effectiveness (for impeller $\varepsilon_i = MR/MR_i$

η efficiency:

$$\eta = \frac{h_{os} - h_{oo}}{W_x}$$

(measuring stations must be specifically defined)

θ boundary layer momentum thickness

θ tangential angular coordinate (see Figure 1)

2θ diffuser divergence angle

λ swirl parameter:

$$\lambda \equiv C_\theta / C_r$$

μ work input coefficient:

$$\mu_i \equiv \frac{W_x}{u^2/g_o}$$

ξ_{WL} Welliver Loss coefficient = $(P_{o2*}-P_{o4})/(P_{o2*}-P_{2*})$

ξ vorticity or loss coefficient:

$$\xi_{IGV} = \frac{\Delta p_o}{(p_o - p)_1}$$

πMi impeller-tip Mach number:

$$\pi Mi \equiv u_2/a_{oo}$$

ρ density

ρ_o stagnation density

σ slip factor:

$$\sigma = 1 - V_s/u_2$$

τ fluid shear stress

τ torque

ψ yaw angle (between velocity vector and null direction of flow angle measuring probe)

Ω impeller angular velocity

Subscripts

0,1,2, 3, -- stations in the stage (see Figure 2)

b blade property

bf backflow

CL centerline

c cover

coll collector station (receiving volume after diffuser)

crit critical value (must be specifically defined)

D diffuser

dm	(impeller) discharge mixing
eff	effective
f	friction
geom	geometrical
h	hub
i	inlet or impeller
i	ideal
IW	internal wake (loss
IGV	inlet guide vane property
j	jet
le	leading edge
m	mean
n	normal thickness
o	stagnation
p	pressure surface of blade
p	polytropic
r	radial component (see Figure 1)
rd	rear disc (friction)
ref	reference state or station (must be specifically defined)
rel	relative to impeller coordinates
s	indicates that process follows an isentropic path

s	suction surface
sep	flow separation value
surf	surface property
T	total (see definitions of h_T, T_T, and p_T)
t	tip or throat
TS	total to static (efficiency)
TT	total to total (efficiency)
WL	Welliver loss
w	wake
x	upstream of shock (e.g., M_x) or axial component (see Figure 1)
y	downstream of shock (e.g., M_y)
θ	tangential component (see Figure 1)

Superscripts

*	mixed-out state (must be specifically defined)
**	impeller discharge state including all work input from fluid angular momentum, cover and rear disc friction and back flow
'	time-varying property
^	instrument-indicated property
∿	mass-flow-averaged property
-	time-averaged property
=	area-averaged property
→	vector quantity

Miscellaneous

ln	natural logarithm
log	base 10 logarithm
exp	exp $a \equiv e^a$
e	base of the natural logarithms ($e = 2.71828...$)
f( )	function of ( )
$\tan^{-1}$( )	inverse operator: $\alpha = \tan^{-1}\lambda$ mean tan $\alpha = \lambda$
Δ	incremental (but finite) change
d	incremental (but infinitesimal) change, total derivative
∂	incremental (but infinitesimal) change, partial derivative
π	3.1416..

D-3. CDR2 COMPUTER OUTPUT LISTINGS

The following pages provide CDR2 data reduction listings for selected compressor stage tests for Runs 6, 7, 8, and 9. See Table IX of the report for a description of the stage configuration used for each series of tests.

Table D-1 lists the CDR2 data presented in this appendix.

TABLE D-1. - LISTING OF CDR2 DATA

Run	Test	Speed (% N_D)
6	6.01 6.06 6.09 6.14	50%
6	6.20 6.24 6.29 6.33	80%
7	7.02 7.10 7.12 7.16	100%
8	8.32 8.36 8.40 8.44	50%
8	8.58 8.64 8.68 8.72	80%
8	8.46 8.48 8.50 8.56	90%
8	8.86 8.90 8.94 8.96	100%

continued

TABLE D-1. - LISTING OF CDR2 DATA (CONTINUED)

Run	Test	Speed (% N_D)
9	9.02	50%
	9.06	
	9.08	
	9.10	
9	9.14	80%
	9.18	
	9.22	
	9.30	
9	9.36	100%
	9.38	
	9.42	
	9.32	

```
CDR2...PROJECT#3305...6.01 HAVE P1T ZBF  SI UNITS...10/10/78  KBA

INPUT VALUES

P00= 101353.   P1= 100066.    P2= 148513.    P4= 123106.
P04= 195990.   P5= 6894.76    P05= 128787.   PCOL= 128787
T00= 288.161   TCOL= 357.222  H= 0 255826    N= 3981.97
MW/M= 0.2      LC= 0          W4= 0.137709   B4= 3.2258 E-3
B1B=-56.3      B2B=-30.       ALPHT= 0       B2= 3.2258 E-3
PR= 1.27068    RSEP= 4.39496 E-2             R1H= 2.16002 E-2
R1T= 4.39496 E-2
R2= 0.079756   # BLADES= 19   # DIFF= 17

INDUCER TIP

TTREL= 288.099    PTREL= 101275.    MRELIT= 0.535298
CIT= 49.5177   RCT= 0          WIT= 181.876
P1T= 100066.   T1T= 286 937    M1T= 0.14574
B1T=-74.2013   IT= 17.7013     UIT= 175.006
P10T= 101353.  IKE= 0.238359

IMPELLER TIP

CT2J= 189.349  CM2J= 134.463  C2J= 232.236
C2W= 292.723   CM2W= 50.7372  CT2W= 288.293
W2W= 58.5863   W2J= 185.808   WT2W= 29.2931
P02J= 196753.  MREL2J= 0.517392
T2J= 321.222   T02J= 348.008  M2J= 0.64724   U2= 317.586
P02W= 223617.  M2W= 0.788309  E= 0.415437    P02MA= 202126
T2W= 344.559   T02W= 387.038
MR= 1.03461    MRI= 1.76792   TN= 1.3208 E-3                DR= 1.02918
WSEP= 176.72

STATES AFTER MIXING

T2*= 329.244   T02*= 355.828  T02**= 357.198
P2*= 151493.   P02*= 198988.
M2*= 0.636906  DP02= 3137.92
CT2*= 209.138  CM2*= 98.7249  C2*= 231.269
T02**-TCOL=-2.42911 E-2
L= 2.11839

SIG*= 0.838

WX= 69389.3    WFC= 1590.09    WFRD= 1325.07 WBF= 54.819

DIFFUSER

P4= 123106.    M4= 0.841868   B= 7 50669 E-3
D*= 1.06155 E-5     CP2*4=-0.5977      HS= 2.5594
CP4C= 7.79491 E-2             CPD=-0.47808
P04= 195990.   WL= 6.31081 E-2

EFFICIENCIES

DETSBF= 7.90021 E-4       DETSFC= 2.29154 E-2     DETSWL= 2.18811 E-2
DETSRD= 1.90962 E-2       DETSI= 0.116613
DETSD= 0.590811           DETSF= 4.20116 E-2
DETSDM= 2.26577 E-2       DETSIW= 5.11534 E-2
ETT= 0.292576  ETS= 0.292576  ETTI= 0.883387

*
```

```
CDR2...PROJECT#3305...6.06 HAVE P1T ZBF  SI UNITS...10/10/78  KBA

INPUT VALUES

P00= 101353.   P1= 100162.    P2= 147562.    P4= 133476.
P04= 202016.   P5= 6894.76    P05= 165247.   PCOL= 165247.
T00= 288.161   TCOL= 358.833  H= 0.246754    N= 3924.68
MW/M= 0.2      LC= 0          W4= 0.137709   B4= 3.2258 E-3
B1B=-56.3      B2B=-30.       ALPHT= 0       B2= 3.2258 E-3
PR= 1.63041    RSEP= 4.39496 E-2             R1H= 2.16002 E-2
R1T= 4.39496 E-2
R2= 0.079756   # BLADES= 19   # DIFF= 17

INDUCER TIP

TTREL= 288.099    PTREL= 101275.    MRELIT= 0.526798
CIT= 47 8896   RCT= 0          WIT= 179.013
P1T= 100162.   T1T= 287.016   M1T= 0.140929
B1T=-74.4833   IT= 18.1833    UIT= 172.498
P10T= 101353.  IKE= 0 225631

IMPELLER TIP

CT2J= 200.021  CM2J= 141.63   C2J= 245.086
C2W= 290.904   CM2W= 44.1322  CT2W= 287.537
W2W= 50.9594   W2J= 181.183   WT2W= 25.4797
P02J= 201685.  MREL2J= 0.504966
T2J= 320.633   T02J= 350.467  M2J= 0.683718  U2= 313.017
P02W= 221379.  M2W= 0.784578  E= 0.462236    P02HA= 205623.
T2W= 343.511   T02W= 385.47
MR= 1.04324    MRI= 1.76552   TN= 1.3208 E-3                DR= 1.03716
WSEP= 172.599

STATES AFTER MIXING

T2*= 329.459   T02*= 357.479  T02**= 358.81
P2*= 151648.   P02*= 201992.
M2*= 0.653673  DP02= 3431.54
CT2*= 217.524  CM2*= 95.1892  C2*= 237.44
T02**-TCOL=-2.34901 E-2
L= 2.28517

SIG*= 0.8705

WX= 71013.5    WFC= 1583.61    WFRD= 1319.68 WBF= 21.3683

DIFFUSER

P4= 133476.    M4= 0.792104   B= 5.22315 E-2
D*= 7.38628 E-5     CP2*4=-0.36096      HS= 2.72253
CP4C= 0.463535                CPD= 0.270117
P04= 202016.   WL=-4.85667 E-4

EFFICIENCIES

DETSBF= 3.00905 E-4       DETSFC= 2.23002 E-2     DETSWL=-1.71737 E-4
DETSRD= 1.85835 E-2       DETSI= 0.115615
DETSD= 0.276622           DETSF= 4.08836 E-2
DETSDM= 2.53307 E-2       DETSIW= 0.0491
ETT= 0.607763  ETS= 0.607763  ETTI= 0.884385

*
```

```
CDR2...PROJECT#3305...6.09 HAVE P1T ZBF  SI UNITS.. 10/10/78  KBA

INPUT VALUES

P00= 101353.   P1= 100745.    P2= 152664.    P4= 174499.
P04= 205498.   P5= 6894.76    P05= 193894.   PCOL= 193894.
T00= 288.161   TCOL= 362.056  H= 0.176447    N= 3948.14
MW/M= 0.2      LC= 0          W4= 0.137709   B4= 3.2258 E-3
B1B=-56.3      B2B=-30.       ALPHT= 0       B2= 3.2258 E-3
PR= 1.91306    RSEP= 4.39496 E-2             R1H= 2.16002 E-2
R1T= 4.39496 E-2
R2= 0.079756   # BLADES= 19   # DIFF= 17

INDUCER TIP

TTREL= 288.099    PTREL= 101275.    MRELIT= 0.521433
CIT= 36.5853   RCT= 0          WIT= 177.334
P1T= 100745.   T1T= 287 493    M1T= 0 107575
B1T=-78.094    IT= 21.794     UIT= 173.519
P10T= 101353.  IKE= 0.211731

IMPELLER TIP

CT2J= 202.907  CM2J= 123.201  C2J= 237.381
C2W= 301.414   CM2W= 25.1592  CT2W= 300 362
W2W= 29.0514   W2J= 166.488   WT2W= 14.5257
P02J= 204287.  MREL2J= 0.461808
T2J= 323.761   T02J= 351 741  M2J= 0.65921   U2= 314.888
P02W= 234186.  M2W= 0.807211  E= 0.568544    P02HA= 210267.
T2W= 348.493   T02W= 393.504
MR= 1.12911    MRI= 2.55248   TN= 1.3208.E-3                DR= 1.11768
WSEP= 158.662

STATES AFTER MIXING

T2*= 333.329   T02*= 360 11   T02**= 362.034
P2*= 156666.   P02*= 205551.
M2*= 0.635611  DP02= 4715.97
CT2*= 222.398  CM2*= 66.6609  C2*= 232.174
T02**-TCOL=-2.19684 E-2
L= 3.33626

SIG*= 0.8285

WX= 74262.6    WFC= 2293.66    WFRD= 1911.38 WBF= 27.0446

DIFFUSER

P4= 174499.    M4= 0.488732   B= 0.124225
D*= 1.75673 E-4     CP2*4= 0.364804      HS= 2.02827
CP4C= 0.625667                CPD= 0.761553
P04= 205498.   WL= 1.07428 E-3

EFFICIENCIES

DETSBF= 3.64176 E-4       DETSFC= 3 08858 E-2     DETSWL= 3.48217 E-4
DETSRD= 2.57382 E-2       DETSI= 0.130569
DETSD= 7.88896 E-2        DETSF= 5.46239 E-2
DETSDM= 3.10127 E-2       DETSIW= 4.25602 E-2
ETT= 0.790541  ETS= 0.790541  ETTI= 0.869431
```

```
CDR2...PROJECT#3305. .6.14 HAVE P1T ZBF  SI UNITS...10/10/78  KBA

INPUT VALUES

P00= 101353.   P1= 100238.    P2= 148878.    P4= 145583.
P04= 202830.   P5= 6894.76    P05= 176251    PCOL= 176251.
T00= 288.161   TCOL= 361.389  H= 0.239043    N= 3947.93
MW/M= 0.2      LC= 0          W4= 0.137709   B4= 3.2258 E-3
B1B=-56.3      B2B=-30.       ALPHT= 0       B2= 3.2258 E-3
PR= 1.73898    RSEP= 4.39496 E-2             R1H= 2.16002 E-2
R1T= 4.39496 E-2
R2= 0.079756   # BLADES= 19   # DIFF= 17

INDUCER TIP

TTREL= 288.099    PTREL= 101275.    MRELIT= 0.528621
CIT= 46.3712   RCT= 0          WIT= 179.651
P1T= 100238.   T1T= 287 079    M1T= 0.137035
B1T=-74.9756   IT= 18.6756    UIT= 173.51
P10T= 101353.  IKE= 0.219286

IMPELLER TIP

CT2J= 207.012  CM2J= 143.949  C2J= 252.141
C2W= 294.478   CM2W= 40.0644  CT2W= 291.74
W2W= 46.2623   W2J= 179.875   WT2W= 23.1312
P02J= 206905.  MREL2J= 0.500697
T2J= 321.448   T02J= 353.021  M2J= 0.70259   U2= 314.871
P02W= 225157.  M2W= 0.792796  E= 0.490677    P02HA= 210555.
T2W= 344.764   T02W= 387.752
MR= 1.05577    MRI= 1.86705   TN= 1.3208 E-3                DR= 1.04893
WSEP= 171.271

STATES AFTER MIXING

T2*= 330.898   T02*= 359.979  T02**= 361.367
P2*= 153538.   P02*= 206407.
M2*= 0.66459   DP02= 4147.79
CT2*= 223.957  CM2*= 91.4772  C2*= 241.919
T02**-TCOL=-2.22736 E-2
L= 2.44823

SIG*= 0.879

WX= 73590.3    WFC= 1673.71    WFRD= 1394.76 WBF= 3.96105

DIFFUSER

P4= 145583.    M4= 0.704652   B= 3.84764 E-2
D*= 5.44112 E-5     CP2*4=-0.150465      HS= 2 76504
CP4C= 0.53571                 CPD= 0.429604
P04= 202830.   WL= 6.76608 E-2

EFFICIENCIES

DETSBF= 5.38257 E-5       DETSFC= 2.27437 E-2     DETSWL= 2.40098 E-2
DETSRD= 1 89531 E-2       DETSI= 0.116905
DETSD= 0.212586           DETSF= 4.16967 E-2
DETSDM= 2.74715 E-2       DETSIW= 4.76828 E-2
ETT= 0.670509  ETS= 0.670509  ETTI= 0.883095
```

ORIGINAL PAGE IS
OF POOR QUALITY

ORIGINAL PAGE IS
OF POOR QUALITY

```
CDR2...PROJECT#3305...6.20 ZBF  SI UNITS...10/10/78  KBA

INPUT VALUES

P00= 101353.   P1= 96292.2    P2= 259726.    P4= 264090.
P04= 470636.   P5=-0           P05= 210083.   PCOL= 210083.
T00= 288.167   TCOL= 473.222   M= 0.553383    N= 6304.86
MW/M= 0.2      LC= 0           W4= 0.137709   B4= 3.2258 E-3
B1B=-56.3      B2B=-30.        ALPHT= 0       B2= 3.2258 E-3
PR= 2.07279    RSEP= 4.39496 E-2              RIH= 2.16002 E-2
RIT= 4.39496 E-2
R2= 0.079756   # BLADES= 19    # DIFF= 17

INDUCER TIP

TTREL= 288.104    PTREL= 101275.    MRELIT= 0.865356
CIT= 93.471    RCT= 0          WIT= 292 436
P1T= 96292.2   T1T= 283.804    M1T= 0.276592
B1T=-71.3596   IT= 15.0596     U1T= 277.096
P10T= 101353.  IKE= 0.228376

IMPELLER TIP

CT2J= 332.293  CM2J= 213.675  C2J= 395.064
C2W= 467.87    CM2W= 69.6068  CT2W= 462.663
W2W= 80.375    W2J= 273.399   WT2W= 40.1875
P02J= 502003.  MREL2J= 0.704201
T2J= 376.716   T02J= 453.554  M2J= 1 01994   U2= 502.85
P02W= 573358.  M2W= 1.12977   E= 0.466398    P02MA= 516274.
T2W= 429.052   T02W= 535.636
HR= 1.22885    HRI= 2.35782   TN= 1.3208 E-3                 DR= 1.20314
WSEP= 243.062

STATES AFTER MIXING

T2#= 397.073   T02#= 470.069  T02##= 473.237
P2#= 274276.   P02#= 499321
M2#= 0.968296  DP02= 16953.4
CT2#= 358.366  CM2#= 142.254  C2#= 385.568
T02##-TCOL= 1.46696 E-2
L= 2.51919

SIG#= 0.876

WX= 187234.    WFC= 3783.03    WFRD= 3152.52 WBF= 93 2612

DIFFUSER

P4= 264090.    M4= 0.949928   B=-9.93288 E-3
D#=-1.40465 E-5     CP2#4=-0.045262     M5= 0
CP4C=-0.261475                 CPD=-0.285244
P04= 470636.   WL= 0.127461

EFFICIENCIES

DETSBF= 4.981 E-4          DETSFC= 2.02048 E-2     DETSWL= 4.08286 E-2
DETSRD= 1.48374 E-2        DETSI= 0.109083
DETSD= 0.534241            DETSF= 3.70422 E-2
DETSDM= 2.33431 E-2        DETSIW= 4.81999 E-2
ETT= 0          ETS= 0.356676  ETTI= 0.890917
```

```
CDR2...PROJECT#3305...6.24  SI UNITS...10/10/78  KBA

INPUT VALUES

P00= 101353.   P1= 96610.7    P2= 259168.    P4= 263236.
P04= 467997.   P5= 0          P05= 302133.   PCOL= 302133.
T00= 288.161   TCOL= 474.606  M= 0.553836    N= 6299.2
MW/M= 0.2      LC= 0          W4= 0.137709   B4= 3.2258 E-3
B1B=-56.3      B2B=-30.       ALPHT= 0       B2= 3.2258 E-3
PR= 2.981      RSEP= 4.39496 E-2             RIH= 2.16002 E-2
RIT= 4.39496 E-2
R2= 0.079756   # BLADES= 19   # DIFF= 17

INDUCER TIP

TTREL= 288.099    PTREL= 101275.    MRELIT= 0.861543
CIT= 90.552    RCT= 0          WIT= 291.28
P1T= 96610.7   T1T= 284.066    M1T= 0.267833
B1T=-71.888    IT= 15.588      U1T= 276.848
P10T= 101353.  IKE= 0.224863

IMPELLER TIP

CT2J= 335.212  CM2J= 216.357  C2J= 398.971
C2W= 467.698   CM2W= 68.9801  CT2W= 462.574
W2W= 79.6514   W2J= 273.426   WT2W= 39.6256
P02J= 507118.  MREL2J= 0.704487
T2J= 376.479   T02J= 454.838  M2J= 1.03033   U2= 502.399
P02W= 572035.  M2W= 1.12964   E= 0.471779    P02MA= 520101.
T2W= 428.82    T02W= 535.327
HR= 1.22294    HRI= 2.34135   TN= 1.3208 E-3                 DR= 1.19806
WSEP= 243.127

STATES AFTER MIXING

T2#= 397.208   T02#= 471.031  T02##= 474.62
P2#= 274390.   P02#= 502565.
M2#= 0.973612  DP02= 17536.5
CT2#= 360.484  CM2#= 142.36   C2#= 387.762
T02##-TCOL= 1.48943 E-2
L= 2.5336

SIG#= 0.881522

WX= 188658.    WFC= 3770.85    WFRD= 3142.37 WBF= 536.634

DIFFUSER

P4= 263236.    M4= 0 947849   B=-0.010168
D#=-2.56922 E-5     CP2#4=-4.88602 E-2     M5= 0
CP4C= 0.189962                 CPD= 0.121589
P04= 467997.   WL= 0.151497

EFFICIENCIES

DETSBF= 2.84449 E-3        DETSFC= 1.99878 E-2     DETSWL= 4.88124 E-2
DETSRD= 1.66565 E-2        DETSI= 0.111349
DETSD= 0.327939            DETSF= 3.66443 E-2
DETSDM= 0.023844           DETSIW= 4.80162 E-2
ETT= 0          ETS= 0.560712  ETTI= 0.888651
```

```
CDR2...PROJECT#3305...6.29  SI UNITS...10/10/78  KBA

INPUT VALUES

P00= 101353.   P1= 97939.3    P2= 257899.    P4= 330253.
P04= 476855.   P5= 0          P05= 430345.   PCOL= 430345.
T00= 288.161   TCOL= 479.494  M= 0.493055    N= 6298.36
MW/M= 0.2      LC= 0          W4= 0.137709   B4= 3.2258 E-3
B1B=-56.3      B2B=-30.       ALPHT= 0       B2= 3.2258 E-3
PR= 4.246      RSEP= 4.39496 E-2             RIH= 2.16002 E-2
RIT= 4.39496 E-2
R2= 0.079756   # BLADES= 19   # DIFF= 17

INDUCER TIP

TTREL= 288.099    PTREL= 101275.    MRELIT= 0.848424
CIT= 77.2833   RCT= 0          WIT= 287.397
P1T= 97939.3   T1T= 285.179    M1T= 0.228148
B1T=-74.4008   IT= 18.1008     U1T= 276.811
P10T= 101353.  IKE= 0.213238

IMPELLER TIP

CT2J= 344.405  CM2J= 225.422  C2J= 411.619
C2W= 474.397   CM2W= 53.6576  CT2W= 471.353
W2W= 61.9584   W2J= 275.238   WT2W= 30.9792
P02J= 525396.  MREL2J= 0.709639
T2J= 375.954   T02J= 459.334  M2J= 1.06403   U2= 502.332
P02W= 577449.  M2W= 1.14109   E= 0.547071    P02MA= 535807.
T2W= 432.356   T02W= 541.839
HR= 1.19557    HRI= 2.63689   TN= 1.3208 E-3                 DR= 1.17431
WSEP= 244.737

STATES AFTER MIXING

T2#= 400.994   T02#= 475.936  T02##= 479.51
P2#= 277571.   P02#= 510162.
M2#= 0.976745  DP02= 25644.3
CT2#= 369.795  CM2#= 126.479  C2#= 390.826
T02##-TCOL= 1.57081 E-2
L= 2.92377

SIG#= 0.881522

WX= 193673.    WFC= 4246.62    WFRD= 3538.85 WBF= 127.55

DIFFUSER

P4= 330253.    M4= 0.747203   B= 0.050033
D#= 7.07530 E-5     CP2#4= 0.226499     M5= 0
CP4C= 0.682743                 CPD= 0.656833
P04= 476855.   WL= 0.1432

EFFICIENCIES

DETSBF= 6.58583 E-4        DETSFC= 2.19268 E-2     DETSWL= 4.52627 E-2
DETSRD= 1.82723 E-2        DETSI= 0.124229
DETSD= 0.112438            DETSF= 4.01991 E-2
DETSDM= 3.34206 E-2        DETSIW= 4.97504 E-2
ETT= 0          ETS= 0.763333  ETTI= 0.875771
```

```
CDR2...PROJECT#3305...6.33 ZBF  SI UNITS...10/10/78  KBA

INPUT VALUES

P00= 101353.   P1= 97030.6    P2= 256240.    P4= 278643.
P04= 479146.   P5= 0          P05= 400040.   PCOL= 400040.
T00= 288.161   TCOL= 473.439  M= 0.539321    N= 6285.17
MW/M= 0.2      LC= 0          W4= 0.137709   B4= 3.2258 E-3
B1B=-56.3      B2B=-30.       ALPHT= 0       B2= 3.2258 E-3
PR= 3.947      RSEP= 4.39496 E-2             RIH= 2.16002 E-2
RIT= 4.39496 E-2
R2= 0.079756   # BLADES= 19   # DIFF= 17

INDUCER TIP

TTREL= 288.099    PTREL= 101275.    MRELIT= 0.855687
CIT= 86.5654   RCT= 0          WIT= 289.477
P1T= 97030.6   T1T= 284.419    M1T= 0.255885
B1T=-72.6001   IT= 16.3001     U1T= 276.231
P10T= 101353.  IKE= 0.223505

IMPELLER TIP

CT2J= 333.921  CM2J= 219.282  C2J= 399.485
C2W= 468.009   CM2W= 65.64    CT2W= 463.383
W2W= 75.7945   W2J= 275.85    WT2W= 37.8972
P02J= 503219.  MREL2J= 0.711855
T2J= 375.264   T02J= 453.837  M2J= 1.03339   U2= 501.28
P02W= 566093.  M2W= 1.13037   E= 0.488338    P02MA= 515794.
T2W= 428.845   T02W= 535.495
HR= 1.20205    HRI= 2.38706   TN= 1.3208 E-3                 DR= 1.17973
WSEP= 245.375

STATES AFTER MIXING

T2#= 397 138   T02#= 470.267  T02##= 473.454
P2#= 272558.   P02#= 496650.
M2#= 0.969104  DP02= 19144.2
CT2#= 359.814  CM2#= 139.536  C2#= 385.922
T02##-TCOL= 1.46527 E-2
L= 2.57864

SIG#= 0.8785

WX= 187461     WFC= 3828.12    WFRD= 3190.1 WBF= 75.5719

DIFFUSER

P4= 278643.    M4= 0.917952   B= 2.92724 E-2
D#= 4 13954 E-5     CP2#4= 2.71503 E-2     M5= 0
CP4C= 0.605462                 CPD= 0.568082
P04= 479146.   WL= 7.81091 E-2

EFFICIENCIES

DETSBF= 4.03133 E-4        DETSFC= 2.04208 E-2     DETSWL= 2.47734 E-2
DETSRD= 1.70174 E-2        DETSI= 0.113907
DETSD= 0.145638            DETSF= 3.74382 E-2
DETSDM= 2.63865 E-2        DETSIW= 4.96796 E-2
ETT= 0          ETS= 0.740455  ETTI= 0 884093
```

ORIGINAL PAGE IS
OF POOR QUALITY

```
CDR2...PROJECT#3305...7.02 P4=.528*P04  SI UNITS...10/11/78  KBA

 INPUT VALUES

 P00= 101353.   P1= 78241.7     P2= 388678.    P4= 449973.
 P04= 852226.   P5= 0           P0S= 503083.   PCOL= 503083.
 T00= 288.167   TCOL= 571.889   M= 0.888134    N= 7846.85
 MW/M= 0.2      LC= 0           W4= 0.137709   B4= 3.2258 E-3
 B1B=-56.3      B2B=-30.        ALPHT= 0       B2= 3.2258 E-3
 PR= 4.96367    RSEP= 4.39496 E-2              R1H= 2.16002 E-2
 R1T= 4.39496 E-2
 R2= 0.079756   # BLADES= 19    # DIFF= 17

 INDUCER TIP

 TTREL= 288.104    PTREL= 101275.    MRELIT= 1.22021
 CIT= 203.573   RCT= 0          W1T= 400.468
 P1T= 78241.7   T1T= 267.422    M1T= 0.620281
 B1T=-59.4469   IT= 3.14685     U1T= 344.866
 P10T= 101353.  IKE= 0.277148

 IMPELLER TIP

 CT2J= 423.017  CM2J= 282.735  C2J= 508.805
 C2W= 585.335   CM2W= 79.5534  CT2W= 579.904
 W2W= 91.8603   W2J= 347.957   WT2W= 45.9301
 P02J= 991435.  MREL2J= 0.84769
 T2J= 422.346   T02J= 548.32   M2J= 1.24235   U2= 625.834
 P02W= 1.0711 E+6              M2W= 1.30114   E= 0.515132    P02MA=
  1.00737 E+6
 T2W= 505.01    T02W= 668.408
 MR= 1.43946    MRI= 3.28099   TN= 1.3208 E-3                DR= 1.35662
 WSEP= 295.196

 STATES AFTER MIXING

 T2*= 458.938   T02*= 572.584  T02**= 571.913
 P2*= 429486.   P02*= 949792.
 M2*= 1.13197   DP02= 57576.3
 CT2*= 454.394  CM2*= 168.516  C2*= 484.635
 T02**-TCOL= 2.43039 E-2
 L= 2.69644

 SIG*= 0.881522

 WX= 289331.    WFC= 5656.22    WFRD= 4713.52 WBF=-5414.49

 DIFFUSER

 P4= 449973.    M4= 1          B= 1.15099 E-2
 D*= 1.62767 E-5     CP2*4= 3.93747 E-2     MS= 0
 CP4C= 0.133488                CPD= 0.14145
 P04= 847838.   WL= 0.19595

 DIFFUSER THROAT IS CHOKED

 EFFICIENCIES

 DETSBF=-1.87138 E-2       DETSFC= 1.95493 E-2     DETSWL= 6.01779 E-2
 DETSRD= 1.62911 E-2       DETSI= 0.106378
 DETSD= 0.313702           DETSF= 3.58404 E-2
 DETSDM= 3.19356 E-2       DETSIW= 5.73156 E-2
 ETT= 0          ETS= 0.57992   ETTI= 0.893622
```

```
CDR2...PROJECT#3305...7.10 P4=.528*P04  SI UNITS...10/11/78  KBA

 INPUT VALUES

 P00= 101353.   P1= 80061.9     P2= 387782.    P4= 454282.
 P04= 860376.   P5= 0           P0S= 727176.   PCOL= 727176.
 T00= 288.167   TCOL= 576.778   M= 0.865001    N= 7853.24
 MW/M= 0.2      LC= 0           W4= 0.137709   B4= 3.2258 E-3
 B1B=-56.3      B2B=-30.        ALPHT= 0       B2= 3.2258 E-3
 PR= 7.17469    RSEP= 4.39496 E-2              R1H= 2.16002 E-2
 R1T= 4.39496 E-2
 R2= 0.079756   # BLADES= 19    # DIFF= 17

 INDUCER TIP

 TTREL= 288.104    PTREL= 101275.    MRELIT= 1.20357
 CIT= 194.727   RCT= 0          W1T= 396.289
 P1T= 80061.9   T1T= 269.191    M1T= 0.591404
 B1T=-60.569    IT= 4.269       U1T= 345.147
 P10T= 101353.  IKE= 0.266683

 IMPELLER TIP

 CT2J= 426.929  CM2J= 286.612  C2J= 513.466
 C2W= 587.741   CM2W= 75.2354  CT2W= 582.906
 W2W= 86.8743   W2J= 349.675   WT2W= 43.4371
 P02J= 1.0049 E+6              MREL2J= 0.852145
 T2J= 422.07    T02J= 550.341  M2J= 1.25427   U2= 626.343
 P02W= 1.07335 E+6             M2W= 1.30442   E= 0.533376    P02MA=
  1.01859 E+6
 T2W= 506.569   T02W= 671.237
 MR= 1.4124     MRI= 3.34648   TN= 1.3208 E-3                DR= 1.33613
 WSEP= 296.595

 STATES AFTER MIXING

 T2*= 460.553   T02*= 574.77   T02**= 576.802
 P2*= 431119.   P02*= 954642.
 M2*= 1.13304   DP02= 63951.9
 CT2*= 457.404  CM2*= 164.08   C2*= 485.943
 T02**-TCOL= 2.43039 E-2
 L= 2.78769

 SIG*= 0.881522

 WX= 294442.    WFC= 5824.8    WFRD= 4854. WBF=-2729.42

 DIFFUSER

 P4= 454282.    M4= 1          B= 4.21247 E-2
 D*= 5.95704 E-5     CP2*4= 4.42437 E-2     MS= 0
 CP4C= 0.679558                CPD= 0.565509
 P04= 855858.   WL= 0.189691

 DIFFUSER THROAT IS CHOKED

 EFFICIENCIES

 DETSBF=-9.26981 E-3       DETSFC= 1.97825 E-2     DETSWL= 5.69959 E-2
 DETSRD= 1.64854 E-2       DETSI= 0.119194
 DETSD= 0.138889           DETSF= 3.62679 E-2
 DETSDM= 3.46512 E-2       DETSIW= 5.75447 E-2
 ETT= 0          ETS= 0.741917  ETTI= 0.880806
```

```
CDR2...PROJECT#3305...7.12 P4=.528*P04  SI UNITS...10/11/78  KBA

 INPUT VALUES

 P00= 101353.   P1= 80799.7     P2= 388375.    P4= 455206.
 P04= 862134.   P5= 0           P0S= 754955.   PCOL= 754955.
 T00= 288.167   TCOL= 579.222   M= 0.862733    N= 7854.08
 MW/M= 0.2      LC= 0           W4= 0.137709   B4= 3.2258 E-3
 B1B=-56.3      B2B=-30.        ALPHT= 0       B2= 3.2258 E-3
 PR= 7.44878    RSEP= 4.39496 E-2              R1H= 2.16002 E-2
 R1T= 4.39496 E-2
 R2= 0.079756   # BLADES= 19    # DIFF= 17

 INDUCER TIP

 TTREL= 288.104    PTREL= 101275.    MRELIT= 1.19669
 CIT= 191.067   RCT= 0          W1T= 394.536
 P1T= 80799.7   T1T= 269.899    M1T= 0.579537
 B1T=-61.0346   IT= 4.73459     U1T= 345.184
 P10T= 101353.  IKE= 0.262052

 IMPELLER TIP

 CT2J= 426.45   CM2J= 286.358  C2J= 513.674
 C2W= 589.016   CM2W= 74.767   CT2W= 583.243
 W2W= 86.3334   W2J= 349.264   WT2W= 43.1667
 P02J= 1.00676 E+6             MREL2J= 0.850965
 T2J= 422.253   T02J= 550.622  M2J= 1.25451   U2= 626.41
 P02W= 1.0755 E+6              M2W= 1.30477   E= 0.534698    P02MA=
  1.02051 E+6
 T2W= 506.763   T02W= 671.575
 MR= 1.40628    MRI= 3.33849   TN= 1.3208 E-3                DR= 1.33181
 WSEP= 296.24

 STATES AFTER MIXING

 T2*= 460.767   T02*= 575.043  T02**= 579.247
 P2*= 431742.   P02*= 956246.
 M2*= 1.13319   DP02= 64261.
 CT2*= 457.808  CM2*= 163.482  C2*= 486.122
 T02**-TCOL= 2.43039 E-2
 L= 2.80036

 SIG*= 0.881522

 WX= 296999.    WFC= 5847.02    WFRD= 4872.51 WBF=-496.4

 DIFFUSER

 P4= 455206.    M4= 1          B= 4.44585 E-2
 D*= 6.28707 E-5     CP2*4= 4.46979 E-2     MS= 0
 CP4C= 0.745009                CPD= 0.616211
 P04= 857549.   WL= 0.188179

 DIFFUSER THROAT IS CHOKED

 EFFICIENCIES

 DETSBF=-1.67138 E-3       DETSFC= 0.019687        DETSWL= 5.63809 E-2
 DETSRD= 1.64058 E-2       DETSI= 0.125897
 DETSD= 0.120217           DETSF= 3.60928 E-2
 DETSDM= 3.44743 E-2       DETSIW= 5.70013 E-2
 ETT= 0          ETS= 0.753886  ETTI= 0.874103
```

```
CDR2...PROJECT#3305 ..7.16 P4=.528*P04  SI UNITS...10/11/78  KBA

 INPUT VALUES

 P00= 101353.   P1= 79827.5     P2= 392650.    P4= 452751.
 P04= 857487.   P5= 0           P0S= 676589.   PCOL= 676589.
 T00= 288.167   TCOL= 576.333   M= 0.885412    N= 7860.99
 MW/M= 0.2      LC= 0           W4= 0.137709   B4= 3.2258 E-3
 B1B=-56.3      B2B=-30.        ALPHT= 0       B2= 3.2258 E-3
 PR= 6.67558    RSEP= 4.39496 E-2              R1H= 2.16002 E-2
 R1T= 4.39496 E-2
 R2= 0.079756   # BLADES= 19    # DIFF= 17

 INDUCER TIP

 TTREL= 288.104    PTREL= 101275.    MRELIT= 1.20669
 CIT= 195.88    RCT= 0          W1T= 397.153
 P1T= 79827.5   T1T= 268.945    M1T= 0.595154
 B1T=-60.4482   IT= 4.14819     U1T= 345.488
 P10T= 101353.  IKE= 0.268271

 IMPELLER TIP

 CT2J= 424.995  CM2J= 281.468  C2J= 509.75
 C2W= 587.017   CM2W= 78.2632  CT2W= 581.776
 W2W= 90.3706   W2J= 346.431   WT2W= 45.1953
 P02J= 1.00223 E+6             MREL2J= 0.842795
 T2J= 423.562   T02J= 549.971  M2J= 1.24288   U2= 626.961
 P02W= 1.08517 E+6             M2W= 1.30329   E= 0.517969    P02MA=
  1.01882 E+6
 T2W= 506.212   T02W= 670.493
 MR= 1.43177    MRI= 3.27434   TN= 1.3208 E-3                DR= 1.35186
 WSEP= 293.783

 STATES AFTER MIXING

 T2*= 460.119   T02*= 574.324  T02**= 576.358
 P2*= 433563.   P02*= 960566.
 M2*= 1.13345   DP02= 58254.
 CT2*= 456.351  CM2*= 166.848  C2*= 485.895
 T02**-TCOL= 2.43208 E-2
 L= 2.73513

 SIG*= 0.881522

 WX= 293977.    WFC= 5735.72    WFRD= 4779.77 WBF=-2653.4

 DIFFUSER

 P4= 452751.    M4= 1          B= 1.66043 E-2
 D*= 2.34809 E-5     CP2*4= 3.64092 E-2     MS= 0
 CP4C= 0.559271                CPD= 0.461147
 P04= 852984.   WL= 0.204141

 DIFFUSER THROAT IS CHOKED

 EFFICIENCIES

 DETSBF=-9.02589 E-3       DETSFC= 1.95108 E-2     DETSWL= 0.062102
 DETSRD= 0.016259          DETSI= 0.114517
 DETSD= 0.177527           DETSF= 3.57698 E-2
 DETSDM= 3.15413 E-2       DETSIW= 5.62315 E-2
 ETT= 0          ETS= 0.707956  ETTI= 0.889483
```

```
CDR2...PROJECT#3305...8.32 HAVE P1T  SI UNITS...10/10/78  KBA

INPUT VALUES

P00= 101353.   P1= 100408.    P2= 157301.    P4= 157301.
P04= 204188.   P5= 6894.76    P05= 181422.   PCOL= 181422
T00= 288.167   TCOL= 374.167  M= 0.127006   N= 3952.12
MW/M= 0.2      LC= 0          W4= 0.137709   B4= 3.2258 E-3
B1B=-56.3      B2B=-30.       ALPHT= 0       B2= 3.2258 E-3
PR= 1.79       RSEP= 4.39496 E-2             R1H= 2.16002 E-2
R1T= 4.39496 E-2
R2= 0.079756   # BLADES= 19   # DIFF= 17

INDUCER TIP

TTREL= 288.104    PTREL= 101275.    MRELIT= 0.526722
CIT= 43.468    RCT= 0          WIT= 179.051
P1T= 100408.   T1T= 287.224    M1T= 0.127872
B1T=-75.95     IT= 19.65       U1T= 173.694
P10T= 101353.  IKE= 0.185355

IMPELLER TIP

CT2J= 236.629  CM2J= 127.12   C2J= 268.613
C2W= 307.242   CM2W= 14.3752  CT2W= 306.906
W2W= 16.5991   W2J= 149.444   WT2W= 8.29954
P02J= 226814.  MREL2J= 0.412795
T2J= 326.546   T02J= 362.361  M2J= 0.74298   U2= 315 205
P02W= 243646.  M2W= 0.81697   E= 0.705374   P02MA= 230180.
T2W= 353.635   T02W= 400.368
MR= 1.27599    MRI= 3.63275   TN= 1.3208 E-3              DR= 1.25547
WSEP= 142.617

STATES AFTER MIXING

T2*= 337.679   T02*= 369.977  T02**= 374.15
P2*= 161785.   P02*= 223070.
M2*= 0.693827  DP02= 7110.65
CT2*= 250.684  CM2*= 47.0703  C2*= 255.065
T02**-TCOL=-1.64074 E-2
L= 5.32574

SIG*= 0.881522

WX= 86480 5    WFC= 3251.03    WFRD= 2709.19 WBF= 1503.07

DIFFUSER

P4= 157301.    M4= 0.622242   B= 0 449191
DR= 6.35221 E-4     CP2*4=-7.31628 E-2     HS= 2.78403
CP4C= 0.51444                 CPD= 0.32042
P04= 204188.   WL= 0.308093

EFFICIENCIES

DETSBF= 1.73805 E-2       DETSFC= 3.75927 E-2     DETSWL= 0.104623
DETSRD= 3.13272 E-2       DETSI= 0.156538
DETSD= 0.240375           DETSF= 6.89199 E-2
DETSDM= 3.77641 E-2       DETSIW= 3.24732 E-2
ETT= 0.603088  ETS= 0.603088  ETTI= 0.843462

*
```

```
CDR2...PROJECT#3305...8.36 HAVE P1T  SI UNITS...10/10/78  KBA

INPUT VALUES

P00= 101353.   P1= 100421.    P2= 150816.    P4= 150816.
P04= 201706.   P5= 6894.76    P05= 177874.   PCOL= 177874.
T00= 288.167   TCOL= 363.778  M= 0.230425   N= 3966.26
MW/M= 0.2      LC= 0          W4= 0.137709   B4= 3.2258 E-3
B1B=-56.3      B2B=-30.       ALPHT= 0       B2= 3.2258 E-3
PR= 1.755      RSEP= 4.39496 E-2             R1H= 2.16002 E-2
R1T= 4.39496 E-2
R2= 0.079756   # BLADES= 19   # DIFF= 17

INDUCER TIP

TTREL= 288.104    PTREL= 101275.    MRELIT= 0.52832
CIT= 43.2331   RCT= 0          WIT= 179.597
P1T= 100421.   T1T= 287.234    M1T= 0.127179
B1T=-76.0708   IT= 19 7708     U1T= 174.316
P10T= 101353.  IKE= 0 21222

IMPELLER TIP

CT2J= 211.795  CM2J= 141.276  C2J= 254.59
C2W= 297.189   CM2W= 37.2095  CT2W= 294.85
W2W= 42.9658   W2J= 175.747   WT2W=-21.4829
P02J= 210642.  MREL2J= 0.488318
T2J= 322.643   T02J= 354.83   M2J= 0.708154  U2= 316.333
P02W= 229447.  M2W= 0.798841  E= 0.504341   P02MA= 214403.
T2W= 345.866   T02W= 389.641
MR= 1.08192    MRI= 1.95173   TN= 1.3208 E-3              DR= 1.07344
WSEP= 167.31

STATES AFTER MIXING

T2*= 332.092   T02*= 361.804  T02**= 363 757
P2*= 155503.   P02*= 210132.
M2*= 0.670639  DP02= 4270.65
CT2*= 228.406  CM2*= 87.3788  C2*= 244.549
T02**-TCOL=-2.11504 E-2
L= 2.61398

SIG*= 0.881522

WX= 75994 2    WFC= 1772.77    WFRD= 1477.31 WBF= 491.648

DIFFUSER

P4= 150816.    M4= 0.657996   B= 3.27912 E-2
DR= 4.63715 E-5     CP2*4=-8.57996 E-2     HS= 2.77108
CP4C= 0.531703                CPD= 0.409514
P04= 201706.   WL= 0.154239

EFFICIENCIES

DETSBF= 6.46954 E-3       DETSFC= 2.33277 E-2     DETSWL= 5.45235 E-2
DETSRD= 1.94398 E-2       DETSI= 0.120914
DETSD= 0.218075           DETSF= 4.27675 E-2
DETSDM= 2.70421 E-2       DETSIW= 4.46353 E-2
ETT= 0.661011  ETS= 0.661011  ETTI= 0.879086

*
```

```
CDR2...PROJECT#3305...8.40 HEAS P1T  SI UNITS  .10/10/78  KBA

INPUT VALUES

P00= 101353.   P1= 98576.4    P2= 142144.    P4= 142144.
P04= 197390.   P5= 6894.76    P05= 170577.   PCOL= 170577
T00= 288.167   TCOL= 355 444  M= 0.331122   N= 3972.33
MW/M= 0.2      LC= 0          W4= 0.137709   B4= 3 2258 E-3
B1B=-56.3      B2B=-30.       ALPHT= 0       B2= 3.2258 E-3
PR= 1.683      RSEP= 4.39496 E-2             R1H= 2.16002 E-2
R1T= 4.39496 E-2
R2= 0.079756   # BLADES= 19   # DIFF= 17

INDUCER TIP

TTREL= 288.104    PTREL= 101275.    MRELIT= 0.554855
CIT= 70.088    RCT= 0          WIT= 188.126
P1T= 98576.4   T1T= 285.714    M1T= 0.206716
B1T=-68.1265   IT= 11.8265     U1T= 174.582
P10T= 101353.  IKE= 0.261802

IMPELLER TIP

CT2J= 186.675  CM2J= 158.512  C2J= 244.896
C2W= 281.379   CM2W= 83.1419  CT2W= 268.815
W2W= 96.004    W2J= 205.093   WT2W= 48.0019
P02J= 194778.  MREL2J= 0.5746
T2J= 317.232   T02J= 347.027  M2J= 0.686538  U2= 316.817
P02W= 208934.  M2W= 0.763327  E= 0.337751   P02MA= 197609.
T2W= 339.442   T02W= 378.724
MR= 0.965637   MRI= 1.35081   TN= 1.3208 E-3              DR= 0.965068
WSEP= 194.935

STATES AFTER MIXING

T2*= 324.208   T02*= 353.376  T02**= 355.418
P2*= 144478.   P02*= 195475.
M2*= 0.67193   DP02= 2133.72
CT2*= 203.107  CM2*= 131.937  C2*= 242.198
T02**-TCOL=-2 62282 E-2
L= 1.53942

SIG*= 0.881522

WX= 67591.9    WFC= 1186.71    WFRD= 988.928 WBF= 1068.4

DIFFUSER

P4= 142144.    M4= 0.70082    B=-0.360551
DR=-5.0987 E-4     CP2*4=-4.57606 E-2     HS= 2.74349
CP4C= 0.514458                CPD= 0 511771
P04= 197390.   WL=-0.037544

EFFICIENCIES

DETSBF= 1.50066 E-2       DETSFC= 0.017557        DETSWL=-1.44043 E-2
DETSRD= 1 46309 E-2       DETSI= 0.119451
DETSD= 0.197167           DETSF= 3.21879 E-2
DETSDM= 1.60461 E-2       DETSIW= 5.54106 E-2
ETT= 0.683382  ETS= 0.683382  ETTI= 0 886549

*
```

```
CDR2...PROJECT#3305...8.44 HEAS P1T  SI UNITS...10/10/78  KBA

INPUT VALUES

P00= 101353.   P1= 97489.8    P2= 128504.    P4= 128504.
P04= 186145.   P5= 6894.76    P05= 159023.   PCOL= 159023.
T00= 288.167   TCOL= 348.444  M= 0.407326   N= 3963.01
MW/M= 0.2      LC= 0          W4= 0.137709   B4= 3.2258 E-3
B1B=-56 3      B2B=-30.       ALPHT= 0       B2= 3.2258 E-3
PR= 1.569      RSEP= 4.39496 E-2             R1H= 2.16002 E-2
R1T= 4.39496 E-2
R2= 0.079756   # BLADES= 19   # DIFF= 17

INDUCER TIP

TTREL= 288.104    PTREL= 101275.    MRELIT= 0.568671
CIT= 81.9992   RCT= 0          WIT= 192.51
P1T= 97489.8   T1T= 284.809    M1T= 0.242224
B1T=-64.7894   IT= 8.48936    U1T= 174.173
P10T= 101353.  IKE= 0.30608

IMPELLER TIP

CT2J= 162.341  CM2J= 189.879  C2J= 249.817
C2W= 273.732   CM2W= 138.101  CT2W= 236.341
W2W= 159.465   W2J= 244.312   WT2W= 79.7326
P02J= 179821.  MREL2J= 0.694226
T2J= 308.219   T02J= 339.243  M2J= 0.709913  U2= 316.074
P02W= 187096   M2W= 0 753128  E= 0.269106   P02MA= 181276
T2W= 329.702   T02W= 366.922
MR= 0.819144   MRI= 1 04312   TN= 1.3208 E-3              DR= 0.829786
WSEP= 231 999

STATES AFTER MIXING

T2*= 313 849   T02*= 344.786  T02**= 348.328
P2*= 129587.   P02*= 180142.
M2*= 0.702563  DP02= 1134 5
CT2*= 177 419  CM2*= 175.169  C2*= 249 323
T02**-TCOL=-0.116158
L= 1 01265

SIG*= 0.881522

WX= 60539.9    WFC= 897.02    WFRD= 747.517 WBF= 2817 6

DIFFUSER

P4= 128501.    M4= 0.746465   B=-0 709387
DR=-1.00318 E-3     CP2*4=-2.14309 E-2     HS= 2.69736
CP4C= 0.529467                CPD= 0.582253
P04= 186145    WL=-0 118741

EFFICIENCIES

DETSBF= 4.65412 E-2       DETSFC= 0.014817        DETSWL=-5.30024 E-2
DETSRD= 1.23475 E-2       DETSI= 0.149903
DETSD= 0.197108           DETSF= 2 71645 E-2
DETSDM= 1.01123 E-2       DETSIW= 6.60849 E-2
ETT= 0.652989  ETS= 0.652989  ETTI= 0.850097

*
```

```
CDR2...PROJECT#3305...8.46 ZBF  SI UNITS...10/10/78  KBA

INPUT VALUES

P00= 101353.   P1= 94161.7    P2= 333337.    P4= 333337.
P04= 657008.   P5= 482633.    P05= 497542.   PC0L= 497542.
T00= 288.167   TC0L= 526.833  M= 0.646823    N= 7094.97
MW/M= 0.2      LC= 0          W4= 0.137709   B4= 3.2258 E-3
B1B=-56.3      B2B=-30.       ALPHT= 0       B2= 3.2258 E-3
PR= 4.909      RSEP= 4.39496 E-2             R1H= 2.16002 E-2
R1T= 4.39496 E-2
R2= 0.079756   # BLADES= 19   # DIFF= 17

INDUCER TIP

TTREL= 288.104    PTREL= 101275.    MRELIT= 0.982706
CIT= 111.181   RCT= 0          W1T= 331.049
P1T= 94161.7   T1T= 281.992    M1T= 0.330037
B1T=-70.3761   IT= 14.0761     U1T= 311.821
P10T= 101353.  IKE= 0.225998

IMPELLER TIP

CT2J= 391.709  CM2J= 228.454  C2J= 444.851
C2W= 533.127   CM2W= 63.2222  CT2W= 529.365
W2W= 73.0027   W2J= 293.437   WT2W= 36.5013
P02J= 717443.  MREL2J= 0.730153
T2J= 404.375   T02J= 501.226  M2J= 1.10954   U2= 565.866
P02W= 835693.  M2W= 1.22956   E= 0.512096   P02MA= 741093.
T2W= 469.821   T02W= 606.731
MR= 1.34589    MRI= 2.92898   TN= 1.3208 E-3              DR= 1.29985
WSEP= 254.683

STATES AFTER MIXING

T2*= 430.664   T02*= 522.507  T02**= 526.855
P2*= 356012.   P02*= 709869.
M2*= 1.04697   DP02= 31224.5
CT2*= 411.24   CM2*= 138.937  C2*= 434.076
T02**-TC0L= 2.19938 E-2
L= 2.95991

SIG*= 0.8685

WX= 242466.    WFC= 5259.06    WFRD= 4382.55 WBF= 117.663

DIFFUSER

P4= 333337.    M4= 1          B= 6.90163 E-2
D*= 9.7599 E-5      CP2*4=-6.40786 E-2      MS= 0 210373
CP4C= 0.555864                CPD= 0.399963
P04= 628741.   WL= 0.229268

DIFFUSER THROAT IS CHOKED

EFFICIENCIES

DETSBF= 4.85278 E-4       DETSFC= 2.16898 E-2     DETSWL= 7.07371 E-2
DETSRD= 1.80749 E-2       DETSI= 0.113371
DETSD= 0.200576           DETSF=3.97647 E-2
DETSDM= 2.56679 E-2       DETSIW= 4.74526 E-2
ETT= 0.686053  ETS= 0.686053  ETTI= 0.886629

*
```

```
CDR2...PROJECT#3305...8.48 ZBF  SI UNITS...10/10/78  KBA

INPUT VALUES

P00= 101353.   P1= 89900.7    P2= 326756.    P4= 326687.
P04= 662345.   P5= 482633.    P05= 495210.   PC0L= 495210.
T00= 288.167   TC0L= 524.556  M= 0.710779    N= 7099.37
MW/M= 0.2      LC= 0          W4= 0.137709   B4= 3.2258 E-3
B1B=-56.3      B2B=-30.       ALPHT= 0       B2= 3.2258 E-3
PR= 4.886      RSEP= 4.39496 E-2             R1H= 2.16002 E-2
R1T= 4.39496 E-2
R2= 0.079756   # BLADES= 19   # DIFF= 17

INDUCER TIP

TTREL= 288.104    PTREL= 101275.    MRELIT= 1.02261
CIT= 140.66    RCT= 0          W1T= 342.255
P1T= 89900.7   T1T= 278.278    M1T= 0.420274
B1T=-65.7336   IT= 9.43364     U1T= 312.014
P10T= 101353.  IKE= 0.243928

IMPELLER TIP

CT2J= 379.898  CM2J= 237.507  C2J= 448.032
C2W= 528.031   CM2W= 75.5498  CT2W= 522.598
W2W= 87.2373   W2J= 301.868   WT2W= 43.6186
P02J= 712918.  MREL2J= 0.753203
T2J= 402.095   T02J= 500.361  M2J= 1.12038   U2= 566.217
P02W= 811570.  M2W= 1.22237   E= 0.476869   P02MA= 732648.
T2W= 466.373   T02W= 600.804
MR= 1.35769    MRI= 2.73337   TN= 1.3208 E-3              DR= 1.30661
WSEP= 261.942

STATES AFTER MIXING

T2*= 427.605   T02*= 520.612  T02**= 524.577
P2*= 349046.   P02*= 704465.
M2*= 1.05697   DP02= 28163.5
CT2*= 408.438  CM2*= 154.615  C2*= 436.723
T02**-TC0L= 2.18836 E-2
L= 2.64164

SIG*= 0.879

WX= 240108.    WFC= 4741.35    WFRD= 3951.12 WBF= 150.976

DIFFUSER

P4= 326687.    M4= 1          B=-4.15046 E-2
D*=-5.86934 E-5      CP2*4=-6.29079 E-2      MS= 0.193382
CP4C= 0.582031                CPD= 0.411245
P04= 616230.   WL= 0.248255

DIFFUSER THROAT IS CHOKED

EFFICIENCIES

DETSBF= 6.28784 E-4       DETSFC= 1.97467 E-2     DETSWL= 7.84613 E-2
DETSRD= 1.64556 E-2       DETSI= 0.109232
DETSD= 0.200521           DETSF= 3 62023 E-2
DETSDM= 0.023558          DETSIW= 4.88433 E-2
ETT= 0.690247  ETS= 0.690247  ETTI= 0.890768

*
```

```
CDR2...PROJECT#3305...8.50  SI UNITS...10/10/78  KBA

INPUT VALUES

P00= 101353.   P1= 83858.9    P2= 309981.    P4= 309981.
P04= 644405.   P5= 448159.    P05= 481021.   PC0L= 481021.
T00= 288.167   TC0L= 517.     M= 0.800137    N= 7099.78
MW/M= 0.2      LC= 0          W4= 0.137709   B4= 3.2258 E-3
B1B=-56.3      B2B=-30.       ALPHT= 0       B2= 3.2258 E-3
PR= 4.746      RSEP= 4.39496 E-2             R1H= 2.16002 E-2
R1T= 4.39496 E-2
R2= 0.079756   # BLADES= 19   # DIFF= 17

INDUCER TIP

TTREL= 288.104    PTREL= 101275.    MRELIT= 1.07997
CIT= 175.343   RCT= 0          W1T= 357.924
P1T= 83858.9   T1T= 272.788    M1T= 0.529066
B1T=-60.6667   IT= 4.36674     U1T= 312.033
P10T= 101353.  IKE= 0.27575

IMPELLER TIP

CT2J= 366.162  CM2J= 251.431  C2J= 444.176
C2W= 518.284   CM2W= 99.9216  CT2W= 508.561
W2W= 115.379   W2J= 321.329   WT2W= 57.6897
P02J= 675097.  MREL2J= 0.807622
T2J= 396.129   T02J= 492.818  M2J= 1.11875   U2= 566.25
P02W= 755482.  M2W= 1.20778   E= 0.42231    P02MA= 691174.
T2W= 460.337   T02W= 590.067
MR= 1.33722    MRI= 2.49624   TN= 1.3208 E-3              DR= 1.28393
WSEP= 278.772

STATES AFTER MIXING

T2*= 420.364   T02*= 512.418  T02**= 517.022
P2*= 329896.   P02*= 668131.
M2*= 1.05966   DP02= 23042.9
CT2*= 394.64   CM2*= 181.038  C2*= 434.184
T02**-TC0L= 2.18158 E-2
L= 2.17987

SIG*= 0.881522

WX= 232294.    WFC= 4072.48    WFRD= 3393.73 WBF= 1362.07

DIFFUSER

P4= 309981.    M4= 1          B=-0.226312
D*=-3.20038 E-4      CP2*4=-5.88768 E-2      MS= 0.321575
CP4C= 0.622325                CPD= 0.446806
P04= 584821.   WL= 0.246307

DIFFUSER THROAT IS CHOKED

EFFICIENCIES

DETSBF= 5.86358 E-3       DETSFC= 1.75316 E-2     DETSWL= 7.95402 E-2
DETSRD= 1.46097 E-2       DETSI= 0.111721
DETSD= 0.191014           DETSF= 3.21412 E-2
DETSDM= 2.07259 E-2       DETSIW= 5.29904 E-2
ETT= 0.697265  ETS= 0.697265  ETTI= 0.888279

*
```

```
CDR2...PROJECT#3305...8.56 ZBF  SI UNITS...10/10/78  KBA

INPUT VALUES

P00= 101353.   P1= 77466.5    P2= 231154.    P4= 231154.
P04= 527394.   P5= 344738.    P05= 390614.   PC0L= 390614.
T00= 288.167   TC0L= 496.     M= 0.865454    N= 7095.07
MW/M= 0.2      LC= 0          W4= 0.137709   B4= 3.2258 E-3
B1B=-56.3      B2B=-30.       ALPHT= 0       B2= 3.2258 E-3
PR= 3.854      RSEP= 4 39496 E-2             R1H= 2.16002 E-2
R1T= 4.39496 E-2
R2= 0.079756   # BLADES= 19   # DIFF= 17

INDUCER TIP

TTREL= 288.104    PTREL= 101275.    MRELIT= 1.14314
CIT= 207.581   RCT= 0          W1T= 374.6
P1T= 77466.5   T1T= 266.595    M1T= 0.633458
B1T=-56.3485   IT= 4.85268 E-2              U1T= 311.826
P10T= 101353.  IKE= 0.333103

IMPELLER TIP

CT2J= 330.893  CM2J= 334.212  C2J= 470.306
C2W= 504.232   CM2W= 142.233  CT2W= 483.756
W2W= 164.237   W2J= 408.551   WT2W= 82.1182
P02J= 584941.  MREL2J= 1.06949
T2J= 364.428   T02J= 473.247  M2J= 1.23484   U2= 565.875
P02W= 550257.  M2W= 1.18939   E= 0.420063   P02MA= 578005.
T2W= 449.367   T02W= 572.499
MR= 1.06886    MRI= 2.37961   TN= 1.3208 E-3              DR= 1.05731
WSEP= 354.296

STATES AFTER MIXING

T2*= 402.43    T02*= 493.25   T02**= 496.023
P2*= 264305.   P02*= 544659.
M2*= 1.0735    DP02= 33345.5
CT2*= 361.458  CM2*= 233.984  C2*= 430.582
T02**-TC0L= 2.25406 E-2
L= 1.5448

SIG*= 0.8775

WX= 210633.    WFC= 3239.46    WFRD= 2699.55 WBF= 153.924

DIFFUSER

P4= 231154.    M4= 1          B=-0.740746
D*=-1.04752 E-3      CP2*4=-0.118249      MS= 0.428517
CP4C= 0.777246                CPD= 0.450534
P04= 436315.   WL= 0.386455

DIFFUSER THROAT IS CHOKED

EFFICIENCIES

DETSBF= 7.3077 E-4        DETSFC= 1.53796 E-2     DETSWL= 0.13629
DETSRD= 1.28163 E-2       DETSI= 0.153638
DETSD= 0.201162           DETSF= 0.028196
DETSDM= 3.79758 E-2       DETSIW= 8.67352 E-2
ETT= 0.645201  ETS= 0.645201  ETTI= 0.846362
```

ORIGINAL PAGE IS OF POOR QUALITY

```
CDR2...PROJECT#3305...8.58 ZBF  SI UNITS...10/10/78  KBA

INPUT VALUES

P00= 101353.   P1= 96781.7    P2= 260760.    P4= 260760.
P04= 473504.   P5= 336478.    P05= 370952.   PCOL= 370952.
T00= 288.167   TCOL= 474.389  M= 0.50757     N= 6287.68
MW/M= 0.2      LC= 0          W4= 0.137709   B4= 3.2258 E-3
B1B=-56.3      B2B=-30.       ALPHT= 0       B2= 3.2258 E-3
PR= 3.66       RSEP= 4.39496 E-2             R1H= 2.16002 E-2
R1T= 4.39496 E-2
R2= 0.079756   # BLADES= 19   # DIFF= 17

INDUCER TIP

TTREL= 288.104    PTREL= 101275.    MRELIT= 0.858433
CIT= 88.9491   RCT= 0          W1T= 299.304
P1T= 96781.7   T1T= 284.216    M1T= 0.263024
B1T=-72.1577   IT= 15.8577     U1T= 276.341
P10T= 101353.  IKE= 0.223628

IMPELLER TIP

CT2J= 333.745  CM2J= 210.655  C2J= 394.646
C2W= 471.134   CM2W= 58.9826  CT2W= 467.427
W2W= 68.1072   W2J= 269.278   WT2W= 34.0536
P02J= 503132.  MREL2J= 0.693204
T2J= 377.142   T02J= 453.922  M2J= 1.01852   U2= 501.48
P02W= 479578.  M2W= 1.13523   E= 0.504965   P02MA= 518421.
T2W= 430.866   T02W= 538.892
MR= 1.23836    MRI= 2.5723    TN= 1.3208 E-3              DR= 1.21193
WSEP= 239.538

STATES AFTER MIXING

T2#= 398.853   T02#= 476.942  T02##= 474.404
P2#= 276521.   P02#= 498839.
M2#= 0.960308  DP02= 19582.6
CT2#= 360.481  CM2#= 129.998  C2#= 383.205
T02##-TCOL= 1.48137 E-2
L= 2.77297

SIG#= 0.8685

WX= 188430.    WFC= 4107.72    WFRD= 3423.1 WBF= 124.438

DIFFUSER

P4= 260760.    M4= 0.966446   B= 7.92793 E-2
D#= 1.12112 E-4     CP2#4=-7.08955 E-2     HS= 0.377694
CP4C= 0.517954                CPD= 0.424756
P04= 473504.   WL= 0.113956

EFFICIENCIES

DETSBF= 6.60395 E-4     DETSFC= 2.17997 E-2     DETSWL= 3.57664 E-2
DETSRD= 1.81664 E-2     DETSI= 0.115407
DETSD= 0.196447         DETSF= 3.99661 E-2
DETSDH= 2.67611 E-2     DETSIW= 4.80191 E-2
ETT= 0.688146  ETS= 0.688146  ETTI= 0.884593

*
```

```
CDR2...PROJECT#3305...8.64 ZBF  SI UNITS...10/10/78  KBA

INPUT VALUES

P00= 101353.   P1= 89790.4    P2= 238000.    P4= 238000.
P04= 455675.   P5= 316814.    P05= 351288.   PCOL= 351288.
T00= 288.167   TCOL= 461.444  M= 0.673131    N= 6285.27
MW/M= 0.2      LC= 0          W4= 0.137709   B4= 3.2258 E-3
B1B=-56.3      B2B=-30.       ALPHT= 0       B2= 3.2258 E-3
PR= 3.46599    RSEP= 4.39496 E-2             R1H= 2.16002 E-2
R1T= 4.39496 E-2
R2= 0.079756   # BLADES= 19   # DIFF= 17

INDUCER TIP

TTREL= 288.104    PTREL= 101275.    MRELIT= 0.927301
CIT= 141.353   RCT= 0          W1T= 310.301
P1T= 89790.4   T1T= 278.18     M1T= 0.422418
B1T=-62.9007   IT= 6.60072     U1T= 276.235
P10T= 101353.  IKE= 0.274836

IMPELLER TIP

CT2J= 314.085  CM2J= 238.345  C2J= 394.282
C2W= 451.192   CM2W= 110 621  CT2W= 437.421
W2W= 127.735   W2J= 303.073   WT2W= 63.8673
P02J= 465681.  MREL2J= 0.790162
T2J= 367 469   T02J= 444.104  M2J= 1.03001   U2= 501.288
P02W= 507881.  M2W= 1.10235   E= 0.380581   P02MA= 474121
T2W= 419.161   T02W= 518.523
MR= 1.17356    MRI= 1.96321   TN= 1.3208 E-3              DR= 1.15145
WSEP= 269.487

STATES AFTER MIXING

T2#= 385.841   T02#= 459.067  T02##= 461.458
P2#= 249666.   P02#= 462152.
M2#= 0.982574  DP02= 11969.7
CT2#= 338.749  CM2#= 184.717  C2#= 385.839
T02##-TCOL= 0.01361
L= 1.83389

SIG#= 0.8885

WX= 175171.    WFC= 2914.43    WFRD= 2428.69 WBF= 16.7948

DIFFUSER

P4= 238000.    M4= 1          B=-0.266535
D#=-3.76919 E-4     CP2#4=-5.49022 E-2     HS= 0.388661
CP4C= 0.5354                  CPD= 0.478253
P04= 449595.   WL= 5.90953 E-2

DIFFUSER THROAT IS CHOKED

EFFICIENCIES

DETSBF= 9.58766 E-5     DETSFC= 1.66376 E-2     DETSWL= 1.99701 E-2
DETSRD= 1.38647 E-2     DETSI= 0.104648
DETSD= 0.192087         DETSF= 3.05022 E-2
DETSDH= 1.86764 E-2     DETSIW= 0.055374
ETT= 0.703265  ETS= 0.703265  ETTI= 0.895352

*
```

```
CDR2...PROJECT#3305...8.68 ZBF  SI UNITS...10/10/78  KBA

INPUT VALUES

P00= 101353.   P1= 86129.3    P2= 212372.    P4= 212372.
P04= 425806.   P5= 293406.    P05= 327880.   PCOL= 327880.
T00= 288.167   TCOL= 451.389  M= 0.738902    N= 6278.68
MW/M= 0.2      LC= 0          W4= 0.137709   B4= 3.2258 E-3
B1B=-56.3      B2B=-30.       ALPHT= 0       B2= 3.2258 E-3
PR= 3.23503    RSEP= 4.39496 E-2             R1H= 2.16002 E-2
R1T= 4.39496 E-2
R2= 0.079756   # BLADES= 19   # DIFF= 17

INDUCER TIP

TTREL= 288.104    PTREL= 101275.    MRELIT= 0.963365
CIT= 162.984   RCT= 0          W1T= 320.484
P1T= 86129.3   T1T= 274.884    M1T= 0.489926
B1T=-59.4323   IT= 3.13229     U1T= 275.945
P10T= 101353   IKE= 0.311446

IMPELLER TIP

CT2J= 295.957  CM2J= 270.266  C2J= 400.792
C2W= 441.474   CM2W= 145.278  CT2W= 416.806
W2W= 167.753   W2J= 339.1     WT2W= 83.8765
P02J= 432764.  MREL2J= 0.898219
T2J= 355.737   T02J= 435.034  M2J= 1.0636    U2= 500.762
P02W= 446080.  M2W= 1.08932   E= 0 349459   P02MA= 435427.
T2W= 410.907   T02W= 506.205
MR= 1.07253    MRI= 1.7841    TN= 1.3208 E-3              DR= 1.06306
WSEP= 301.472

STATES AFTER MIXING

T2#= 375.09    T02#= 449.339  T02##= 451.404
P2#= 224076.   P02#= 424487.
M2#= 1 00228   DP02= 10940.7
CT2#= 320.131  CM2#= 219.627  C2#= 388.226
T02##-TCOL= 0.015564
L= 1.45761

SIG#= 0.8925

WX= 164892.    WFC= 2473.51    WFRD= 2061.26 WBF= 47.5476

DIFFUSER

P4= 212372.    M4= 1          B=-0.340367
D#=-7.64156 E-4     CP2#4=-5.83962 E-2     HS= 0.40315
CP4C= 0.61147                 CPD= 0.517958
P04= 401274.   WL= 0.115825

DIFFUSER THROAT IS CHOKED

EFFICIENCIES

DETSBF= 2.88356 E-4     DETSFC= 1.50008 E-2     DETSWL= 4.21138 E-2
DETSRD= 1.25006 E-2     DETSI= 0.113778
DETSD= 0.187971         DETSF= 2.75014 E-2
DETSDH= 1.92779 E-2     DETSIW= 6.67107 E-2
ETT= 0.69825   ETS= 0.69825   ETTI= 0.886222

*
```

```
CDR2...PROJECT#3305...8.72 ZBF  SI UNITS...10/10/78  KBA

INPUT VALUES

P00= 101353.   P1= 83860.9    P2= 149892.    P4= 149892.
P04= 357493.   P5= 235022.    P05= 269495.   PCOL= 269495.
T00= 288.167   TCOL= 432.     M= 0.777457    N= 6274.07
MW/M= 0.2      LC= 0          W4= 0.137709   B4= 3.2258 E-3
B1B=-56.3      B2B=-30.       ALPHT= 0       B2= 3.2258 E-3
PR= 2.65898    RSEP= 4.39496 E-2             R1H= 2.16002 E-2
R1T= 4.39496 E-2
R2= 0.079756   # BLADES= 19   # DIFF= 17

INDUCER TIP

TTREL= 288.104    PTREL= 101275.    MRELIT= 0.98595
CIT= 175.332   RCT= 0          W1T= 326.765
P1T= 83860.9   T1T= 272.79     M1T= 0.529031
B1T=-57.5496   IT= 1.24964     U1T= 275.743
P10T= 101353.  IKE= 0.367889

IMPELLER TIP

CT2J= 259.934  CM2J= 352 889  C2J= 438.288
C2W= 433.367   CM2W= 219.531  CT2W= 373.648
W2W= 253.493   W2J= 427.027   WT2W= 126.746
P02J= 373001.  MREL2J= 1.18753
T2J= 322.078   T02J= 417.203  M2J= 1.22078   U2= 500.395
P02W= 317857.  M2W= 1.09652   E= 0.327538   P02MA= 361972.
T2W= 370.36    T02W= 482.529
MR= 0.830256   MRI= 1.68401   TN= 1.3208 E-3              DR= 0.860841
WSEP= 379.589

STATES AFTER MIXING

T2#= 350.542   T02#= 430.324  T02##= 431.997
P2#= 169468.   P02#= 349045.
M2#= 1.07178   DP02= 12927.1
CT2#= 282.693  CM2#= 285.554  C2#= 401.817
T02##-TCOL=-3.42475 E-3
L= 0.989983

SIG#= 0.895

WX= 145120.    WFC= 1958.8    WFRD= 1632.33 WBF= 69.874

DIFFUSER

P4= 149892.    M4= 1          B=-1.24467
D#=-1.76014 E-3     CP2#4=-0.109008     HS= 0.448004
CP4C= 0.896236                CPD= 0.557018
P04= 283343.   WL= 0.365872

DIFFUSER THROAT IS CHOKED

EFFICIENCIES

DETSBF= 4.81493 E-4     DETSFC= 1.34978 E-2     DETSWL= 0.164299
DETSRD= 1.12482 E-2     DETSI= 0.156303
DETSD= 0.202339         DETSF= 0.024746
DETSDH= 2.96624 E-2     DETSIW= 0.101413
ETT= 0.641358  ETS= 0.641358  ETTI= 0.843697

*
```

```
CDR2...PROJECT#3305...8.86 P1T/105  SI UNITS...10/10/78  KBA

INPUT VALUES

P00= 101353.   P1= 85784.6    P2= 423766.    P4= 423766.
P04= 901028.   P5= 620528.    P05= 658691.   PCOL= 658691.
T00= 288.167   TCOL= 591.611  M= 0.772468    N= 7868.32
MW/M= 0.2      LC= 0          W4= 0.137709   B4= 3.2258 E-3
B1B=-56.3      B2B=-30.       ALPHT= 0       B2= 3.2258 E-3
PR= 6.49898    RSEP= 4.39496 E-2             RIH= 2.16002 E-2
R1T= 4.39496 E-2
R2= 0.079756   # BLADES= 19   # DIFF= 17

INDUCER TIP

TTREL= 288.104    PTREL= 101275.    MRELIT= 1.15229
CIT= 164.905   RCT= 0          W1T= 383.116
P1T= 85784.6   T1T= 274.568    M1T= 0.495981
B1T=-64.5051   IT= 8.20512     U1T= 345.81
P10T= 101353.  IKE= 0.236754

IMPELLER TIP

CT2J= 442.932  CM2J= 260.564  C2J= 513.889
C2W= 596.711   CM2W= 58.363   CT2W= 593.85
W2W= 67.3918   W2J= 319.336   WT2W= 33.6958
P02J= 1.07668 E+6             MREL2J= 0.768787
T2J= 432.785   T02J= 561.019  M2J= 1.23962   U2= 627.546
P02W= 1.18934 E+6             M2W= 1.31479   E= 0.569908    P02MA=
 1.09921 E+6
T2W= 513.807   T02W= 683.194
MR= 1.49884    MRI= 3.66892   TN= 1.3208 E-3                 DR= 1.41476
WSEP= 270.799

STATES AFTER MIXING

T2*= 468.354   T02*= 585.712  T02**= 591.635
P2*= 463155.   P02*= 1.03431 E+6
M2*= 1.13996   DP02= 64903.7
CT2*= 473.115  CM2*= 138.703  C2*= 493.026
T02**-TCOL= 2.41682 E-2
L= 3.411

SIG*= 0.881522

WX= 309981.    WFC= 6867.37    WFRD= 5722.81 WBF= 488.766

DIFFUSER

P4= 423766.    M4= 1          B= 7.06944 E-2
D*= 9.7972 E-5      CP2*4=-6.89647 E-2      M5= 0.29584
CP4C= 0.627606                CPD= 0.342354
P04= 798085.   WL= 0.413586

DIFFUSER THROAT IS CHOKED

EFFICIENCIES

DETSBF= 1.57676 E-3       DETSFC= 2.21542 E-2     DETSWL= 0.128703
DETSRD= 1.84618 E-2       DETSI= 0.122579
DETSD= 0.218236           DETSF= 0.040616
DETSDM= 3.15613 E-2       DETSIW= 4.88254 E-2
ETT= 0.659184  ETS= 0.659184  ETTI= 0.877421

*
```

```
CDR2...PROJECT#3305...8.90  SI UNITS...10/10/78  KBA

INPUT VALUES

P00= 101353.   P1= 82109.7    P2= 418002.    P4= 418002.
P04= 897601.   P5= 620528.    P05= 656464.   PCOL= 656464.
T00= 288.167   TCOL= 586.833  M= 0.829167    N= 7873.45
MW/M= 0.2      LC= 0          W4= 0.137709   B4= 3.2258 E-3
B1B=-56.3      B2B=-30.       ALPHT= 0       B2= 3.2258 E-3
PR= 6.47701    RSEP= 4.39496 E-2             R1H= 2.16002 E-2
R1T= 4.39496 E-2
R2= 0.079756   # BLADES= 19   # DIFF= 17

INDUCER TIP

TTREL= 288.104    PTREL= 101275.    MRELIT= 1.18668
CIT= 184.448   RCT= 0          W1T= 392.124
P1T= 82109.7   T1T= 271.146    M1T= 0.558194
B1T=-61.941    IT= 5.64101     U1T= 346.035
P10T= 101353.  IKE= 0.252093

IMPELLER TIP

CT2J= 436.191  CM2J= 262.901  C2J= 509.293
C2W= 593.113   CM2W= 66.906   CT2W= 589.327
W2W= 77.2563   W2J= 325.408   WT2W= 38.6281
P02J= 1.04983 E+6             MREL2J= 0.784878
T2J= 431.115   T02J= 557.131  M2J= 1.2308    U2= 627.955
P02W= 1.16667 E+6             M2W= 1.31065   E= 0.537925    P02MA=
 1.0732 E+6
T2W= 510.898   T02W= 678.386
MR= 1.51193    MRI= 3.49123   TN= 1.3208 E-3                 DR= 1.42128
WSEP= 275.894

STATES AFTER MIXING

T2*= 465.447   T02*= 581.635  T02**= 586.858
P2*= 456136.   P02*= 1.01545 E+6
M2*= 1.13741   DP02= 57743.3
CT2*= 466.818  CM2*= 150.236  C2*= 490.397
T02**-TCOL= 0.024253
L= 3.10723

SIG*= 0.881522

WX= 304971.    WFC= 6357.99    WFRD= 5298.32 WBF= 173.311

DIFFUSER

P4= 418002.    M4= 1          B=-6.97657 E-3
D*=-9.86588 E-6      CP2*4=-6.81814 E-2      M5= 0.287217
CP4C= 0.645693                CPD= 0.358165
P04= 787319.   WL= 0.407879

DIFFUSER THROAT IS CHOKED

EFFICIENCIES

DETSBF= 5.68289 E-4       DETSFC= 2.08479 E-2     DETSWL= 0.127825
DETSRD= 1.73732 E-2       DETSI= 0.117756
DETSD= 0.213792           DETSF= 3.82211 E-2
DETSDM= 2.89839 E-2       DETSIW= 4.99825 E-2
ETT= 0.660452  ETS= 0.660452  ETTI= 0.882244
```

```
CDR2...PROJECT#3305.. 8.94 ZBF  SI UNITS...10/10/78  KBA

INPUT VALUES

P00= 101353.   P1= 78538.2    P2= 400985.    P4= 400985.
P04= 881757.   P5= 586054.    P05= 640551.   PCOL= 640551.
T00= 288.167   TCOL= 580.833  M= 0.886773    N= 7886.12
MW/M= 0.2      LC= 0          W4= 0.137709   B4= 3.2258 E-3
B1B=-56.3      B2B=-30.       ALPHT= 0       B2= 3.2258 E-3
PR= 6.32       RSEP= 4.39496 E-2             RIH= 2.16002 E-2
R1T= 4.39496 E-2
R2= 0.079756   # BLADES= 19   # DIFF= 17

INDUCER TIP

TTREL= 288.104    PTREL= 101275.    MRELIT= 1.2219
CIT= 202.149   RCT= 0          W1T= 401.236
P1T= 78538.2   T1T= 267.712    M1T= 0.615613
B1T=-59.7473   IT= 3.44726     U1T= 346.592
P10T= 101353.  IKE= 0.269499

IMPELLER TIP

CT2J= 425.93   CM2J= 276.003  C2J= 507.537
C2W= 589.354   CM2W= 77.4665  CT2W= 584.24
W2W= 89.4506   W2J= 342.639   WT2W= 44.7253
P02J= 1.01125 E+6             MREL2J= 0.831166
T2J= 426.084   T02J= 551.355  M2J= 1.23382   U2= 628.966
P02W= 1.11239 E+6             M2W= 1.30611   E= 0.515033    P02MA=
 1.03148 E+6
T2W= 508.015   T02W= 673.523
MR= 1.4701     MRI= 3.33962   TN= 1.3208 E-3                 DR= 1.38185
WSEP= 290.361

STATES AFTER MIXING

T2*= 461.621   T02*= 576.044  T02**= 580.859
P2*= 440494.   P02*= 975183.
M2*= 1.13289   DP02= 56299.6
CT2*= 457.592  CM2*= 165.012  C2*= 486.435
T02**-TCOL= 2.43378 E-2
L= 2.77308

SIG*= 0.879

WX= 298685.    WFC= 5839.42    WFRD= 4866.18 WBF= 170.906

DIFFUSER

P4= 400985.    M4= 1          B=-0.1166
D*=-1.64889 E-4      CP2*4=-0.073892      M5= 0.361635
CP4C= 0.675992                CPD= 0.374155
P04= 755376.   WL= 0.411093

DIFFUSER THROAT IS CHOKED

EFFICIENCIES

DETSBF= 5.69181 E-4       DETSFC= 1.95504 E-2     DETSWL= 0.129536
DETSRD= 0.016292          DETSI= 0.120561
DETSD= 0.208436           DETSF= 3.58424 E-2
DETSDM= 2.97054 E-2       DETSIW= 5.44441 E-2
ETT= 0.671003  ETS= 0.671003  ETTI= 0.879439

*
```

```
CDR2...PROJECT#3305...8.96 ZBF  SI UNITS...10/10/78  KBA

INPUT VALUES

P00= 101353.   P1= 75035.6    P2= 377067.    P4= 377067.
P04= 840940.   P5= 551581.    P05= 612475.   PCOL= 612475.
T00= 288.167   TCOL= 576.389  M= 0.909453    N= 7878.9
MW/M= 0.2      LC= 0          W4= 0.137709   B4= 3.2258 E-3
B1B=-56.3      B2B=-30.       ALPHT= 0       B2= 3.2258 E-3
PR= 6.04299    RSEP= 4.39496 E-2             R1H= 2.16002 E-2
R1T= 4.39496 E-2
R2= 0.079756   # BLADES= 19   # DIFF= 17

INDUCER TIP

TTREL= 288.104    PTREL= 101275.    MRELIT= 1.25515
CIT= 218.611   RCT= 0          W1T= 409.508
P1T= 75035.6   T1T= 264.233    M1T= 0.670047
B1T=-57.7349   IT= 1 4349      U1T= 346.275
P10T= 101353.  IKE= 0.285165

IMPELLER TIP

CT2J= 419.562  CM2J= 296.653  C2J= 513.844
C2W= 586.015   CM2W= 83.8338  CT2W= 579.988
W2W= 96.8029   W2J= 362.783   WT2W= 48.4014
P02J= 984980.  MREL2J= 0.887504
T2J= 418.739   T02J= 547.272  M2J= 1.26019   U2= 628.389
P02W= 1.04048 E+6             M2W= 1.30212   E= 0.516381    P02MA= 996081.
T2W= 505.406   T02W= 669.164
MR= 1.41425    MRI= 3.32064   TN= 1 3208 E-3                 DR= 1.33192
WSEP= 307.457

STATES AFTER MIXING

T2*= 458.282   T02*= 571.904  T02**= 576.413
P2*= 421643.   P02*= 933176.
M2*= 1.13257   DP02= 62904.8
CT2*= 451.647  CM2*= 175.52   C2*= 484.553
T02**-TCOL= 2.43462 E-2
L= 2.5732

SIG*= 0.88

WX= 294035.    WFC= 5510.5    WFRD= 4592.08 WBF= 121.808

DIFFUSER

P4= 377067.    M4= 1          B=-0.212901
D*=-3.01073 E-4      CP2*4=-8.71403 E-2      M5= 0.392801
CP4C= 0.706237                CPD= 0 37306
P04= 710394.   WL= 0.435517

DIFFUSER THROAT IS CHOKED

EFFICIENCIES

DETSBF= 4.14264 E-4       DETSFC= 0.018741        DETSWL= 0.138508
DETSRD= 1.56173 E-2       DETSI= 0.130001
DETSD= 0.209542           DETSF= 3.43584 E-2
DETSDM= 0.034694          DETSIW= 0.060534
ETT= 0.660457  ETS= 0.660457  ETTI= 0.869999

*
```

```
CDR2...PROJECT#3305...9.02 BL2 DIF HAVE PIT  SI UNITS...10/11/78  KBA

INPUT VALUES

P00= 101353.   P1= 100734.    P2= 152308.    P4= 176430
P04= 201768.   P5= 0          P05= 191557.   PCOL= 191557.
T00= 288.167   TCOL= 363.378  H= 0.177808    N= 3935.16
MW/M= 0.2      LC= 0          W4= 0.149352   B4= 3.2258 E-3
B1B=-56.3      B2B=-30.       ALPHT= 0       B2= 3.2258 E-3
PR= 1.89       RSEP= 4.39496 E-2             R1H= 2.16002 E-2
R1T= 4.39496 E-2
R2= 0.079756   # BLADES= 19   # DIFF= 17

INDUCER TIP

TTREL= 288.104    PTREL= 101275.    MRELIT= 0.519933
CIT= 36.8151   RCT= 0          W1T= 176.824
P1T= 100734.   T1T= 287.49     M1T= 0.108251
B1T=-77.983    IT= 21.683      U1T= 172.949
P10T= 101353.  IKE= 0.207092

IMPELLER TIP

CT2J= 222.435  CM2J= 138.354  C2J= 261.953
C2W= 301.147   CM2W= 23.5721  CT2W= 300.243
W2W= 27.2188   W2J= 165.828   WT2W= 13.6094
P02J= 216545.  MREL2J= 0.460122
T2J= 323.552   T02J= 357.623  M2J= 0.727749  U2= 313.852
P02W= 233600.  M2W= 0.807028  E= 0.612181   P02MA= 219956.
T2W= 348.067   T02W= 393.006
MR= 1.12999    MRI= 2.51866   TN= 1.3208 E-3  0          DR= 1.1185
WSEP= 158.089

STATES AFTER MIXING

T2#= 334.351   T02#= 364.712  T02##= 363.256
P2#= 157603.   P02#= 213913.
M2#= 0.6758    DP02= 4043.19
CT2#= 237.997  CM2#= 66.9803  C2#= 247.242
T02##-TCOL=-2.13835 E-2
L= 3.55323

SIG#= 0.881522

WX= 75489.9    WFC= 2261.45    WFRD= 1884.54 WBF=-3352.02

DIFFUSER

P4= 176430.    M4= 0.441624   B= 0.104018
D#= 1.48523 E-4     CP2#4= 0.334346     MS= 0
CP4C= 0.597007              CPD= 0.602986
P04= 201768.   WL= 0.215676

EFFICIENCIES

DETSBF=-4.44036 E-2       DETSFC= 2.99569 E-2     DETSWL= 7.85978 E-2
DETSRD= 2.49641 E-2       DETSI= 0.090921
DETSD= 0.147333           DETSF= 5.49211 E-2
DETSDM= 3.79302 E-2       DETSIW= 4.24734 E-2
ETT= 0         ETS= 0.761746  ETTI= 0.909079

*
```

```
CDR2.. PROJECT#3305...9.04 BL2 DIF HAVE PIT  SI UNITS...10/11/78  KBA

INPUT VALUES

P00= 101353.   P1= 100654.    P2= 151485.    P4= 173365.
P04= 201361.   P5= 0          P05= 189125.   PCOL= 189125.
T00= 288.167   TCOL= 363.444  H= 0.189602    N= 3924.89
MW/M= 0.2      LC= 0          W4= 0.149352   B4= 3.2258 E-3
B1B=-56.3      B2B=-30.       ALPHT= 0       B2= 3.2258 E-3
PR= 1.866      RSEP= 4.39496 E-2             R1H= 2.16002 E-2
R1T= 4.39496 E-2
R2= 0.079756   # BLADES= 19   # DIFF= 17

INDUCER TIP

TTREL= 288.104    PTREL= 101275.    MRELIT= 0.519794
CIT= 38.5661   RCT= 0          W1T= 176.756
P1T= 100654.   T1T= 287.424    M1T= 0.113413
B1T=-77.3974   IT= 21.0974     U1T= 172.498
P10T= 101353.  IKE= 0.206474

IMPELLER TIP

CT2J= 218.766  CM2J= 138.22   C2J= 258.772
C2W= 298.968   CM2W= 26 3834  CT2W= 297.801
W2W= 30 4649   W2J= 167.306   WT2W= 15.2324
P02J= 213741.  MREL2J= 0.464575
T2J= 323.051   T02J= 356.302  M2J= 0.719417  U2= 313.034
P02W= 231284.  M2W= 0.80244   E= 0.584451   P02MA= 217249.
T2W= 346.911   T02W= 391.204
MR= 1.11886    MRI= 2.3447    TN= 1.3208 E-3              DR= 1.10806
WSEP= 159.519

STATES AFTER MIXING

T2#= 333.411   T02#= 363.294  T02##= 363.423
P2#= 156638.   P02#= 211789.
M2#= 0.671341  DP02= 5459.87
CT2#= 234.573  CM2#= 71.6608  C2#= 245.275
T02##-TCOL=-2.13072 E-2
L= 3.27338

SIG#= 0.881522

WX= 75658.     WFC= 2098.89    WFRD= 1749.07 WBF=-1619.32

DIFFUSER

P4= 173365.    M4= 0.467103   B= 8.25627 E-2
D#= 1.17888 E-4     CP2#4= 0.303282     MS= 0
CP4C= 0.562922              CPD= 0.589042
P04= 201361.   WL= 0.189081

EFFICIENCIES

DETSBF=-2.14031 E-2       DETSFC= 2.77418 E-2     DETSWL= 6.76285 E-2
DETSRD= 2.31182 E-2       DETSI= 0.10642
DETSD= 0.150246           DETSF= 5.08599 E-2
DETSDM= 3.44663 E-2       DETSIW= 4.24968 E-2
ETT= 0         ETS= 0.743334  ETTI= 0.89358

*
```

```
CDR2...PROJECT#3305...9.08 BL2 DIF HAVE PIT  SI UNITS...10/11/78  KBA

INPUT VALUES

P00= 101353.   P1= 100228.    P2= 149761.    P4= 150940.
P04= 199196.   P5= 0          P05= 175645.   PCOL= 175645.
T00= 288.167   TCOL= 360.222  H= 0.240404    N= 3942.49
MW/M= 0.2      LC= 0          W4= 0.149352   B4= 3.2258 E-3
B1B=-56.3      B2B=-30.       ALPHT= 0       B2= 3.2258 E-3
PR= 1.733      RSEP= 4.39496 E-2             R1H= 2.16002 E-2
R1T= 4.39496 E-2
R2= 0.079756   # BLADES= 19   # DIFF= 17

INDUCER TIP

TTREL= 288.104    PTREL= 101275.    MRELIT= 0.528082
CIT= 46.7528   RCT= 0          W1T= 179.467
P1T= 100228.   T1T= 287.076    M1T= 0.13757
B1T=-74.8998   IT= 18.5998     U1T= 173.271
P10T= 101353.  IKE= 0.22241

IMPELLER TIP

CT2J= 207.292  CM2J= 144.036  C2J= 252.421
C2W= 293.843   CM2W= 40.5353  CT2W= 291.034
W2W= 46.8061   W2J= 179.517   WT2W= 23.4031
P02J= 206897.  MREL2J= 0.499752
T2J= 321.382   T02J= 353.025  M2J= 0.703431  U2= 314.437
P02W= 224661.  M2W= 0.791355  E= 0.497786   P02MA= 210450.
T2W= 344.526   T02W= 387.33
MR= 1.05669    MRI= 1.85081   TN= 1.3208 E-3              DR= 1.04979
WSEP= 170.956

STATES AFTER MIXING

T2#= 330.746   T02#= 359.897  T02##= 360 199
P2#= 153386.   P02#= 206371.
M2#= 0.665539  DP02= 4078.22
CT2#= 224.04   CM2#= 72.0463  C2#= 242.212
T02##-TCOL=-2.28288 E-2
L= 2.43399

SIG#= 0.881522

WX= 72408.3    WFC= 1657.01    WFRD= 1380.84 WBF=-1076.18

DIFFUSER

P4= 150940.    M4= 0.642021   B= 5.01574 E-2
D#= 7.16178 E-5     CP2#4=-4.61693 E-2     MS= 0
CP4C= 0.511945              CPD= 0.420087
P04= 199196.   WL= 0.135415

EFFICIENCIES

DETSBF=-1.48626 E-2       DETSFC= 2.28843 E-2     DETSWL= 4.92622 E-2
DETSRD= 1.90702 E-2       DETSI= 0.102713
DETSD= 0.220421           DETSF= 4.19545 E-2
DETSDM= 2.74589 E-2       DETSIW= 4.81622 E-2
ETT= 0         ETS= 0.676866  ETTI= 0.897287

*
```

```
CDR2 ..PROJECT#3305. .9.10 BL2 DIF HAVE PIT  SI UNITS...10/11/78  KBA

INPUT VALUES

P00= 101353    P1= 99985.     P2= 146670.    P4= 122967.
P04= 195935.   P5= 0          P05= 150408.   PCOL= 150408.
T00= 288.167   TCOL= 358.389  H= 0.264444    N= 3942.7
MW/M= 0 2      LC= 0          W4= 0.149352   B4= 3.2258 E-3
B1B=-56.3      B2B=-30.       ALPHT= 0       B2= 3.2258 E-3
PR= 1.484      RSEP= 4.39496 E-2             R1H= 2.16002 E-2
R1T= 4.39496 E-2
R2= 0.079756   # BLADES= 19   # DIFF= 17

INDUCER TIP

TTREL= 288.104    PTREL= 101275.    MRELIT= 0.531548
CIT= 50.8387   RCT= 0          W1T= 180.584
P1T= 99985.    T1T= 286.877    M1T= 0.149644
B1T=-73.6489   IT= 17.3489     U1T= 173.28
P10T= 101353.  IKE= 0.231085

IMPELLER TIP

CT2J= 201.091  CM2J= 148.291  C2J= 249.856
C2W= 290.271   CM2W= 49.1422  CT2W= 286.081
W2W= 56.7446   W2J= 186.658   WT2W= 28.3723
P02J= 202937.  MREL2J= 0.520661
T2J= 320.085   T02J= 351.092  M2J= 0.697602  U2= 314.454
P02W= 219751.  M2W= 0.783217  E= 0.44717    P02MA= 206300.
T2W= 343.2     T02W= 384.979
MR= 1.02091    MRI= 1.67462   TN= 1.3208 E-3              DR= 1.01631
WSEP= 177.686

STATES AFTER MIXING

T2#= 329.032   T02#= 357.88   T02##= 358.365
P2#= 150911    P02#= 202721.
M2#= 0 663666  DP02= 3570.37
CT2#= 218.089  CM2#= 102.379  C2#= 240.924
T02##-TCOL=-0.023702
L= 2.13022

SIG#= 0.881522

WX= 70559.8    WFC= 1492 19    WFRD= 1243.49 WBF=-754.967

DIFFUSER

P0= 122967.    M4= 0.84273    D= 5.24685 E-2
D#= 7.49178 E-5     CP2#4=-0.539352     MS= 0
CP4C= 0.376068              CPD=-9.76947 E-3
P04= 195935.   WL= 0.130982

EFFICIENCIES

DETSBF=-1.06997 E-2       DETSFC= 2.11479 E-2     DETSWL= 4.84025 E-2
DETSRD= 1.76232 E-2       DETSI= 0.104764
DETSD= 0.408571           DETSF= 3.87711 E-2
DETSDM= 0.025059          DETSIW= 5.16335 E-2
ETT= 0         ETS= 0.486665  ETTI= 0.895236

*
```

```
CDR2...PROJECT#3305...9.14 BL2 DIF  SI UNITS...10/11/78  KBA

 INPUT VALUES

P00= 101353.    P1= 97298.8     P2= 262339.     P4= 349921.
P04= 477165.    P5= 0           P05= 424263.    PCOL= 424263.
T00= 288.167    TCOL= 479.      M= 0.496684     N= 4314.18
MW/M= 0.2       LC= 0           W4= 0.149352    B4= 3.2258 E-3
B1B=-56.3       B2B=-30.        ALPHT= 0        B2= 3.2258 E-3
PR= 4.186       RSEP= 4.39496 E-2               RIH= 2.16002 E-2
R1T= 4.39496 E-2
R2= 0.079756    # BLADES= 19    # DIFF= 17

 INDUCER TIP

TIREL= 288.104     PTREL= 101275.     MRELIT= 0.856653
CIT= 83.9269    RCT= 0          W1T= 289.919
P1T= 97298.8    T1T= 284.65     M1T= 0.247987
B1T=-73.173     IT= 16.873      U1T= 277.506
P10T= 101353.   IKE= 0.217574

 IMPELLER TIP

CT2J= 345.826   CM2J= 220.077   C2J= 409.914
C2W= 475.448    CM2W= 54.0976   CT2W= 472.36
W2W= 62.4665    W2J= 270.785    WT2W= 31.2332
P02J= 529918.   MREL2J= 0.696499
T2J= 377.79     T02J= 460.464   M2J= 1.05702    U2= 503.594
P02W= 588496.   M2W= 1.1426     E= 0.538322     P02MA= 541634.
T2W= 433.127    T02W= 543.076
MR= 1.22994     MRI= 2.65422    TN= 1.3208 E-3                  DR= 1.20458
WSEP= 240.681

 STATES AFTER MIXING

T2#= 401.72     T02#= 477.088   T02##= 479.016
P2#= 280991.    P02#= 517605.
M2#= 0.978713   DP02= 24028.6
CT2#= 371.133   CM2#= 126.086   C2#= 391.966
T02##-TCOL= 1.56403 E-2
L= 2.94349

SIG#= 0.881522

WX= 193160.     WFC= 4281.97    WFRD= 3568.31 WBF=-1590.56

 DIFFUSER

P4= 349921.     M4= 0.683968    B= 8.32149 E-2
D#= 1.18819 E-4      CP2#4= 0.291319      HS= 0
CP4C= 0.584247              CPD= 0.60551
P04= 477165.    WL= 0.17091

 EFFICIENCIES

DETSBF=-8.23443 E-3       DETSFC= 0.022168        DETSWL= 5.47987 E-2
DETSRD= 1.84733 E-2       DETSI= 0.112037
DETSD= 0.131775           DETSF= 4.06413 E-2
DETSDM= 3.11146 E-2       DETSIW= 4.85158 E-2
ETT= 0          ETS= 0.756188   ETTI= 0.887963

*
```

```
CDR2...PROJECT#3305...9.18 BL2 DIF  SI UNITS...10/11/.  KBA

 INPUT VALUES

P00= 101353.    P1= 96724.5     P2= 260794.     P4= 331373.
P04= 478365.    P5= 0           P05= 414939.    PCOL= 414939.
T00= 288.167    TCOL= 476.611   M= 0.532064     N= 6312.5
MW/M= 0.2       LC= 0           W4= 0.149352    B4= 3.2258 E-3
B1B=-56 3       B2B=-30.        ALPHT= 0        B2= 3.2258 E-3
PR= 4.094       RSEP= 4.39496 E-2               R1H= 2.16002 E-2
R1T= 4.39496 E-2
R2= 0.079756    # BLADES= 19    # DIFF= 17

 INDUCER TIP

TIREL= 288.104     PTREL= 101275.     MRELIT= 0.862064
CIT= 89.4886    RCT= 0          W1T= 291.508
P1T= 96724.5    T1T= 284.168    M1T= 0.264641
B1T=-72.1224    IT= 15.8224     U1T= 277.432
P10T= 101353.   IKE= 0.222792

 IMPELLER TIP

CT2J= 339.863   CM2J= 218.421   C2J= 403.999
C2W= 471.539    CM2W= 62.4927   CT2W= 467.38
W2W= 72.1604    W2J= 272.895    WT2W= 36.0802
P02J= 517720.   MREL2J= 0.702503
T2J= 377.156    T02J= 457.483   M2J= 1.0425     U2= 503.46
P02W= 580331.   M2W= 1.13616     E= 0.499574     P02MA= 530242.
T2W= 430.898    T02W= 539.108
MR= 1.22713     MRI= 2.46638    TN= 1.3208 E-3                  DR= 1.2018
WSEP= 242.56

 STATES AFTER MIXING

T2#= 399.33     T02#= 473.906   T02##= 476.626
P2#= 277670.    P02#= 510047.
M2#= 0.976195   DP02= 20195.5
CT2#= 365.366   CM2#= 135.87    C2#= 389.812
T02##-TCOL= 1.52334 E-2
L= 2.68908

SIG#= 0.881522

WX= 190709.     WFC= 3972.1     WFRD= 3310.08 WBF=-520.664

 DIFFUSER

P4= 331373.     M4= 0.746897    B= 6.05198 E-2
D#= 8.64138 E-5      CP2#4= 0.231104      HS= 0
CP4C= 0.568506              CPD= 0.590717
P04= 478365.    WL= 0.136338

 EFFICIENCIES

DETSBF=-2.73015 E-3       DETSFC= 0.020828        DETSWL= 4.36783 E-2
DETSRD= 1.73567 E-2       DETSI= 0.110755
DETSD= 0.137794           DETSF= 3.81847 E-2
DETSDM= 2.68329 E-2       DETSIW= 4.84627 E-2
ETT= 0          ETS= 0.75145    ETTI= 0.889245

*
```

```
CDR2...PROJECT#3305...9.22 BL2 DIF  SI UNITS...10/11/78  KBA
 INPUT VALUES

P00= 101353.    P1= 95778.5     P2= 259527.     P4= 300942.
P04= 473539.    P5= 0           P05= 397101.    PCOL= 397101.
T00= 288.167    TCOL= 473.333   M= 0.557465     N= 6305.17
MW/M= 0.2       LC= 0           W4= 0.149352    B4= 3.2258 E-3
B1B=-56.3       B2B=-30.        ALPHT= 0        B2= 3.2258 E-3
PR= 3.918       RSEP= 4.39496 E-2               RIH= 2.16002 E-2
R1T= 4.39496 E-2
R2= 0.079756    # BLADES= 19    # DIFF= 17

 INDUCER TIP

TTREL= 288.104     PTREL= 101275.     MRELIT= 0.870434
CIT= 98.0078    RCT= 0          W1T= 293.931
P1T= 95778.5    T1T= 283.369    M1T= 0.290236
B1T=-70.5225    IT= 14.2225     U1T= 277.11
P10T= 101353.   IKE= 0.230576

 IMPELLER TIP

CT2J= 335.137   CM2J= 216.337   C2J= 398.897
C2W= 467.814    CM2W= 69.7963   CT2W= 462.578
W2W= 80.5939    W2J= 273.748    WT2W= 40.2969
P02J= 507572.   MREL2J= 0.705174
T2J= 376.634    T02J= 454.963   M2J= 1.02992    U2= 502.875
P02W= 572943.   M2W= 1.1298     E= 0.468784     P02MA= 520646.
T2W= 428.926    T02W= 535.488
MR= 1.23435     MRI= 2.35128    TN= 1.3208 E-3                  DR= 1.20776
WSEP= 243.368

 STATES AFTER MIXING

T2#= 397.245    T02#= 471.163   T02##= 473.348
P2#= 274613.    P02#= 503307.
M2#= 0.974192   DP02= 17339.3
CT2#= 360.625   CM2#= 143.19    C2#= 388.013
T02##-TCOL= 1.4678I E-2
L= 2.51851

SIG#= 0.881522

WX= 187348.     WFC= 3758.46    WFRD= 3132.05 WBF=-892.545

 DIFFUSER

P4= 300942.     M4= 0.834576    B= 4.55238 E-2
D#= 6.50017 E-5      CP2#4= 0.11513       HS= 0
CP4C= 0.557129              CPD= 0 535598
P04= 473539.    WL= 0.130164

 EFFICIENCIES

DETSBF=-4.76411 E-3       DETSFC= 2.00614 E-2     DETSWL= 4.21302 E-2
DETSRD= 1.67179 E-2       DETSI= 0.104089
DETSD= 0.159804           DETSF= 3.67793 E-2
DETSDM= 2.37196 E-2       DETSIW= 4.83546 E-2
ETT= 0          ETS= 0.736106   ETTI= 0.895911
```

```
CDR2...PROJECT#3305...9.30 BL2 DIF  SI UNITS...10/11/78  KBA

 INPUT VALUES

P00= 101353.    P1= 95204.2     P2= 257778.     P4= 259007.
P04= 456826.    P5= 0           P05= 328181.    PCOL= 328181.
T00= 288.167    TCOL= 471.722   M= 0.571073     N= 6303.6
MW/M= 0.2       LC= 0           W4= 0.149352    B4= 3.2258 E-3
B1B=-56.3       B2B=-30.        ALPHT= 0        B2= 3.2258 E-3
PR= 3.238       RSEP= 4.39496 E-2               R1H= 2.16002 E-2
R1T= 4.39496 E-2
R2= 0.079756    # BLADES= 19    # DIFF= 17

 INDUCER TIP

TTREL= 288.104     PTREL= 101275.     MRELIT= 0.875882
CIT= 102.862    RCT= 0          W1T= 295.52
P1T= 95204.2    T1T= 282.882    M1T= 0.30487
B1T=-69.6306    IT= 13.3306     U1T= 277.041
P10T= 101353.   IKE= 0.235149

 IMPELLER TIP

CT2J= 332.503   CM2J= 217.461   C2J= 397.3
C2W= 466 009    CM2W= 73.833    CT2W= 460.122
W2W= 85.255     W2J= 276.176    WT2W= 42.6275
P02J= 502265.   MREL2J= 0.712098
T2J= 375.911    T02J= 453.625   M2J= 1.02672    U2= 502.75
P02W= 566919.   M2W= 1.12674     E= 0.456004     P02MA= 515196.
T2W= 427.945    T02W= 533.712
MR= 1.23        MRI= 2.29732    TN= 1.3208 E-3                  DR= 1.20361
WSEP= 245.529

 STATES AFTER MIXING

T2#= 396.106    T02#= 469.736   T02##= 471.737
P2#= 272313.    P02#= 498754.
M2#= 0.973572   DP02= 16441.6
CT2#= 358.026   CM2#= 147.5     C2#= 387.22
T02##-TCOL= 1.44153 E-2
L= 2.4273

SIG#= 0.881522

WX= 185696      WFC= 3648.69    WFRD= 3040.57 WBF=-991.211

 DIFFUSER

P4= 259007.     M4= 0,940708    B= 1.06818 E-2
D#= 1.52521 E-5      CP2#4=-5.87625 E-2      HS= 0
CP4C= 0.349682              CPD= 0.24672
P04= 456826.    WL= 0.185161

 EFFICIENCIES

DETSBF=-5.33782 E-3       DETSFC= 1.96487 E-2     DETSWL= 6 08358 E-2
DETSRD= 1.63739 E-2       DETSI= 0.102503
DETSD= 0.276903           DETSF= 3.60226 E-2
DETSDM= 2.28525 E-2       DETSIW= 4.89656 E-2
ETT= 0          ETS= 0.620594   ETTI= 0.897497

*
```

ORIGINAL PAGE IS
OF POOR QUALITY

```
CDR2...PROJECT#3305...9.32  SI UNITS...10/10/78  KBA

 INPUT VALUES

 P00= 101353.   P1= 75541.7     P2= 365691.    P4= 442306.
 P04= 814691.   P5= 0           P05= 508792.   PCOL= 508792.
 T00= 288.167   TCOL= 575.611   M= 0.896299    N= 7856.59
 MW/M= 0.2      LC= 0           W4= 0.137709   B4= 3.2258 E-3
 B1B=-56.3      B2B=-30.        ALPHT= 0       B2= 3.2258 E-3
 PR= 5.02       RSEP= 4.39496 E-2              RIH= 2.16002 E-2
 R1T= 4.39496 E-2
 R2= 0.079756   # BLADES= 19    # DIFF= 17

 INDUCER TIP

 TTREL= 288.104    PTREL= 101275.    MRELIT= 1.24761
 CIT= 216.278   RCT= 0          WIT= 407.436
 P1T= 75541.7   T1T= 264.743    M1T= 0.662267
 B1T=-57.9387   IT= 1.63873     U1T= 345.294
 P10T= 101353.  IKE= 0.28307

 IMPELLER TIP

 CT2J= 418.768  CM2J= 305.817  C2J= 518.547
 C2W= 584.521   CM2W= 83.2116  CT2W= 578.568
 W2W= 96.0845   W2J= 369.76    WT2W= 48.0422
 P02J= 977545.  MREL2J= 0.908392
 T2J= 415.125   T02J= 546.076  M2J= 1.27735   U2= 626.61
 P02W= 1.00678 E+6             M2W= 1.3004    E= 0.527389    P02MA= 983393.
 T2W= 504.184   T02W= 667.163
 RR= 1.37343    RRI= 3.33096   TN= 1.3208 E-3                DR= 1.29939
 WSEP= 313.56

 STATES AFTER MIXING

 T2*= 457.205   T02*= 570.543  T02**= 575.635
 P2*= 413315.   P02*= 914512.
 M2*= 1.13234   DP02= 68880.3
 CT2*= 450.728  CM2*= 176.052  C2*= 483.89
 T02**-TCOL= 2.43208 E-2
 L= 2.5602

 SIG*= 0.881522

 WX= 293222.    WFC= 5467.9    WFRD= 4556.59 WBF= 765.767

 DIFFUSER

 P4= 442306.    M4= 0.980065   B=-4.22889 E-2
 D*=-5.98026 E-5     CP2*4= 5.78423 E-2     HS= 0
 CP4C= 0.178541                CPD= 0.190497
 P04= 814691.   WL= 0.199165

 EFFICIENCIES

 DETSBF= 2.61157 E-3       DETSFC= 1.86477 E-2     DETSWL= 5.97969 E-2
 DETSRD= 1.55397 E-2       DETSI= 0.138236
 DETSD= 0.284507           DETSF= 3.41874 E-2
 DETSDM= 3.85527 E-2       DETSIW= 6.28841 E-2
 ETT= 0          ETS= 0.577257  ETTI= 0.861764

 *
```

```
CDR2...PROJECT#3305...9.36  SI UNITS...10/10/78  KBA

 INPUT VALUES

 P00= 101353.   P1= 82231.      P2= 399533.    P4= 514907.
 P04= 865961.   P5= 0           P05= 771192.   PCOL= 771192.
 T00= 288.167   TCOL= 584.556   M= 0.837332    N= 7864.63
 MW/M= 0.2      LC= 0           W4= 0.137709   B4= 3.2258 E-3
 B1B=-56.3      B2B=-30.        ALPHT= 0       B2= 3.2258 E-3
 PR= 7.60898    RSEP= 4.39496 E-2              RIH= 2.16002 E-2
 R1T= 4.39496 E-2
 R2= 0.079756   # BLADES= 19    # DIFF= 17

 INDUCER TIP

 TTREL= 288.104    PTREL= 101275.    MRELIT= 1.18445
 CIT= 183.827   RCT= 0          WIT= 391.467
 P1T= 82231.    T1T= 271.261    M1T= 0.556198
 B1T=-61.9927   IT= 5.69274     U1T= 345.621
 P10T= 101353.  IKE= 0.25323

 IMPELLER TIP

 CT2J= 431.852  CM2J= 279.13   C2J= 514.208
 C2W= 591.222   CM2W= 69.4018  CT2W= 587.134
 W2W= 80.1383   W2J= 340.699   WT2W= 40.0691
 P02J= 1.03048 E+6             MREL2J= 0.826873
 T2J= 425.647   T02J= 554.203  M2J= 1.2598    U2= 627.203
 P02W= 1.1123 E+6              M2W= 1.30874   E= 0.546022    P02MA=
  1.04684 E+6
 T2W= 509.153   T02W= 675.653
 RR= 1.43244    RRI= 3.43426   TN= 1.3208 E-3                DR= 1.35499
 WSEP= 288.908

 STATES AFTER MIXING

 T2*= 463.427   T02*= 578.746  T02**= 584.58
 P2*= 442080.   P02*= 981661.
 M2*= 1.13534   DP02= 65181.1
 CT2*= 462.908  CM2*= 155.86   C2*= 488.443
 T02**-TCOL= 2.42784 E-2
 L= 2.97002

 SIG*= 0.881522

 WX= 302584.    WFC= 6137.49    WFRD= 5184.58 WBF= 993.669

 DIFFUSER

 P4= 514907.    M4= 0.899062   B= 0.068316
 D*= 9.66087 E-5     CP2*4= 0.134969     HS= 0
 CP4C= 0.730046                CPD= 0.609941
 P04= 865961.   WL= 0.214426

 EFFICIENCIES

 DETSBF= 3.28395 E-3       DETSFC= 2.02836 E-2     DETSWL= 6.40234 E-2
 DETSRD= 0.016903          DETSI= 0.128455
 DETSD= 0.121261           DETSF= 3.71867 E-2
 DETSDM= 3.36844 E-2       DETSIW= 5.42999 E-2
 ETT= 0          ETS= 0.750284  ETTI= 0.871545

 *
```

```
CDR2...PROJECT#3305...9.38  SI UNITS...10/10/78  KBA

 INPUT VALUES

 P00= 101353.   P1= 79496.5     P2= 393139.    P4= 593976.
 P04= 877613.   P5= 0           P05= 761457.   PCOL= 761457.
 T00= 288.167   TCOL= 585.833   M= 0.860011    N= 7870.31
 MW/M= 0.2      LC= 0           W4= 0.137709   B4= 3.2258 E-3
 B1B=-56.3      B2B=-30.        ALPHT= 0       B2= 3.2258 E-3
 PR= 7.51293    RSEP= 4.39496 E-2              RIH= 2.16002 E-2
 R1T= 4.39496 E-2
 R2= 0.079756   # BLADES= 19    # DIFF= 17

 INDUCER TIP

 TTREL= 288.104    PTREL= 101275.    MRELIT= 1.21092
 CIT= 197.502   RCT= 0          WIT= 398.311
 P1T= 79496.5   T1T= 268.645    M1T= 0.600431
 B1T=-60.2744   IT= 3.97438     U1T= 345.897
 P10T= 101353.  IKE= 0.261007

 IMPELLER TIP

 CT2J= 428.681  CM2J= 284.664  C2J= 514.588
 C2W= 589.891   CM2W= 73.4458  CT2W= 585.301
 W2W= 84.8078   W2J= 347.338   WT2W= 42.4039
 P02J= 1.01917 E+6             MREL2J= 0.844856
 T2J= 423.711   T02J= 552.499  M2J= 1.25459   U2= 627.705
 P02W= 1.09215 E+6             M2W= 1.30714   E= 0.537467    P02MA=
  1.03376 E+6
 T2W= 508.127   T02W= 673.927
 RR= 1.43328    RRI= 3.41153   TN= 1.3208 E-3                DR= 1.35264
 WSEP= 294.47

 STATES AFTER MIXING

 T2*= 462.09    T02*= 577.037  T02**= 585.658
 P2*= 436517.   P02*= 968894.
 M2*= 1.13497   DP02= 64868.
 CT2*= 460.005  CM2*= 161.654  C2*= 487.582
 T02**-TCOL= 2.42615 E-2
 L= 2.84561

 SIG*= 0.881522

 WX= 303923.    WFC= 5940.08    WFRD= 4950.07 WBF= 4284.89

 DIFFUSER

 P4= 593976.    M4= 0.772907   B= 1.52617 E-2
 D*= 2.15823 E-5     CP2*4= 0.295766     HS= 0
 CP4C= 0.590476                CPD= 0.610357
 P04= 877613.   WL= 0.17146

 EFFICIENCIES

 DETSBF= 1.40986 E-2       DETSFC= 1.95447 E-2     DETSWL= 5.02951 E-2
 DETSRD= 1.62873 E-2       DETSI= 0.139031
 DETSD= 0.120106           DETSF= 0.035832
 DETSDM= 3.36872 E-2       DETSIW= 5.54333 E-2
 ETT= 0          ETS= 0.740843  ETTI= 0.860949

 *
```

```
CDR2...PROJECT#3305...9.42  SI UNITS...10/10/78  KBA

 INPUT VALUES

 P00= 101353.   P1= 76589.      P2= 371053.    P4= 469129.
 P04= 843677.   P5= 0           P05= 673288.   PCOL= 673288.
 T00= 288.167   TCOL= 576.889   M= 0.893577    N= 7864.97
 MW/M= 0.2      LC= 0           W4= 0.137709   B4= 3.2258 E-3
 B1B=-56.3      B2B=-30.        ALPHT= 0       B2= 3.2258 E-3
 PR= 6.643      RSEP= 4.39496 E-2              RIH= 2.16002 E-2
 R1T= 4.39496 E-2
 R2= 0.079756   # BLADES= 19    # DIFF= 17

 INDUCER TIP

 TTREL= 288.104    PTREL= 101275.    MRELIT= 1.23831
 CIT= 211.404   RCT= 0          WIT= 405.184
 P1T= 76589.    T1T= 265 791    M1T= 0.646083
 B1T=-58.5505   IT= 2.25053     U1T= 345.662
 P10T= 101353.  IKE= 0.278679

 IMPELLER TIP

 CT2J= 420.648  CM2J= 302.296  C2J= 518.003
 C2W= 585.804   CM2W= 81.7705  CT2W= 580.068
 W2W= 94.4204   W2J= 366.168   WT2W= 47.2102
 P02J= 986544.  MREL2J= 0.897767
 T2J= 416.839   T02J= 547.479  M2J= 1.27337   U2= 627.279
 P02W= 1.02379 E+6             M2W= 1.30204   E= 0.528286    P02MA= 993992.
 T2W= 505.104   T02W= 668.756
 RR= 1.37932    RRI= 3.32727   TN= 1.3208 E-3                DR= 1.30517
 WSEP= 310.445

 STATES AFTER MIXING

 T2*= 458.243   T02*= 571.986  T02**= 576.913
 P2*= 417991.   P02*= 925848.
 M2*= 1.13321   DP02= 68144.2
 CT2*= 452.532  CM2*= 173.947  C2*= 484.812
 T02**-TCOL= 2.43123 E-2
 L= 2.60155

 SIG*= 0.881522

 WX= 294558.    WFC= 5542.31    WFRD= 4618.59 WBF= 533.011

 DIFFUSER

 P4= 469129.    M4= 0 959247   B=-5.73278 E-3
 D*=-8.10698 E-6     CP2*4= 0.100693     HS= 0
 CP4C= 0.54508                 CPD= 0.502693
 P04= 843677.   WL= 0.1618

 EFFICIENCIES

 DETSBF= 1.80953 E-3       DETSFC= 1.88157 E-2     DETSWL= 4.81769 E-2
 DETSRD= 1 56797 E-2       DETSI= 0.135689
 DETSD= 0.160105           DETSF= 3.44954 E-2
 DETSDM= 0.037652          DETSIW= 6.17318 E-2
 ETT= 0          ETS= 0.704296  ETTI= 0.864311

 *
```

REFERENCES

1. Fowler, H. S.; SOME MEASUREMENTS OF THE FLOW PATTERN IN A CENTRIFUGAL COMPRESSOR IMPELLER: ASME Paper No. 65-WA/GTP-7, 1965.

2. Welliver, A. D. and Acurio, J.; DESIGN AND DEVELOPMENT OF SMALL, SINGLE-STAGE CENTRIFUGAL COMPRESSORS; The Boeing Company, USAAVLABS Technical Report 67-47, U. S. Army Aviation Materiel Laboratory, Fort Eustis, Virginia, September 1967 AD385595.

3. Eckardt, D.; INSTANTANEOUS MEASUREMENTS IN THE JET-WAKE DISCHARGE FLOW OF A CENTRIFUGAL COMPRESSOR IMPELLER; ASME Paper 74-GT-90, 1974.

4. Senoo, Y. and Ishida, M.; BEHAVIOR OF SEVERELY ASYMMETRIC FLOW IN A VANELESS DIFFUSER; ASME Paper No. 74-GT-64, 1974.

5. Eckardt, D.; JET-WAKE MIXING IN THE DIFFUSER ENTRY REGION OF A HIGH-SPEED CENTRIFUGAL COMPRESSOR; Joint Symposium on Design and Operation of Fluid Machinery; Colorado State University, Fort Collins, Colorado, June, 1978.

6. Yeh, Y. and Cummins, H. Z.; LOCALIZED FLUID FLOW MEASUREMENTS WITH A HE-NE LASER SPECTROMETER; Applied Physics Letter, Volume 4, No. 10, May, 1964.

7. Wisler, D. C. and Mossey, P. W.; GAS VELOCITY MEASUREMENTS WITHIN A COMPRESSOR ROTOR PASSAGE USING THE LASER DOPPLER VELOCIMETER; ASME Paper No. 72-WA/GT-2.

8. Wisler, D. C.; SHOCK WAVE AND FLOW VELOCITY MEASUREMENTS FOR A HIGH SPEED FAN ROTOR USING THE LASER VELOCIMETER; Journal of Engineering for Power, April, 1977.

9. Schodl, R.; ADVANCED TESTING TECHNIQUES IN TURBOMACHINES; Von Karman Institute for Fluid Dynamics, April, 1975.

10. Seasholtz, R. G.; LASER DOPPLER VELOCIMETER SYSTEM FOR TURBINE STATOR CASCADE STUDIES AND ANALYSIS OF STATISTICAL BIASING ERRORS; NASA TN D-8297, February, 1977.

11. Schodl, R.; THE LASER-DUAL-FOCUS FLOW VELOCIMETER; AGARD-CP-193, May, 1976.

12. Eckardt, D.; DETAILED FLOW INVESTIGATIONS WITHIN A HIGH-SPEED CENTRIFUGAL COMPRESSOR IMPELLER; Journal of Fluids Engineering; Vol. 98, Series 1, No. 3, September, 1976.

13. Block, J. A., Runstadler, P. W., Jr. and Dean, R. C., Jr.; LOW SPEED OF SOUND MODELING OF A HIGH PRESSURE RATIO CENTRIFUGAL COMPRESSOR: Proceedings of Second International JSME Symposium, Vol. II, p. 141-150, September, 1972.

14. Osborne, C., Runstadler, P. W. Jr., and Stacy, W. D.; AERODYNAMIC AND MECHANICAL DESIGN OF AN 8:1 PRESSURE RATIO CENTRIFUGAL COMPRESSOR; NASA CR-134782, Creare TN-204, April, 1975.

15. Kogelnik, H.; IMAGING OF OPTICAL MODES-RESONATORS WITH INTERNAL LENSES; Bell Systems Technical Journal, March, 1965.

16. Berman, N. S.; PARTICLE FLUID INTERACTION CORRECTIONS FOR FLOW MEASUREMENTS WITH A LASER DOPPLER FLOWMETER; Arizona State University, NASA George C. Marshall Space Flight Center, Contract NASA8-21397, 1972.

17. Melling, A.; SCATTERING PARTICLES FOR LASER ANEMOMETRY IN AIR: SELECTION CRITERIA AND THEIR REALIZATION; Imperial College of Science and Technology, Report No. ET/TN/B/7, April, 1971.

18. Farmer, W. M.; MEASUREMENT OF PARTICLE SIZE, NUMBER DENSITY AND VELOCITY USING A LASER INTERFEROMETER: Applied Optics, Volume 11, November, 1972.

19. Yanta, W. J.; TURBULENCE MEASUREMENTS WITH A LASER DOPPLER VELOCIMETER; Naval Ordinance Laboratory, Technical Report 73-94, (AD766781), May, 1973.

20. McLaughlin, D. K. and Tiederman, W. G.; STATISTICAL BIASING IN INDIVIDUAL REALIZATION LASER ANEMOMETRY; Oklahoma State University, Report ER-73-J-19, November, 1972.

21. Smith, W. J.; MODERN OPTICAL ENGINEERING; McGraw-Hill Book Company, 1966.

22. Toyama, K., Runstadler, P. W., Jr., Dean, R. C., Jr.; AN EXPERIMENTAL STUDY OF SURGE IN CENTRIFUGAL COMPRESSORS; Proceedings of the Centrifugal Compressor and Pump Stability, Stall and Surge Symposium, ASME Symposium, New Orleans, La., March 21-25, 1976, Journal of Fluids Engineering, Volume 99, Series 1, pp. 115-131, March 1977.

23. Dean, R. C., Jr. and Young, L. R.; THE TIME DOMAIN OF CENTRIFUGAL COMPRESSORS AND PUMP STABILITY AND SURGE; Proceeding of the Centrifugal Compressor and Pump Stability, Stall and Surge Symposium, ASME Symposium, New Orleans, La., March 21-25, 1976